Analysis of sector-coupling effects between the mobility sector and the energy system under consideration of energy transport and charging infrastructure

Zur Erlangung des akademischen Grades Doktor-Ingenieur (Dr.-Ing.)
genehmigte Dissertation von Dominik Husarek, geboren in Mönchengladbach
Darmstadt, Tag der Einreichung: 26.06.2022, Tag der Prüfung: 11.11.2022

1. Gutachten: Prof. Dr.-Ing. Stefan Niessen, MBA
2. Gutachten: Prof. Dr. rer. nat. Florian Steinke
Fachbereich Elektrotechnik und Informationstechnik, Technische Universität Darmstadt

TECHNISCHE
UNIVERSITÄT
DARMSTADT

Analysis of sector-coupling effects between the mobility sector and the energy system under consideration of energy transport and charging infrastructure

Accepted doctoral thesis by Dominik Husarek

Fachbereich Elektrotechnik und Informationstechnik, Technische Universität Darmstadt

Darmstadt

Date of submission: 26.06.2022
Date of thesis defense: 11.11.2022

Jahr der Veröffentlichung der Dissertation auf TUprints: 2023

Erklärung laut Promotionsordnung

§8 Abs. 1 lit. c PromO

Ich versichere hiermit, dass die elektronische Version meiner Dissertation mit der schriftlichen Version übereinstimmt.

§8 Abs. 1 lit. d PromO

Ich versichere hiermit, dass zu einem vorherigen Zeitpunkt noch keine Promotion versucht wurde. In diesem Fall sind nähere Angaben über Zeitpunkt, Hochschule, Dissertationsthema und Ergebnis dieses Versuchs mitzuteilen.

§9 Abs. 1 PromO

Ich versichere hiermit, dass die vorliegende Dissertation selbstständig und nur unter Verwendung der angegebenen Quellen verfasst wurde.

§9 Abs. 2 PromO

Die Arbeit hat bisher noch nicht zu Prüfungszwecken gedient

Dominik Husarek, Munich, 22.05.2022

Abstract

Within the next decades, energy systems must be decarbonized and rely on renewable energy sources in the electricity, heat, and mobility sectors. This requires sector-coupling technologies such as electrolyzers, heat pumps, or charging infrastructure for electric vehicles. Additionally, energy transport networks for electricity and gas, including hydrogen, must be expanded. To design future energy systems cost-efficiently, those sectors and the energy transport infrastructure can no longer be considered independently but require an integrated assessment approach.

While the decarbonization of Germany's electricity and heat sectors has progressed since 1990, the emissions in the mobility sector stagnate. The decarbonization of the mobility sector requires new powertrain technologies and energy infrastructure enabling the utilization of electricity, hydrogen, or electricity-based fuels. Especially a carbon-neutral hydrogen supply chain and the charging infrastructure for battery electric vehicles are new, disruptive elements in the energy system. Electrolyzers, hydrogen storage, and the corresponding transport infrastructure couple the mobility sector indirectly with the electricity sector. This affects the electricity demand and provides flexibility for intermittent renewable energy sources. Charging stations couple the mobility sector directly with the electricity sector. The upcoming electrical charging demand is driven by electric vehicle drivers' heterogenous driving and charging behavior, which can differ significantly from conventional refueling behavior today.

In the present thesis, a model framework is developed and applied to analyze the interdependencies of a decarbonized mobility sector and the energy supply, energy transport, and charging infrastructure of a carbon-neutral, multi-modal energy system. The analysis aims at assessing cost-optimal energy carriers in the mobility sector and the correspondingly required renewable energy sources, energy imports, storage capacities, and transport infrastructure for electricity and hydrogen in Germany. Further, it aims at assessing the required charging infrastructure for battery electric vehicles, including slow and fast charging technologies at various locations. The impact of differently designed charging infrastructure networks on the multi-modal energy system is analyzed regarding the electricity charging peak load and the available flexibility from controlled charging processes.

The developed framework consists of a mathematical energy system optimization model and an agent-based electric vehicle simulation. The energy system model is parametrized to optimally design a carbon-neutral German multi-modal energy system in 2045 with its energy supply, transport, and demand infrastructure. It considers 38 administrative areas in Germany and 13 energy exchange countries in Europe. A scenario-based local sensitivity analysis is applied to assess the impact of different energy carriers in the mobility sector on the multi-modal energy system and to assess the cost-optimal energy carriers in the mobility sector under consideration of different energy supply and transport scenarios.

The agent-based simulation focuses on the charging and driving behavior of battery electric passenger vehicles. It is applied to identify Pareto optimal charging infrastructure network designs for rural and urban areas. The output is used to parametrize the charging infrastructure and electric vehicle charging demand time series in the energy system optimization model. A sensitivity analysis is applied by varying the availability of slow and fast charging stations at different locations in an urban and a rural area to assess the impact of different charging infrastructure network designs on the electricity charging peak load and the available flexibility from electric vehicle charging.

The analysis in the energy system model shows that efforts to enable a high electrification rate in the mobility sector can be considered no-regret measures. However, uncertainties in the availability and costs of energy supply and transport infrastructure primarily affect the cost-optimal electrification rate of capital-intensive technologies such as heavy-duty vehicles and buses. While electricity-based fuels are mainly consumed by heavy-duty vehicles, busses, ships, and airplanes, hydrogen can cost-optimally complement the electrification of light-duty vehicles and passenger cars. Both generation of hydrogen and electricity-based fuels can be cost-competitive at locations with large wind power generation in Germany, with electrolyzers operating in hours with low marginal electricity costs, compared to international locations. If hydrogen is used directly in the

mobility sector, the required hydrogen transport infrastructure must be expanded from connecting only hydrogen generation and import regions with industrial demand regions towards a country-wide coverage.

Furthermore, the results show that each 10%-increase of the electrification rate in the mobility sector requires an additional stationary energy storage capacity of 250 GWh, including thermal storage, hydrogen storage, and battery storage. However, the required battery storage capacity can be reduced by up to 45 GWh by controlled charging of electric passenger vehicle fleets.

The charging infrastructure network design significantly affects the volume of dispatched flexibility from battery electric vehicles and, correspondingly, the required battery storage capacity within the energy system. Fostering a dense network of fast chargers can significantly reduce the required number of slow chargers in the initial market phase of electric vehicles. With a growing number of electric vehicles, the design of regional charging infrastructure networks can be used increasingly effectively to reduce the electricity charging peak load and increase the available flexibility of a fleet of electric vehicles.

This thesis contributes to the research on decarbonized energy systems and shows the need for an integrated design process for future energy systems. It additionally reveals the relevance of comprehensively designing charging infrastructure networks for battery electric vehicles by quantifying the impact of different charging infrastructure networks on the charging peak load, on the available flexibility of charging processes, and on a fully multi-modal energy system.

Kurzfassung

Um die Klimaerwärmung zu begrenzen, müssen Energiesysteme in den nächsten drei Jahrzehnten vollständig dekarbonisiert und die Sektoren Strom, Wärme und Verkehr durch erneuerbare Energien versorgt werden. Dazu sind sektorkoppelnde Technologien, wie Elektrolyseure, Wärmepumpen und Ladeinfrastruktur für Elektrofahrzeuge notwendig. Stromnetze müssen ausgebaut und Gaspipelinesysteme für den Transport von Wasserstoff befähigt werden. Aufgrund der Komplexität von solch integrierten Energiesystemen, können die Verbrauchssektoren und die Energietransportinfrastruktur nicht mehr unabhängig voneinander betrachtet werden, sondern erfordern einen integrierten Bewertungsansatz.

Während die CO_2 Emissionen im Strom- und Wärmesektor in Deutschland seit 1990 reduziert werden konnten, emittiert der Verkehrssektor noch die gleichen Emissionen wie im Jahr 1990. Die Transformation des Verkehrssektors benötigt neue Antriebstechnologien und neue Energieinfrastruktur, die die Nutzung von Strom, Wasserstoff oder strombasierten Kraftstoffen ermöglichen. Neue und disruptive Schlüsselelemente im Energiesystem sind dabei die Versorgungsinfrastruktur für CO_2-neutralen Wasserstoff und der Aufbau von Ladeinfrastruktur für Elektrofahrzeuge. Elektrolyseure, Wasserstoffspeicher und die entsprechende Pipelineinfrastruktur koppeln den Mobilitätssektor indirekt mit dem Stromsektor. Dies wirkt sich auf die Stromnachfrage aus und bietet Flexibilität für die intermittierenden erneuerbaren Energiequellen. Ladestationen koppeln den Mobilitätssektor direkt mit dem Stromsektor, wobei der entstehende Stromladebedarf durch das heterogene Fahr- und Ladeverhalten von Fahrzeughaltern beeinflusst wird.

In der vorliegenden Doktorarbeit wird ein agenten-basiertes Modell entwickelt und mit einer mathematischen Optimierung gekoppelt, um die Wechselwirkungen eines dekarbonisierten Verkehrssektors mit der Energieversorgungs-, der Energietransport- und der Ladeinfrastruktur zu analysieren. Die Analyse identifiziert kostenoptimale Energieträger im Verkehrssektor und die benötigten Erneuerbare-Energien-Anlagen, Energieimporte, Speicherkapazitäten, sowie die Strom- und Wasserstofftransportinfrastruktur. Darüber hinaus soll die erforderliche Ladeinfrastruktur für batterieelektrische Fahrzeuge, einschließlich Langsam- und Schnellladetechnologien zu Hause, am Arbeitsplatz, an öffentlichen Plätzen und auf den Autobahnen, sowie die Auswirkungen unterschiedlich gestalteter Ladeinfrastrukturnetze auf das multimodale Energiesystem bewertet werden. Diese Auswirkungen werden in Bezug auf die elektrische Spitzenlast durch gleichzeitig auftretende Ladevorgänge und die verfügbare Flexibilität durch gesteuerte Ladevorgänge bestimmt.

Das mathematische Optimierungsmodell ist so parametrisiert, dass ein CO_2-neutrales, deutsches, multimodales Energiesystem im Jahr 2045 mit seiner Energieversorgungs-, Transport- und Nachfragestruktur optimiert werden kann. Dabei wird das deutsche Energiesystem in 38 Regionen unterteilt abgebildet und der Energieaustausch mit 13 europäischen Ländern modelliert. Eine Szenario-basierte, lokale Sensitivitätsanalyse wird angewandt, um die Auswirkungen verschiedener Energieträger im Verkehrssektor auf das multi-modale Energiesystem zu bewerten und die kostenoptimalen Energieträger im Verkehrssektor unter Berücksichtigung unterschiedlicher Energieversorgungs- und Transportkosten sowie verschiedener Technologieausbaugrenzen und Importverfügbarkeiten von strombasierten Energieträgern zu bewerten.

Die agentenbasierte Simulation bildet das Lade- und Fahrverhalten batterieelektrischer PKWs ab. Sie wird genutzt, um Pareto-optimale regionale Ladeinfrastrukturausgestaltungen für einen ländlichen und einen städtischen Raum zu untersuchen. Die Ergebnisse werden zur Parametrisierung der Ladeinfrastruktur und der zeitlich aufgelösten Ladeprozesse im Optimierungsmodell des Energiesystems verwendet. Des Weiteren wird eine Sensitivitätsanalyse durchgeführt, bei der die Verfügbarkeit von Langsam- und Schnellladestationen an verschiedenen Standorten in der agentenbasierten Simulation variiert wird, um die Auswirkungen verschiedener Ausgestaltungen des Netzwerks an Ladeinfrastruktur auf die elektrische Spitzenlast und die verfügbare Flexibilität der Ladevorgänge zu bewerten.

Die durchgeführte Analyse im Energiesystemmodell zeigt, dass eine hohe Elektrifizierungsrate im Verkehrssektor in allen Szenarien kosten-optimal ist. Veränderungen der Verfügbarkeit und der Kosten der Energieversorgungs- und - Energietransportinfrastruktur wirken sich hierbei vor allem auf die Elektrifizierungsrate von kapitalintensiven Fahrzeugtechnologien – schweren Nutzfahrzeuge und Busse – aus.

Während strombasierte Kraftstoffe vor allem Anwendung bei schweren Nutzfahrzeugen wie Bussen, Schiffen und Flugzeugen finden, kann Wasserstoff die Elektrifizierung von leichten Nutzfahrzeugen und Personenkraftwagen kostenoptimal ergänzen. Die Analyse zeigt, dass Wasserstoff und strombasierte Kraftstoffe an Standorten mit hoher Windstromerzeugung in Deutschland in Stunden mit niedrigen Stromgrenzkosten kostenoptimal erzeugt werden können. Für den Einsatz von Wasserstoff im Verkehrssektor muss die erforderliche Wasserstofftransportinfrastruktur von Wasserstofferzeugungs- und Importregionen im Norden des Landes von einem auf Industrieregionen begrenzten Pipelinenetzwerk zu einer flächendeckenden Pipelineinfrastruktur ausgebaut werden.

Darüber hinaus zeigen die Ergebnisse, dass bei einer Erhöhung der Elektrifizierungsrate im Verkehrssektor um 10% eine zusätzliche stationäre Energiespeicherkapazität von 250 GWh – thermische Speicher, Wasserstoffspeicher und Batteriespeicher – erforderlich ist. Die insgesamt benötigte stationäre Batteriespeicherkapazität kann durch gesteuertes Laden von Elektro-Pkw-Flotten um bis zu 45 GWh reduziert werden.

Die Ausgestaltung von regionalen Ladeinfrastrukturnetzwerken hat einen erheblichen Einfluss auf die von batteriebetriebenen Elektrofahrzeugen bereitgestellte Flexibilität und dementsprechend auf die erforderliche stationäre Batteriespeicherkapazität im Energiesystem. Besonders in der Anfangsphase des Markthochlaufs für Elektrofahrzeuge kann das Schnellladen die Anzahl der benötigten Ladesäulen signifikant reduzieren. Mit zunehmender Anzahl von Elektrofahrzeugen kann ein effizientes regionales Ladeinfrastrukturnetz so ausgestaltet werden, dass die Spitzenlast beim Laden von Strom minimiert und die verfügbare Flexibilität der Elektrofahrzeugflotte maximiert wird.

Diese Arbeit leistet einen Beitrag zur Forschung über die Ausgestaltung eines dekarbonisierten Energiesystems und zeigt die Notwendigkeit eines integrierten Prozesses für zukünftige Energiesysteme. Darüber hinaus wird die Relevanz einer umfassenden Ausarbeitung von Ladeinfrastrukturnetzen für batterieelektrische Fahrzeuge aufgezeigt, um Herausforderungen bei der Integration von Elektrofahrzeugen gezielt zu reduzieren.

Table of Contents

List of Figures

List of Tables

1 Introduction

Societies today consume large amounts of energy to power different applications across all sectors. In 2019, fossil energy carriers account for a significant share of the overall energy consumption. While Germany uses 612 TWh of natural gas and oil to heat buildings, warm water, and for industrial process heating in the year 2019 [1], its people drive 739 billion kilometers [2] in vehicles consuming 725 TWh of energy [3], mainly by combusting oil derivatives in internal combustion engines (ICE) [4]. Beyond that, lights, computers, medical equipment in hospitals, and large industry processes are powered by 578 TWh of electricity per year. 60% of the electricity is still generated in conventional power plants in 2019 [1]. The supply chain for fossil energy carriers was established over many decades. Oil and Gas, which are consumed in Germany, are mainly produced in Russia, Norway, and Northern Africa, and transported via pipelines and ships to Germany. The oil then is refined in 20 refineries in Germany and, inter alia, fueled at 14000 refueling stations across the country [5].

When burning fossil fuels 711-million tons of carbon dioxide were released into the atmosphere in Germany in 2019 [6]. A substance, which is proven to be primarily liable for the anthropogenic climate warming. This poses one of the main challenges in the 21st century, namely, keeping climate warming below 1.5°C as 195 countries worldwide agreed to in the Paris Agreement in 2015.

Renewable energy sources (RES) must be utilized within the sectors heat, electricity, and mobility [7]. This can be enabled by sector-coupling technologies such as heat pumps and electric vehicles, which gain increasing importance [2], [7]. In addition, electricity-based energy carriers, such as electrolysis hydrogen or Fischer-Tropsch (FT) diesel increase the number of applications for RES, where a direct electrification is not economically or technically reasonable today. RES will be at the center of most energetic applications within a decarbonized energy system, which thus will contain many sector-coupling technologies [7], [8].

The German government agreed to CO_2 reduction targets in the Kyoto protocol and tightened its targets yet again in 2021 with the amendment of the Climate Change Act [9] to reach carbon-neutrality in 2045 instead of 2050. Furthermore, sector-specific targets were announced prior to the amendment of the Climate Change Act [9]. The mobility sector must cut its emissions until 2030 by 40-42%, and thus 1.5 million[1] public charging points for 15 million Battery Electric passenger Vehicles (BEVs) shall be installed [12].

To make the transformation of the energy system efficient across all sectors, the interactions between sectors and investments in new key energy infrastructure, such as hydrogen pipelines or charging stations, must be understood. The present thesis analyzes those interactions for a future carbon-neutral energy system of Germany.

1.1 Motivation

The annual CO_2 emissions in Germany have been reduced by 32% from 1990 to 2019 (cf. Figure 1-1) [1]. Considering the climate targets of Germany further 68% of CO_2 reduction are necessary in the upcoming 25 years. Differentiating the development by sectors reveals that the electricity and heat sector each reduced the CO_2 emissions by almost 40%. In contrast, the mobility sector's decarbonization did not progress and it contributed with 23% to the total emissions in Germany in 2019. Thereof, the road transportation sector is the mode of transportation consuming the most energy and contributing with 96% to the emissions in the mobility sector [6].

As the transformation across all sectors, especially the mobility sector, must start and gain momentum immediately, less carbon intense technologies, need to enter the market or increase their market share soon. The need is not only relevant to reach short-term targets of a total of 65% CO_2 reduction until 2030 but ultimately

[1] One public charging point per ten BEVs is required according to the 'Masterplan Ladeinfrastruktur' and the Directive 2014/94/EU [10, p. 94], [11].

to not miss the chance of limiting climate warming by reaching carbon-neutrality by 2045 [9]. Less carbon intense technologies comprise, for instance, vehicles with alternative powertrains including BEVs and fuel cell vehicles fueled by carbon-neutrally generated hydrogen. However, ICEs could still have relevant market share in a decarbonized mobility sector if powered with carbon-neutrally generated electricity-based methane (e-methane) or fuels (e-fuels).

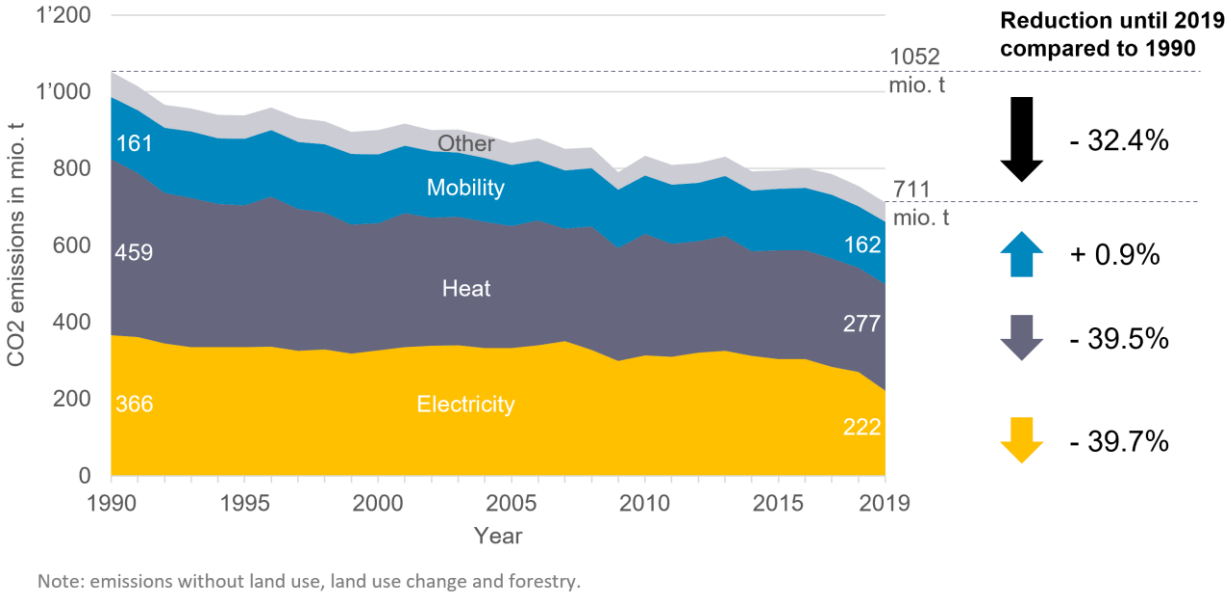

Figure 1-1 - Development of CO_2 emissions in Germany from 1990 to 2019 [1].

Independently of the technology that dominates in the mobility sector, major energy infrastructure investments arise: first, for converting wind and solar radiation into electricity, hydrogen, e-methane, and e-fuels, second, for energy transport and distribution, and finally, for new charging and refueling infrastructure. Especially the charging infrastructure differs significantly from the existing refueling infrastructure and so does the refueling behavior of drivers [5]. Charging points need to greatly outnumber the existing refueling stations, due to longer charging times and shorter driving ranges [13], [14]. In contrast to existing refueling infrastructure, they can be distributed across different types of locations: at home for private use, at workplaces for employees, along highways for public, and in public locations for public or semi-public (e.g., customers of, e.g., supermarkets) usage. The investment in such a future charging infrastructure might even exceed the costs for electricity distribution grid extensions [14], [15]. Charging stations are not only a prerequisite for an increasing market share of BEVs but also a sector-coupling element, linking the mobility and electricity sectors directly. The complex charging behavior across different locations, the high investments, and the impact on the electricity sector show the relevance of analyzing future designs of charging infrastructure networks in a carbon-neutral energy system.

Furthermore, the utilization of electricity, hydrogen, or e-fuels has different advantages and disadvantages as well as impacts on the overall energy system. While directly using electricity is energetically the most efficient path [14], [16], the intermittency of RES, the additional stress to an only slowly expanding electricity grid and the challenges of battery electric storages must be tackled. Those challenges are, e.g., the usage of metals that are rare, the need to improve recycling, a low gravimetric energy density limiting the range of BEVs, and no fit as seasonal storage for the energy system [14], [17], [18]. Hydrogen conversely seems to overcome some of those challenges. Due to better storage capabilities, and better international long-distance transport than electricity, it can help to harness more RES – even in international locations with excellent wind and solar conditions. But hydrogen requires a completely new generation and transport infrastructure and sacrifices in

energy efficiency. Finally, even if utilizing e- fuels would result in the lowest energy efficiency compared to the direct use of electricity or hydrogen, they come with the lowest efforts for transport, distribution and refueling infrastructure adjustments and the least disruptive changes on the automotive market [19], [20].

An effective utilization of RES is crucial for a decarbonized energy system independent of the utilized energy carrier in the end application to minimize system costs. Flexible technologies on the demand side and energy storage, which can balance the intermittent availability of RES, increase the effectiveness of RES in an integrated energy system. While sector-coupling increases the complexity of a multi-modal energy system (MMES), it has the potential to provide flexibility [21], [22]. A decarbonized mobility sector can offer different sources of flexibility in dependency of the developments in the automotive market. Those sources of flexibility are, for instance, electrolyzers with hydrogen storages or controlled charging processes of BEVs. The aggregated capacity of batteries installed in BEVs reaches already today the total capacity of the German national pumped-hydrogen storages [23]. Nevertheless, understanding the availability of those batteries in BEVs for the balancing needs of the MMES is crucial for the integrated decarbonization.

Sector-coupling and the new infrastructure contribute significantly to increasing the complexity of a decarbonized MMES, since developments in the mobility sector directly impact other sectors while competing for RES. Simultaneously, sharing energy transport infrastructure across sectors allows to increase the utilization of cost-intensive infrastructures to transport the energy from the generation region to the demand region. The arising complexity can be handled by applying mathematical optimization models to plan the decarbonization of an MMES [24], [25]. They help to handle the complexity and to analyze interactions between different technologies in the country-energy system.

To sum up the challenge, the decarbonization of the mobility sector becomes increasingly important and requires an integrated energy system assessment including the sectors of electricity, heat, and mobility as well as the relevant energy transport, charging, and refueling infrastructure. The complex task of planning the decarbonization of an MMES can be abstracted in mathematical energy system models [24], [25], commonly used to assess investments under consideration of their projected operation. To assess the role of the mobility sector within an MMES under fair competition between different energy carriers and technologies, the following five aspects need to be considered in a model:

(a) Multi-modality: The electricity, heat, and mobility sectors, and their interactions, including the competition for RES between these sectors must be considered.

(b) Mobility technologies: Different vehicle types and different suitable fuels require the coverage of the transportation modes road, rail, ship, and aviation with powertrain technologies allowing the utilization of electricity, gaseous, or liquid energy carriers.

(c) Energy supply infrastructure: The inland conversion of electricity, heat, hydrogen, and electricity-based energy carriers considering the competition for intermittent RES and the competition with energy imports in terms of overall energy supply costs must be considered.

(d) Energy transport infrastructure: Since energy supply and consumption sites differ in location, the national energy transport infrastructure for electricity, hydrogen, methane, and liquid fuels needs to be considered.

(e) Charging and refueling infrastructure: The refueling and charging infrastructure costs need to be represented as indispensable prerequisite for the mobility sector's transformation.

1.2 Literature review

The existing literature is grouped here into four categories and assessed based on the five aspects (a)-(e) (cf. Section 1.1). The four categories are firstly, studies focusing on **multi-modal energy systems**, secondly **energy transport infrastructure,** thirdly **charging and refueling infrastructure**, and finally **mobility sector studies** assessing a variety of different mobility technologies. While the categories are derived based on the aspects (a)-

(e), a separate category for the energy supply infrastructure (aspect (c)) is not outlined since this aspect is considered in **multi-modal** and **mobility sector studies**. Even though the existing literature already provides extensive insights into different aspects of the energy system transformation, the following analysis identifies a gap in the analysis of cross-sectoral effects rooted in the mobility sector under consideration of energy infrastructure.

Multi-modal energy system studies

Several MMES studies, which focus on the decarbonization of the German energy system until 2030 or 2050 have been published [8], [26]–[28]. Their distinctive mark is to include sector-coupling technologies such as heat pumps and electric vehicles and to analyze several energy sectors simultaneously, including their interactions. Inherently, the consideration of several sectors requires modeling a variety of different technologies, which can lead to increasing complexity requiring extensive computation power [25]. One way to deal with that is to focus on specific technologies and neglect others.

Regarding the coverage of the mobility sector, some MMES studies include only the road transportation sector [16], [29]. While Felgenhauer [16] tailors his analysis to the comparison of BEVs and FCEVs on a regional level, Robinius et al. [29] determine hydrogen demands for the road transportation sector exogenously.

A more comprehensive picture of the mobility sector is covered by other modelers by adding rail, water, and air transportation technologies in the optimization model [21], [30]–[36]. This can result in increased utilization of electricity-based energy carriers [32]. Bartholdsen et al. [30] consider internal combustion engines, fuel cells and electric powertrains, but the considered technologies are still limited in the scope of powertrain and transportation mode combinations. Focusing on cross-sectoral interactions, Palzer [36] optimizes only road transportation technologies and only covers the energy demands for trains, ships, and aviation by liquid hydrogen. The same approach is used by Sterchele [21] to assess load balancing options within an MMES. The author founds that controlled charging of BEVs and heat generators with thermal storage are suitable options to balance intermittent renewables. None of these studies considers refueling and charging infrastructure and only Bartholdsen et al. [30], Brown et al. [32], Müller et al. [35] and Metzger et al. [34] include electricity transport restrictions but no gas transport restrictions. Further, the electricity transport restrictions in Müller et al. [35] and Metzger et al. [34] are implemented in a separate model, which allows for conducting load flow calculations on the electricity line level. Nevertheless, similar to Robinius et al. [29], who apply seven sub-models, including energy transport infrastructure modeling, this restricts the capability of investigating interactions between the energy transport infrastructure and the MMES. Further, Lester et al. [33] and Bramstoft et al. [31] only include transport costs for biomass, which is converted to biofuel, but do not consider the electrification of the road transportation sector. Finally, the above mentioned MMES studies show a shortcoming with regard to modeling the import of electricity-based energy carriers.

Finally, there is a variety of MMES studies, which publish different scenarios for the German energy system. Some of those studies show a detailed representation of energy supply and the mobility sector and partly energy transport infrastructure. These studies are referenced and discussed subsequently and can be considered as relevant literature for the German energy system. However, they do not target an analysis of the interaction of the mobility sector with the MMES.

In 2020, Robinius et al. published a comprehensive MMES study focusing on the transformation of the German energy system until 2050, including various coupled and iteratively applied models [27]: an energy system investment model with a system cost minimization target optimizing the electricity, heat, and mobility sectors simultaneously; models for the electricity transmission grid simulation with a direct current load flow calculation; an international trade model for commodity import prices and restrictions; and a hydrogen infrastructure model. Still, while, e.g., hydrogen refueling is covered, this comprehensive study does not include a detailed charging infrastructure network modeling and it does not rely on a model-based derivation of controlled charging assumptions for BEVs. Further, the model framework does not include a combined electricity, methane and hydrogen transport infrastructure optimization. A similar gap due to a variety of applied models exists in another comprehensive study from the Federal Ministry for Economic Affairs and Energy

(BMWi) [7]. This study models the decarbonization of the German energy system, including the most relevant aspects with a high degree of detail.

Furthermore, the 'Dena Leitstudie' [26] from 2018 assesses an 80% and a 95% decarbonization scenario for 2050. While this study covers a multi-modal technology optimization with a mobility sector covering road, rail, water, and air transportation, it only considers the electricity transmission system, including a DC load flow calculation for a reduced transmission system. The studies **'**Klimapfade für Deutschland 2.0' [8], 'Klimschutzszenario' [37], 'Energiemarkt 2030 und 2050' [38], 'Wege zu einem Klimaneutralen Energiesystem' [28], 'Sektorkopplung' [39] and 'Interaktion EE-Strom, Wärme und Verkehr' [40] publish MMES decarbonization pathways for 80% and 95% CO_2 reduction targets until 2050 without covering the energy transport infrastructure in detail. The same gap is valid for the study 'Klimaneutrales Deutschland 2045' [41] but for the target year 2045.

With some of the MMES studies mentioned above (e.g. [29]–[31], [34], [35]) also considering energy transport infrastructures, the importance of this element in a model is emphasized. Nevertheless, the representation of infrastructure in these studies is either on a low spatial resolution or focuses solely on electricity or hydrogen transport. This restriction eliminates the option to fully evaluate the cost-optimal energy transport routes in an MMES. In a nutshell, it could be shown, that there is a lack of consideration of multi-modal energy transport, refueling and charging infrastructure in MMES studies. Moreover, only few studies cover all mobility sector technologies comprehensively.

Energy transport infrastructure studies

Publications in the category of energy transport infrastructure model the transport infrastructure for energy carriers with a high spatial or temporal resolution and under consideration of a physical power or gas flow calculation. The focus of the analyzed literature is on the long-term planning of energy transmission infrastructure with a target year of 2030 or 2050.

Most infrastructure studies focus on a single energy carrier. Their target is to derive explicit measures for electricity grid or pipeline extensions und upgrades. The most relevant studies for the German electricity or gas transport system are the 'Grid Development Plan Electricity' and the 'Grid Development Plan Gas' [42], [43]. Driven by the Energiewirtschaftsgesetz (§ 12b I 2 EnWG), both studies are released biennially by the electricity transmission system operators and the gas transmission system operators. The grid extension measures are identified for the next ten to 15 years based on exogenously defined scenario assumptions for technology projections. This includes, e.g., the electrification rate in the mobility and heat sector, and electricity supply technologies. Even though a planning process integrating the gas and electricity infrastructure does not exist yet, the relevance is accentuated by current developments regarding a 'System Development Plan' [44]. Nevertheless, both electricity and gas infrastructure studies are independently conducted and lack multi-modality as well as a representation of the mobility sector.

The equivalent to the Grid Development Plan on the European level is the 'Ten Year Network Development Plan'. Further, studies and articles focusing solely on the development of the electricity transmission grid with a reduced granularity exist on the European level [45]–[47] and for Germany [48].

Different approaches for assessing the required gas transport system extensions exist, which all result in deviating conclusions. Haumeier et al. conclude from a GIS-based area potential and gas power flow analysis that the gas pipeline infrastructure can limit the power to gas capacities in Germany [49]**.** Gillesen et al. evaluate the integration of the renewable gases into the German gas system until 2050 using an optimization model, which incorporates gas flows, and conclude that further extension of natural gas pipelines is not necessary [50]. Hauser et al. apply a gas market model to assess congestions in the German gas transmission network in 2030 [51]. Their linear optimization includes more than 1400 pipelines, and the gas demand is regionalized to 400 regions in Germany. The authors argue that a projected increasing gas demand could overload the pipelines during a few hours per year.

In contrast, research dealing with hydrogen transport infrastructure is found to explicitly center the analysis on the mobility sector as hydrogen sink. A first approach of modeling a spatially highly resolved hydrogen pipeline

network for Germany was conducted by Krieg in 2012 [52]. In 2016, Robinius extended this analysis by introducing an electricity and gas market into the model [53]. Reuss and Stöckl et al. focus on the competition between liquid, gaseous and organic hydrogen carriers for the inner-German transport [54]–[56]. The three doctoral theses from Krieg, Reuß and Robinius suggest explicit hydrogen transport routes from electrolyzer locations in Germany to hubs on municipality level and its further distribution to refueling stations. Still, no integrated consideration of the mobility sector and its technology mix is conducted, which goes beyond assuming refueling stations as hydrogen sink.

All infrastructure studies mentioned to this point show that energy transport infrastructure studies focus specifically only on transport infrastructure for one energy carrier, neglect an integrated multi-modal optimization of supply and demand technologies, consider no representation of different mobility sector technologies, and finally omit the consideration of energy import routes.

After all, the following two studies from the United Kingdom (UK) go beyond a pure hydrogen scope by including electricity transport technologies. Samsatli et al. [57] conducted an analysis focusing on supplying hydrogen for fuel cell electric passenger vehicles to different regions in the UK. Thereby, he analyzed the competition of electricity and hydrogen transport options. A further analysis from Samsatli and Samsatli [58] assesses the hydrogen and electricity transport infrastructure for a hydrogen demand in the heat sector including the option to repurpose natural gas infrastructure. While this analysis improves the multi-modal energy transport representation it does not focus on the different technologies in the mobility sector.

Finally, two studies incorporate a combined optimization of electricity, hydrogen, and methane transport infrastructure for the case of Germany. In a study from TenneT and Gasunie [59] a joint energy transport system extension for electricity, methane, and hydrogen is modeled based the administrative NUTS2 level in Germany and Netherlands for three different scenarios until 2050. A similar consideration of energy transport infrastructure with an increased scope in terms of multi-modal technologies is modeled in Gils et al. [22]. They integrate hydrogen, methane, and electricity infrastructure into a sector-coupling energy system optimization model. They focus on the interaction of the hydrogen infrastructure with the energy system and an assessment of the robustness of the outcome against different infrastructure-based measures such as a limited power grid extension. Nevertheless, the regional scope is limited to ten regions in Gils et al. and both studies define end use technologies and energy demands in the mobility sector exogenously.

In conclusion, this section shows that most of the literature in the energy transport infrastructure category focuses on a high degree of detail but only for a single commodity to derive specific grid extension measures. Studies focusing on more than one commodity for the energy transport reduce the degree of detail regarding infrastructure elements, and do not optimize end use technologies in the mobility sector jointly with the infrastructure. The importance of an integrated planning process of different energy transport options is additionally outlined by the potential of increased flexibility for the MMES through interactions of the electricity, methane, and hydrogen systems which in turn results in decreased overall system costs [60]. Finally, refueling or charging infrastructure is also under-represented in the category of energy transport infrastructure studies. It is solely considered in the hydrogen network studies as hydrogen sink.

Charging and refueling infrastructure studies

Since modelers try to limit the complexity of their models, they usually do not consider the refueling and charging infrastructure as shown above. However neglecting this cost term in a cost-optimal model can cause significant deviations since the buildup for new refueling and charging infrastructure contributes significantly to the overall mobility costs [14], [15], [61]. There are basically three approaches to be distinguished in literature covering refueling and charging infrastructure.

- First, studies that allocate hydrogen refueling infrastructure [52]–[54] or charging infrastructure [14] within Germany and use these allocated stations as sink in their model. While this allows for a detailed modeling of energy transport and distribution infrastructure, the number of refueling stations and the demand are defined exogenously.

- Second, studies that incorporate cost terms for refueling and charging infrastructure into their model [62]. This approach represents a less detailed coverage without geographic allocation of refueling and charging infrastructure, but the required total capacity and costs can be optimized, and level out the field of competition between technologies in the mobility sector. Nevertheless, the cost terms and infrastructure demand are not assessed fundamentally.
- And third, studies that focus entirely on refueling and charging network design but lack the integration of insights into a broader energy system scope, as described below.

Grüger [63] identifies in his dissertation the required hydrogen refueling infrastructure for commercial fleets using an optimization model. Rose [64] develops in his dissertation an optimization model to assesses the hydrogen refueling investments for heavy-duty trucks in Germany in 2050. Melaina and Bremson [65] analyze the required alternative refueling infrastructure for passenger cars on a city scope for the US.

While the number of publications on BEV charging and its impact on distribution grids is large, the subsequent focus lies on explicit charging infrastructure network studies. Grube et al. estimate the cost of charging infrastructure for Germany with consideration of regional differences but without a fundamental model-based assessment of required chargers [66]. While Funke et al. [67], Gnann et al. [13], and Jochem et al. [68] assess the demand for fast charging infrastructure along the German highway, other studies such as Nicholas and Wappelhorst [69], Brost et al. [70], and Pagany et al. [71] allocate charging infrastructure on a regional level. These regional studies reveal a more accurate assessment, but they cannot be generalized easily to the country level and neglect interactions between different types of chargers. Finally, a meta study from VDE|FNN and BDEW assesses 157 publications for the integration of BEVs into the electricity system [72]. Some of the gaps in research they derive are that the consideration of regional differences as well as interactions between different charger types and locations are not covered in literature accurately. Further, the analysis in this section shows, that a detailed representation of charging infrastructure is not covered in energy system studies but only as stand-alone.

Mobility studies:

The following paragraphs analyze publications focusing on the German mobility sector. In comparison to the MMES studies, the authors deal distinctively with the decarbonization of the mobility sector. Those studies have in common that they consider numerous different technologies in the mobility sector and comprehensively integrate alternative energy carriers in the assessment.

Hacker et al. [73] investigate the impact of an increased electrification in the mobility sector on the German electricity sector until 2050. They assess various vehicle technologies in the TEMPS model and couple it with a linear optimization model representing the electricity sector. While Hacker et al. focus on electrification strategies, the TEMPS model is also used to derive a detailed strategy to decarbonize the mobility sector until 2050 in Kasten et al. [74], but without an assessment of impacts on the electricity sector. In contrast, Weger et al. [75] assess the shift towards a hydrogen-based mobility sector in terms of greenhouse gas emissions. They assess different emission factors similar to Matthias et al. [76], who built up a tool chain to model spatiotemporal transport sector emission distributions for 2040. Both articles do not cover interactions with the entire MMES.

Millinger et al. [77] use a linear optimization model to assess the potential of electricity-based energy carriers and biofuels for the entire German mobility sector. While timely varying excess electricity from RES is considered in the optimization, the installed capacities in the electricity sector are fixed and not optimized. In contrast, Helgeson and Peter [62] model the transformation of the road transport sector until 2050 in Europe considering direct electrification and different electricity-based energy carriers. Thereby, they include the electricity sector and different power-to-x technologies in the optimization. By additionally modeling the mobility sector decoupled from the electricity sector they conclude that a coupled framework is important to lift synergies between the sectors. This ultimately results in lower system transformation costs. The authors focus strongly on the interaction of both sectors and include cost terms for charging and refueling infrastructure. However, they do not elaborate on the derivation of the charging infrastructure costs. Further, it was not in their scope to include the heat sector, energy transport infrastructure, or rail and inland navigation.

Bramstoft and Skytte [78] model Sweden's MMES considering different alternative fuels for the mobility sector in the STREAM model in 2050. However, the energy transport infrastructure is not considered. A similar gap exists in Shafiei et al. [96], who focus on a comparison between BEVs and fuel cell passenger vehicles, and their refueling and charging infrastructure costs in Iceland. Therefore, a system-dynamics simulation model is built but no MMES assessment and no energy transport infrastructure costs are mentioned.

As a concluding remark, it is emphasized that different scenarios for the direct and indirect electrification of the mobility sector exist in literature. A comprehensive multi-modal model framework is required, inter alia, to not neglected the competition about scarce RES between the electricity, heat and mobility sector [79]. Further, the above literature analysis identifies the additional shortcoming of not considering energy transport infrastructure costs.

Research gap:

The analysis above shows that a variety of research exists in the field of analyzing a decarbonized mobility sector. It also reveals the need for further research as a variety of MMES studies with different granularity levels and varying representations of energy transport systems are available and none of these studies covers the integrated optimization of the energy transport infrastructure. The publications [22], [44], [59], [60] emphasize the relevance of a combined optimization. Nevertheless, analyzing the impact of a MMES optimization, including multi-modal energy transport, on a decarbonized energy system remains open.

Figure 1-2 shows the identified research gap and summarizes the analysis above using a qualitative classification for each group of studies regarding the five aspects (a)-(e) described above. From the inside of the spider chart to the outside the classifications are 'out of scope', 'limited consideration', most aspects are 'covered' and 'detailed representation and evaluation'. The three dotted lines represent each one group of studies. Charging and refueling infrastructure studies are excluded in the figure since the aspects (a)-(d) are out of scope in today's existing scientific literature on this topic. As shown in the figure, MMES studies and energy transport infrastructure studies have a detailed representation of the aspects in the categories multi-modality and energy transport, respectively. Additionally, they complementarily cover the three remaining categories. In contrast, the assessed group of mobility studies represents mobility technologies and their energy supply up to a detailed level but is limited in terms of energy transport and multi-modality.

The present thesis fills the research gap of MMES studies by integrating an enhanced coverage of energy transport infrastructure and a more detailed representation charging and refueling infrastructure. While contributing to closing this gap might sacrifice details of infrastructure and mobility studies, the here developed approach can be considered Pareto optimal compared to existing MMES studies.

Four distinct statements regarding this gap are derived from the literature analysis and ultimately support the allocation of the research gap in Figure 1-2:

(1) First, the assessment of the role of the mobility sector in a decarbonized German MMES lacks consideration of the associated energy transport as well as charging and refueling infrastructure.
(2) Second, a lack of multi-modality while simultaneously optimizing the technologies in the mobility sector and corresponding energy carrier supply is identified. Therefore, only limited statements can be made about the competition between the heat, electricity, and mobility sector in terms of scarce RES.
(3) Third, there is no joint analysis of the required electricity grid and gas pipeline capacities between regions within an MMES optimization while assessing the decarbonization of the mobility sector.
(4) Finally, there is no analysis and representation of detailed charging infrastructure networks considering the charging and driving behavior of drivers, which includes the interactions between different types of charging locations and the impact of charging infrastructure on electrical load profiles and flexibility. A specific representation of charging infrastructure within MMES still needs to be analyzed.

There are comprehensive studies such as [7], [27], covering most of the aspects (a)-(e), and thus represent some aspects on a very detailed level. Nevertheless, since they use a variety of different models, the capability of

analyzing interactions between, for instance, transport infrastructure and the decarbonization of the mobility sector is limited. Moreover, these studies focus on specific scenarios and not on a more fundamental understanding of the interactions within a MMES.

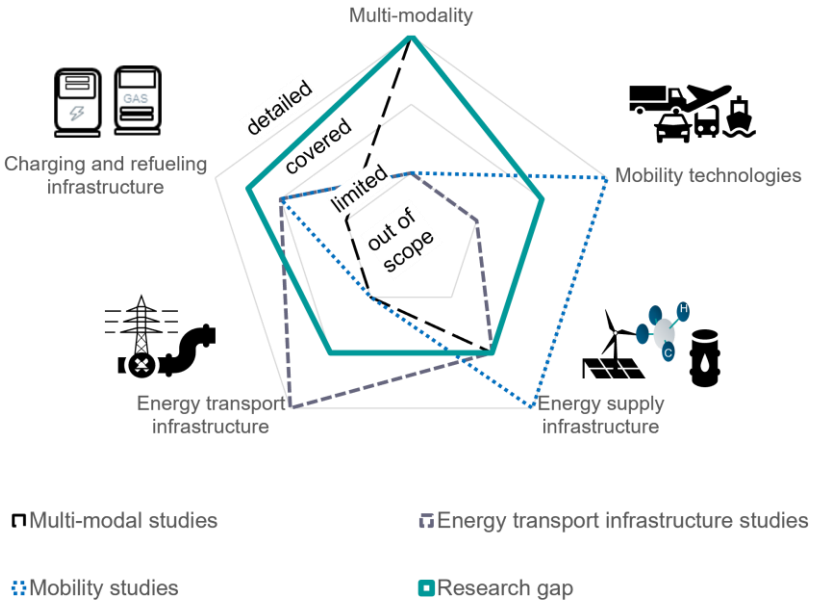

Figure 1-2 – Identification of the research gap by classification of existing literature and assessment based on five derived key aspects for the decarbonization of a multi-modal energy system.

1.3 Research questions and objective

Planning a complex system like the German MMES requires modeling tools to assess the interactions between different sectors. Since the mobility sector in Germany is by far the sector with the least decarbonization progress until 2021 compared to 1990 (cf. Figure 1-1), the present thesis focuses on the assessment of a decarbonized mobility sector within the German MMES. It is fundamental to incorporate costs and restrictions of relevant national energy transport, charging, and refueling infrastructure in this process. Aiming to contribute to the literature by addressing the research gaps (1) – (4) (cf. Section 1.2), the following objective and research questions are derived.

The present doctoral thesis aims to cost-optimally identify the required and inter-regional energy infrastructural measures to decarbonize the mobility sector as part of the German MMES. Those infrastructural measures are identified on an aggregated regional level based on a resolution of 38 regions in Germany. Further, the impact of different energy carriers in the mobility sector on the energy supply and energy transport under consideration of charging and refueling infrastructure is assessed. Two significant new infrastructure elements are examined in greater detail: charging infrastructure and hydrogen transport infrastructure. Both elements are underrepresented in the MMES literature while still gaining increased public and political attention. In Table 1-1, the three central research questions of the present thesis are identified.

	Research questions
RQ1	What are the optimal energy carriers to fuel a decarbonized mobility sector and how does the required energy supply and transport infrastructure impact the share of those energy carriers in a cost-optimally decarbonized Multi-modal Energy System?
RQ2	How does a decarbonized mobility sector generally impact the energy supply, transport, and demand structure of the Multi-modal Energy System, and in particular, what is the impact of the charging infrastructure network design and battery electric vehicles' flexibility?
RQ3	How to design charging infrastructure networks and how does the infrastructure affect the battery electric vehicles' charging peak load and available flexibility?

Table 1-1 – Research questions.

To answer the research questions, an MMES model framework is extended and parametrized to incorporate mobility sector characteristics such as distributed controlled charging, as well as electricity, methane, and hydrogen transport restrictions. This framework is based on an existing linear optimization model called Energy System Development Planner (ESDP) [35], which is extended and parametrized according to the requirements formulated in Section 2. Furthermore, an agent-based model to incorporate driving and charging behavior into the charging infrastructure planning process is developed and coupled to ESDP. The model coupling approach derived in the present thesis allows to derive general statements about charging infrastructure networks in the agent-based model and enables an accurate representation of BEVs and its charging infrastructure in ESDP, including a model-based derivation of controlled charging restrictions.

The complex nature of an MMES does not allow considering all elements to the same extent. Hence, the following restrictions to the scope of the present thesis are made. First, the alternative energy carriers considered in the mobility sector focus on electricity and electricity-based energy carriers, which are derivatives of hydrogen. A detailed assessment of biofuels produced from biomass are intentionally out of scope here due to competing interests of area usage for biomass crops with food production and photovoltaics (lower areal efficiency for energy production of biomass). Biomass from residues is not elaborated due to its limited potential [77], [80], [81]. Second, the energy transport is modeled for electricity, methane, and gaseous hydrogen. The transport of liquid energy carriers is not focused since it is assumed that this transport mode is regarding its complexity and its costs similar to the existing liquid energy carrier transport of oil and its derivatives (cf. [5], [19]). Third, since this study focuses on the country-level modeling, no assessment and detailed modeling of energy distribution networks is conducted. Finally, it is not meant to derive explicit infrastructural measures on an individual asset level, such as power transmission line extensions as, e.g., in the Grid Development Plan. This limitation is applied here since detailed planning for single assets in 2045 would imply too many uncertainties to derive meaningful statements. Therefore, assets in the energy system are not modeled individually but aggregated on a regional level. Furthermore, the present thesis focuses on the role of the mobility sector within an MMES and assesses energy-related measures for the decarbonization. This means that consequences of a modal shift, e.g., from road to rail, and new concepts such as autonomous driving, are not analyzed here.

1.4 Structure of thesis

The present thesis is structured in eight sections, including the introduction section. The requirements of a model framework to answers the research questions are analyzed in Section 2. This includes, for instance, the questions of which technologies need to be considered to which spatial and temporal resolution. The applied ESDP model and the here newly developed agent-based model are described in Sections 3 and 4. The method

of assessing charging infrastructure networks, the coupling process of both models, including implemented expansions in ESDP, as well as the techno-economic parametrization of the MMES follow in Section 5. The techno-economic parametrization of the MMES in ESDP includes the derivation of input parameters for BEVs in the agent-based model. Finally, Section 6 shows the results and answers the research questions. A discussion of the results follows in Section 7, and Section 8 contains the conclusion and outlook.

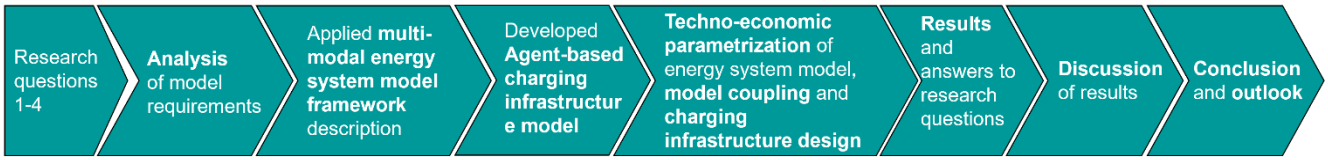

Figure 1-3 – Structure of thesis.

2 Analysis

A model framework to assess the role of the mobility sector in an MMES under consideration of energy transport infrastructure and charging infrastructure must consist of a variety of technologies and energy carriers. The analysis identifies first the technologies and energy carriers in the mobility sector that must be considered in a model (cf. Section 2.1). Second, the technologies in the MMES and subsequently the model implications such as the required spatial and temporal resolution are derived (cf. Section 2.2). And third, the specific requirements for modeling electric vehicles and charging infrastructure are analyzed (cf. Section 2.3).

2.1 Energy carriers and technologies to decarbonize the mobility sector

Transportation demand

The mobility sector in Germany can be subdivided into freight and passenger transportation with an annual passenger transportation capacity of 1169 billion passenger kilometers (Gpkm) and an annual freight transportation capacity of 701 billion ton-kilometers (Gtkm) in 2019 [4]. These units of transportation measurement describe the factor of distance and weight of transported goods and passengers respectively and are shown in Figure 2-1.

While 71% of the freight transportation capacity is provided by heavy and light-duty trucks, shipping and rail transportation make up another 26%. Since the freight transportation capacity for crude oil via pipeline and the aviation capacity account for only 2.5% and 0.2% of the total transportation capacity, they can be neglected with only a minor loss of accuracy in an MMES. International freight vehicles and vessels accounted for 30% of Germany's total freight transportation capacity in 2019 [4].

Passengers are transported to 78% in cars and 22% in busses, coaches, trains, and aviation. While those modes of transportation need to be considered, there is only a minor share of inland passenger transportation by ships in Germany, which can here be neglected in the context of an MMES. A more detailed view of passenger cars to assess energy carriers in the mobility sector is reasonable due to the large share of total passenger transportation. Therefore, to reduce the complexity of the overall MMES, the number of considered inland shipping and aviation technologies should be limited primarily and powertrain technologies for passenger cars should be considered comprehensively. This is further supported by the required energy of passenger cars amounting to 56% of the total energy demand in the mobility sector (cf. Figure 2-2). Further, differentiating between regional and long-distance traffic for busses, coaches, and trains is considered not relevant for answering the research questions in the present thesis. Hence, regional, and long-distance traffic is considered together as aggregated demand served by the same set of technologies.

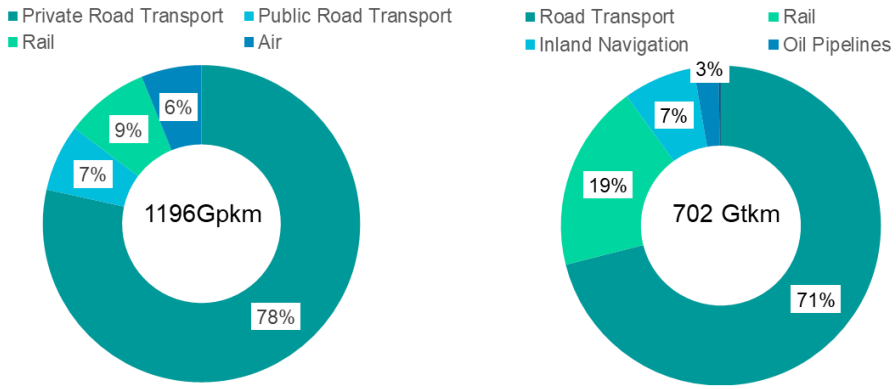

Figure 2-1 – Transportation capacity in Passenger-distance (left) and freight-distance (right) in 2019 based on [4].

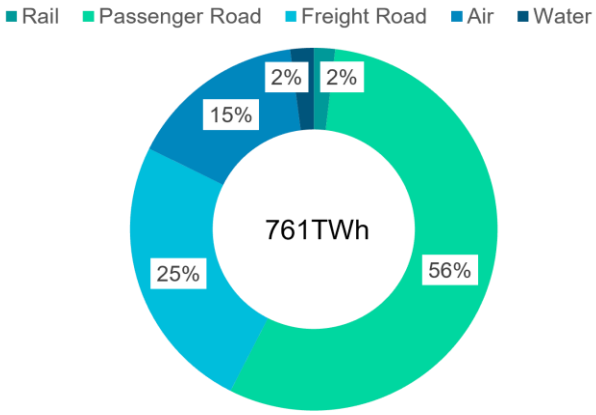

Figure 2-2 – Energy consumption in the mobility sector in 2019 based on [4].

Powertrains

Different technologies for each modality in the freight and passenger transportation sector exist. Those technologies are differentiated by their powertrains and by their consumed fuel. The powertrain converts electrical or chemical energy in the engine into kinetic energy and finally into propulsion. Three main powertrains are distinguished: ICE, fuel cell electric, and battery electric.

First, an ICE is a thermal engine that converts chemical energy in the form of a fuel-air mixture into mechanical energy by combustion. The most common ICEs are the Otto and Diesel engines, which ignite fuel by external spark ignition or internal compression ignition, respectively [82].

Second, the fuel cell electric powertrain uses an electric machine to convert electrical energy into mechanical energy analogously to an electric powertrain. In contrast to the battery electric powertrain, the fuel is stored as gas or liquid and uses a fuel cell to convert the chemical energy into electrical energy by a chemical reaction of the fuel and an oxidant [82]. In the present thesis, the term fuel cell is referred to the most relevant fuel cell for vehicles, the hydrogen-oxygen fuel cell with Proton Exchange Membrane technology [83].

Third, the electric powertrain with a battery as electrochemical energy storage or with a direct electricity supply from overhead lines, a so-called catenary system. Catenary systems exist today primarily along railways, but first pilot systems are installed along the German highway for heavy-duty trucks and in cities for busses [84].

Finally, different combinations of these powertrains exist in hybrid vehicles. To increase the overall powertrain efficiency, the most suitable combination uses the electric powertrain as one component to improve the overall efficiency and reduce operational carbon emissions. A mild hybrid electric vehicle uses electric energy primarily during acceleration and starting. A plug-in hybrid electric vehicle can drive fully electric and recharge its battery via a plug. Since no full-electric driving is possible in mild hybrid electric vehicles, they do not differ significantly from ICEs in terms of fuel consumption and thus do not need to be explicitly considered in an MMES optimization. Therefore, electric hybrids considered in the scope here can incorporate ICEs or fuel cell powertrains.

Alternative energy carriers

The discussed powertrains can use different energy carriers. While ICEs can burn a variety of different fuels, the application of fuel cells in the mobility sector and electric powertrains can be limited to hydrogen and electricity, respectively, in an MMES. Using other energy carriers such as methanol in fuel cells can be neglected in an MMES study due to a low relevance in the literature (cf. analysis below in Table 2-1). Considering electricity and hydrogen as energy carriers will be of utmost relevance for assessing the decarbonization of the mobility sector [5], [74]. Further, an MMES study needs to consider different types of fuels to account for different well-to-wheel efficiencies and greenhouse gas emissions. Even though the final energy demand of, e.g., inland shipping is relatively low, all modes of transportation, including shipping, aviation, train, heavy and light-duty vehicles, busses, and passenger cars, need to be considered. This is because different fuels can be expected to be used for road, rail, water, and air transportation and additionally to accurately account for the competition for energy carriers that are generated from RES. Based on CO_2 emissions of the generated electricity, hydrogen from electrolysis and its derivatives reduce the overall emissions in the mobility sector.

Today, the crude oil derivatives gasoline and diesel are the dominant fuels in the mobility sector. Compared to hydrogen, the two crude oil derivatives have similar chemical characteristics as well as similar production, transport, and distribution procedures. Thus, a differentiation is not necessary for a macro-economic model focusing on the interactions of the mobility sector with the energy system. Therefore, diesel, gasoline, and electricity-based liquid fuels (e-Fuels), which also show similar combustion characteristics [19], can be considered, following literature, as perfect substitutes without significant loss of accuracy [62]. Subsequently, mixtures of liquid fuels with, e.g., ethanol (E5, E10), an alcohol produced from bio-organic materials, need no explicit representation in a macro-economic MMES optimization. This might be evaluated differently in a mobility sector study.

As a by-product of the refinery process or the oil and gas extraction process, a mixture of Butane and Propane is used as Liquified Petroleum Gas. While it is worldwide used, its future application in Germany and the European Union is not prioritized [10]. Further, crude oil utilization in the mobility sector must decrease, and subsequently, the need for refineries as of today might decline as well. This would result in lower availability of Liquified Petroleum Gas as a byproduct. In addition, its characteristics, and requirements for engines, as well as the extraction and distribution, do not differ significantly from other fuels. Therefore, a consideration in an MMES is considered not necessary.

Furthermore, in 2019 about 81 thousand passenger vehicles used natural gas in an ICE [4]. This is either compressed natural gas (CNG) or liquified natural gas (LNG); both chemically consist primarily of methane. The European Commission supports the buildup of CNG and LNG infrastructures for cars and trucks to meet climate targets [10]. Since the major difference of the gas in both states of aggregation is the volumetric energy density, they are suitable for different applications in the mobility sector as discussed below.

Hydrogen

Hydrogen (H_2) is increasingly discussed as an enabler for the energy transition due to the versatile applications in the electricity, heat, and mobility sector [7], [27], [75]. Its high gravimetric energy density of a lower heating value of 33.33 kWh per kg can be an advantage for applications in the mobility sector. Contrary, its low volumetric energy density of 0.09 kg per m^3 at atmospheric pressure to 42 kg per m^3 at 700bar can pose design challenges in terms of onboard space. Today hydrogen is mainly produced by steam methane reforming from natural gas [85]. Still, water electrolysis using renewable electricity has the potential to generate carbon-neutral hydrogen, often referred to as green hydrogen.

To create propulsion in a vehicle, hydrogen can be burned in ICEs or used in fuel cell powertrains. Hydrogen's high laminar flame speed and the availability of lean unthrottled operation improve the engine's thermal efficiency compared to a gasoline-operation mode. Nevertheless, pre-ignition and backfiring are critical issues [86], which are not further analyzed here but reveal requirements to adjust today's ICEs for the use of hydrogen [87]. Alternatively, fuel cell powertrains are already available at a low scale today, revealing higher efficiencies than combustion [82].

Hydrogens' low volumetric energy density is a limiting factor for the range of a vehicle or vessel. Hydrogen tanks require more space and, therefore, new design concepts. This is especially relevant for freight transport applications. Thus, liquid hydrogen with its higher volumetric energy density of 71kg per m^3 than gaseous compressed hydrogen is discussed for ships and HDV [74]. Anyway, Liquified Hydrogen (LH_2) must be cooled down and kept at a temperature of -252.9 centigrade. Even though LH_2 and Gaseous Hydrogen (GH_2) are considered across all transportation modes in [88], a reduced consideration of hydrogen is reasonable by including only one state of aggregation per transportation mode. The same reduced scope is, for instance, used in [62], [74], and it is regarded as reasonable in the MMES context as analyzed below.

e-Fuels

Chemical synthesis processes can process hydrogen to products that chemically resemble conventional fuels and gases. The main reason to consider these hydrogen derivatives is the increased volumetric energy density compared to hydrogen, the usability of existing transport, distribution and refueling infrastructure, and the compatibility with existing ICE technologies [20], [77], [89].

A variety of e-Fuels can be distinguished based on the production process. The most relevant processes in the an MMES context are the methanation, the Fischer Tropsch (FT) synthesis and the methanol synthesis [26], [62], [77], [90]. Due to the assumed hydrogen production from water electrolysis with electricity, these fuels are considered e-Fuels even though the exotherm reactions used to convert hydrogen to a hydrocarbon do not require additional electricity input. The generated heat can be used for the direct air capture process of CO_2 [89]. Considering the CO_2 supply in detail for synthesis processes is out of scope here, but it is covered in the cost estimation of those processes to guarantee an accurate representation of the costs.

The process of methanation generates methane from hydrogen utilizing the exact reverse reaction as the steam methane reforming process, which converts methane to hydrogen. If the used hydrogen is generated from electricity, its output is considered e-methane. It is produced from hydrogen and carbon dioxide (CO_2) or carbon monoxide (CO) according to the chemical Sabatier reaction shown in Equations (2-1)-(2-2). As an exotherm reaction it does not require additional electricity or heat input. The efficiency can be as high as 80%, and it requires 0.198 kg of CO_2 for 1 kWh of methane [89]. The resulting chemically pure methane (CH_4) resembles natural gas, which consist of 85-98% of methane depending on its origin [91]. Therefore, in the context of an MMES, gaseous e-methane can be considered a perfect substitute for natural gas using the same transport and refueling infrastructure [89].

$$CO + 3H_2 \rightarrow CH_4 + H_2O \quad (2\text{-}1)$$

$$CO_2 + 4H_2 \rightarrow CH_4 + 2H_2O \quad (2\text{-}2)$$

Liquid e-fuels such as e-gasoline, e-diesel, e-methanol, Dimethyl ether, Polyoxymethylene ethers, or n-alkalines are discussed as alternatives for fossil diesel and gasoline [89], [92]. They can be used in ICEs with only minor adjustments, and all but Dimethyl ether and Polyoxymethylene ethers can rely on existing infrastructure for transport, distribution, and refueling [86], [89]. With its additional specifications for infrastructure but its assumed minor impact on the overall energy system compared to other e-fuels, Dimethyl ether and Polyoxymethylene can be neglected in an MMES optimization. A further elaboration of e-methanol and e-diesel generation processes follows.

The methanol synthesis uses hydrogen and carbon dioxide as reactants similar to the methanation process, as shown in Equations (2-3)-(2-4). To yield methanol (CH_3OH), the reverse water gas shift reaction converts carbon dioxide into carbon monoxide, and the hydrogenation further converts it into the alcohol methanol. Methanol is liquid at ambient temperature and standard pressure. Even though methanol fuel cells exist, the more relevant use case discussed in literature is the combustion of methanol. According to Yugo and Soler, current infrastructures can be used with only minor adjustments for methanol transport, distribution, and refueling [20].

$$CO_2 + 3H_2 \rightarrow CH_3OH + H_2O \quad (2\text{-}3)$$

$$CO + 2H_2 \rightarrow CH_3OH \quad (2\text{-}4)$$

The FT synthesis converts gas to a liquid. Hydrogen and a carbon monoxide mixture as input of the reverse water gas shift reaction result in different hydrocarbons with FT diesel assumed here as the most relevant for the mobility sector. Equation (2-5) shows the chemical reactions. Due to its high chemical similarity to diesel, it can use today's infrastructure at no additional costs [5].

$$n\,CO + 2n\,H_2 \rightarrow (CH_2)_n + n\,H_2O \quad (2\text{-}5)$$

To summarize, the most relevant fuels to consider in the mobility sector as part of an MMES optimization are electricity, hydrogen, methane, FT diesel, and methanol. The category of liquid fuels can represent fossil and liquid e-fuels for which no further specification of vehicle technologies is required due to its similar combustion characteristics and infrastructure requirements. Still, the consideration of different generation pathways for hydrogen or liquid fuels is reasonable to account for different efficiencies.

Analysis of powertrain-fuel combinations for different transport modes

Different powertrain-fuel combinations are relevant for a decarbonized mobility sector, which are analyzed subsequently. Table 2-1 summarizes the combinations which are appropriate based on a literature review. The most relevant fuel-powertrain combinations are marked in green. This table is not meant to give a complete overview of all considered technologies in each assessed publication but rather to identify relevant and non-relevant combinations by exemplarily highlighting sources that cover certain combinations.

The following limitations regarding the technologies are derived as reasonable. Due to its high infrastructural investments, the catenary system is only assessed for HDVs and trains. Even though catenary systems for busses exist today, the application and its costs depend significantly on local factors, which require detailed regional analyses and are therefore not considered [74]. This decision reflects the set of assessed technologies in the literature. Due to the low volumetric energy density, compressed gas and GH_2 are not combined with HDV, ships, and aviation since the additional space for a larger tank compared to liquified gas would require major changes regarding the design of the vehicles and vessel [5], [62], [93], [94]. Batteries are not considered for vessels in analogy to [74]. Furthermore, powertrains and fuels for aviation have specific requirements regarding volumetric and gravimetric energy densities. For inland aviation, with its small overall demand, liquid e-jet fuels burned in ICEs are the most relevant technology to consider. Therefore, no other technology is considered for aviation.

Further, it can be derived from the literature that an aggregated modeling of technologies based on powertrain and fuel type as, e.g., in [36], is sufficient. There is no need to further disaggregate the vehicle market into different vehicle sizes since this is not assumed to impact the market shares of the power trains [95].

	ICEV	FCEV	BEV	PHEV	Catenary
Passenger Cars					
Electricity			[5], [20], [62], [73], [74], [88]		
GH_2		[20], [26], [62], [78], [83], [88]		[83], [95], [96]	
LH_2	[95]	[26], [83]		[95]	
CG	[20], [62], [83], [84], [88], [95]			[62], [88]	
LG	[26], [83], [95]				
e-Fuel	[20], [26], [62], [78], [84], [88]	[95] methanol		[62], [73], [88]	
Busses and Coaches					
Electricity			[26], [78]		
GH_2		[26], [88]			
LH_2		[26]			
CG	[74]				
LG					
e-Fuel	[73], [78]			[26]	
Light Duty Vehicles (LDV)					
Electricity			[62], [73], [78], [88]		
GH_2		[26], [62], [74], [78], [88]			
LH_2					
CG	[62], [73], [74]			[62]	
LG					
e-Fuel	[62], [78]			[62], [73]	
Heavy Duty Vehicles (HDV)					
Electricity			[26], [62], [73], [78], [88]		[5], [73]
GH_2		[20]			
LH_2	[19], [62], [74], [97]	[19], [74]			
CG	[19], [20], [26], [73], [93]				
LG	[5], [10], [19], [62], [62], [74]			[62]	
e-Fuel	[19], [20], [62], [78], [84], [93]			[62], [73], [74]	[73], [88]
Trains					
Electricity					[73], [78]
GH_2		[26], [88]			
LH_2		[26], [88]			
CG					
LG					
e-Fuel	[26], [78], [88]				
Ships (Inland Navigation)					
Electricity					
GH_2					
LH_2	[74], [93]				
CG	[20], [26], [88]				
LG	[10], [26], [74], [78], [93], [98]				

e-Fuel	[20], [78], [98]				
Aviation					
Electricity					
GH_2		[88]			
LH_2		[26]			
CG					
LG					
e-Fuel	[20], [78]				

Table 2-1 – Identification of relevant powertrain and fuel combinations based on the literature. White – not considered here; green – high relevance in literature; ICEV – Internal Combustion Engine Vehicle; FCEV – Fuel Cell Electric Vehicle; CG & LG – compressed & liquid gas (methane)

Charging, refueling, and fuel distribution infrastructure

Refueling and charging infrastructure investments are critical cost factors when assessing the mobility sector's decarbonization and need to be included in the analysis [95]. For liquid e-fuels, the existing distribution and refueling infrastructure can be used [5], [20], [33], [77], [89]. Only minor adjustments in refueling infrastructure are required depending on the characteristics of the fuel at dispensers, pumps, or valves, which are considered non-significant compared to the investments in new infrastructure for hydrogen and electric vehicles [5]. Hence, differentiation of technologies for liquid fuel refueling infrastructure is not required here.

Using hydrogen in the mobility sector requires a new refueling, distribution, and transport infrastructure. A reassignment of existing natural gas transport and distribution infrastructure is discussed, and about 91 hydrogen refueling stations exist in Germany in November 2021 already [99], [100]. Even though different dispensers with different pressure levels between 350 - 700 bar exist, the convergency to only one technology in the future is assumed here. Further, differentiation is assumed with high uncertainties for cost developments for both technologies and with only a minor impact on the energy system. The number of required stations in Germany per vehicle is supposed across the literature to be about nine to eleven thousand if the penetration exceeds 50% for FCEV cars [14], [63], [65]. Apart from the initial infrastructure network, there is a high consensus about the required network and costs. Due to the duration of a refueling process below 5 minutes, the refueling behavior and required refueling network of hydrogen, methane, and e-fuels are similar to today's systems [5]. Hence, a fundamental assessment of those refueling modes is not required here.

In contrast, charging infrastructure for BEVs differs significantly from todays' refueling systems in terms of the number of chargers, costs, spatial distribution, and charging behavior. Additionally, there is no consensus about the required number of charging points. Projections range from 2 to 70 BEVs per 3.7 kW-22 kW charging point [14]. Charging at different locations such as home, work, or highways with varying charging speeds increases complexity and interactions between different types of charging stations (cf. Section 2.3). Compared to refueling stations, charging stations are considered a sector-coupling element, directly coupling the electricity and mobility sector. Therefore, the timing of the charging processes impacts the electricity sector immediately. Finally, there are high costs associated with building up a charging infrastructure network [8], [14], [15]. The Federation of German Industry (BDI) [8] estimates investments of 75 billion € in (semi-)public charging infrastructure between 2021 and 2030, which is 9% of the total required climate protection measure investments until 2030. Robinius et al. [14] state that the total infrastructure investments for distribution grid components and a charging infrastructure network consisting of Mode 1, 2, 3, and 4 chargers (cf. Section 2.3) amounts to 40 – 62 billion € for 20 million BEVs. Up to 73% of this investment is allocated to the charging infrastructure. This is valid for passenger BEVs and shows the importance of analyzing and planning charging infrastructure accurately. Therefore, Section 2.3 investigates the requirements for a representation of BEVs in detail.

A major requirement for assessing a carbon-neutral mobility sector is a technology-neutral assessment within an integrated energy system. Therefore, the following subsection analyses the MMES requirements beyond the mobility sector.

2.2 Multi-modal energy supply and transport infrastructure

To assess a decarbonized MMES, different aspects need to be considered and result in specific requirements for an optimization model. Those are:

1. Consideration of supply and transport infrastructure as well as demands in the electricity, heat, and mobility sector to consider competition for scarce RES between different applications.
2. Technology-neutral competition between carbon-neutral energy carriers in the mobility sector, including energy transport infrastructures.
3. Modeling of sector-coupling elements between the mobility and electricity sector, including the provision of flexibility.
4. Limited computational effort.

The first aspect requires a complete picture of an MMES enabling the optimized utilization of RES and imported energy carriers across different applications in all sectors. Figure 2-3 shows the main technologies of a decarbonized MMES, including the energy transport, refueling, and charging infrastructure. The required mobility sector technologies and energy carriers are identified in Section 2.1.

Further, all electricity demands must be considered, such as the electricity demand for information and communication technologies, lightning, cooling, motors, or electrical heating. The heat sector demands consist of process heating at high temperatures for the industry, space heating primarily in buildings, and water heating. Integrating technologies that cover those demands by utilization of electricity, methane, hydrogen, or e-fuels enables modeling of the competition of energy carriers in the MMES. Therefore, the optimization of investments and the optimized dispatch of different technologies per sector must be integrated. That means that the optimizer needs the degree of freedom to choose, for instance, in the case of an applied CO_2 restriction and scarce RES due to land availabilities and weather patterns, whether the electrification of the heat or the mobility sector should be prioritized.

In addition, hydrogen, e-fuels, or e-methane can be imported to satisfy the end energy usages in the heat, mobility, or electricity sector. A comprehensive model must optimize the buildup and operation of electrolyzers and synthesis processes in Germany in competition with import costs for those energy carriers. To enable the competition for energy carriers between the mobility and the heat sector, it can be followed that the technologies for heat generation need to comprise electrical heat pumps, gas, and hydrogen boilers and furnaces, gas power plants for combined heat, as well as power generation fueled by methane or hydrogen.

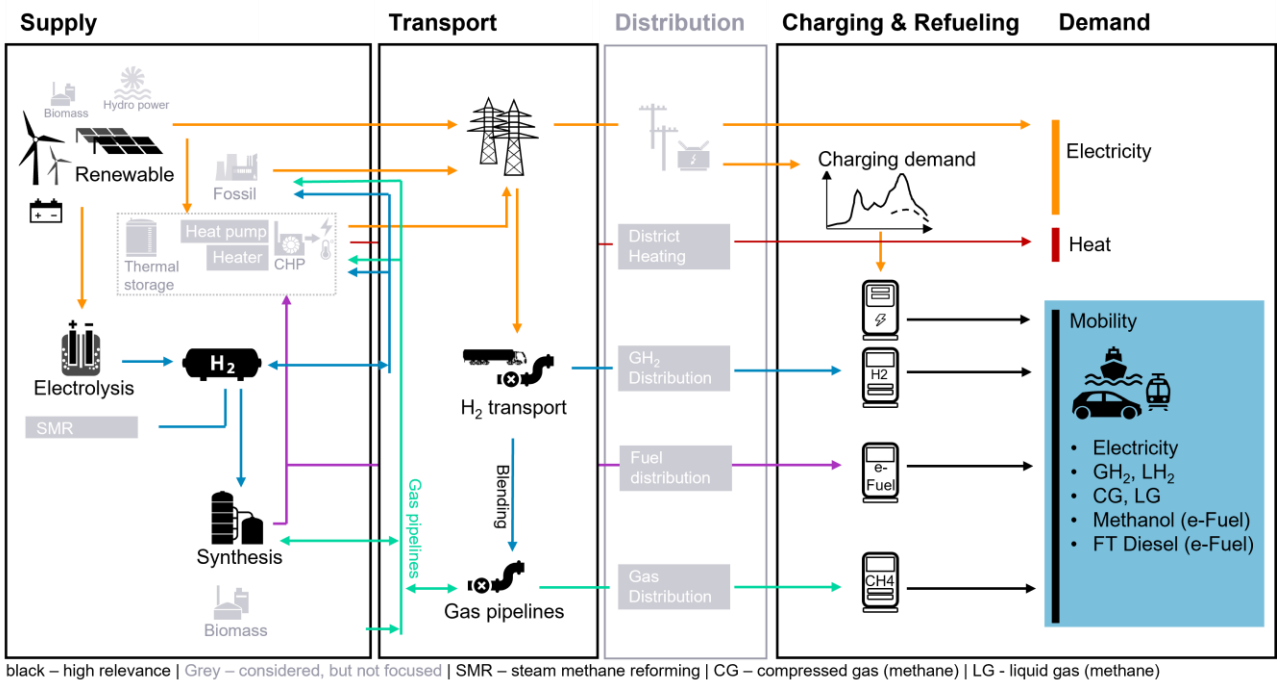

Figure 2-3 – The mobility sector as part of a multi-modal energy system.

Furthermore, aspect two requires incorporating investments in electricity, hydrogen, and methane transport infrastructure into a model since literature reveals that this can be a substantial cost factor in the decarbonization of the mobility sector [95]. The transport of liquid fuels can be assumed to use existing infrastructure to significantly lower costs and is out of scope here. The relevance of the methane infrastructure also in a decarbonized energy system is underlined in the meta-study from VNG [101]. Incorporating energy transport constraints of these commodities enables optimized decisions. For instance, if an electrolyzer should be installed in the hydrogen demand region supplied by electricity from the electricity transmission grid or it can be installed in another area with higher renewable electricity availability and subsequent hydrogen transport via pipeline or trailer to the demand region. For a fair competition between the energy transport options, models must have the same degree of detail regarding the modeled physical principles of the energy transport.

Modeling multi-modal energy transport infrastructure requires a spatial resolution high enough not to underestimate required investments and to cover major bottlenecks in the electricity grid and pipeline networks. Since the computational effort (cf. aspect four) of an MMES can be significant already for just one single region, the spatial resolution must be chosen carefully [25]. The state of the art in so-called multi-region models is to reduce the representation of energy transport constraints to aggregated constraints between regions [102], [103]. A representation of physical constraints such as a pressure drop is commonly not considered for gas flows in MMES models, as the meta-study from Groissböck et al. showed based on 33 open source energy system models [104]. Further, a linearized approach regarding electricity and gas flows, including hydrogen and energy transport asset costs, is not only commonly used [24], [57], [59], [105] but also recommended for MMES studies, which do not focus on strategic asset planning, based on an analysis in [105], [106]. This is due to a minor impact on the overall system and comparatively high costs of the computational effort. Even a highly detailed gas grid model from Hauser et al. considers pressure and flow rate constant within gas pipelines [107]. To aggregate the electricity transport capacities between regions, a power flow calculation is commonly used to derive Net Transfer Capacities (NTCs) for the electricity transport, representing the maximum physical electricity flow between both regions [108]. The actual transport distance can vary from connection to connection between two regions. A simplified way is to model distance to distance matrices from the center of each region, which is considered state of the art in energy system modeling [22], [57], [59], [109].

A higher spatial resolution can counteract the herewith introduced inaccuracy. It is concluded that modeling inter-regional transport capacities is sufficient for long-term investment planning and operational utilization in an MMES. The physical representation of energy flows can be substituted in the optimization by an approach of optimally controlled energy flows between regions to answer the research questions in the present thesis.

Following the temporal and spatial requirements for a model are derived. In a fully decarbonized MMES, wind and solar RES must be utilized across all sectors. Their weather-dependent volatility is crucial to be considered in a model in a temporal as well as in a spatial dimension. Modeling one-hour time steps can achieve a temporally sufficient resolution for the operation of RES and other generators as it is state of the art in energy system modeling and sufficient to depict short-term variations [110], [111]. This temporal resolution is also sufficient for modeling flexible loads such as a fleet of BEVs [112]. Further, locational differences of solar radiation and wind need to be taken into account by disaggregating the model into several sub-regions [25]. Sub-regions are also important for modeling energy transport routes as described above. It can be differentiated between single point, multi-region, and grid node resolutions. The single point resolution for an entire country like Germany cannot guarantee a sufficient representation of weather patterns leading to a significant inaccuracy in residual energy demands [29]. Furthermore, energy transport restrictions cannot be considered, but only cost terms based on country-wide energy generation and demand patterns can be estimated. This can result in solid deviations of installed capacities and generated energies per technology as analyzed by Robinius et al. [29]. A representation of each grid node as a single region with up to 500 regions is used in studies focusing on the energy transport of a single commodity. Nevertheless, this detailed representation is non-trivial for studies considering several energy transportation systems. Furthermore, a lack of accurate data in a high spatial resolution can lead to errors in energy system studies with grid load resolution such as an overestimated energy curtailment and renewable energy surpluses [29], [110]. A high spatial resolution increases computational efforts, which can be exponentially increasing with the number of regions, which is a limiting factor in large MMES models [25], [60], [113]. In contrast, a multi-region approach can overcome the challenges and drawbacks of single point and grid node models while still capturing renewable energy feed-in and energy transport restrictions sufficiently. A study from Frysztacki et al. [110] showed on a European level that 181 regions could represent the spatial differences of solar and wind patterns in a model, and 90 regions could be sufficient for covering major bottlenecks in the considered electricity grid. Applying the higher number to the size of Germany holding about 6.7% of the European land area (without Russia, Turkey, Ukraine, Moldavia, Belarus, and Greenland), since they were not modeled by Frysztacki et al.) reveals that a resolution of at least 13 regions in Germany should be modeled. This number is derived presuming that the number of regions can be linearly scaled to Germany and by assuming that the same variations in weather patterns exist across the entire continent. Only the electricity transportation system was considered in this publication. Due to the simplified estimation of the required 13 regions and since only the electricity transport system is considered by Frysztacki et al. a higher resolution is reasonable in the MMES here. With the NUTS2 representation of administrative areas, 38 inner German regions exist, with relatively high availability of spatially resolved data. Energy system or weather-based clustering approaches for regions within a country are not considered here [114], [115]. This decision is made since the energy system-based clustering does not incorporate gaseous infrastructures, and the weather-based clustering does not include energy system parameters, which are assumed to be required to gain a substantial benefit over the chosen administrative areas. Further development of these approaches is out of scope here.

MMES optimizations are commonly formulated as linear programs [25]. Following state of the art, the MMES here is also based on a linear programming approach without integer variables. The model complexity and thus the computational effort of linear programs depends on the number of decision variables and constraints. Since increasing temporal and spatial resolution increases the number of variables and constraints significantly, methods for complexity reduction are commonly used [25], [116]. The approach of time-series aggregation is used to reduce the number of time steps within the year. Here, a selection of representative weeks is primarily conducted under consideration of the maximum and minimum residual electric load, consideration of weeks within different months of the year as well the criteria that the potential average full load hours of PV and wind turbines over the time step selection should meet the average full load hours of the entire year. Figure 2-4 benchmarks a time series reduction to four, six, and eight representative weeks against an optimization with

twelve representative weeks. A carbon-neutral German energy system is therefore optimized considering different numbers of representative weeks. It shows the deviation of key parameters of the model such as CAPEX, OPEX, and electricity prices. Thin weeks represent here an additional time step reduction to three hours instead of an hourly interval, which is here not influencing the observed model outputs. It shows that selecting six instead of four weeks can reduce the deviation compared to the twelve thin weeks for all key variables to below 3%. An extended investigation showed that a similar behavior, with a deviation less than 8% in the six thin weeks scenario. This is analyzed for all generation, demand, transport, and storage technologies in terms of the optimized capacities and operation. Therefore, all optimizations in the present thesis use the representative six thin weeks.

Figure 2-4 – Impact of the number of modeled representative weeks and the time interval compared to a twelve-week optimization in a carbon-neutral German energy system. 'Thin weeks' refer to a three-hour time step, and 'weeks' refer to an hourly time step.

As one great advantage, all considered liquid fuels, but liquid hydrogen and liquid gas can be stored easily at ambient temperature and normal pressure (Yugo & Soler). This provides flexibility to the MMES. Therefore, the storage capabilities of other energy carriers must be considered in a model as well. Further, due to the hourly and seasonally varying demand for electricity and heat as well as the availability of renewable energies, storage technologies need to be considered. In the context of the analysis here, the most relevant technologies are hydrogen storages and Li-Ion Batteries – stationary and in electric vehicles. The mobile batteries require a unique representation to make up for the fact that the batteries are not always connected to the grid, and the electricity is consumed for driving purposes. Further, this flexibility from charging processes is restricted in time due to BEVs' parking duration, and it therefore needs a different representation compared to a stationary battery. This is analyzed in Section 2.3.

2.3 Requirements to model electric vehicles and charging infrastructure

BEVs require a more detailed representation as indicated in Sections 2.1-2.2 due to the fundamentally new charging behavior compared to todays' refueling behavior, the new requirements for charging infrastructure, the insufficient representation in literature, and due to the potential of BEVs to provide flexibility to the electricity sector. The flexibility potential of BEVs differs in its modeling requirements fundamentally from stationary storages. This is mainly since the primary use case of the BEV's battery is driving and due to the restricted temporal availability of shifting charging processes in time. The latter depends on the power rating of charging stations, the remaining energy in the BEV's battery at arrival, and the driver's preferences. The flexible

share of charging processes varies significantly in time [117], and it is often not assessed fundamentally but only estimated as a constant share of the total battery capacity of a vehicle's fleet, such as in [27], [36]. It could be shown in a fundamental analysis in [118] that the size of the installed batteries in electric vehicles does not correlate with the available flexibility of charging processes. This is primarily because the essential drivers of the available flexibility of a fleet of BEVs are short parking durations, short recharging times due to relatively high SOCs in general, the type of charging infrastructure that can be used during a day, and the energy consumption of BEVs. Therefore, it is of high relevance here to fundamentally derive the temporally resolved flexibility. Additional flexibility can be leveraged from the vehicle's batteries if vehicles are enabled to feed electricity back into the electricity grid. This is commonly known as vehicle-to-grid concept. However, the challenge of incentivizing vehicle owners to participate must be increasingly considered. Since the flexibility is already large even without vehicle-to-grid, and here incentives are only covered from a systemic point of view, the vehicle-to-grid mode is not covered in the present thesis.

Additionally, the charging infrastructure network design must be assessed fundamentally to accurately derive the flexibility [118] and determine the charging infrastructure's costs. This is not covered in the literature yet. Based on the 'Directive 2014/94/EU on the deployment of alternative fuels infrastructure (AFID)', charging stations are categorized by their power rating into normal charging ($\leq$22 kW) and fast charging (>22 kW) [10]. Additionally, in DIN EN IEC 61851-1, four different charging modes are differentiated [119]:

- **Mode 1:** alternating current charging at a domestic or industrial 1-phase or 3-phase socket without communication between vehicle and infrastructure
- **Mode 2:** alternating current charging at a domestic or industrial 1-phase or 3-phase socket with 'In Cable Control and Protection Device' in the vehicle for control and protection
- **Mode 3:** alternating current (AC) 1-phase or 3-phase charging via installed charging device (e.g., wallbox) with 'Type 2' plug. This mode is available for a power rating of 3.7 kW-44 kW.
- **Mode 4:** direct current (DC) charging at installed charging device with 'Combo 2' plug. This mode is commonly used with power ratings greater 50 kW, even though smaller power ratings are available.

Finally, the following aspects must be covered to enhance the representation of electric vehicles and their charging infrastructure as a sector-coupling element in energy system analyses:

- **Heterogenous driving and charging behavior:** end consumers are highly heterogeneous in their driving and charging behavior. This heterogeneity must be covered, which requires representing individual vehicles in a model.
- **Dynamic electricity demand:** the electricity demand increases with each driven trip of a vehicle. But this demand can only be satisfied at locations where a charging station is installed. Therefore, this demand must be considered depending on the BEVs' location and the charging availabilities along its daily or even weekly route. The availability of chargers at different locations also impacts the timing of the electricity demand. This raises the requirement for a spatial representation and a representation of charging stations at different locations in a model.
- **High spatial resolution:** the spatial resolution must consider different locations such as workplaces, homes, or public places. The required spatial resolution deviates, depending on the assessed region.
- **Charging stations:** the availability of charging stations across different locations must be covered to model the competition for chargers as this impacts the timing of the electricity demand. Different charger types, including alternating current technology with 3.7 kW-22 kW (Mode 3) and direct current technology with power rating greater than 50 kW (Mode 4), have different roles in an overall charging infrastructure network. The demand for those types of chargers must be considered systematically. The demand cannot be assessed independently for each mode or location since the deployment of one charger impacts the demand for chargers at other locations. For the assessment of the electrical charging load, its flexibility, and the total required number of charging stations, a differentiation between those chargers is here sufficient in terms of charging power.
- **Temporally resolved assessment of shiftable charging processes:** the flexibility of a fleet varies over time and depends on the charging infrastructure network design, as well as the BEVs charging and driving behavior.

- **Country-level:** derived temporally resolved electricity demands, including their flexibility and the need for charging infrastructure, must be able to be interpreted in the linear MMES optimization model on country level. Modeling on individual BEV and charger level would require large computational efforts if modeled for an entire country. Therefore, the model should focus on a regional level such as municipalities. This requires a model setup, which can be applied to different types of regions. Modeling than, for instance, rural and urban areas allow to scale up the results to country level or to NUTS2 level, which is used in the MMES optimization.

Those aspects cannot be covered in an MMES optimization on country level directly. Therefore, it is required to introduce another model capable of assessing the spatial and temporal electrical charging demand, including its flexibility and capable of deriving suitable charging infrastructure network designs. While the model must represent individual vehicles and assets, it must still be able to be generalized to a country-level representation. Finally, the derived outputs must be integrated into the energy system optimization tool.

3 Applied multi-modal energy system model

The present thesis uses a linear optimization approach to assess an MMES. An existing modeling framework is parametrized to represent the commodities and technologies of a MMES as defined in Section 2. The applied model framework can be considered as state of the art in energy system optimization models and satisfies the modeling requirements in Section 2.2. Those are the temporal and spatial resolution, the aggregated consideration of technologies within each modeled region, modeling of different commodities and sector-coupling technologies, and the possibility to optimize supply, transport, and demand infrastructure simultaneously with different technologies competing about RES.

Subsequently, the model framework is described in Section 3.1, and a mathematical formulation of the model follows in section 3.2. Implemented extensions to the model to meet the specific requirements of eMobility charging are described in Section 5.2.1. The derived techno-economic parametrization of the model follows in Section 5.3.

3.1 Model framework

The multi-modal model of the German energy system is here set up in the 'Energy System Planner' (ESDP). This modeling framework is depicted in Figure 3-1 and can be applied to build and optimize Linear Programs (LP) and Mixed Integer Linear Programs representing, for instance, large, complex MMESs. The model is based on developments from Schaber and Steinke [120], was first presented in 2015 by Raths et al. [121], and extended and applied in several further publications [34], [35], [117], [122]–[125].

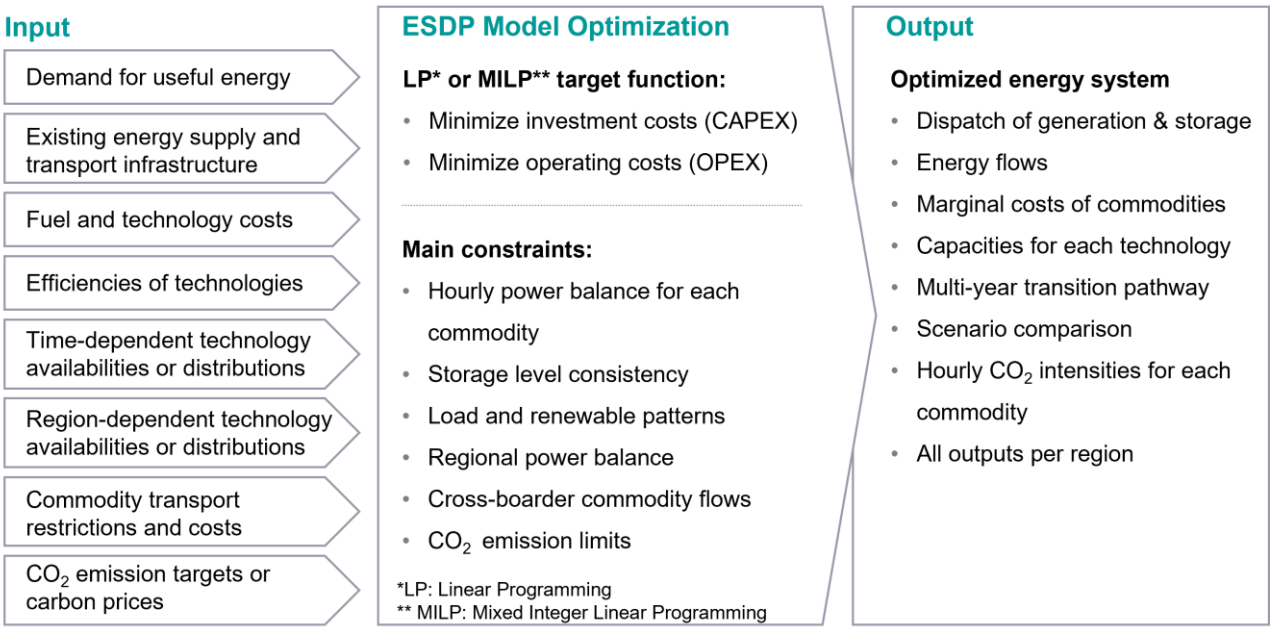

Figure 3-1 – Input-Output model framework of the ESDP.

ESDP is implemented as a cost-optimizing macroeconomic equilibrium model, optimizing the dispatch of modeled technologies, for instance, on an hourly basis. Simultaneously, it optimizes the capacity investments for a specified target year or multiple years. The model can be parametrized for various possible technologies and commodities across different sectors such as the heat, electricity, or mobility sector. Further, single point and multiple-region models, including energy flows between regions, can be differentiated.

Parameters such as lifetime, investment costs, operational costs, capacity restrictions, and energy restrictions can be defined for each technology per year and region. Further, general parameters for an optimization scenario apply, for instance, the Weighted Average Capital Costs (WACC) and the yearly CO_2 emission limits. The optimization output includes for all technologies their capacities and hourly dispatch, energy flows across regions, system costs, and marginal commodity prices.

The modeling approach is based on so-called conversion processes as illustrated in Figure 3-3. Each conversion process *cp* takes one or multiple input commodities and converts them in one or multiple conversion subprocesses *cs* into output commodities using a subprocess-specific, yearly efficiency $\eta_{cs,y}$ (cf. Eq. 3.8). An entire country energy system model consists of multiple interconnected conversion processes representing different technologies and optional transport processes defining the inter-regional energy transport technologies such as the electricity transmission grid or gas pipelines. If multiple regions are considered, each conversion process and commodity is defined for each region, and the optimization balances supply, demand, imports, and exports for each commodity on a regional level. Energy transport processes allow and restrict the

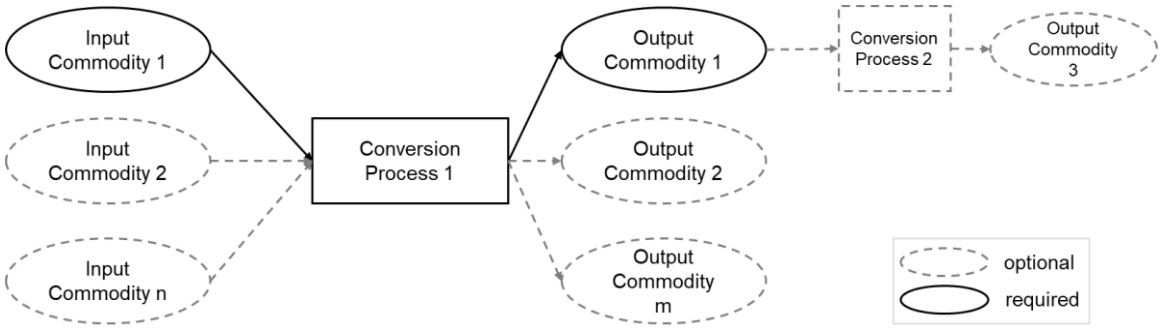

Figure 3-3 – Representation of a conversion process in ESDP. Several input and output commodities can be applied.

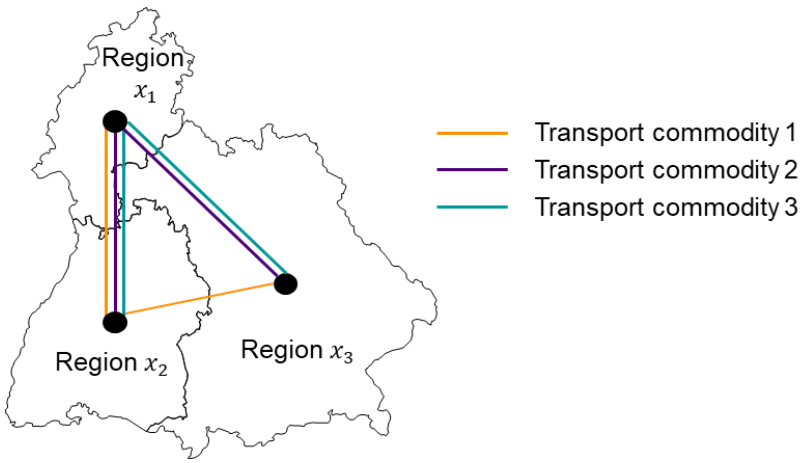

Figure 3-2 – Illustration of center-to-center commodity transport between three exemplary regions in ESDP.

transfer of commodities from one region to another, as depicted in Figure 3-2.

This modeling approach can be considered state of the art for large-scale energy system optimization compared to other energy system models as reviewed in [24], [104], [126]. Since it can be applied to meet the requirements formulated in Section 2, it is considered reasonable to address the research questions RQ 1-4 derived in Section 1.3.

The ESDP framework uses GAMS 30.3.0 Minor Release from March 6, 2020, and the CPLEX optimization package 12.12.0. The parametrization of different technologies and scenarios is managed using Excel and a PostgreSQL database controlled via a MATLAB interface.

3.2 Mathematical description of the model

Subsequently, the main applied equations of the linear problem are described. This contains the objective function, the power balance equation for conversion processes and commodities, power restrictions for conversion processes, global emission constraints, and the energy transport equations. Not explicitly stated here are, e.g., time consistency of capacities over multiple years, and special restrictions setting variables according to time-dependent input parameters.

In order to minimize the social-welfare the objective of the model is to minimize the capital and operational expenditures $C^{\text{capex,conv}}, C^{\text{opex,conv}}$ and $C^{\text{capex,trsp}}, C^{\text{opex,trsp}}$ of all energy conversion processes $cp \in CP$, which consist of one or more conversion subprocesses $cs \in CS$, and all energy transport processes of all commodities $co \in CO^{\text{trsp}}$ over all considered years $y \in Y$ and regions $x \in X$ (cf. Eq 3.1-3.5). *CP*, *CS*, *CO*, *Y*, and *X* are the corresponding sets.

$$\mathbf{min}(\boldsymbol{C}^{\mathbf{capex,conv}} + \boldsymbol{C}^{\mathbf{capex,trsp}} + \boldsymbol{C}^{\mathbf{opex,conv}} + \boldsymbol{C}^{\mathbf{opex,trsp}}) \tag{3-1}$$

with

$$C^{\text{capex,conv}} = \sum_{cp} \sum_{y} \left(F_y^{\text{d}} \cdot \sum_{cs \in cp} \left(N_{cs,y} \cdot \sum_{x} \left(k_{cs,x,y}^{\text{new}} \cdot C_{cs,y}^{\text{inv}} + k_{cs,x,y}^{\text{sto,new}} \cdot C_{cs,y}^{\text{sto,inv}} \right) \right) \right) \tag{3-2}$$

$$C^{\text{capex,trsp}} = \sum_{co} \sum_{y} \left(F_y^{\text{d}} \cdot N_{co,y} \cdot g_{co,y}^{\text{new,tot}} \cdot C_{co,y}^{\text{trsp,inv}} \right) \tag{3-3}$$

$$C^{\text{opex,conv}} = \sum_{cp} \sum_{y} \left(F_y^{\text{d}} \cdot \sum_{cs \in cp} \left(e_{cs,y}^{\text{out,tot}} \cdot C_{cs,y}^{\text{om,eout}} + k_{cs,y}^{\text{tot}} \cdot C_{cs,y}^{\text{om,cap}} + k_{cs,y}^{\text{sto,tot}} \cdot C_{cs,y}^{\text{om,sto}} \right) \right) \tag{3-4}$$

$$C^{\text{opex,trsp}} = \sum_{co} \sum_{y} \left(F_y^{\text{d}} \cdot g_{co,y}^{\text{tot}} \cdot C_{co,y}^{\text{om,trsp}} \right) \tag{3-5}$$

The annuity factors of a conversion subprocess and transport processes are $N_{cs,y}$ and $N_{co,y}$ respectively, which are calculated based on the weighted average cost of capital and the lifetime. The applied macro-economic discount factor is F_y^{d}. The newly build capacities of a conversion subprocess and storage subprocess are $k_{cs,x,y}^{\text{new}}$ and $k_{cs,x,y}^{\text{sto,new}}$, the total capacities of subprocesses are $k_{cs,y}^{\text{tot}}$ and $k_{cs,y}^{\text{sto,tot}}$, and $g_{co,y}$ is the transport process capacity. $C_{cs,y}^{\text{inv}}$ and $C_{cs,y}^{\text{sto,inv}}$ are the specific investment cost for conversion and storage subprocesses, $C_{co,y}^{\text{trsp,inv}}$ and $C_{co,y}^{\text{om,trsp}}$ are the specific investment and operational cost parameters for transport processes, $C_{cs,y}^{\text{om,eout}}$ and $C_{cs,y}^{\text{om,cap}}$ are the variable and fixed operational cost parameters of conversion subprocesses, $C_{cs,y}^{\text{om,sto}}$ is the operational cost parameter for storages.

This is subject to the balance equation matching supply and demand within each time step $t \in T$ and each region $x \in X$ for each conversion process $cp \in CP$ (Equation (3-6)) and for each commodity (Equation (3-7)). The efficiency $\eta_{cs,y}$ connects the input and output of a conversion process. The energy imported at each time step into region x_0 is $p_{co,t,x_2,x_0,y}^{\text{out,trp}}$ and the exported energy is $p_{co,t,x_0,x_1,y}^{\text{in,trp}}$ (cf. Equation (3-12)).

$$\sum_{cs \in cp} p_{cs,y,t,x}^{\text{in}} = \sum_{cs \in cp} \left(\frac{p_{cs,y,t,x}^{\text{out}}}{\eta_{cs,y}} \right), \forall cp, y, t, x \tag{3-6}$$

$$\sum_{cs} p_{cs,co,y,t,x_0}^{\text{in}} + \sum_{x_1 \in X} p_{co,t,x_0,x_1,y}^{\text{in,trp}} = \sum_{cs} p_{cs,co,y,t,x_0}^{\text{out}} + \sum_{x_2 \in X} p_{co,t,x_2,x_0,y}^{\text{out,trp}}, \forall co, y, t, x_0 \in X \tag{3-7}$$

As optional constraint, global CO_2 emissions $o_y^{\mathrm{tot,Y}}$ are limited according to Equations (3-8)-(3-9) based on the product of the total annual energy output $e_{cs,y}^{\mathrm{out,tot}}$ from a conversion process and the emission factor of a commodity $F_{cs,y}^{\mathrm{CO_2}}$, which is defined for the commodity generating conversion process cs.

$$o_y^{\mathrm{tot,Y}} = \sum_{cs} \left(e_{cs,y}^{\mathrm{out,tot}} \cdot F_{cs,y}^{\mathrm{CO_2}} \right) \tag{3-8}$$

$$o_y^{\mathrm{tot,Y}} \leq O_y^{\mathrm{CO_2,Y}} \tag{3-9}$$

In a multi-region model the total energy output of a conversion process is defined as the sum of its power output $p_{cs,y,x,t}^{\mathrm{out}}$ over all regions and time steps (cf. Equation (3-10)).

$$e_{cs,y}^{\mathrm{out,tot}} = \sum_t \sum_x \left(p_{cs,y,x,t}^{\mathrm{out}} \cdot \Delta t \cdot w \right), \forall y \in Y, cs \in CS \tag{3-10}$$

To reduce the computational effort, different time step lengths Δt, for instance, 1 hour or 3 hours, can be applied. A weighting factor

$$w = \frac{N^{\Delta \mathrm{t}}}{8760} \tag{3-11}$$

for the power output is therefore introduced with $N^{\Delta \mathrm{t}}$ as the total number of considered time steps within a year.

Further, in a multi-region model as considered here, commodity flows between regions and their corresponding transport capacities can be described as follows. The set of equations (3-12)-(3-16) is valid for all commodities *co*, which are modeled as transport commodities and between two regions x_0 and x_1, for which a link between the regions is considered with a distance $L_{co,x_0,x_1}^{\mathrm{link}}$, which is greater than zero. The energy flow between regions x_0,$x_1 \in X$ is then

$$p_{co,t,x_0,x_1,y}^{\mathrm{out,trp}} = p_{co,t,x_0,x_1,y}^{\mathrm{in,trp}} \cdot \eta_{co,y}^{\mathrm{trp}} \cdot L_{co,x_0,x_1}^{\mathrm{link}}, \forall t \in T, y \in Y \tag{3-12}$$

with the distance-dependent transport efficiency $\eta_{co,y}^{\mathrm{trp}}$ and its incoming power being limited by the installed transport capacity $g_{co,x_0,x1,y}$ according to Equation (3-13).

$$p_{co,t,x,x_1,y}^{\mathrm{in,trp}} \leq g_{co,x_0,x_1,y}, \forall t \in T, y \in Y \tag{3-13}$$

This installed transport capacity is the sum of the capacity existing before the optimization period $g_{co,x_0,x_1,y}^{\mathrm{res}}$ and the additional transport capacity $g_{co,x_0,x_1,y_1}^{\mathrm{new}}$ installed by the optimizer in each considered year y_1.

$$g_{co,x_0,x_1,y} = g_{co,x_0,x_1,y}^{\mathrm{res}} + \sum_{y_1} g_{co,x_0,x_1,y_1}^{\mathrm{new}} \tag{3-14}$$

The total and new transport capacity of a commodity, as shown in equations (3-15)-(3-16), is used for the cost calculation and defined by adding up all capacities in all modeled regions.

$$g_{co,y}^{\mathrm{tot}} = \frac{1}{2} \sum_{x_0} \sum_{x_1} \left(g_{co,x_0,x_1,y} \cdot L_{co,x_0,x_1}^{\mathrm{link}} \right), \forall y \in Y \tag{3-15}$$

$$g_{co,y}^{\mathrm{new,tot}} = \frac{1}{2} \sum_{x_0} \sum_{x_1} \left(g_{co,x_0,x_1,y}^{\mathrm{new}} \cdot L_{co,x_0,x_1}^{\mathrm{link}} \right), \forall y \in Y \tag{3-16}$$

Finally, the energy storage balance equation defines the stored energy $E_{cs,x,y,t}^{\mathrm{st}}$ within a conversion step and its time consistency including a self-discharge rate $\eta_{cs,y}^{\mathrm{selfdischar}}$ as well as storage efficiency for incoming energy $\eta_{cs,y}^{\mathrm{st}}$ and for outflowing energy $\eta_{cs,y}$. Equation (3-17) is only valid for conversion steps with storage capability as indicated during the parametrization of the model. If only selected time slices within a year, e.g., six representative weeks, are modeled, it is assumed that the energy storage level changes in unmodeled time steps

exactly according to the change in the last modeled time slice. A time slice is here represented, e.g., by a representative week.

$$e^{\mathrm{st}}_{cs,x,y,t} = e^{\mathrm{st}}_{cs,x,y,t-1} \cdot (1 - \eta^{\mathrm{selfdischar}}_{cs,y}) \cdot \Delta t + \eta^{\mathrm{st}}_{cs,y} \cdot p^{\mathrm{in}}_{cs,x,y,t} \cdot \Delta t - p^{\mathrm{out}}_{cs,x,y,t} \cdot \frac{\Delta t}{\eta_{cs,y}} \quad (3\text{-}17)$$

4 Developed e-Mobility charging infrastructure model

As derived in Section 2, it is required to explicitly model eMobility charging behavior and infrastructure to answer the research questions. Therefore, a new approach is developed in the present thesis focusing on charging demand and charging infrastructure. The implemented framework is described in Section 4.2, and the model behavior, including a validation based on empirical data, is shown in Section 4.3.

4.1 Relevant simulation techniques

Simulation models can be used to assess future charging infrastructure requirements and the integration of BEVs into the energy system using electrical load profiles and the available flexibility of BEVs. Several simulation and modeling techniques exist in the literature, which were already applied to the case of BEV charging. The suitability of three different methods is subsequently described based on the requirements derived in Section 2.

Equation-based models apply a set of differential equations expressing relations between measurable characteristics of interest [127]. This allows modeling a temporally dynamic charging demand. As top-down models, they are not found suitable due to their high complexity when modeling spatially resolved systems and their shortcomings in modeling heterogeneity.

In contrast, using the stochastic process of Markov-chains allows to model BEV charging behavior as a bottom-up approach, including a spatial resolution. Individually parametrized vehicles are modeled by their likelihood of being in a current state, such as ‘driving’ or ‘parking’, and their probability of transition into another state [128]–[130]. The probabilities are usually derived from travel statistics. Nevertheless, these models are limited when it comes to modeling charging infrastructure networks with individual chargers interacting with BEVs [131].

The model class of Agent-based Simulations is the most suitable for the derived requirements, beneficial for highly distributed and heterogeneous systems with discrete decision processes [131]. The basic idea of an agent-based model is to represent individuals, entities and their socio-economic interactions with their environment or technical subsystems [132]. So-called agents, consisting of a set of attributes and rules, interact within each time step with other agents or with the environment. These interactions following the rules of each agent emerge then into a complex system behavior. A general set-up of an agent-based model is depicted in Figure 4-1. Agents, which can, e.g., represent a vehicle driver or a charging station, and their environment, consisting of time and space, are parametrized based on empirical data and from literature derived theory about their behavior and interactions.

Furthermore, the suitability regarding the requirements formulated in Section 2 is also underlined by the application of this model class in literature [133], [134]. Additionally, the published literature reveals the gap of a detailed spatial resolution and an accurate representation of charging station networks. This gap is filled with the framework implemented in the present thesis. A first version is presented in [117], and an extended version is published in [118]. Anyway, since agent-based models gain complexity quickly with an increasing number of agents and different behavioral rules, the applied rules and attributes must be designed to be as simple as possible. Therefore, the parametrization here follows, for instance, the currently predominant ‘charge at arrival’ strategy for all agents and the system behavior is validated based on empirical data. The implemented model and its behavior are described in the following.

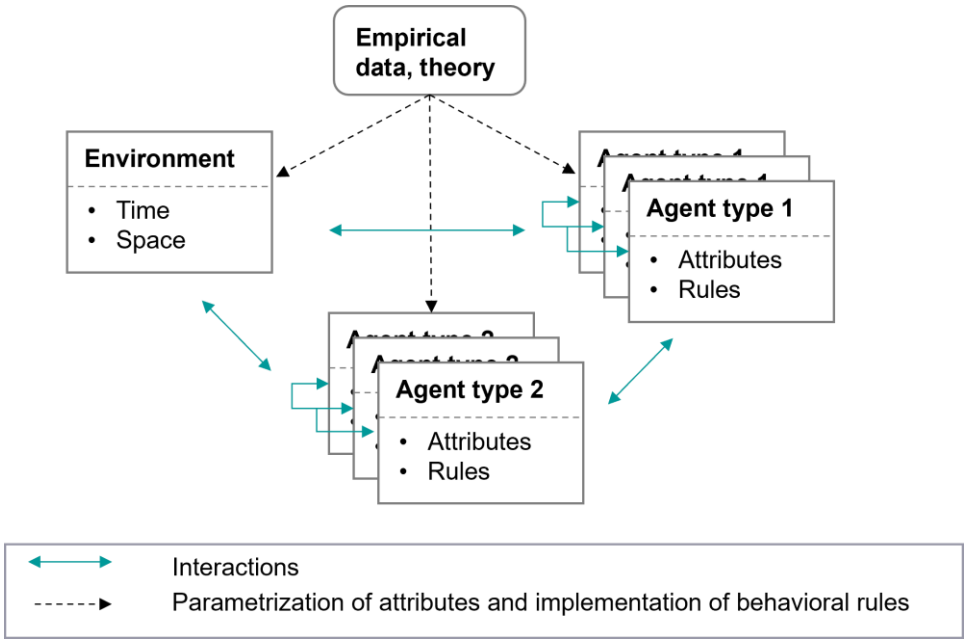

Figure 4-1 – General principle of Agent-based Simulations based on [132].

4.2 Agent-based eMobility model framework

The here developed Agent-based eMobility Model (ABM eMob) is implemented in NetLogo 6.1.0, a programmable modeling environment [135]. Figure 4-2 shows the implemented user interface with a section for input parameters on the left-hand side, on the right-hand side a representation of the considered region, including geographical information system data such as streets, administrative areas, and allocated charging stations, as well as several figures representing the output behavior of the system. This figure only illustrates the implemented graphical user interface in NetLogo; all relevant inputs are described in Figure 4-3. The ABM eMob simulates BEV agents' driving and charging behavior within a region across different locations such as home, work, or public over a defined period. The individual behavior of each BEV over time emerges into a measurable system behavior, which is here primarily the electrical charging load over time, the available flexibility of charging processes measured in shiftable energy per hour, and the Service Quality of the deployed Charging Infrastructure network (SQCI) within the simulated region. The SQCI indicates if the number of charging stations applied in the simulation is sufficient to supply the charging demand of the simulated BEVs.

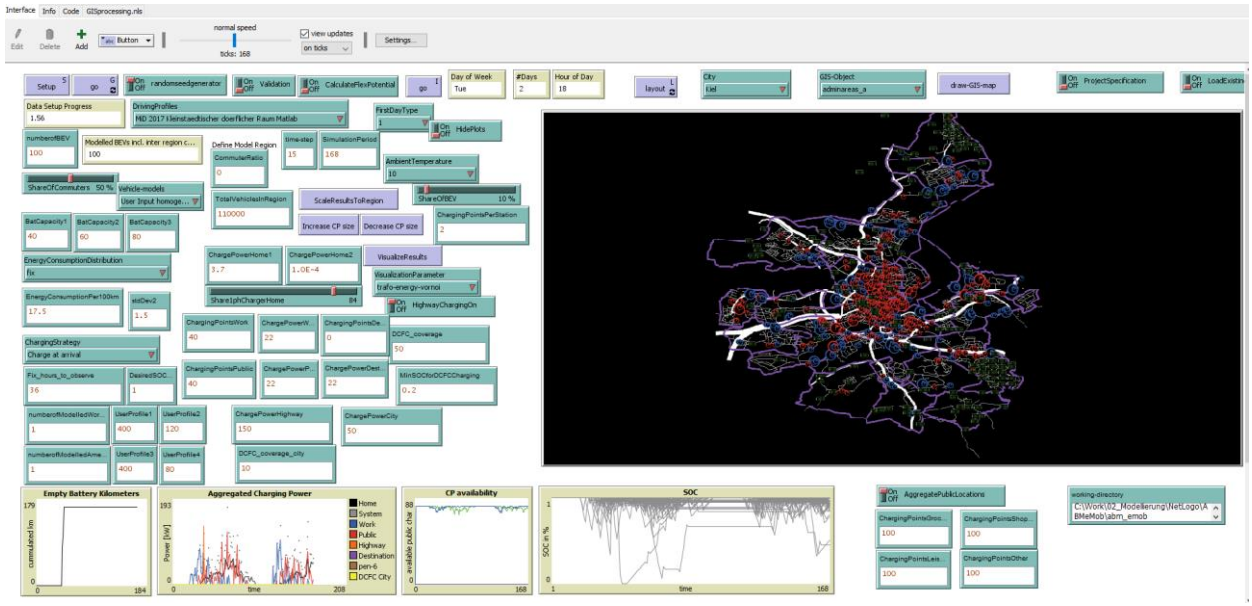

Figure 4-2 – Graphical user interface of implemented Agent-based eMobility Model (ABM eMob) in NetLogo.

Figure 4-3 shows the input parameters of the model, which can be divided into general, regional, technology, and behavioral parameters. They allow an individual parametrization of the simulation for different scenarios and regions. While the model is designed for simulating a 'regional charging system', inter-regional trips are considered to represent the charging demand of commuters traveling into or out of a region. The model consists of three types of agents: BEVs, charging stations, and Locations.

BEV agents represent the vehicle technology in terms of battery size, energy consumption, onboard charger, and its driver's charging and driving behavior (cf. Section 4.2.1).

The charging demand of BEVs is dynamic in time and space. This means that the demand can be fulfilled at different locations at different times because vehicles drive from one location to another. Therefore, the location of a placed charging station can impact the location of the electricity demand as well as the timing of the charging processes within a region. Locational agents represent this spatial resolution in the model. They can be differentiated by multiple types of locations and represent in the following the locations home, work, and public. Several instances of each type of location can be modeled. The number of locational instances of the same type, in the following called 'location duplicates', combined with the number of modeled BEVs defines the spatial resolution of the model (cf. Section 4.2.3). Further, this ratio also reflects the modeled BEV penetration level within a region. The more BEVs per location are simulated, the higher the BEVs penetration level. Consequently, lower BEV penetration levels require more charging stations per BEV to reach a sufficient spatial coverage level in the simulation. This reflects, for instance, the requirements of large initial charging infrastructure networks during the market introduction phase of BEVs due to the spatial distribution of charging demands.

Charging station agents represent the charging station technology. Each charging station is assigned to a particular type of location and randomly located at a specific locational duplicate. Therefore, some public locations may be equipped with several charging stations, while other public locations are not equipped with any charging station. This feature represents that a BEV cannot charge at every destination. Nevertheless, when overbuilding the charging infrastructure, this discrepancy diminishes. The number of plugs (charging points) and the maximum charging power per plug can be defined for each charging station. If a BEV connects to a charging point of a charging station, this agent's charging point is not available for other BEVs until the BEV disconnects. This represents a charging point scarcity and competition within the region. Home chargers are allocated stochastically according to a specified home charger access rate within the modeled region. They are assigned to the houses of individual BEVs, represented by the location home. Consisting of only one charging point they can only be accessed by the single corresponding BEV, which is assigned to the same house. Each modeled BEV

is assigned randomly to a house before the simulation commences. Further, DCFC charging is not represented with these charging station agents, but its modeling follows a stochastic approach, as explained in Section 4.2.1.

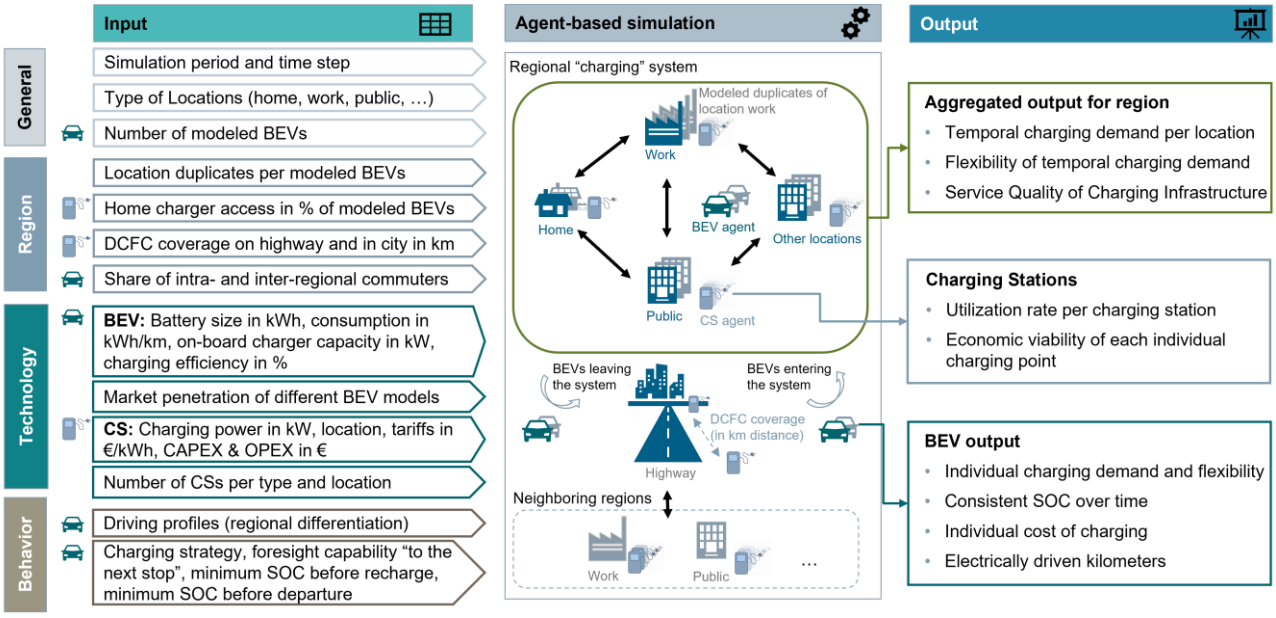

Note: BEV – Battery Electric Vehicle; CS – Charging Station; DCFC – Direct Current Fast Charging; SOC - State of Charge.

Figure 4-3 – Input-Output model framework of the ABM eMob. Input parameters with a BEV agent or charging station agent symbol represent the parametrization of the corresponding main agents' attributes.

4.2.1 Mobility and charging demand modeling

The driving behavior of BEVs is characterized by the driving profiles, which are randomly assigned for the entire simulation period to each BEV from the pool of driving profiles. These driving profiles can either be taken from a set of trips from a mobility study or are derived as synthetic driving profiles based on travel statistics. Since here, a data set of authentic trips from the Mobility in Germany 2017 (MiD17) [136] study is available, the synthetic profile generation is not further described. The dataset contains daily mobility routes of 316 thousand people and a classification of the region to which each route is allocated. For a single BEV, a daily route consists of several trips driven by the same vehicle during a day, including data about the origin, destination, speed, and distance. The availability of driving profiles based on routes, leads to consecutive changes in the state of charge of a BEV's battery. In total 525 thousand trips with cars are recorded in the dataset. Empty and unreasonable data, such as trips above 1000km and a speed greater 180km/h are not considered thus reducing the pool of driving profiles to 457 thousand trips.

The regional classification of a route is based on the 'Regional Statistical Spatial Typology for Mobility and Transport Research' (RegioStaR) of the Germany Federal Ministry of Transport and Digital Infrastructure and the German Federal Ministry for Building Transport and Urban Development. This enables regionally differentiated driving profiles. The profiles are additionally categorized regarding different user groups of BEVs, which here are commuters and non-commuters. The share of both is a regionally differentiated input parameter (cf. Figure 4-3) and, therefore, varies with regard to the simulated region (cf. [118]). Additionally, a daily mobility quote based on MiD17 is considered per day to account for the fact that not all vehicles are used every day. Those data reveal, for instance, that 17% fewer people are leaving their homes on Sundays compared to an average weekday in Germany [137]. Figure 4-4 shows the flow chart of the simulation, including the driving and charging rules of BEVs and the interactions between different types of agents.

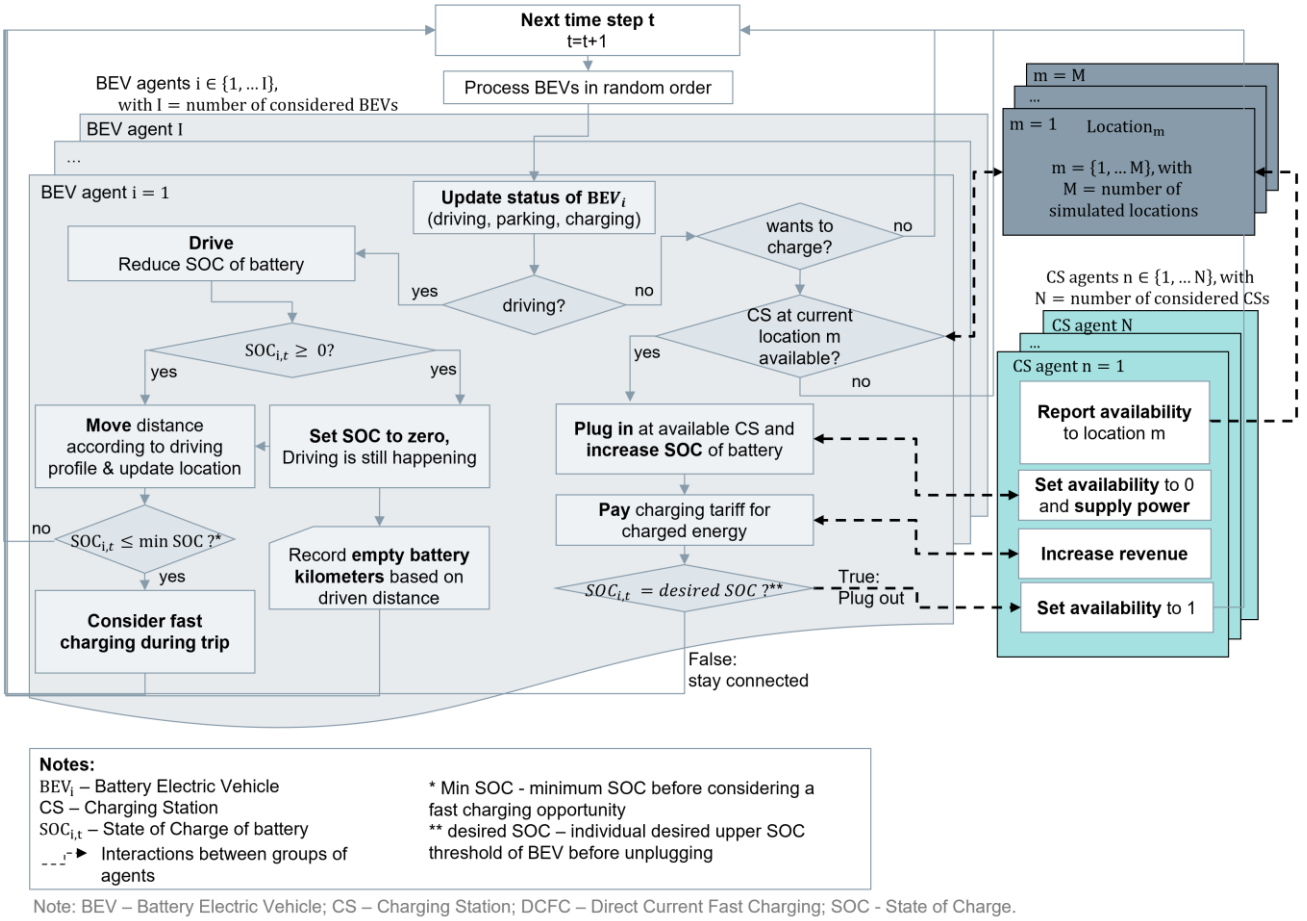

Note: BEV – Battery Electric Vehicle; CS – Charging Station; DCFC – Direct Current Fast Charging; SOC - State of Charge.

Figure 4-4 – Flow chart of the ABM eMob showing the main procedures and the interactions between BEVs, Charging Stations, and Locations. This flow chart only shows a 'charge at arrival' charging strategy for BEVs.

Each BEV drives and parks according to its driving profiles without any deviation. Equation (4-1) describes the change of the SOC of a BEV *i* within time step t if the vehicle is driving. K_i is the battery's capacity in kWh.

$$SOC_{i,t} = SOC_{i,t-1} - \frac{C_i \cdot D_{i,t} \cdot \beta_{T^{\text{ambient}},V_{i,t}}}{K_i} \quad (4\text{-}1)$$

The consumed energy is based on the BEVs' energy consumption rate C_i in kWh per km at a speed of 50km/h and an ambient temperature T^{ambient} of 20 °C, as well as on the driven distance $D_{i,t}$. To account for different energy consumption rates in dependence of the ambient temperature T^{ambient} and the current BEVs speed $V_{i,t}$, an adjustment factor β is introduced. It is derived based on Schmidt [138]. The derived adjustment factors for different temperatures are shown in Figure 4-5.

One abstract but a central feature of the approach of BEVs driving according to their driving profiles without any deviation independent of their SOC is that BEVs can drive with an empty battery in the model (cf. Figure 4-4). Even though this deviates from reality, the driven kilometers with an empty battery can be measured in the model and used as an indicator for the SQCI. The lower the total number of driven kilometers with an empty battery in the simulated system, the better the charging infrastructure coverage in the simulation for the simulated dynamic charging demand. It is assumed to be an appropriate measure since the preferred charging location is at destinations where the driver of the BEV parks anyway. A similar measure is, for instance, used in Nicholas et al. and van der Kam et al. [134], [139]. An analysis in the ABM eMob showed that in a scenario with strong overbuilding of AC charging infrastructure at home, work, and public and without any DCFC charging opportunities, the empty battery kilometers occur only due to long trips, which the type of vehicle cannot cover

without stopping in between for recharging. By reducing the AC charging availability, additional empty battery kilometers occur due to several consecutive trips without available recharging at the parking destinations and subsequently also due to trips starting with an empty battery.

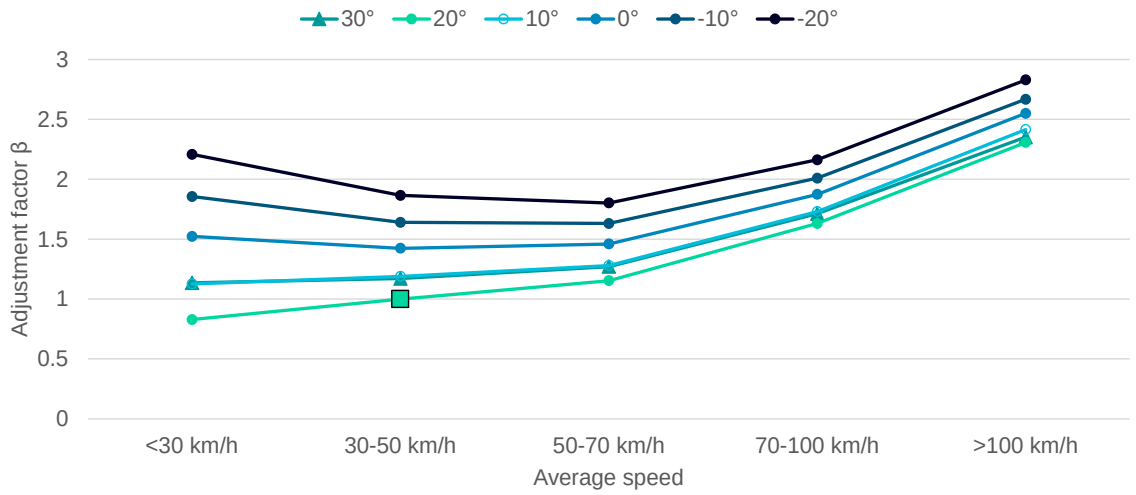

Figure 4-5 – Adjustment factor β for BEVs energy consumption in dependency of the ambient temperature and the average driving speed of a trip derived based on Schmidt, 2016 [138].

In the scope here, each BEV follows the charging strategy 'Charge at Arrival' to recharge the battery. A BEV charges its battery immediately after arrival at a destination until its battery reaches the BEV's desired minimum SOC threshold before departure or until the BEV departs again. The charging strategy defines whether a BEV wants to charge within the current time step, but the charging process can only start if a charging station is available at the current location (cf. Figure 4-4). The change of SOC of a BEV *i* in time step *t* in which a charging process occurs is defined by

$$SOC_{i,t} = SOC_{i,t-1} + \frac{p_j \cdot \Delta t}{K_i} \tag{4-2}$$

with K_i being the batteries capacity and P_j the available power supply

$$p_j = \begin{cases} P_j^{\max}, & if\ SOC_{i,t-1} + \dfrac{P_j^{\max} \cdot \Delta t}{K_i} \leq 1 \\ \left(1 - SOC_{i,t-1}\right) \cdot K_i, & if\ SOC_{i,t-1} + \dfrac{P_j^{\max} \cdot \Delta t}{K_i} > 1 \end{cases} \tag{4-3}$$

from the BEVs onboard charger and the charging station *j*, to which the BEV is connected. Equation (4-3) represents a simplified constant current constant voltage charging process of the battery with its characteristic of reduced charging power at the end of the charging process. $P_j^{\max}$ is the maximum power rating of the charging station. The equation shows that the charging power in the last time step before reaching a SOC of 100% is reduced from the maximum available charging power $P_j^{\max}$ of the charging system to the required charging power to exactly meet an SOC of 100% within this time step. This simultaneously prevents the SOC from increasing above 100% in the simulation.

Suppose the selected time step within a simulation is greater than a vehicle's charging time t^{charge}. In that case, the charging power p_j is reduced for that charging process to not overestimate the simultaneity of several short charging processes within one time step and to still ensure a consistent SOC for each BEV according to Equation (4-1) (cf. Equation (4-4)).

$$p_{j,t} = \begin{cases} p_{j,t} & ,\forall t^{\text{charge,ac}} \geq \Delta t \\ p_{j,t} \cdot \dfrac{t^{\text{charge,ac}}}{\Delta t} & ,\forall\, t^{\text{charge,ac}} < \Delta t \end{cases} \quad (4\text{-}4)$$

In this case, the assumed charging time for AC charging is fixed to $t^{\text{charge,ac}}$, which is assumed in the following to 20 minutes if the simulation time step is set to one hour. While the actual charging peak can be underestimated for single BEVs, it is regarded as a valid simplification for large BEV fleets.

Charging station agents only represent charging activities at BEVs destinations such as home, work, supermarkets, restaurants, or other points of interest. A charging infrastructure network, which focuses on these charging locations, maximizes the driver's comfort since no detours or additional stops are required [140]. AC chargers can usually provide these charging services with a power rating between 3.7 kW and 22 kW. In contrast, fast charging activities are assumed to occur only to avoid the SOC from dropping below a threshold defined by the vehicle's charging strategy. To minimize the time for a designated fast charging stop, these chargers are assumed to be DCFC chargers with 50 kW or more. The model applies a stochastic representation of these chargers. If the SOC of a currently driving BEV drops below its individual minimum threshold, and if the trip of the BEV is at least 30 minutes, the BEV starts to look for a fast-charging opportunity along its way. The minimum SOC threshold is assumed to 30% here. The probability χ_i to find a charging station along its way within the time step t is assumed to be

$$\chi_{i,t} = \frac{D_{i,t}}{DCFC\ coverage} \quad (4\text{-}5)$$

with the assumed distance between DCFC stations in the region as set by the input parameter 'DCFC coverage'. This parameter can be interpreted as the distance between two stations on, for instance, the highway. A differentiation between DCFC charging within the considered city and on highways is made based on the current traveling speed of the BEV. Trips with a recorded speed which is on average faster than 50km/h, are presumed as trips outside of the considered region. This classification is relevant to exclude fast charging activities outside the region when measuring the charging power within the considered region. All fast-charging processes are assumed to last for a fixed period $t^{\text{charge,dcfc}}$, which is subsequently assumed to ten minutes. If the simulated time step is greater than the assumed charging period, the charged energy in the charging period with the maximum power $P_i^{\text{dcfc,max}}$ is averaged over the entire time step Δt to obtain the charging power p_t^{dcfc}. This charging power is then accounted for in the aggregated charging demand profile. This is considered a reasonable simplification in modeling large fleets in analogy to the AC charging described above. Equation (4-6) defines the fast-charging power $P_{t,i,z}^{\text{dcfc}}$ for a BEV $i \in I$, which is charging at a fast-charging station of type $z \in \{highway, city\}$ in time step t.

$$p_{t,i,z}^{\text{dcfc}} = \begin{cases} P_z^{\text{dcfc,max}} & ,\forall t^{\text{charge,dcfc}} > \Delta t \\ P_z^{\text{dcfc,max}} \cdot \dfrac{t^{\text{charge,dcfc}}}{\Delta t} & ,\forall t^{\text{charge,dcfc}} \leq \Delta t \end{cases} \quad (4\text{-}6)$$

Finally, the aggregated charging demand p_t of all charging processes in the considered region can be derived as a sum over all charging processes, excluding the fast-charging activities on highways. Highway charging is still accounted for but assumed to be not within the assessed regional scope.

$$p_t = \sum_j p_{j,t} + \sum_z p_{z,t} \quad ,\forall j \in J, z \in Z \backslash highway \quad (4\text{-}7)$$

4.2.2 Flexibility of charging processes

With the introduction of electric vehicles in the mobility sector, many Lithium-Ion batteries are installed. Using these batteries is broadly discussed to integrate renewables, reduce grid congestions, or reduce vehicle owners' charging costs [141]–[144]. It could be shown by Husarek et al. in [118] that even a simple shift in time of a

planned charging process during the same parking process yields enormous flexibility potentials. In the present thesis, flexibility from a charging process is subsequently defined as the energy per time step P^{flex} that can be shifted in time for t^{delay} time steps. The flexibility is assessed only for the charging strategy 'Charge at Arrival'. To determine the flexibility, the difference of the planned parking duration t_{i,t^a}^{park} of a BEV according to its driving profile and the required charging time $t_{i,t^{\text{a}}}^{\text{charge}}$ to reach a predefined SOC is calculated at each arrival of a BEV in $t^{\text{a}} \in T$ if a charging station is available at the BEVs location according to Equation (4-8).

$$t_{i,t^a}^{\text{delay}} = t_{i,t^a}^{\text{charge}} - t_{i,t^a}^{\text{park}} \quad ,\forall i \in I, t^{\text{a}} \in T \tag{4-8}$$

Suppose $t_{i,t^{\text{a}}}^{\text{delay}}$ is greater zero. In that case, it indicates that a charging process can be shifted, and it defines the maximum available delay time of the process under the condition that the SOC of the BEV still reaches the desired SOC before departure. The corresponding flexible charging power is then derived according to Equation (4-9) based on the charging power $p_{j,t}$ for all time steps starting from the arrival time t^{a} until the latest time step in which the charging process must start to still reach the desired SOC before the next departure.

$$p_{j,t}^{\text{flex}} = p_{j,t} \quad ,\forall\, t^{\text{a}} \leq t \leq t^{\text{a}} + t^{dely} - 1 \tag{4-9}$$

The total flexibility categorized by its realizable delay time is then

$$p_{t^{\text{delay}}}^{\text{flex}} = \sum_{t} \sum_{j} p_{j,t}^{\text{flex}} \quad ,\forall t^{\text{delay}} \in T^{delay} \tag{4-10}$$

for all uniquely occurring delay times t^{delay} in the set of potentially realizable delay times T^{delay} for the entire simulation period and all locations.

4.2.3 Representation of spatial resolution and BEV penetration

Since the computational effort of the ABM eMob increases significantly with an increasing number of modeled BEVs, high penetration levels within a region are not efficiently modeled by simply increasing the number of BEVs. Therefore, the following hypothesis is made to model a high penetration rate without increasing the number of BEVs: The number of modeled BEVs and the number of modeled locational duplicates can be substituted based on a linear relationship while the total energy demand per type of location is constant. This relation is formulated in Equation (4-11) with $m_{places,s,M^{\text{BEV}}}$ being the number of modeled workplaces and public places with $places \in \{workplaces, public\ places\}$, M^{BEV} the number of modeled BEVs, and S^{BEV} the share of BEVs in relation to the total number of cars $N^{\text{cars,tot}}$ within the region. N_{places}^{tot} is the total number of potential charging locations in the region (cf. Section 5.1).

$$m_{places,s,M^{\text{BEV}}} = \frac{N_{places}^{\text{tot}}}{N^{\text{cars,tot}}} \cdot \frac{M^{\text{BEV}}}{S^{BEV}}, \forall\, places \in \{workplaces, public\ places\} \tag{4-11}$$

Figure 4-6 (a) shows exemplarily the linear substitution rates for workplaces in an urban area, and Figure 4-6 (b) compares the number of modeled public and workplaces in dependency of the electrification rate of passenger cars for the same urban area.

The hypothesis stated above can be validated by defining a BEV penetration scenario and varying the ratio so that this scenario is represented with different numbers of BEVs and modeled locational duplicates. If the energy consumed, for instance, over all public locations, stays the same, the hypothesis can be verified. An analysis varying the number of BEVs between 500 and 1000 and the number of modeled public and workplaces according to the defined substitution rate is conducted to verify the hypothesis above. Thereby, the number of public chargers is set so that each public location has exactly one public charger with a power rating of 22 kW in all scenarios. This analysis revealed that the same energy output aggregated over all public locations can be obtained. Therefore, this approach is considered as validated subsequently and applied in all further analyses to define different penetration rates for a specific region.

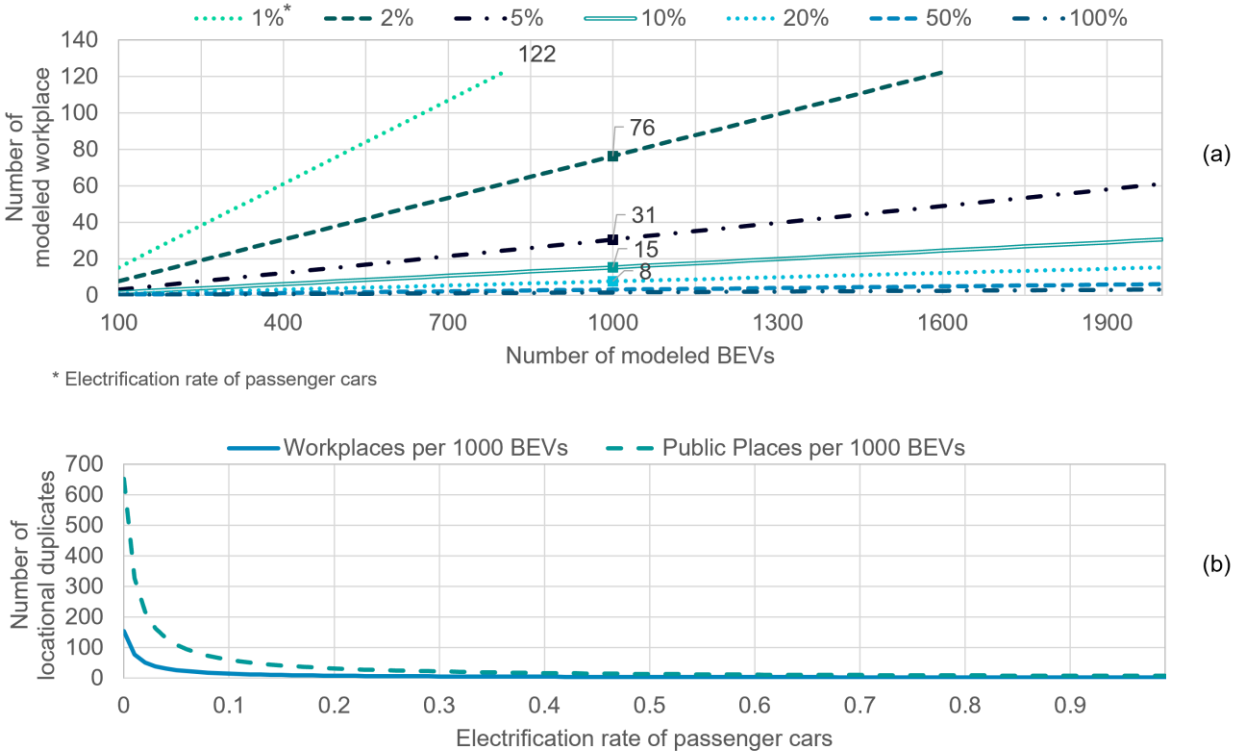

Figure 4-6 – (a) Linear substitution rate of modeled BEVs m^{BEV} and modeled places $m_{places,s,m^{\mathrm{BEV}}}$ exemplarily depicted for workplaces, and (b) number of modeled places $m_{places,s,m^{\mathrm{BEV}}}$ in dependence of the electrification rate. Both depicted curves relate to an urban area with 110 thousand passenger cars, 168 industrial and commercial work areas, and 719 identified relevant public locations.

4.3 Model behavior and benchmarking

Subsequently, the model behavior described in Section 4.2.1 is investigated for the 'charge at arrival' strategy. Therefore, first, the SOC over time is evaluated, second, aggregated charging profiles for a BEV fleet are presented and validated, and finally, a global sensitivity analysis of the ABM eMob is conducted.

State of charge assessment

Driving profiles are taken from the MiD17 study and filtered by commuter and non-commuter profiles. Figure 4-7 shows a two-weekly SOC curve for a single BEV of type commuter. The SOC changes due to charging and driving activities according to Equations 4.23-4.24. The figure shows additionally that the BEV is driving every weekday to work and stops along its way infrequently at public places before parking at home overnight. While the observed BEV charges every day at home to a SOC of 100%, no charging activities at work occur due to a lack of charging infrastructure. Regular charging also occurs in public places. The plot indicates that only short trips occur for the observed vehicle each day with a minimum SOC of 87% on Wednesday of the first week. Additionally, due to the charge at arrival strategy, many short charging processes occur.

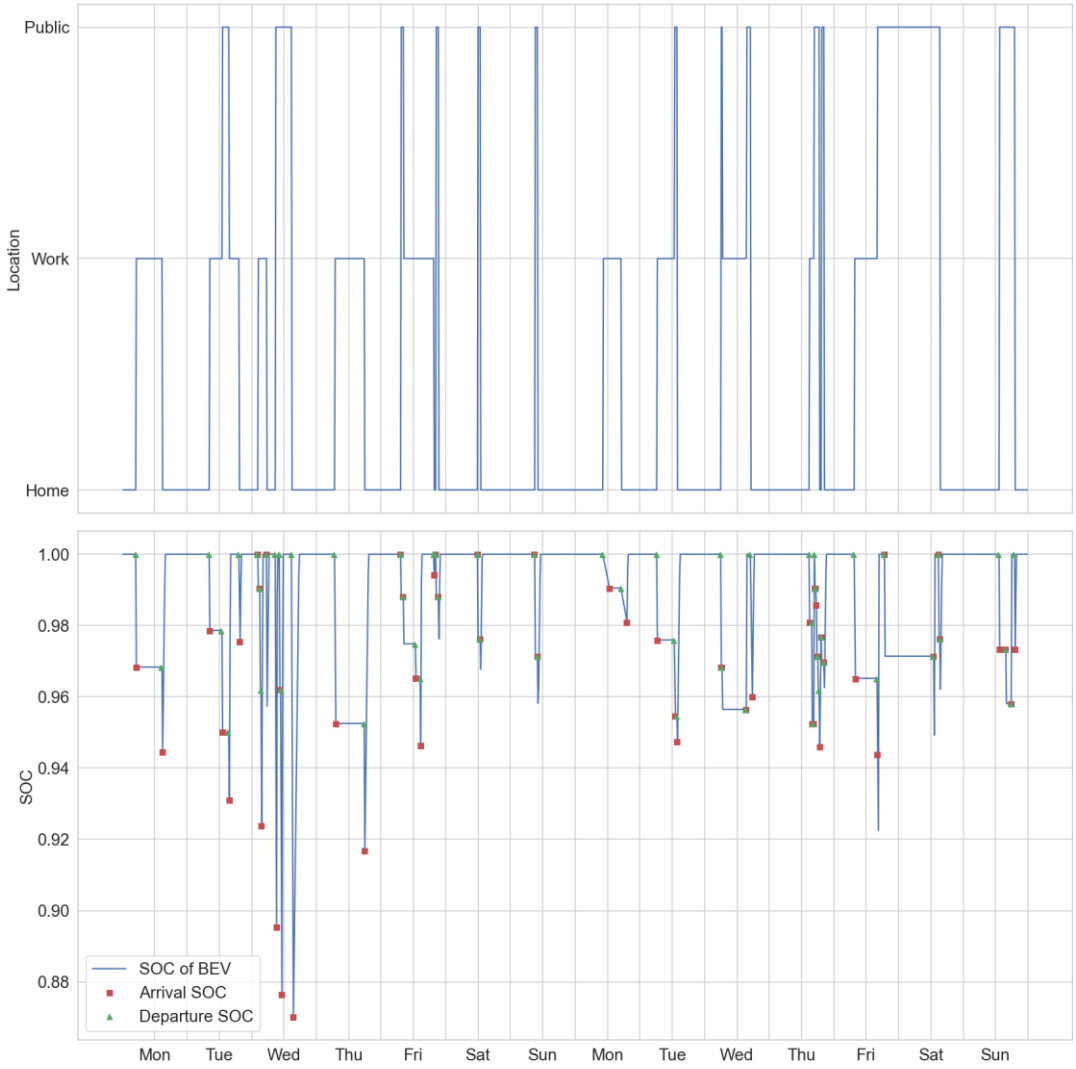

Figure 4-7 – State of charge over time on a 15-minute time interval of an exemplary BEV with the user profile 'commuter'. The upper figure shows the location of the BEV over time according to the driving profile, and the lower plot indicates the resulting SOC over time.

Figure 4-8 shows the mean SOC of a fleet of 1000 BEVs over time, including its standard deviation. The SOC stays above 95% during the week and only drops at weekends below that value due to longer driving distances. The standard deviation drops below 85% on Sundays. The relatively high average SOC indicates that sufficient charging infrastructure is available to recharge the consumed energy.

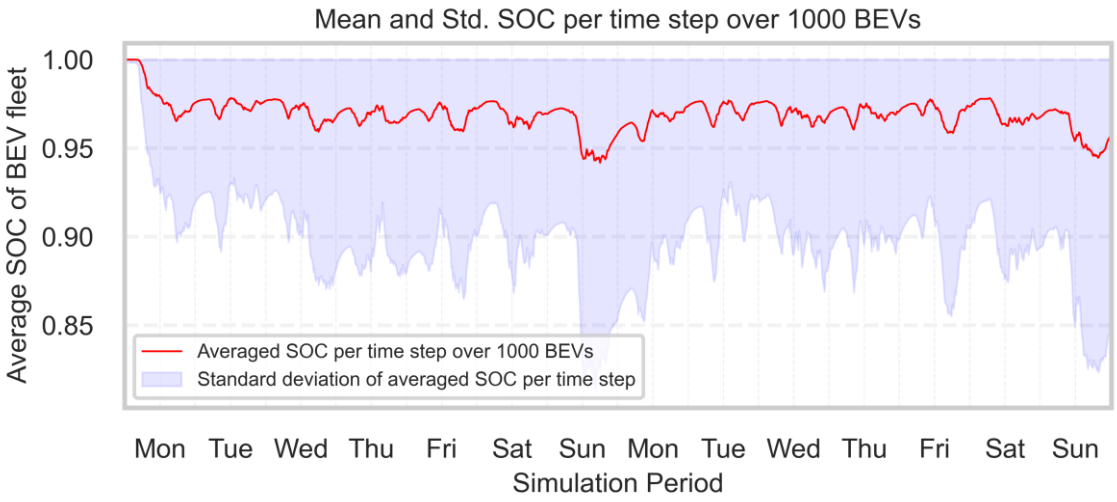

Figure 4-8 – State of Charge of a fleet of 1000 BEVs averaged in each 15-minute time step for two exemplary weeks.

Finally, Figure 4-9 exemplifies the aggregated charging profile of a fleet of 1000 BEVs in a rural area subdivided into the charging categories home, work, public, city, and highway (cf. 4.26). It shows that a morning and evening peak occur around 8 am and 6 pm. The morning peak is mainly caused by work charging and the evening peak due to the home and public charging load. In this example, public and work charging are the dominating charging modes for the electrical load due to the high assumed availability of work and public chargers with 5 BEVs per charging point at public and work locations each. Finally, fast-charging power increases on the weekend when driving distances increase and vehicles cannot recharge at workplaces. The overall electrical load from charging within this region occurs on Friday at 5 pm with about 1.6 MW per 1000 BEVs. It is to mention that this is

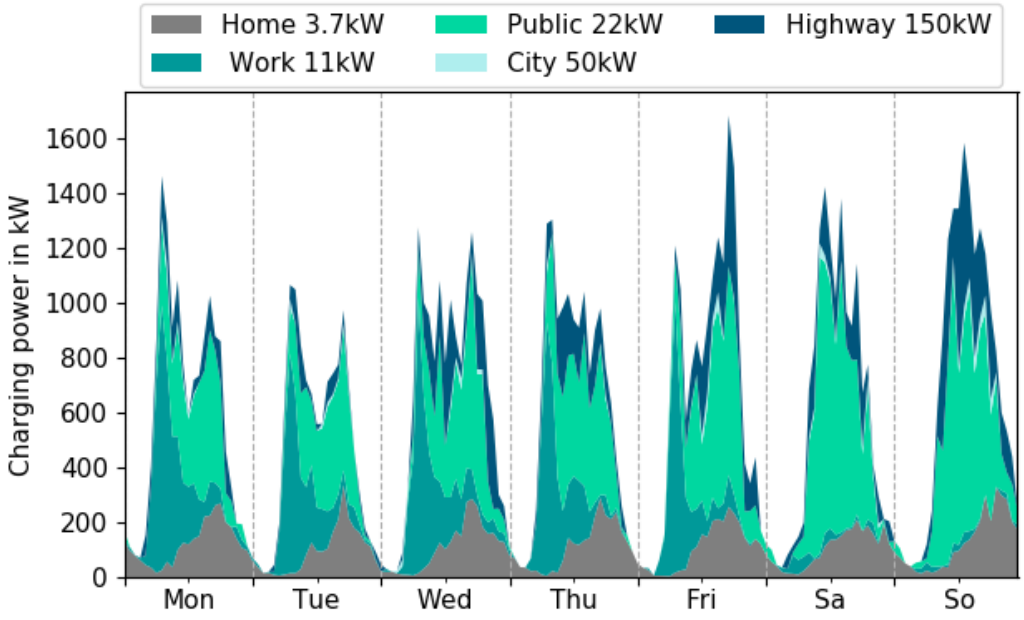

Figure 4-9 – Aggregated charging power per 1000 BEVs subdivided by location and power rating of charging stations for one exemplary week in an urban area, assuming a high availability of charging stations.

obtained from a single simulation run for a specific scenario. Different parameter settings and different driving processes drawn from the pool of driving processes impact the aggregated charging profile within each simulation run. However, the overall tendency of morning and evening peaks is constant over different simulations if the model parametrization is unchanged.

Charging profile validation

The model output is used to assess the impact of BEVs on the energy system and identify BEVs' charging infrastructure requirements. A high accuracy compared to real-world data is essential for the quality of the derived insights. Hecht et al. published an empirical data set of usage patterns of 26,951 charging stations between December 2019 and March 2020 across Germany [145]. The published data are subsequently compared to the ABM eMob model output.

The observed data in the dataset are taken from different websites such as 'Chargemap' reporting the status of public charging stations on a five- or 20-minute interval. Newly starting charging events within one time step are derived from these data. About 71% of the recorded data belong to charging stations with a power rating of 22 kW, including industrial, residential, suburban, and urban locations [145].

Therefore, the newly starting charging events in the ABM eMob are observed for 22 kW public chargers and 11 kW work chargers and compared to the empirical data. It is assumed that in 2019 most of the BEV owners are early adopters having access to home charging. The corresponding input parameter 'home charger access' is subsequently set to 90%. Additionally, 10% of these home charging processes are accounted for to represent on-street charging. With 83 thousand registered BEVs in Germany in 2019 [146], excluding Hybrid Electric Vehicles, and with about 30 thousand publicly reported charging points until the end of 2019, there are between two and three BEVs per public charging station [147]. This ratio is applied in the ABM eMob with 250 charging points at public locations and 100 at work locations. As the empirical data set represents the entire country by Hecht et al., the MiD17 driving profiles are not filtered according to a regional classification.

Figure 4-10 shows the newly starting charging events of the ABM eMob compared to the empirical data. The dotted line represents the hourly mean value of new public charging events from 50 simulations in the ABM eMob, and the corresponding shadowed area shows the standard deviation per hour. The solid line shows the new events of an exemplary week as published in the empirical data. Since the data set contains only one week of the new starting events, the standard deviation is taken from the active events per hour as published in the appendix in [145].

The comparison shows that the ABM eMob can represent the temporal resolution of public charging events for a day with high accuracy. Differences between weekdays and weekends are modeled accurately, and the charging peak times around 8 am to 9 am and 6 pm align temporally with the empirical data. Additionally, the decreased charging events after 7 pm in the ABM eMob match the decline in the empirical data.

The average standard deviation over the week is with 14.5% around the mean value on average significantly lower in the ABM eMob than the weekly averaged standard deviation of 22% around the mean in the empirical data. One reason could be that the penetration of BEVs in 2019 is still below 1%, and the utilization of public chargers is therefore very low. This can decrease the simultaneity and, in turn, increase the standard deviation shown here. It can be assumed that this standard deviation would decrease with an increasing penetration level. Further, the standard deviation of the ABM eMob, in contrast, is limited by the number of different driving profiles in the pool of MiD17. Additionally, the model is parametrized here with only one public and one workplace, which increases the charging station availability for BEVs in the model and decreases the standard deviation. This was chosen since determining an accurate number of public and work charging locations on country level seems unreasonable. Finally, the standard deviation decreases with an increasing number of repeated simulations in the model.

Nevertheless, the lower standard deviation is not considered to decrease the accuracy of the model, which could be shown in the above. The validation focuses only on public chargers. Further modes of charging are not validated due to a lack of empirical data.

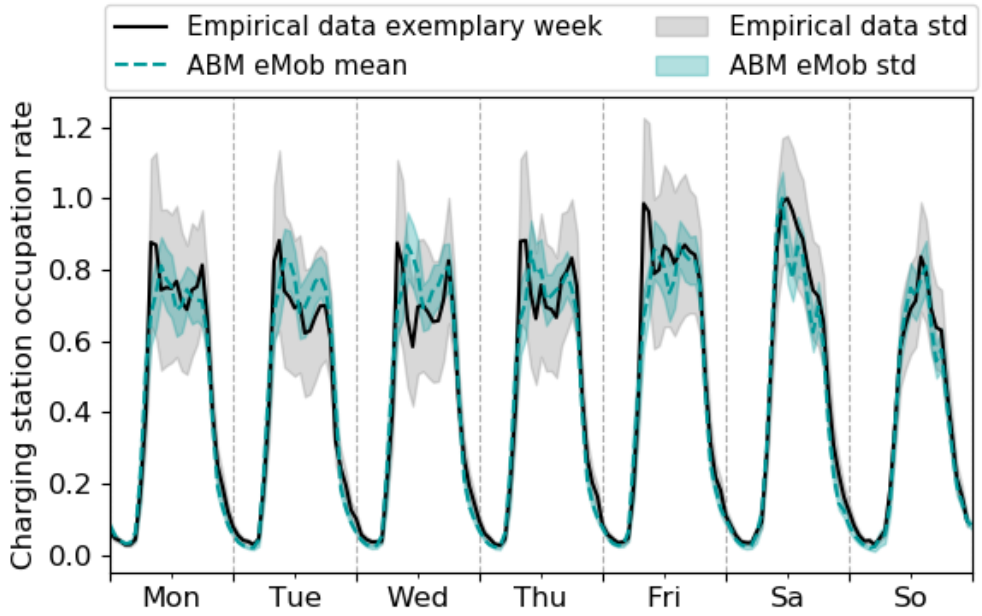

Figure 4-10 – ABM eMob validation comparing empirical data of newly starting charging events per hour from public 12 kW-25 kW charging stations with a mean value of 50 ABM eMob simulations. The shadowed areas show the standard deviation (std).

Global sensitivity analysis of model

The parametrization of the model can significantly impact the observed outputs [118]. A reasonable parametrization is therefore a central step for the analysis of a 'regional charging system'. To comprehensively assess the behavior of the ABM eMob, a multi-output global Sobol Sensitivity analysis [148]–[150] is conducted and published in Husarek et al. 2021 [118]. It shows the impact of different input parameters on multiple output parameters. In a global sensitivity analysis, all input parameters are simultaneously varied over their full range. The approach from Sobol aims especially at non-linear and non-monotonic models such as Agent-based models. Sobol indices are calculated describing the impact of each individual input parameter on the total observed output variance of an output parameter based on a variance decomposition.

Here, potential parameter ranges are defined for 10 BEV and charging station agent input parameters based on the literature, and subsequently, 8800 experiments were obtained applying a Saltelli sampling method [150] with a sample size of 400. The Saltelli sampling allows an efficient experimental design for a Sobol sensitivity analysis [151], [152]. It was conducted for a rural and an urban area. To assess the ABM eMob output, a combined evaluation of total order Sobol indices and the Pearson Correlation coefficient was derived, allowing to interpret the explained output parameter variance by a single input parameter and simultaneously the direction of a linear correlation. To obtain the Sobol indices, the output variances are decomposed into partial variances referring to each input parameter by calculating the variance while varying one input parameter and keeping all other inputs constant. Further, Total Order Sobol indices additionally contain the effect of varying several parameters together. Compared to the first-order indices, they also contain second-order effects, which describe the impact of varying more than one parameter simultaneously. This means, for instance, that the combined effect on the required number of charging stations in a region by small battery sizes and high vehicle consumption rates can be measured.

Figure 4-11 shows the derived Total Order Sobol indices for 17 output parameters[2] and ten input parameters, including the sign of the Pearson Correlation Coefficient for the assessed urban system. It shows that the energy consumption of BEVs has a significant impact on most output parameters. Showing a positive correlation, it explains 78% of the variance of the peak load of the modeled system and an additional 40% of the highway charging peak. Simultaneously but negatively correlating, an increasing energy demand explains 80% of the daily shiftable energy demand output variance and 45% of the region's SQCI output variance. Therefore, this is a highly relevant input parameter, which needs to be chosen carefully to design a sufficient charging infrastructure network and assess the integration into energy systems. In contrast, the battery size of a BEV is highly relevant for the SQCI, but it does not impact the available flexibility significantly. This is because the average SOC of a BEVs fleet is relatively high over the course of one week (cf. Figure 4-8), and, therefore, the flexibility is primarily defined by the parking duration. Further, the charging power of charging stations reveals less impact on the model output than the number of deployed charging stations.

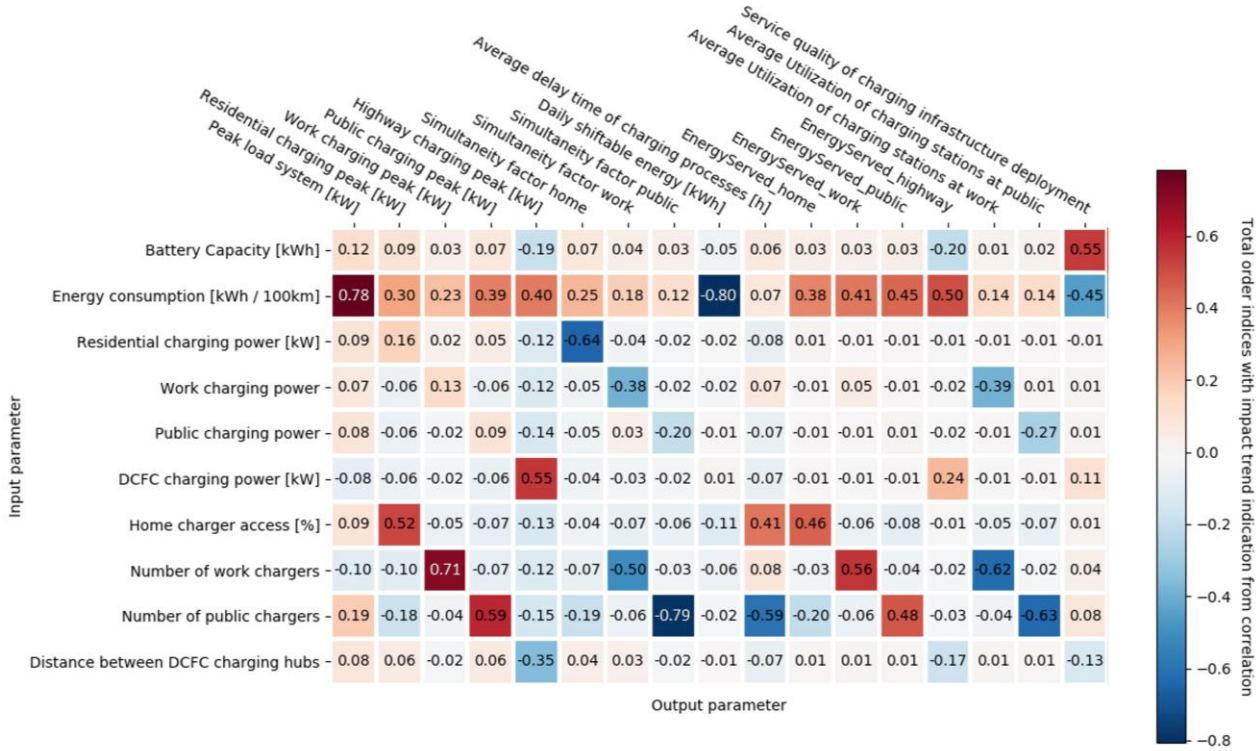

Figure 4-11 – Total Order Sobol indices and sign of Pearson Correlation Coefficient for an urban area for 17 output and ten input parameters from [118].

The conducted analysis concludes the following key impacts on the output parameters of the ABM eMob [118]:

> *"Energy demand and battery size of BEVs are the main driver for the required charging infrastructure. • Charging power (except highway) explains less than 16% of the peak load variance and is therefore significantly less influential compared to BEVs' energy consumption and charger availability; • Highway charging peak load is explained by up to 55% by highway charging power; • Residential peak load explained by up to 51% by home charger access; • Cross-locational effects matter: home charging peak explained up to 18% by public charger availability; • Low effect of charging station parameters on shiftable*

[2] The output parameters labeled with EnergyServed refer to the served energy in kWh per indicated location (home, work, public, highway).

energy, but the average delay time is explained up to 59% by charger's availability; • Highly competitive market: number of public chargers explain up to 69% of the utilization of public chargers."

5 Method

Interactions of the mobility sector and the MMES are assessed by applying the ESDP and the ABM eMob (cf. Sections 3 and 4). The combined model framework allows identifying optimal capacities and their operation in the MMES as well as fundamental insights about the necessary charging infrastructure for an electrified passenger car sector. Figure 5-1 shows the procedure to answer the three research questions (cf. Table 1-1).

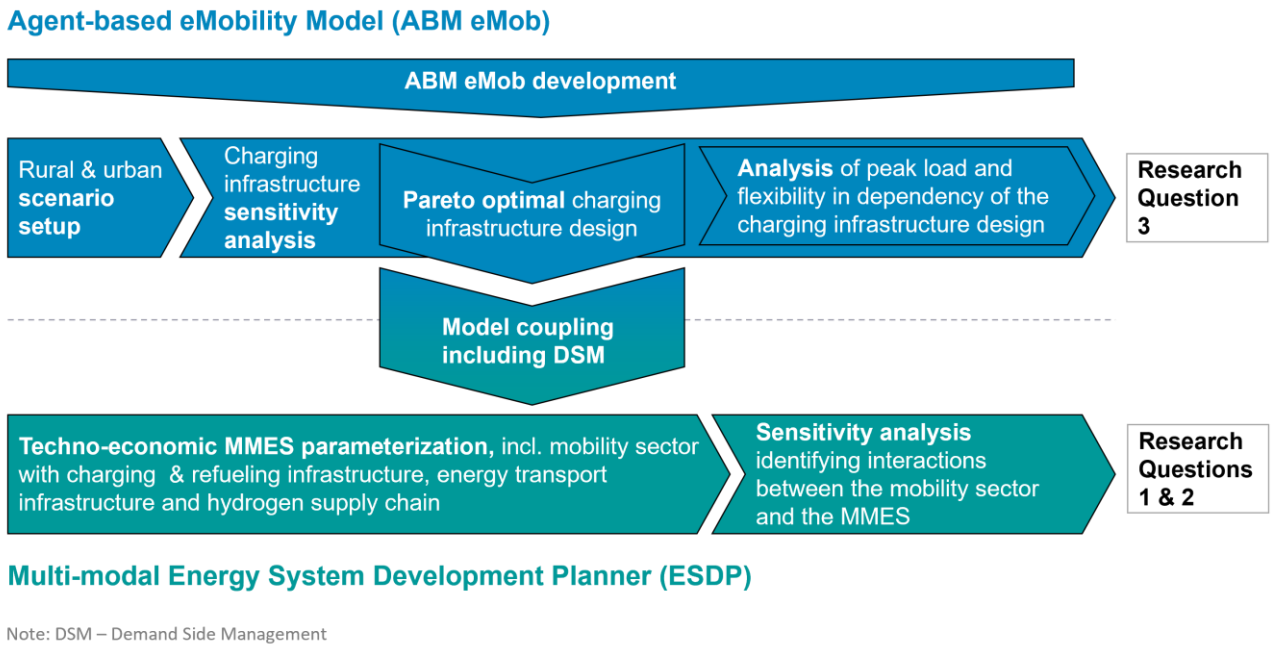

Note: DSM – Demand Side Management

Figure 5-1 – Overview of the procedure of thesis.

The developed ABM eMob is applied to answer Research Question 3. A rural and an urban area are investigated to assess the different charging demand and charging infrastructure requirements. A sensitivity analysis of the charging infrastructure is conducted for both regions to explore potential charging infrastructure network designs and their impact on the BEVs' charging peak load and flexibility. A charging infrastructure network design is defined here as a specific combination of the number of charging points per power rating at different locations. The sensitivity analysis is further used to define Pareto-optimal charging infrastructure designs (cf. Section 5.1). Subsequently, two Pareto optimal scenarios are used to parametrize eMobility conversion processes in ESDP as described in Section 5.2. This parametrization focuses primarily on the derived charging infrastructure network costs, temporally resolved electricity charging demand, and temporally resolved flexibility potential of the charging processes (cf. Sections 5.2.2-5.2.3).

Assessing interactions of the mobility sector with the energy transport infrastructure for electricity, methane, and hydrogen simultaneously within an MMES requires a comprehensive parameterization of these processes in ESDP. The derived parametrization of the most relevant conversion and transport processes within the MMES is described in Section 0. Finally, a local sensitivity analysis is conducted in the ESDP to answer Research Questions 1 and 2 (cf. Section 5.4). Thereby, the interactions of the mobility sector with the energy transport infrastructure, the energy supply, and the flexibility of BEVs are investigated.

Figure 5-2 shows the applied model framework, including the MMES model, which is parametrized in ESDP and the ABM eMob. It indicates the fundamental differences between both model techniques and that the model coupling focuses only on BEVs for passengers and their charging infrastructure. This applied framework allows simulating driving and charging behavior of individual BEVs, including their charging infrastructure, with a high degree of detail and to incorporate it into the German multi-region MMES. While the ESDP assumes perfect foresight for all considered time steps and years, the ABM eMob does not. This means that a BEV in the discrete

event simulation, which drives towards a location where it can charge, does not know if the charging point is available at time of arrival or if it is occupied.

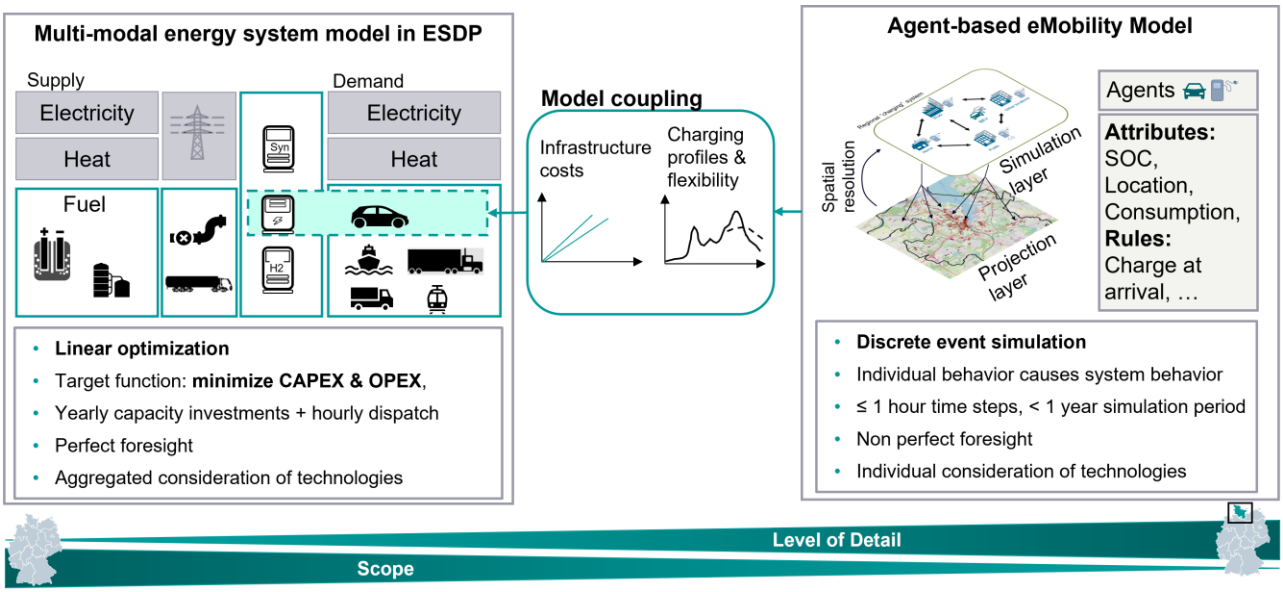

Figure 5-2 – Applied model framework, including the model coupling of the ESDP and the ABM eMob.

5.1 Designing regional charging infrastructure networks

The ABM eMob is designed to assess regional charging infrastructure networks and to simulate the electricity charging demand of BEV charging processes at different locations over time. Due to the spatial and temporal dynamics of BEVs' charging demand, a charging infrastructure analysis is conducted, considering an entire region, including different modes of charging and locations. Since the ABM eMob simulates several consecutive days, weeks, or months, with consistent SOCs in time and space, the model allows considering cross-locational effects and regional differences (cf. [118]). Cross-locational effects include that charging demand served at one location must not be served at another location anymore and are considered in designing charging infrastructure networks.

A simulated region is defined here as a system, commonly based on administrative borders, where driving and charging activities are simulated. Such a system interacts with its neighboring regions by modeling inter-regional commuters as described in Section 4.2. A region is characterized by its population, the number of cars per inhabitant, the employment rate, the number of inter-region commuters traveling into or out of the simulated system, the rate of vehicles having access to private parking as an indicator for the access to home charging, and by its driving patterns. Additionally, the number of potential workplaces and public places for charging infrastructure are identified for each region as a measure of the required spatial resolution in the model.

Table 5-1 shows the parametrization for an urban and rural area. The parametrization of the urban area is based on the city of Kiel and the rural area is based on the municipality of Steinburg (cf. [118]). Both regions are in the state and NUTS2 region of Schleswig Holstein in Northern Germany. The driving profiles are obtained from MiD17 [136] and filtered by the municipality type. One major difference is that BEVs commute into the urban area during the day and commute out of the rural area. This is reflected in the parameter 'inter-regional commuters', which is an import parameter to differentiate the charging infrastructure design in both regions. The vehicle parameters are assumed equal for both subsequently considered regions, with consumption rates between 16 kWh/km and 24 kWh/km, and battery sizes between 40 kWh and 80 kWh.

Regional parameters	Rural	Urban
Driving profiles based in MiD17 filtered by municipality type	Small-town area, village	Regiopolis
Home charger access	84%	60%
Share of commuters	49%	46%
Inter-regional commuters	-23%	36%
BEVs in region	8,400	11,000
Assessed BEV penetration levels	1%, 20%, 80%	1%, 20%, 80%

Table 5-1 – Regional parametrization of ABM eMob based on [118].

The number of potential available public places for charging stations is estimated based on points of interest, which are considered relevant, such as supermarkets, parking lots, or shopping malls. The geoinformation system data of these relevant points of interest are extracted from OpenStreetMaps and intersected with a raster of the size 150m x 150m. This is presumed comfortable walking distance. For each square with one or more relevant points of interest allocated, only one public place is modeled, and scaled according to Equation (4-11). Aggregating all points of interest within a square is used to not overestimate a high density of points of interest within a vicinity. To obtain the number of workplaces in a region, industrial and commercial areas are counted based on land use data from OpenStreetMap. It is assumed that those are areas with a high density of workplaces, and it reflects joint charging hubs in these areas rather than individual charging stations at each workplace. The estimated numbers here can vary significantly in reality. However, applying a consistent method to estimate them enables comparability between different regions, while their main characteristics in terms of spatial resolution are still assumed to be reflected.

The charging infrastructure sensitivity analysis (cf. Figure 5-1) is applied to assess different charging infrastructure combinations, their impact on the peak load and flexibility, and to derive Pareto optimal designs. This procedure, which is applied to a rural and an urban area for the three different BEV penetration levels of 1%, 20%, and 80%, is shown in Figure 5-3. A variation of the number of charging points per location with different power ratings is conducted. A full factorial design combining all possible factor variations is applied to obtain the set of scenarios. This experimental design allows gaining full insight into various specific combinations of charging stations, which is required to derive specific combinations. However, it comes with an exponentially increasing number of scenarios by 2^k with k describing the number of assessed factors. Therefore, the assessed parameter variations are kept to a minimum as defined in Table 5-2. Home chargers are assumed to be built to their maximum availability and are not included in the parameter variations. Highway and city fast charging are assessed with two different values for the DCFC coverage each. Hence, the assessment focuses on public and work chargers and their interactions with low and high DCFC coverages.

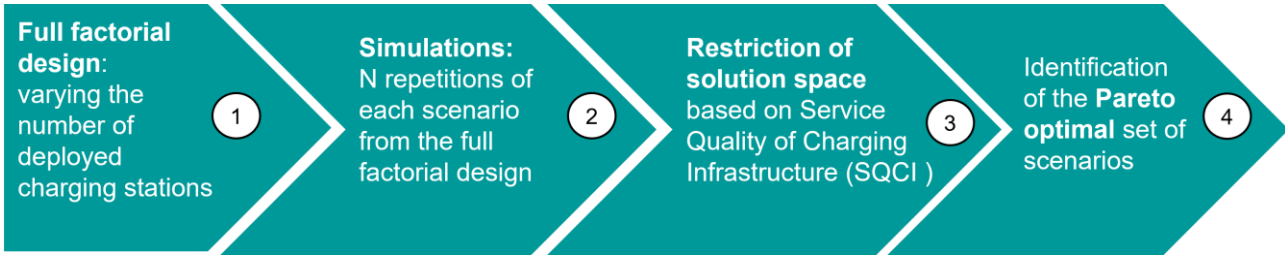

Figure 5-3 – Method for determining the Pareto optimal set of charging infrastructure designs.

Charger type	3.7kW	11kW	22kW	50kW	150kW
Location	Home	Work	Public	City	Highway
BEVs per charging point	Not varied	5, 10, 15, 20, 25, 32, 42, 50, 100, 250	5, 10, 15, 20, 25, 32, 42, 50, 100, 250	-	-
DCFC coverage in km	-	-	-	5, 25	25, 50

Table 5-2 – Parameter variations for charging infrastructure sensitivity analysis. DCFC – Direct Current Fast Charging

In step two, each defined scenario is repeated 40 times resulting in a total simulation number of 4 thousand per region and assessed penetration level. Repetition of each scenario is necessary to account for the stochastic factors in the model. Those are predominantly the different driving profiles, which are randomly drawn from the pool of driving profiles and assigned to BEVs within each simulation. Further, factors are the random order of simulating each BEV in each time step, the probabilistic assignment of home charger access to each BEV according to the overall home charger availability, and the probabilistic assignment of vehicle parameters to each BEV agent. The required sample size of 40 is derived as sufficient following the procedure described in Appendix A.

To increase the speed of all simulations, the pyNetLogo extension [153] is used and set up to run the ABM eMob from Python in combination with the multiprocessing package [154]. This enables a parallelization of the simulation runs on multiple threads.

In step three, the solution space of all scenarios is restricted based on the SQCI. This leaves only the simulations with a sufficient number of charging points to supply the charging demand. In step four, the Pareto optimal set of scenarios is obtained. While the Pareto-optimum is primarily derived for the model coupling procedure, steps one to three are simultaneously used to analyze the impact on the charging peak and flexibility as required for research question three. Steps three and four are described in detail in the following Section.

5.1.1 Method to derive a Pareto optimal charging infrastructure design

Three essential criteria are considered here to design regional charging infrastructure networks. First, is the SQCI (cf. Section 4.2.1), which guarantees a sufficient supply of charging stations covering the dynamic charging demand within the entire region. Second is the regionally aggregated electrical charging peak of all charging processes, and the third is the regionally aggregated flexibility of all charging processes measured in shiftable electrical energy demand per day. The latter could be used, for instance, to relieve grid congestions or to integrate volatile energy sources if incentivized effectively. The aggregated charging peak load within the region is considered an indicator of the electricity grid's additional stress due to electric vehicles. Further, minimizing this peak load reduces the impact on the overall electricity system peak load of BEVs on the country energy system level. The effect of charging infrastructure on the occurring regional charging peak load is shown in Figure 4-11 in the first column.

To integrate all three criteria a multi-objective optimization is used. The suggested procedure finds a Pareto optimal charging infrastructure design regarding the three key model outputs SQCI, aggregated charging peak load within the region, and flexibility of the charging processes. The Pareto optimum is allocated by minimizing the charging peak within the region and maximizing the total available flexibility under the restriction of reaching a sufficient SQCI, as described below.

Suppose a scenario ω from the set of all scenarios Ω is defined by its output parameters $\mathrm{SQCI}_\omega \in SQCI$, the peak load $p_\omega \in P$, and the flexibility $f_\omega \in F$. The sets SQCI, P and F describe the service quality of the charging

infrastructure network, the peak load, and the available flexibility for all scenarios $\omega \in \Omega$. Those parameters define the mean values over all simulations of the same scenario ω. Each scenario ω is simulated 40 times and the set of scenarios Ω corresponds to the full factorial design according to the parameter variations in Table 5-2.

First, SQCI_ω defines, whether a simulated charging infrastructure network is sufficient to supply the regional charging demand. The set of feasible allocations is denoted as Ω^{S}, i.e.,

$$\Omega^{\mathrm{S}} = \{\omega \in \Omega: \mathrm{SQCI}_\omega \geq L\}, \tag{5-1}$$

where *L* is the threshold for the SQCI. A threshold of 99.6% is defined by taking the upper 95% confidence interval of the SQCI of 40 repeated simulations of a scenario with unlimited charging stations at work, public, and home locations. Not reaching an SQCI of 100% is because the considered driving profiles are based on ICE cars and not BEVs, while the modeled charging station network is designed to maximize the driver's comfort without consideration of detours and additional stops for recharging (cf. Section 4).

Further, Pareto optimal scenarios are identified based on two objectives: the minimization of p_ω (Equation (5-2)) and the maximization of f_ω (Equation (5-3)). Thereby, p_ω is the maximum charging power in one time step as sum over all vehicles *i* (Equation (5-4)). And f_ω is defined as the daily averaged flexibility over all charging processes (Equation (5-5)).

$$\min_{\omega \in \Omega^{\mathrm{S}}} p_\omega \tag{5-2}$$

$$\min_{\omega \in \Omega^{\mathrm{S}}} f_\omega \tag{5-3}$$

$$with\ p_\omega = \max_{\mathrm{t} \in \mathrm{T}} \sum_{i=1}^{M^{\mathrm{BEV}}} p_{\omega,i,t}^{\mathrm{charge}}, \forall \omega \in \Omega^{\mathrm{s}} \tag{5-4}$$

$$and\ f_\omega = \frac{\left(\sum_{i=1}^{M^{\mathrm{BEV}}} \sum_{t=1}^{T} f_{\omega,i,t}^{\mathrm{charge}}\right)}{N^{\mathrm{days}}}, \forall \omega \in \Omega^{\mathrm{s}} \tag{5-5}$$

$p_{\omega,i,t}^{\mathrm{charge}}$ is the electrical charging power of BEV *i* in scenario ω at time step $t \in T = \{1, \dots T^{\mathrm{s}}\}$. T^{s} is the last time step of the simulation period T. $f_{\omega,i,t}^{\mathrm{charge}}$ is the available shiftable energy of a BEV's charging process with N^{days} representing the number of simulated days and M^{BEV} is the total number of simulated BEVs.

Both objectives can be formulated as maximization by introducing the set of target values $u_j(\omega)\ with\ j \in \{p, f\}$ for each scenario ω, with

$$u_p(\omega) = -p_\omega, u_f(\omega) = f_\omega. \tag{5-6}$$

Finally, the strongly Pareto optimal allocation with $\omega', \omega'' \in \Omega^{\mathrm{s}}$ is formulated as:

$$\omega' \text{ is pareto optimal:} \Leftrightarrow \neg\left(\exists \omega'': \left(\forall j: u_j(\omega'') \geq u_j(\omega')\right) \wedge \left(\exists j: u_j(\omega'') > u_j(\omega')\right)\right) \tag{5-7}$$

The set of all Pareto efficient scenarios, for which Equation (5-7) is valid, is then summarized as $\Omega^{\mathrm{po}} \subseteq \Omega^{\mathrm{s}}$.

5.1.2 Comparison of two Pareto optimal charging infrastructure designs

Reasonable compositions of different charging stations at different locations are derived as Pareto optimal set through multiple simulations in the ABM as described in Section 5.1. Two different charging infrastructure designs are assessed and subsequently used in the ESDP (cf. Section 5.2). This allows here to compare the impact of different designs on the MMES.

Therefore, two Pareto optimal charging infrastructure designs are selected from the set of all Pareto optimal scenarios Ω^{po} with respect to the objectives as formulated in Equations (5-8)-(5-9). Following the procedure presented in [155], this is firstly the Pareto optimal scenario ω^{p} from the set of Pareto optimal scenarios Ω^{po} with the lowest charging peak

$$\omega^{\mathrm{p}} = \arg\min_{\omega \in \Omega^{\mathrm{po}}} p_{\omega} \tag{5-8}$$

and secondly, the scenario ω^{f} with the highest flexibility

$$\omega^{\mathrm{f}} = \arg\max_{\omega \in \Omega^{\mathrm{po}}} f_{\omega}. \tag{5-9}$$

Figure 5-4 shows the Pareto frontier and the two selected scenarios ω^{f} and ω^{p}, which are used to parametrize two scenarios in the ESDP (cf. Section 5.2).

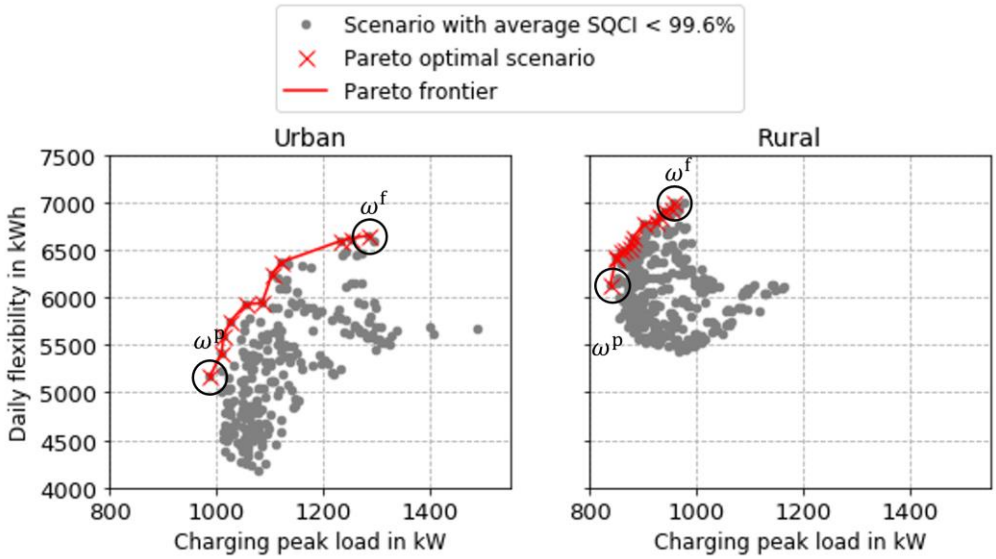

Figure 5-4 – Pareto optimal charging infrastructure scenarios and identified extreme scenarios ω^{f} and ω^{p} for the urban and rural areas.

Table 5-3 summarizes the simulated number of charging points in both scenarios, and Table 5-4 summarizes the key differences of both scenarios, which are used as input parameter in the model coupling. The charging costs for 2045 in Table 5-4 presume a cost reduction potential of 20% compared to 2020.

The charging infrastructure network scenario with the minimal peak load requires only up to 50% of the number of chargers of the High Flexibility scenario ω^{f} (cf. Table 5-3). Work chargers exceed the public chargers in rural areas by factor three in the Low Peak scenario ω^{p}. A balanced number of work and public chargers occurs in the urban area in ω^{p} as well as in the High Flexibility scenario in both regions. The DCFC coverage is converted to a required number of fast chargers so that the maximum fast charging peak load is satisfied. This results in two to three DCFC chargers of 50 kW and three to five 150 kW DCFC chargers per 1000 BEVs. To interpret this number, it needs to be reminded that transit and long-distance travel during holiday is not explicitly considered in this scenario, which could result in a higher number. The table shows that the highest flexibility occurs by maximizing the number of work and public chargers.

Both scenarios differ by factor two in terms of charging infrastructure network utilization (cf. Table 5-4). This is defined based on the maximum number of simultaneously occupied chargers (3.7 kW-150 kW). The maximum utilization here is 26.6% occurring in the simulated urban area. It means that serving a maximum charging peak load of 5.2 MW per 1000 BEVs (cf. Figure 5-4) requires four times as much charger capacity in the entire charging network in the region. This utilization rate is relevant for the model coupling procedure. The capital expenditures per 1000 BEVs for a Low Peak network reach from 1.8 million € (urban) to 2 million € (rural) and for a High

Flexibility network from 2.9 million € (urban) to 3.2 million € (rural)[3]. Lower costs in urban areas are mainly due to the assumed lower number of home chargers. The specific capital expenditure of a charging infrastructure network ranges from 239 €/kW to 330 €/kW. Those specific costs must be considered jointly with the maximum utilization rate of the network in an MMES optimization.

	Minimum peak load scenario, ω^p	**Maximum flexibility scenario, ω^f**
Number of home chargers (3.7kW)	Rural: 840 Urban: 600	Rural: 840 Urban: 600
Number of public chargers (22kW)	Rural: 20 Urban: 50	Rural: 200 Urban: 200
Number of work chargers (11kW)	Rural: 66 Urban: 50	Rural: 200 Urban: 200
Number of city chargers (50kW)	Rural: 3 Urban: 3	Rural: 2 Urban: 3
Number of highway chargers (150kW)	Rural: 3 Urban: 5	Rural: 3 Urban: 5

Table 5-3 – Pareto optimal number of charging points in a rural and urban area per 1000 BEVs.

The assumed individual charging station cost for the conducted network cost calculation, including a 20% cost reduction until 2045, are 1360 € for a home charger, 4400 € for 11 kW-22 kW charging stations with two plugs, 20 thousand € per 50 kW charging point, and 50 thousand € per 150 kW charging point. Those assumptions are derived based on [14], [156], [157].

	Minimal peak load scenario, ω^p	**Maximum flexibility scenario, ω^f**
Total charging network capacity	Rural:4874kW Urban: 4770kW	Rural: 10258kW Urban: 9720kW
Maximum utilization factor of charging network	Rural: 21.7% Urban: 26.6%	Rural: 11.9% Urban: 17.2%
Capital expenditures of charging network in 2020	Rural: 2.01mio. € Urban: 1.78mio. €	Rural: 3.17mio. € Urban: 2.9mio. €
Capital expenditures of charging network in 2045	Rural: 1.6mio. € Urban: 1.4mio. €	Rural: 2.5mio. € Urban: 2.3mio. €
Specific costs of charging infrastructure network in 2045	Rural: 330.4€/kW Urban: 299€/kW	Rural: 247€/kW Urban: 239€/kW

Table 5-4 – Comparison of key parameters of two Pareto optimal charging infrastructure networks. Individual charging station costs for network cost calculation are based on [14], [156], [157], assuming a 20% cost reduction by 2045.

[3] The here calculated costs are in the range of the costs stated by Robinius et al. [14]: 40 billion € to 62 billion € of infrastructure costs per 20 million BEVs (about 40% BEV penetration), with charger network costs of about 73% of those total infrastructure costs. This amounts to 2 million € to 3.1 million € per 1000 BEVs. However, calculated costs in this thesis focus on a BEV penetration level of 80% in Germany.

5.2 Model coupling

The ABM eMob is used to generate input parameters for the charging processes of BEVs in ESDP, including their charging power, their flexibility, the charging infrastructure network costs, and its utilization rate. Parametrizing ESDP by applying the ABM eMob enables an accurate representation of the highly heterogeneous BEV charging processes in a linear country energy system optimization. The individual parametrization of charging stations, urban and rural regions, as well as vehicle technologies and behaviors, can be analyzed in the ABM eMob and then be aggregated for use in ESDP. Coupling both models enables a modeling framework from individual BEV and charger levels to an MMES representation on country.

Figure 5-5 shows the implemented soft coupling approach between the ABM eMob and the ESDP and the applied tools. The coupling is realized by three consecutive steps. The simulation of multiple scenarios in the ABM eMob, a data analysis and handover procedure, including the identification of Pareto optimal scenarios, and the ESDP model. Data from the ABM eMob are analyzed in Python and transferred to an Excel format, which can be used to parametrize the ESDP model. Time series for charging demand and available flexibility are prepared in Python, saved in Excel, and then uploaded to an SQL database, which is part of the ESDP model framework. Cost parameters and average utilization of the charging infrastructure network are derived in an additional assessment in Python and are assigned together with the corresponding time series for charging demand and flexibility to the conversion process of charging infrastructure networks in the MMES parametrization in ESDP.

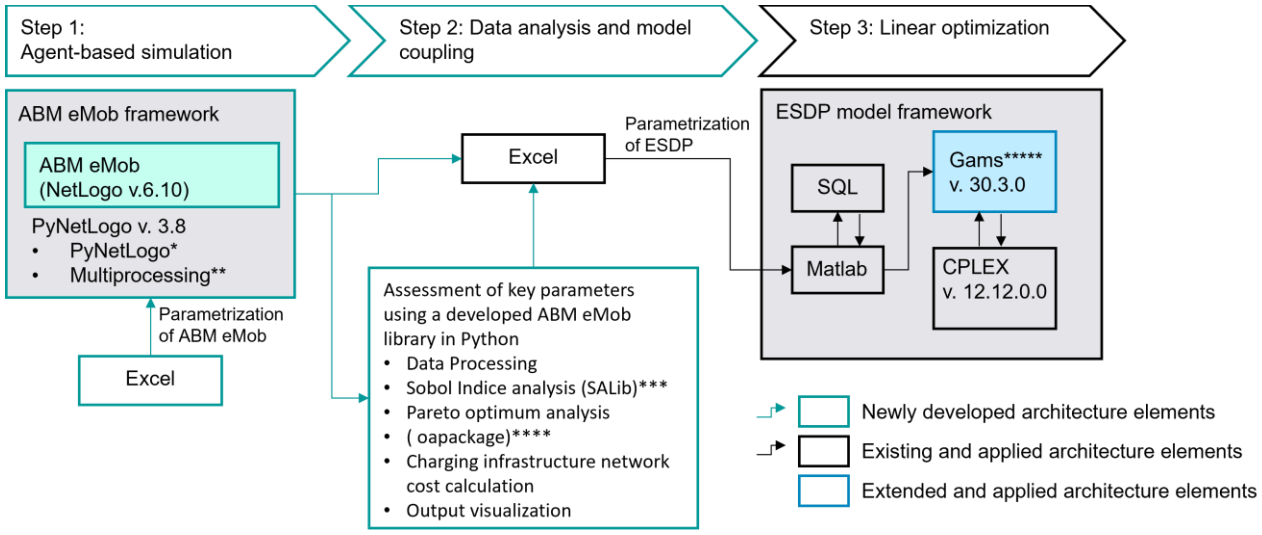

Figure 5-5 – Soft coupling of the ABM eMob and the ESDP in three steps.

As shown in Figure 5-6, two charging infrastructure network conversion processes are modeled in ESDP. Electricity from the distribution grid can flow into both conversion processes. The commodity ‘electricity BEV’ as conversion process output represents the energy flowing into the BEVs’ battery in a consecutive conversion process. Both charging infrastructure conversion processes represent an entire charging infrastructure network, including 3.7-22 kW AC chargers at home, work, and public, and DCFC chargers with 50 kW to 150 kW. To accurately represent the flexibility of a fleet of BEVs with different possible delay times of each charging processes, the aggregated charging profiles are disaggregated according to their possible delay times. Therefore, each charging network conversion process generates four different output commodities. One of them is a static output, representing charging processes, which cannot be shifted in time. Another one reflects charging processes with short-term flexibility of delay times up to three hours. These processes occur predominantly in public locations. The second flexible process represents medium-term delay times between four and nine hours, occurring predominantly at work. And finally, long-term shiftable processes with more than ten-hour delay times

predominantly occur at home. The share of each output commodity from the total energy output is predefined by the annual energy share of the total aggregated charging profile, and the energy of each output commodity, e1, e2, e3, and e4. The temporal distribution of e1 to e4 follows a predefined charging demand profile.

To incorporate an accurate representation of the BEVs' flexibility, a demand-side management method is newly integrated into ESDP, which is applied to the charging infrastructure representation with respect to the output commodities that have a delay time other than zero (e2, e3, e4). This method enables the optimizer to alter the predefined charging profile in the range of the corresponding delay time. A detailed description of the demand side management for electric vehicle charging follows in Section 5.2.1, the derivation of the electric charging demand profiles from the ABM eMob in Section 5.2.2, and the corresponding flexibility parameters for the demand side management approach are derived in Section 5.2.3.

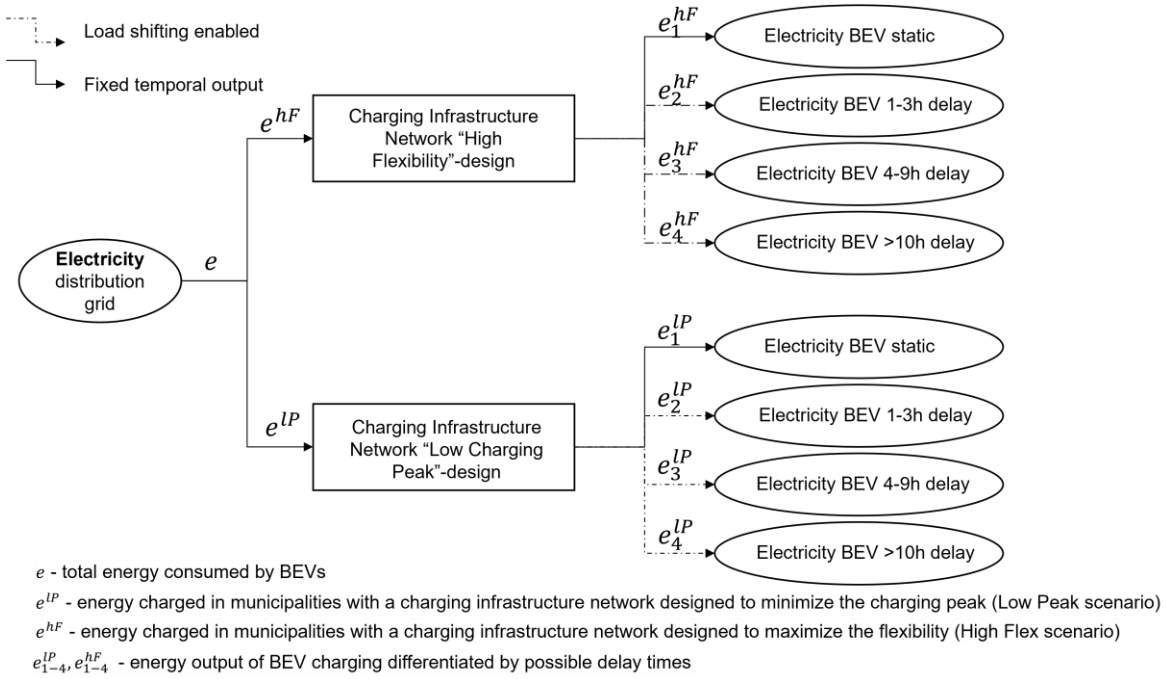

Figure 5-6 – Representation of charging infrastructure networks for electric passenger vehicle fleets and their flexibility in ESDP.

5.2.1 Demand side management for battery electric vehicles in ESDP

The model coupling procedure is developed to accurately parametrize charging infrastructure, BEV charging processes, and their corresponding flexibility. Several challenges exist when modeling electric vehicles in a large energy system model with a regionally aggregated representation of technologies. First, the charging of vehicles depends on time and location of each BEV, and the corresponding flexibility is restricted to the parking duration. Those aspects are not trivial to represent in an energy system model but might be approximated by modeling a virtual battery for the BEV charging process. Such a model only represents, e.g., one huge battery for all vehicles or, if differentiated, e.g., one for each user group. However, using a battery cannot circumvent the effect that one vehicle charges electricity and another vehicle drives with this electricity from the single modelled battery. The high flexibility of a large battery for all BEVs without temporal restrictions of how long energy can be stored does also not consider regular charging and parking behaviors such as modeled in the ABM eMob. If driving and charging behavior is considered, only approximately 10% to 20% of the battery capacity of a fleet of BEVs can

be used for flexibility provision [118]. Additionally, the timing of delayed charging processes is restricted by the SOC of each BEVs battery and the parking duration. If the SOC of each BEV and the parking duration are not considered, unrealistic state of charges might be neglected. In contrast to the approach of modeling a battery, considering a fixed load profile ensures a reasonable temporal distribution of the electricity demand of BEVs but it would not allow covering the flexibility of charging processes. Finally, a more realistic and flexible charging load can be obtained if the number of parking vehicles is used to derive the maximum possible power input and output of a battery in each time step. But this approach still considers a single large battery and cannot ensure the temporal and spatial consistency of the SOC of the fleet of vehicles.

As one particular requirement for the accurate representation of the flexibility of BEVs in an MMES, it must be assured that the parking duration can be considered to only charge the battery when a vehicle is parking at the corresponding charging station. Therefore, the battery equation (3-17) is not suitable, but an alternative set of equations needs to be able to restrict the charged energy to only occur during the parking time of vehicles.

In the following, a procedure for dealing with these challenges is proposed in three steps:

1. A fixed charging profile is derived from the ABM eMob and set in ESDP for BEV charging.
2. A charging infrastructure network design consisting implicitly of different types of chargers and locations to ensure a consistent charging station network design together with the derived charging profiles is modeled (cf. Figure 5-6).
3. The flexibility of charging processes is represented based on an existing, but here adjusted, and extended load shifting method for linear energy system optimization, as described in the following. Its parametrization using the ABM eMob is described in subsections 5.2.2-5.2.3.

The integrated demand-side management implementation here is based on Zerrahn et al. [158], who published a method to represent load shifting in linear energy system models. This method is applied in other energy system models and can therefore be considered as state of the art here [159], [160]. To couple the ESDP and the ABM eMob, this method is, on the one hand, tailored to the use of BEV charging processes and, on the other hand, kept general enough to represent additional load shifting processes in future applications, which are not in the scope of the present thesis.

The following adjustments to the approach presented in [158] are made:

- Introduction of investment cost for investments in, for instance, load management systems and variable costs for the shifted energy (cf. Equation 5.55-5.56)
- Differentiation between forward and backward load shift time and therefore, allowing asymmetric shift times: This is, e.g., required to couple the model based on the charging strategy ‘charge at arrival’, for which only a forward shift in time is reasonable because the original load profile is based on BEVs starting to charge immediately at their arrival.
- Upshift and downshift restrictions relative to the conversion process variables instead of restrictions based on absolute input parameters: This allows optimizing the capacity of the entire conversion process for a target year or over multiple years while the relative maximum load shift potential is restricted to the optimized conversion process capacity.
- The equations are adjusted to be used in a multi-region model and thus contain a regional variable component.

The method, which is implemented in GAMS, is described subsequently. It is based on an energy demand time series as input and enables the optimizer to deviate from that profile as illustrated in Figure 5-7.

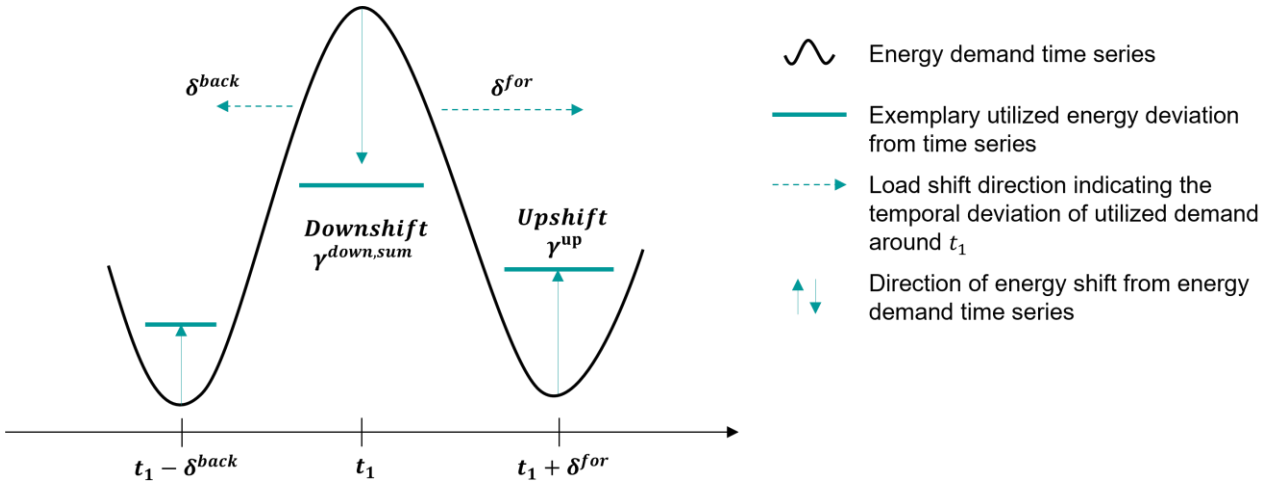

Figure 5-7 – Illustration of load shifting approach based on a given energy demand time series with asymmetric forward and backward shift times.

Three newly introduced variable sets $\gamma^{\text{up}}_{cs,y,t,x}$, $\gamma^{\text{down}}_{cs,y,t,\text{tt},x}$ and $\gamma^{\text{down,sum}}_{cs,y,t,x}$ with

$$\gamma^{\text{up}}_{cs,y,t,x} \geq 0 \; and \; \gamma^{\text{down}}_{cs,y,t,\text{tt},x} \geq 0 \tag{5-10}$$

$$\sum_{tt=t-\delta^{\text{back}}_{cs}}^{t+\delta^{\text{for}}_{cs}} \gamma^{\text{down}}_{cs,y,t,tt,x} = \gamma^{\text{down,sum}}_{cs,y,t,x} \tag{5-11}$$

represent the total power being shifted upwards ($\gamma^{\text{up}}_{cs,y,t,x}$) in one time step *t* and the power shifted downwards ($\gamma^{\text{down}}_{cs,y,t,\text{tt},x}$, $\gamma^{\text{down,sum}}_{cs,y,t,x}$) from the demand time series. The indices indicate that the implementation allows a regional differentiation of shifted load, which means that a downshift in a region $x_1 \in X$ must be accompanied by an upshift in region x_1 according to Equation (5-12), which couples the up- and downshift variables in time to temporally redistribute the energy demand within the allowed shift times $\delta^{\text{back}}_{cs}$ and δ^{for}_{cs}. $\gamma^{\text{down}}_{cs,y,t,\text{tt},x}$ is a downshift in time step *tt*, which is linked to an upshift in t. $\gamma^{\text{down,sum}}_{cs,y,t,x}$ is a variable, which is used to simplify the equations and can be interpreted as the total downshift in one time step *t*. This total downshift ($\gamma^{\text{down,sum}}_{cs,y,t,x}$) can consist of multiple downshifts ($\gamma^{\text{down}}_{cs,y,t,\text{tt},x}$) each being linked to upshifts in different time steps.

Potential efficiency losses due to the load shift are set by the parameter η^{dsm}_{cs}. The following set of equations (5-12)-(5-22) is valid for each time step $t \in T$, each region $x \in X$, each year $y \in Y$, and for each conversion subprocess $cs \in CS$ with the forward or backward shift time being greater than zero.

$$\eta^{\text{dsm}}_{cs} * \gamma^{\text{up}}_{cs,y,t,x} = \sum_{tt=t-\delta^{\text{for}}_{cs}}^{t+\delta^{\text{back}}_{cs}} \gamma^{\text{down}}_{cs,y,t,tt,x} \tag{5-12}$$

Equation (5-12) allows shifting a unit of load, which was scheduled according to a specified normalized time series $P^{\text{out,norm}}_{cs,x,t}$, forward or backward in time. Corresponding load shift restrictions are formulated in equations (5-13)-(5-16), defining the maximum deviation from the energy demand time series in each time step t.

$$\gamma^{\text{up}}_{cs,y,t,x} \leq k_{cs,y,x} \cdot V^{\text{avg}}_{cs,y,x} \cdot K^{\text{up,max}}_{cs,y,x} \tag{5-13}$$

$$\gamma^{\text{down,sum}}_{cs,y,t,x} \leq p^{\text{out}}_{cs,y,t,x} \cdot K^{\text{do,max}}_{cs,y,x} \tag{5-14}$$

$$\gamma^{\text{up}}_{cs,y,t,x} + \gamma^{\text{down,sum}}_{cs,y,t,x} \leq \max\left\{K^{\text{up,max}}_{cs,y,x} \cdot P^{\text{out,max,norm}}_{cs,x}, K^{\text{do,max}}_{cs,y,x} \cdot P^{\text{out,norm}}_{cs,x,t}\right\} \cdot \frac{e^{\text{out,tot}}_{cs,y,x}}{\Delta t \cdot w} \tag{5-15}$$

$$\gamma^{\text{up}}_{cs,y,t,x} + \gamma^{\text{down,sum}}_{cs,y,t,x} \leq k^{\text{dsm}}_{\text{cs,y,x}} \tag{5-16}$$

Equations (5-13) and (5-14) restrict the upshifted and downshifted energy within a single time step. Deviating from the formulation from Zerrahn and Scholl, the upshifted and downshifted energy here are not restricted based on an absolute capacity. Instead, the maximum upshift is set in percent of the variable defining the installed conversion process capacity $k_{cs,y,x}$ of the conversion process, its average technical availability $V^{\text{avg}}_{cs,y,x}$ parameter and the parameter $K^{\text{up,max}}_{cs,y,x}$, which describes the maximum upshift in percent of the installed conversion subprocess capacity. This allows optimizing the conversion process capacity and its load shift capacity simultaneously, with the load shift capacity being restricted in relation to the installed conversion process capacity. Applying this to BEV charging, it can be interpreted in a way that the available controlled charging capacity is restricted based on the installed charging stations. In contrast, the parameter $k^{\text{do,max}}_{cs,y,x}$ in Equation (5-14) restricts the downshifted energy in time step *t* in percent of the load of the energy demand time series in *t*. For a fleet of BEVs, it means that if, e.g., 90% of the charging load in *t* would be available for a shift in time and that at least 10% of the charging vehicles are not available for flexibility provision. According to the changes in equations (5-13) and (5-14) and the formulation presented by Zerrahn and Scholl, Equation (5-15) restricts the combined up and downshift energy as the maximum of the restrictions in Equations (5-13) and (5-14). The formulation here must rely on the energy output $e^{\text{out,tot}}_{cs,y,x}$ of the conversion process to avoid a non-convex formulation if variables such as $p^{\text{out}}_{cs,y,t,x}$ (cf. Section 3) would be considered within the 'max'-statement. Therefore, the formulation refers to $P^{\text{out,norm}}_{cs,x,t}$, the given time series with 8760 values normalized to the sum over all its values, and its maximum value $P^{\text{out,max,norm}}_{cs,x} \in P^{\text{out,norm}}_{cs,x,t}$. Finally, the capacity $\text{k}^{\text{dsm}}_{\text{cs,y,x}}$ within a region *x* is defined here as the maximum simultaneously occurring upshift and downshift per time step according to Equation (5-16). This is here interpreted as the capacity of the required load management systems to realize the maximum occurring load shift in time.

Further, the power balance equation for each conversion process[4] needs to be formulated as in Equation (5-17) with $p^{\text{out}}_{cs,y,t,x}$ and $p^{in}_{cs,y,t,x}$ being the input and output energy per time step and η_{cs} the overall conversion process efficiency. This power balance equation is valid for conversion processes with a load shift time parameter greater zero.

$$p^{\text{in}}_{cs,y,t,x} - \gamma^{\text{up}}_{cs,y,t,x} + \gamma^{\text{down,sum}}_{cs,y,t,x} = \frac{p^{\text{out}}_{cs,y,t,x}}{\eta_{cs}} \tag{5-17}$$

This ensures the power balance within each time step. The time consistency of load shift capacities of a conversion process over multiple years is defined in Equation (5-18) as a sum over all years from the first considered year y^{first} to the year *y*.

$$k^{\text{dsm}}_{cs,y,x} = \sum_{y'=y^{\text{first}}}^{y} k^{\text{dsm,new}}_{cs,y',x} \tag{5-18}$$

$$k^{\text{dsm,new,tot}}_{cs,y} = \sum_{x \in X} k^{\text{dsm,new}}_{cs,y,x} \tag{5-19}$$

$$k^{\text{dsm,tot}}_{\text{cs,y}} = \sum_{x \in X} k^{\text{dsm}}_{cs,y,x} \tag{5-20}$$

[4] Only the power balance for the sum over all conversion processes is formulated in Section 3 (cf. Equation (3-6)), which now is only valid for all conversion subprocesses without demand side management.

Equations (5-19) to (5-20) define, as the sum over all regions, the total annually new and the total installed load shift capacity of a corresponding conversion process for each year, respectively.

Finally, three parameters representing the capital and operational expenditures of a load shift process are introduced (cf. Equations (5-21)-(5-22)) and integrated into the total cost equation here.

$$C_{cs,y}^{\text{capex,DSM}} = C_{cs}^{\text{inv}} \cdot k_{\text{cs,y}}^{\text{dsm,new,tot}} \tag{5-21}$$

$$C_{cs,y}^{\text{opex,DSM}} = \frac{1}{2}\sum_{t,x} C_{cs}^{\text{m}} \cdot (\gamma_{cs,y,t,x}^{\text{up}} + \gamma_{cs,y,t,x}^{\text{down,sum}}) \cdot \Delta t \cdot w + k_{\text{cs,y}}^{\text{dsm,tot}} \cdot C_{cs}^{\text{om}} \tag{5-22}$$

Capital expenditures C_{cs}^{inv} are based on the annual new installed capacity in Euro per kW. These costs can occur, for instance, for load management systems and communication technology that need to be installed to enable the load shift. The operational expenditures are set as marginal costs C_{cs}^{m} in Euro per kWh of the shifted load and as fixed operational and maintenance costs C_{cs}^{om} in Euro per kW per year of the total installed load shift capacity of a conversion process.

5.2.2 Electric charging profiles

Two annual charging profiles are generated for the two Pareto optimal scenarios with the minimum charging peak and the maximum flexibility of BEVs (cf. Equation (5-8)-(5-9)). The procedure is described for one region and then applied to a rural and an urban area.

As a first step, charging profiles for three representative periods, which each consist of four consecutive weeks, with low, medium, and high average ambient temperatures are simulated in the ABM eMob with an hourly time step. An hourly interval was chosen to match the time step in ESDP. Since ESDP requires yearly profiles of 8760 hours, the three simulated representative periods[5] are scaled to a full yearly profile based on the expected temperature-dependent energy consumption of the fleet of BEVs within each month of the year. The expected energy consumption for each period is derived based on the energy consumption in the three simulated representative periods. For that, a piecewise linear scaling is applied in dependency of the actual monthly averaged temperatures T^{avg}, the considered ambient temperatures T^{ambient} (cf. Section 4.2.1) in the three representative periods (set here to $T^{\text{low}}, T^{\text{mid}}, \text{and } T^{\text{high}}$), and the total energy demand of all BEVs within the considered region for each simulated representative period ($E^{\text{tot,low}}$, $E^{\text{tot,mid}}, \text{and } E^{\text{tot,high}}$).

Equation (5-23) defines the temperature-dependent scaling factor $f(T^{\text{avg}})$, which is interpreted as the energy demand of 1000 BEVs in dependency of the ambient temperature per period (cf. Figure 4-5 for the effect of temperature on the BEVs energy demand). If a normalized charging profile is multiplied by the scaling factor, one obtains charging profiles for the corresponding ambient temperature. This is used to create a yearly charging profile based on monthly deviating ambient temperatures. The scaling factor is obtained by interpolating between the BEVs' energy demand of the simulated representative period with the lowest and the medium temperatures $E^{\text{tot,low}}$ and $E^{\text{tot,mid}}$, as well as between the medium and the highest temperatures $E^{\text{tot,mid}}$ and $E^{\text{tot,high}}$. The actual monthly temperatures are here taken from the weather year 2012. T^{low} and T^{high} are chosen for the simulations so that they represent the lowest monthly averaged temperature and the highest monthly averaged temperature in 2012. Each representative period is simulated 100 times and the average energy demand is considered in the following.

[5] A total of 2016 hours was simulated: 4 weeks of 168 hours for three representative periods with low, medium, and high temperatures

$$f(T^{\text{avg}}(t)) = \begin{cases} E^{\text{tot,low}} + \dfrac{\left(E^{\text{tot,mid}} - E^{\text{tot,low}}\right)}{T^{\text{mid}} - T^{\text{low}}} \cdot T^{\text{avg}}, if\ T^{\text{avg}} \leq T^{\text{mid}} \\ E^{\text{tot,mid}} + \dfrac{\left(E^{\text{tot,high}} - E^{\text{tot,mid}}\right)}{T^{\text{high}} - T^{\text{mid}}} \cdot T^{\text{avg}}, if\ T^{\text{avg}} > T^{\text{mid}} \end{cases} \quad (5\text{-}23)$$

Then, the three simulated representative time series are normalized each to their monthly BEVs' energy demand and multiplied with the scaling factor $f(T^{\text{avg}}(t))$ (cf. Equation (5-24)). In other words, the normalized monthly charging profiles ($P^{\text{low}}_{t'(t)}, P^{\text{mid}}_{t'(t)}, P^{\text{high}}_{t'(t)}$) are multiplied by the expected energy demand within each month of the year. P_t with $t \in \{1, \dots, 8760\}$ is the resulting yearly charging profile, whereas the time of the year t defines the corresponding temperature $T^{\text{avg}}(t)$ according to the curve in Figure 5-8. $T^{\text{avg}}(t)$ is constant for each t in the same month. $P^{\text{low}}_{t'(t)}$, $P^{\text{mid}}_{t'(t)}$ and $P^{\text{high}}_{t'(t)}$ are the normalized charging profiles for the representative periods with the lowest, medium, and highest temperatures respectively and with $t'(t) = \{t \in \{1, \dots, 8760\} | t\ mod\ 672\}$ defined for exactly 4 weeks with hourly resolution (672 hours). The formulation of $t'(t)$ is used to link each hourly energy demand of, e.g., $P^{\text{low}}_{t'(t)}$ to an hour of the year with the same weekday and time of day.

$$P_t = \begin{cases} P^{\text{low}}_{t'(t)} f\left(T^{\text{avg}}(t)\right), if\ T^{\text{avg}}(t) \leq T^{\text{mid}} - \left(\dfrac{T^{\text{mid}} - T^{\text{low}}}{3}\right) \\ P^{\text{mid}}_{t'(t)} f(T^{\text{avg}}(t)), if\ T^{\text{mid}} - \left(\dfrac{T^{\text{mid}} - T^{\text{low}}}{3}\right) < T^{\text{avg}}(t) \leq T^{\text{mid}} + \left(\dfrac{T^{\text{mid}} - T^{\text{low}}}{3}\right) \\ P^{\text{high}}_{t'(t)} f\left(T^{\text{avg}}(t)\right), if\ T^{\text{avg}}(t) > T^{\text{mid}} + \left(\dfrac{T^{\text{mid}} - T^{\text{low}}}{3}\right) \end{cases} \quad (5\text{-}24)$$

Figure 5-8 shows the scaling factor (total charged energy within four consecutive weeks per 1000 BEVs) for each month of the year. Additionally, the average temperatures $T^{\text{avg}}(t)$, including day and night temperatures of the year 2012, are depicted for the location Schleswig within the NUTS2 region Schleswig-Holstein. Adjusting the average temperatures to the hours of the day in which most driving activities are expected is not considered as hourly and daily temperature variations are not considered in the simulation. This is justifiable here since the introduced error by predicting hourly temperature variations based on historic data is assumed significantly greater than the error by using a monthly average value. The latter still accounts reasonable for the seasonal differences in temperature, which cause larger temperature deviations than hourly variations.

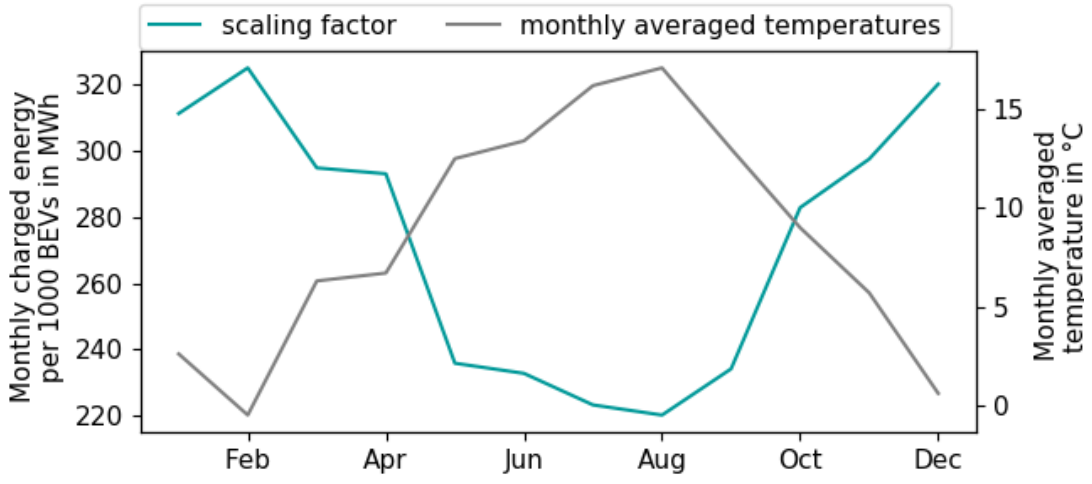

Figure 5-8 – Temperature-dependent scaling of monthly charging demand based on the weather year 2012. The scaling factor refers to the monthly charged energy normalized to a fleet of 1000 BEVs.

Finally, the yearly charging profiles P_t, which are derived for the rural (P_t^{rural}) and the urban area (P_t^{urban}), are scaled from the municipality level to the NUTS2 level (cf. Equation (5-25)). The same scaling procedure is also applied for the flexibility, the average utilization of the charging infrastructure network, and the charging infrastructure costs. In Equation (5-25), weighting factors ($N_x^{\text{cars,tot,urban}}$ and $N_x^{\text{cars,tot,urban}}$) representing the total numbers of all vehicles in urban and rural municipalities within one NUTS2 region *x* are multiplied with the rural and urban charging profiles based on each municipality's RegioStaR classification and the BEV penetration rate S^{BEV} of the scenario. This represents for each NUTS2 region *x* the corresponding mixture of BEVs in urban and rural municipalities. The number of urban and rural vehicles is divided by 1000 since P_t^{urban} and P_t^{rural} are normalized to 1000 BEVs.

$$P_{x,t}^{\text{charge}} = \left(P_t^{\text{urban}} \frac{N_x^{\text{cars,tot,urban}}}{1000} + P_t^{\text{rural}} \frac{N_x^{\text{cars,tot,rural}}}{1000} \right) \cdot S^{\text{BEV}}, \quad \forall x \in X, t \in T \tag{5-25}$$

Figure 5-9 shows exemplarily the regional charging infrastructure requirements of public chargers on the municipality level for 20% BEV penetration in Germany. Values of zero indicate a lack of data in the data set. The resulting seasonal variations of the electrical charging demand as well as regional differences on the NUTS2 level are shown in Figure 5-10 as overlapping line plots. Here, regional differences in electrical charging demand are predominantly determined by the population and the number of vehicles per region. It reveals that the electricity demand and its corresponding peak load decrease in summer to 64% of the winter charging peak. Further, it shows the region Duesseldorf as the region with the highest expected electricity demand from electric vehicles and the state of Bremen with the lowest expected demand. The difference in charging demand can be explained by the differences in population and number of vehicles.

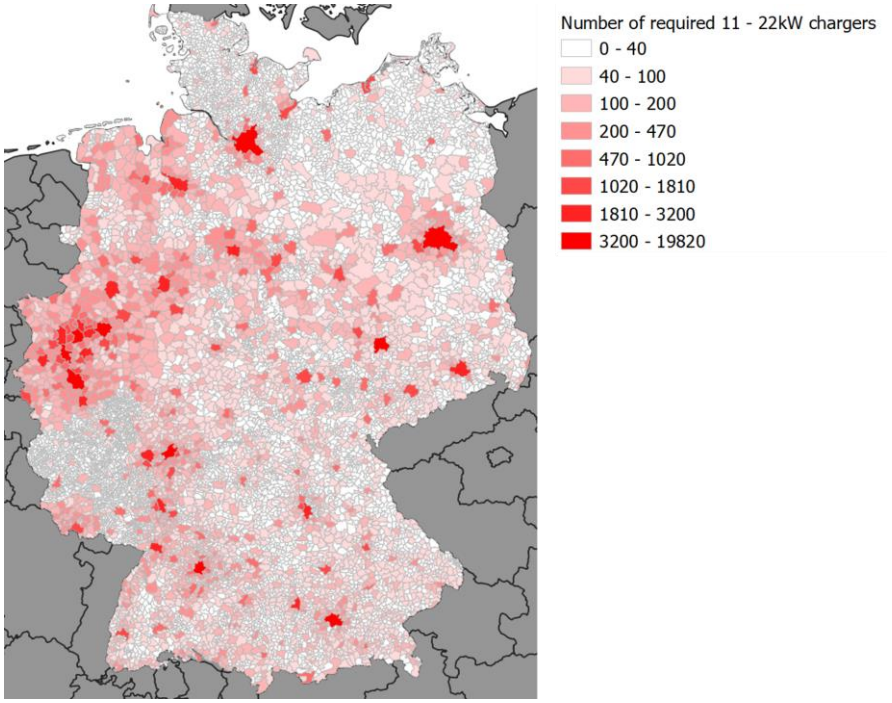

Figure 5-9 – Regional requirements of 11 – 22 kW chargers at work and public places on the municipality level for a BEV penetration of 20%.

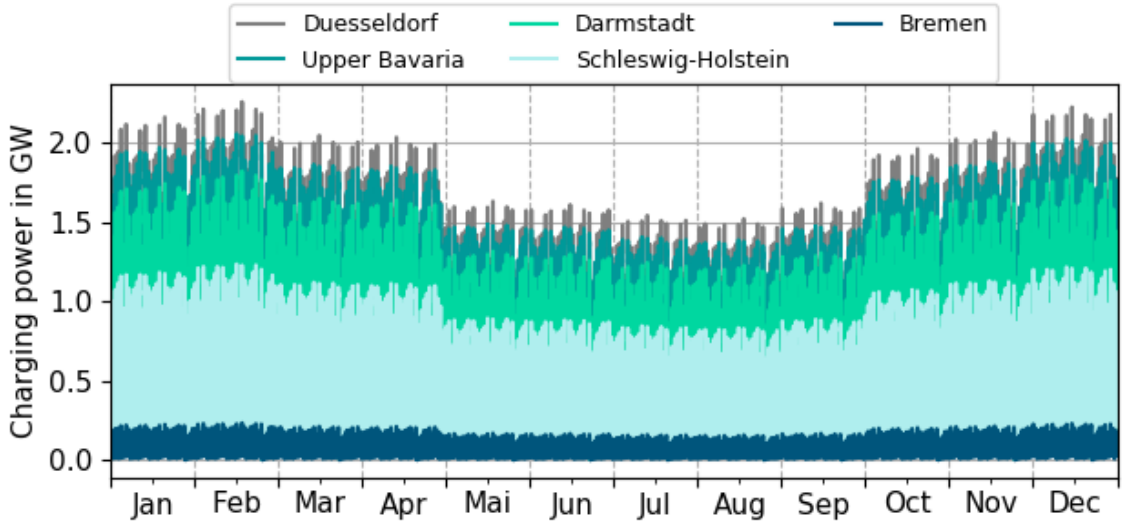

Figure 5-10 – Aggregated charging profiles at 80% BEV penetration in five exemplary NUTS2 regions for 8760 hours of the year, considering the Pareto optimal charging infrastructure design with the minimal charging peak load. Curves are overlapping each other.

Figure 5-11 shows the final derived aggregated charging profiles for the entire country for one exemplary week normalized to the annual BEVs' energy demand. The shown two charging profiles represent the two considered Pareto optimal charging infrastructure network designs. The figure shows that the 'high Flexibility' charging infrastructure design significantly increases the morning and evening charging load. In contrast, the 'low Peak' design has a more evenly distributed charging demand over the day, resulting in a lower peak and higher demand during midday and at night compared to the 'high Flexibility' scenario. The difference between both charging profiles shows the importance of accurately considering charging infrastructure networks when assessing the electrical charging load. In general, the figure indicates that a high availability of charging infrastructure as in the 'high Flexibility' scenario - or even not restricting the availability of charging infrastructure in a BEV simulation - can result in significantly higher projected charging peaks of a fleet of BEVs of up to 30% compared to a charging infrastructure design scenario, which minimizes the peak load.

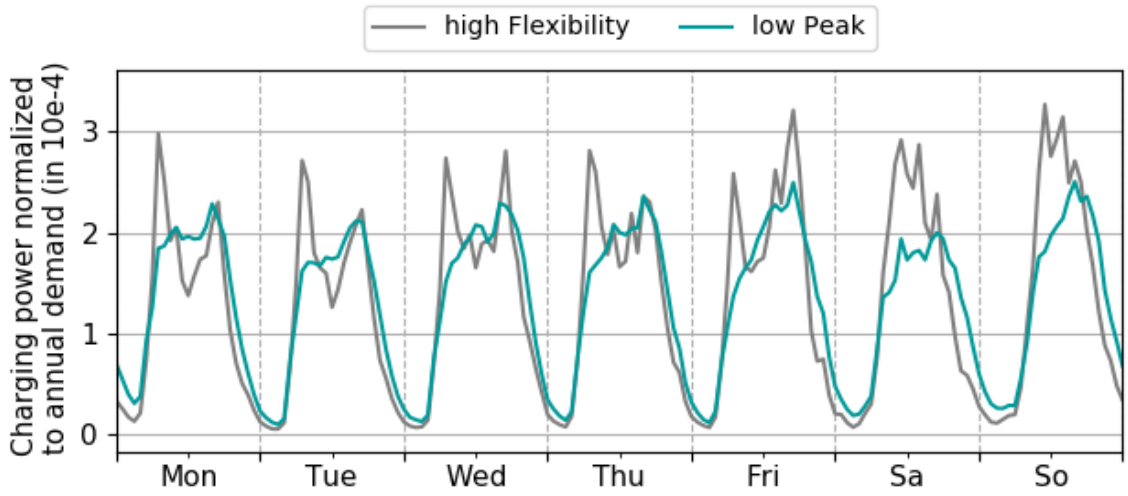

Figure 5-11 – Aggregated charging profile for Germany for an exemplary week normalized to the total annual charging demand in Germany for the two Pareto optimal charging infrastructure designs with the minimal charging peak (low Peak) and the maximum available flexibility (high Flexibility).

5.2.3 Flexibility of charging profiles

The applied representation of charging infrastructure and the demand side management method for the output commodities with a delay time greater than zero (cf. Figure 5-6) requires the following inputs to characterize the flexibility: one or multiple flexible charging profiles per NUTS2 region with a corresponding maximal delay time, one static charging profile per NUTS2 region representing the charging processes, which cannot be shifted in time, and the share of energy output per applied charging and flexibility time series. The fixed energy share guarantees that the optimizer does not use, e.g., only the process with the highest flexibility. This fixed energy share is required, since the aggregated profiles originate from individual charging processes of BEVs in the ABM eMob, which correspond to exact parking durations, states of SOC and available charging power ratings.

A yearly charging profile $P_{x,t}^{\text{charge}}$ is subdivided into a static time series $P_{x,t}^{\text{static}}$ and multiple flexible charging time series $P_{x,t,D_1,D_2}^{\text{flex}}$. The flexible time series are charging profiles, which are defined by a range of realizable minimum and maximum delay times (D_1 and D_2) of the individual charging processes. This allows to derive multiple flexible charging time series for parametrization of the MMES in ESDP which correspond to charging processes

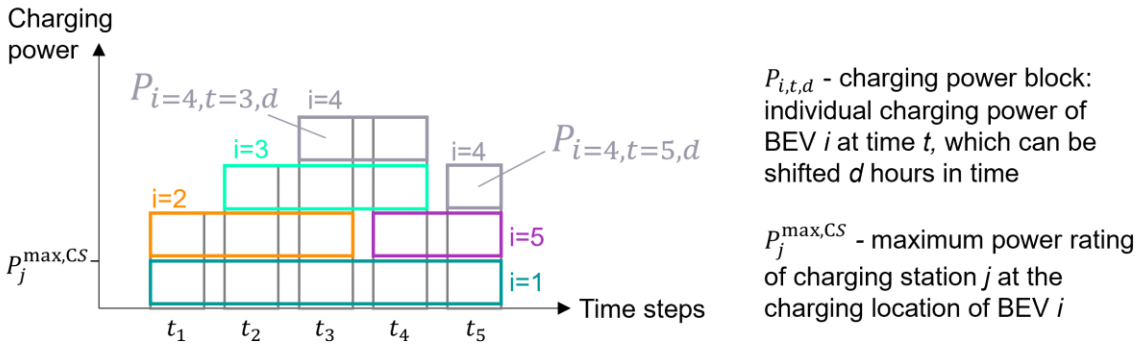

Figure 5-12 – Decomposition of charging processes of BEVs into individual charging blocks $P_{i,t,d}$.

with different realizable delay times. To obtain the decomposed charging profiles, the profile $P_{x,t}^{\text{charge}}$ is decomposed into its individual charging power blocks $P_{x,i,t,d}$ as indicated in Figure 5-12, keeping for each block the information of its potential delay time *d*. All charging power blocks are obtained from the ABM eMob. One charging power block is here defined as the charged energy of a single BEV *i* in time step *t*, which can be shifted in time for up to *d* hours. Then, for each hour of the year the charging power blocks of all BEVs $i = \{1, \dots, I\}$, which correspond to a specified range of realizable delay times[6] $D_1 \leq d < D_2$, are aggregated according to Equations (5-26) and (5-27).

Equation (5-26) describes the static charging demand, which cannot be shifted in time. Equation (5-27) shows the aggregation of flexible charging power blocks with a specified time shift range between D_1 and D_2. The flexible charging blocks are clustered by applying Equation (5-27) with the delay times 1-3 hours, 4-9 hours, and greater than ten hours to differentiate between different delay times.

$$P_{x,t}^{\text{static}} = \sum_{i=0}^{I} P_{x,i,t,d=0} \quad \forall t \in T, x \in X \tag{5-26}$$

$$P_{x,t,D_1,D_2}^{\text{flex}} = \sum_{i=0}^{I} \sum_{d=D_1}^{D_2} P_{x,i,t,d} \quad \forall t \in T, x \in X \tag{5-27}$$

[6] $d_{i,1}$ and $d_{i,2}$

Figure 5-13 shows the final subdivided charging profiles ($P_t^{\text{static}}, P_{t,1,3}^{\text{flex}}, P_{t,4,9}^{\text{flex}}, P_{t,10,50}^{\text{flex}}$) and the total charging profile P_t^{charge} for the two assessed Pareto optimal scenarios aggregated for Germany (sum over all NUTS2 regions *x*) considering 80% of BEV penetration. The charging peak differs in both charging infrastructure scenarios by 10 GW. It reveals that significantly more electricity demand cannot be shifted in time in the Low Peak scenario than in the High Flexibility scenario. The short-term flexibility below 3 hours delay time is scattered across the day, reaching its maximum on the weekend. Medium-term flexibility between 4 - 9 hours delay time occurs predominantly during the morning hours at workplaces. This flexibility is significantly higher in the flexible charging infrastructure scenario due to the higher availability of work chargers. While at the evening charging peak around 5 pm, a high share of long-term flexibility with delay times greater than ten hours is available, the possible delay time reduces during late evening and night hours. The available long-term flexibility reaches its maximum on Friday to Sunday since most vehicles are not leaving home as early in the next morning compared to weekdays. In general, the Low Peak scenario has a higher share of potential delay times greater than ten hours, and the High Flexibility scenario has a larger share of charging processes, which can be shifted for 1-3 hours. This is mainly due to an increased charging demand at home in the Low Peak scenario due to lower public and work charger availability. This statement is valid for the here applied charge at arrival strategy.

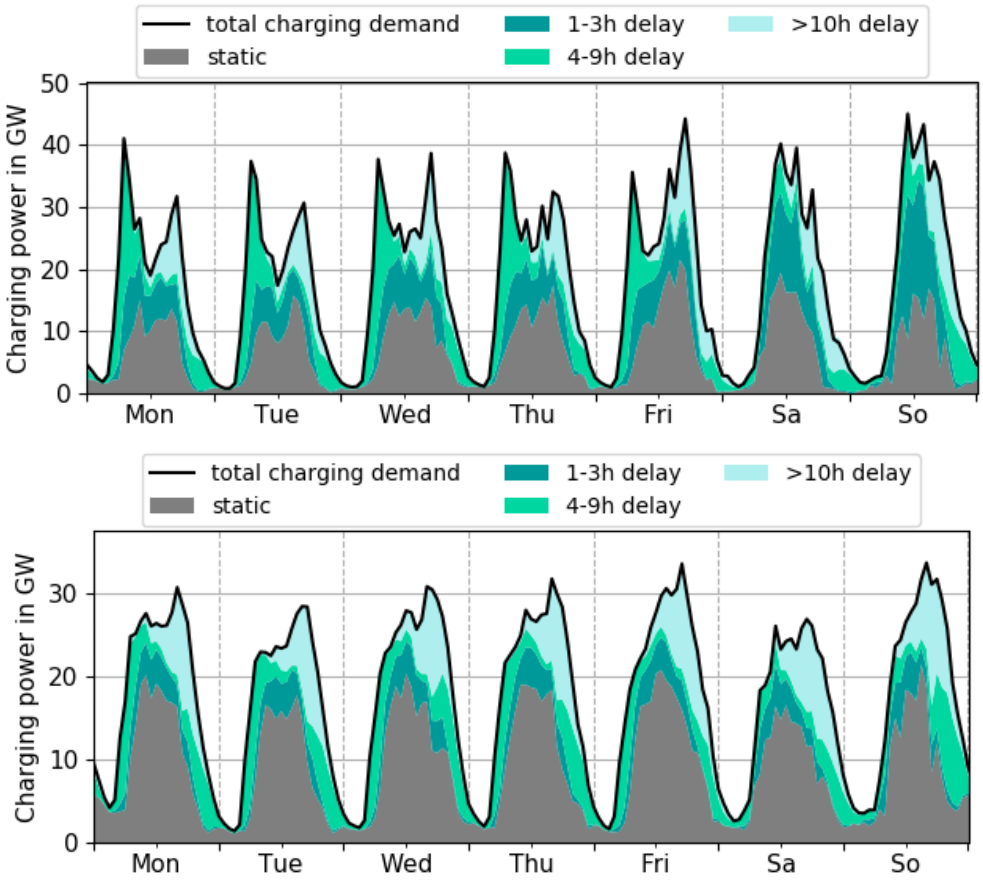

Figure 5-13 – Charging demand of High Flexibility (upper) and Low Peak (lower) charging infrastructure scenario for an exemplary week (Monday-Sunday) decomposed into different realizable delay times.

5.3 Techno-economic parametrization of the MMES

The implemented MMES model in ESDP is based on a model of the German electricity sector as published by Kolster et al. [123]. It is spatially resolved to 38 NUTS2 regions in Germany and twelve energy exchange countries, resolved to the country-level: Austria, Belgium, Switzerland, Czech Republic, Denmark, France, Luxembourg, Netherlands, Norway, Poland, and Sweden. All 38 NUTS2 region names are shown in Appendix B and referred to throughout the thesis. The original model includes electricity and heat sector technologies relevant for the application to the year 2030 and to assess the potential of flexibility provision from distribution grids to the transmission grid. It consists of a representation of the German AC and DC grid as planned for the year 2030. The implementation here sets up on the same set of technologies but extends the scope towards an MMES adding the mobility sector, including charging and refueling infrastructure, energy transport infrastructure for methane and hydrogen, synthesis technologies for electricity-based fuel production, and technologies for the supply of hydrogen, including, for example, international import routes, and hydrogen usage in gas turbines. Further, all technologies in the model are parametrized for the year 2045 regarding capacity and energy constraints where applicable, as well as cost assumptions. All following parametrizations described in Section 0 are exclusively used in the present thesis. The regional scope of the energy exchange countries with infrastructure connection to Germany was expanded by Russia as a gas supplier to include methane import routes. Nevertheless, the energy system of Russia is not included since no electricity grid connections exist. The model generally applies end energy usages in the different modeled sectors and cost-optimizes the energy supply, transport, storage, and demand technologies and their dispatch, considering a carbon emission restriction for the modeled year 2045.

5.3.1 Electricity and heat sector

The modeled electricity demand is subdivided into an exogenously fixed demand and an electricity demand arising from technologies optimized in the model, such as electrolysis or heat pumps. The exogenous demand represents the demand in the electricity sector, such as the electricity demand for information and communication technologies, lighting, electric motors, and cooling. A constant annual demand of 377 TWh from 2019 to 2045 is assumed due to contrary effects of increasing electrical efficiencies and demands due to digitalization and communication technologies between 2019 and 2045 [161]. Electricity demand for electric heating and usage in the mobility sector is excluded since it is modeled explicitly as a technology supplying the end energy demand in the heat or mobility sector. The electricity demand in the electricity sector is disaggregated based on population and gross domestic product on the NUTS2 level, as shown in Figure 5-14. The temporal distribution is based on Germany's normalized historical electricity load data for 2012 provided from ENTSO-E, as shown in Figure 5-15.

The heat demand is split into process heating and space and water heating. A constant yearly process heat demand of 551 TWh as in 2018 [162] is assumed with a uniform distribution over 8760 hours. Regional differences occur mainly based on the distribution of industrial sites per NUTS2 region. The industrial gas demand from the data set published in [163] for 2015 is considered to distribute the process heat demand in space. It is assumed that no major locational changes in industrial sites will occur until 2045. In 2018, space and water heating accounted for 757 TWh of heat demand [162]. This is assumed to decline by 51% until 2045 due to efficiency measures in buildings to 500 TWh. Gas heating is one of the major technologies for heating in today. Hence, the gas demand of households is used to spatially disaggregate the demand to the NUTS2 regions based on the data published in [163]. The temporal distribution is based on the heating demand in Germany in 2015 based on data published in the EU project ‘Heat Roadmap Europe 4’ for Germany [164].

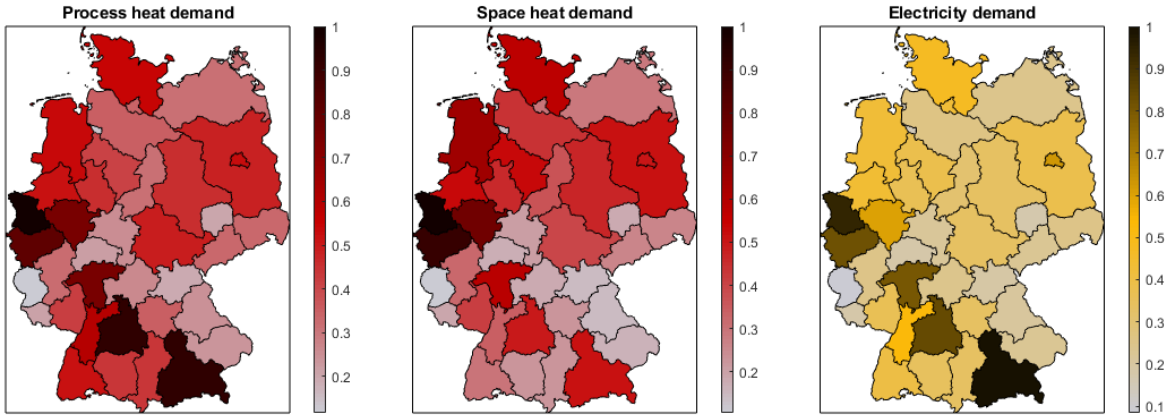

Figure 5-14 – Regional distribution of annual heat and electricity demand on NUTS2 level normalized to the highest occurring value within one region.

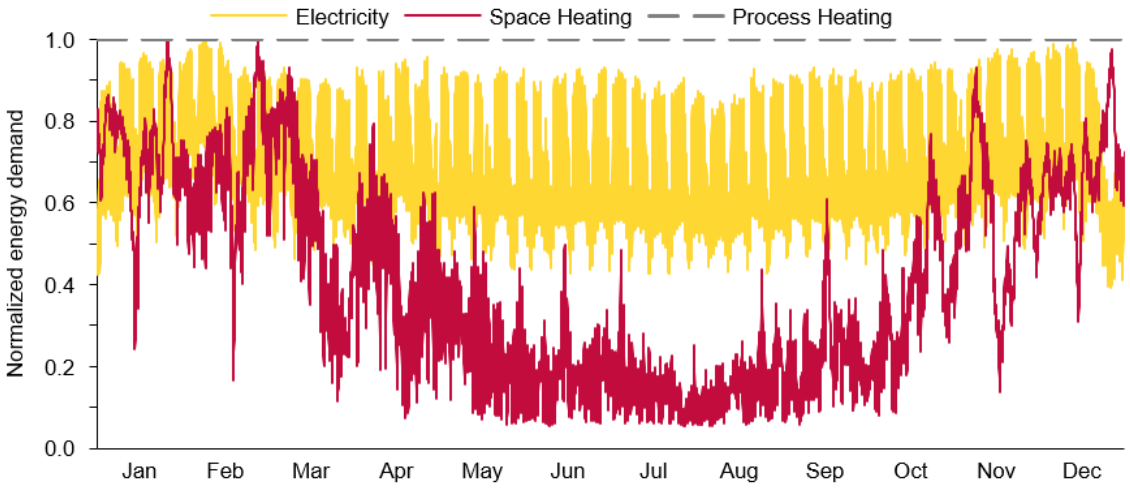

Figure 5-15 - Temporal distribution of electricity and heat demand in Germany normalized to the maximum demand within one hour of the year.

The model converts energy from solar radiation and wind into electricity. The efficiency is incorporated in the hourly capacity factors for the technologies on a regional level. It differs between regions based on historical weather data of 2012 as derived from the MERRA-2 database from the Modern-Era Retrospective analysis for Research and Applications, Version 2 database (MERRA-2) from NASA. Here, it is differentiated between Wind onshore and offshore turbines, as well as rooftop and ground-mounted PV. This allows distinguishing in terms of costs as well as temporal and regional availabilities. The used hourly and regionally differentiated capacity factors are described in the following.

For each hour and region, the capacity factor describes the available capacity of, for instance, all installed wind onshore turbines within a region. This temporal availability of PV and Wind energy is modeled based on weather data of the year 2012. Therefore, hourly averaged data for solar radiation and wind speeds at different heights are taken from the MERRA-2 database. The spatial resolution of the weather data is available on a raster of 0.625 longitude and 0.5° latitude, which corresponds approximately to 48 km x 57 km in Germany. The MERRA-2 cells are then intersected with the NUTS 2 regions to obtain regional availability profiles for onshore wind turbines, offshore wind turbines, rooftop PV, and ground-mounted PV on the NUTS 2 level. Offshore wind

capacity factors are based on international exclusive economic zones, which are then allocated to the nearest NUTS2 region in Germany.

To generate the available wind generation from the weather data, an optimized wind turbine for the characteristic full load hours in each cell, the air pressure at the hub height as well as the rotor area and the rotor efficiency, which depends on the corresponding wind speed and the chosen turbine are considered. The availability profiles or time-dependent capacity factors for wind are normalized to the highest available capacity factor over all regions and all hours of the weather year 2012.

The hourly capacity factors for PV are based on the horizontal solar radiation, divided into diffuse and direct radiation by the Erbs model [165]. To obtain the hourly capacity factors, the angle of incidence of the radiation at each hour of the year, the albedo effect, the ambient temperature, the low light behavior of a module, as well as the optimal orientation with a 40° angle for the PV modules are considered. Further, an efficiency reduction factor of 0.8 is applied to the hourly available capacities due to, for instance, electrical losses and module degradation. Hourly capacity factors for rooftop and ground-mounted PV are not differentiated.

Figure 5-16 shows the full load hours (FLH) for PV and wind onshore turbines, ranging from 1033 hours in Schleswig-Holstein to 1271 hours in Tubingen. For comparison, the country-wide averaged full load hours of the modeled European countries are 874 hours in Norway and 1335 hours in Switzerland for PV. Further, the maximum assumed capacity per region is restricted based on land restrictions of the ENSPRESO dataset [166].

Wind and PV energy generation in the model follows the weather patterns but can be curtailed by the optimizer. In addition, gas power plants running on hydrogen or the gas mix from the pipeline system as well as waste, biomass, and hydro powerplants are considered. The heat demand can be supplied by solar thermal systems, electric heat pumps, gas power plants, boilers, and furnaces. The last three technologies can be fueled by the gas mix from the modeled gas pipelines or pure hydrogen. Further, a district heating grid can distribute centrally produced heat from, e.g., bulk generation to meet the end demand. Maximum capacities for heat and electricity generating technologies are restricted based on [167].

The electricity generation capacities in non-German regions are not optimized but fixed here according to the TYNDP scenario ‘National Trends’ [168]. Since the capacity projections in this data set are only available from 2025 to 2040, they are extrapolated linearly to 2045 here. A decrease in nuclear capacities in the EU is assumed in this scenario in all countries but not in the UK. The electricity demand in the modeled twelve non-German countries is 1941 TWh, including mobility and heat applications since those are only modeled explicitly for German regions. Further, natural gas demand in the modeled European countries is integrated to model gas

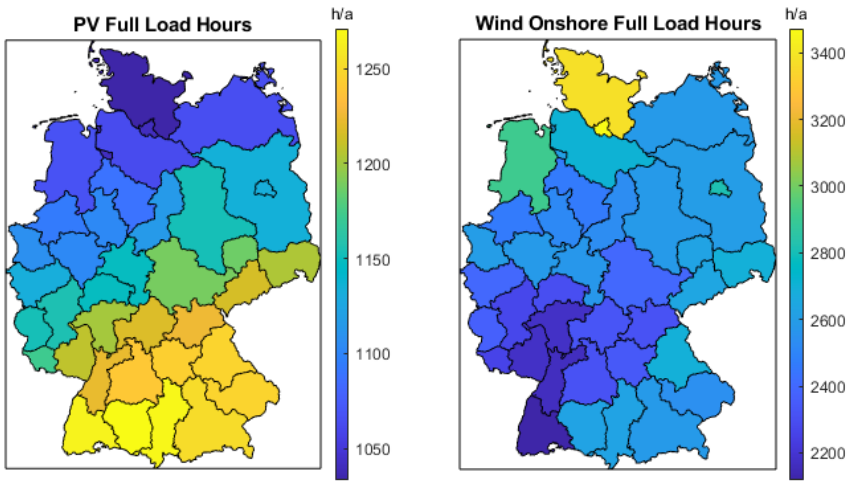

Figure 5-16 – Regionally distributed full load hours of Wind onshore turbines and photovoltaics based on the weather year 2012.

exports from Germany to represent an accurate utilization of the gas transmission pipelines (cf. Section 5.3.4). Other energy demands in non-German countries are not considered in the model.

Electricity transport infrastructure

Supplying electricity from different sources to the demand requires transmission and distribution infrastructure with 220 kV-380 kV or 0.4 kV-110 kV, respectively. Here, two main assumptions apply to the parametrization. First, electricity is only transported between NUTS2 regions using the transmission grid, and second, it is distributed within a NUTS2 region using the distribution grid. The distribution grid is only considered in terms of costs per kilowatt-hour, representing grid fees of five cents per kilowatt-hour in total, from which 20% are presumed at the transmission level. Most loads are assumed to be connected to the distribution grid. They, therefore, access electricity to its hourly generation costs from the electricity generation mix, including losses of 6% per kWh, transmission costs if transported to another region, and distribution costs of four cents per kWh. Only central batteries, central electrolysis as well as rail and catenary systems are modeled to be connected to the transmission grid directly or free of distribution grid charges. Other bulk consumers, e.g., in the industry, are not explicitly modeled, and hence, no exception for distribution grid costs for their electricity consumption is integrated.

The Alternating Current (AC) electricity transmission grid capacities are optimized for 2045 endogenously. Anyway, this transmission infrastructure, as it existed in 2017, is considered an initial grid for the 2045 optimization. Challenges regarding the social acceptance of newly built overhead transmission lines exist. Therefore, it is assumed that the existing connections can only be reinforced, but no new connections between regions, which are not connected in 2017, are available. In addition, planned Direct Current (DC) corridors, as considered in [169], are integrated into the initial grid for 2045. Those DC links connected regions in northern Germany with regions in Southern Germany, directly reaching across multiple NUTS2 regions. They include ‘Ultranet’, ‘Southlink 1’ and ‘Southlink 2’as well as ‘East-South link’, and they are not further optimized. The AC electricity transmission grid is implemented as Net Transfer Capacities (NTCs) between the NUTS2 regions. Those consider thermal limits of power lines, including an AC power flow calculation and security of supply as an n-1 criterium. The resulting initial AC and DC grid is shown in Figure 5-17. Grid extensions in the optimization are considered with costs of 500 €/km per 1 MW capacity [170]. Costs for substations are considered in the distribution grid fees.

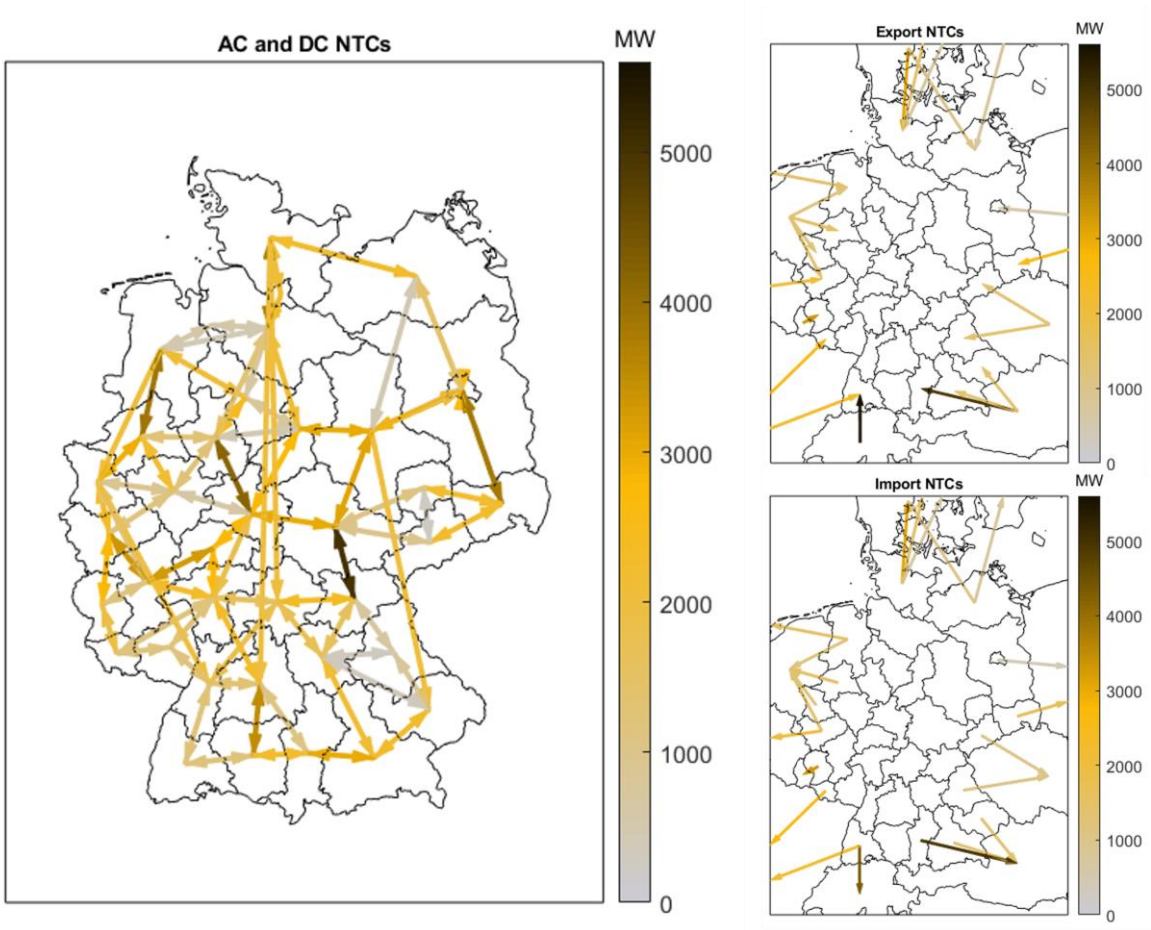

Figure 5-17 – Initial net transfer capacities (NTCs) of electricity transmission grid based on publicly available data from 2016 and 2017 for the AC grid and planned DC links for 2030.

5.3.2 Mobility sector, including refueling and charging infrastructure

The mobility sector is modeled, analog to the electricity and heat sector, based on its useful energies, which are split into freight and passenger demands and further into the modalities of car, bus, Light-Duty Vehicles (LDV), Heavy-Duty Vehicles (HDV), train, ship, and aviation. Figure 5-18 and Figure 5-19 illustrate the modeled technologies and demands in the freight and passenger transportation sectors based on the most relevant powertrain-fuel combinations derived in Section 2.1. Each demand process is fixed in its annual output representing the corresponding mobility demand in Gtkm or Gpkm in Germany. The modal split is not optimized in the model. To convert the Gpkm and Gtkm to energy demands that can be supplied in the form of energy, three values are required per technology: The average payload or an average number of passengers per vehicle and vessel, the annually averaged covered kilometers, and the vehicles energy consumption per kilometer. The efficiency parameter of a conversion process (cf. Equation 3.11) is then used to convert the units. Figure 5-20 illustrates the unit conversion exemplarily for BEVs. The present approach is adopted from Most, who implemented the mobility sector in the European context in the plan4res project [171]. Further, the modeled vehicle technologies are shown in the figure. These technologies are optimized, including the required refueling and charging infrastructure as described below.

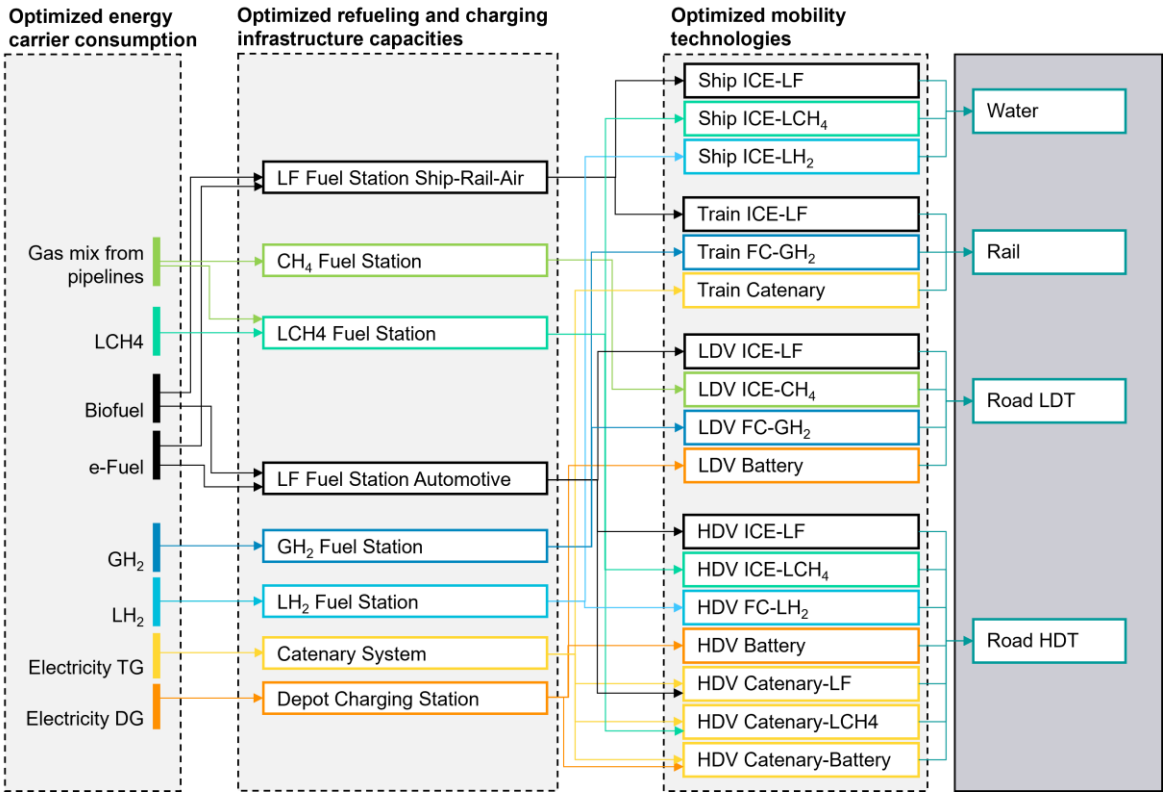

Figure 5-18 – Freight transportation modeling. For abbreviations, see the caption of Figure 5-19.

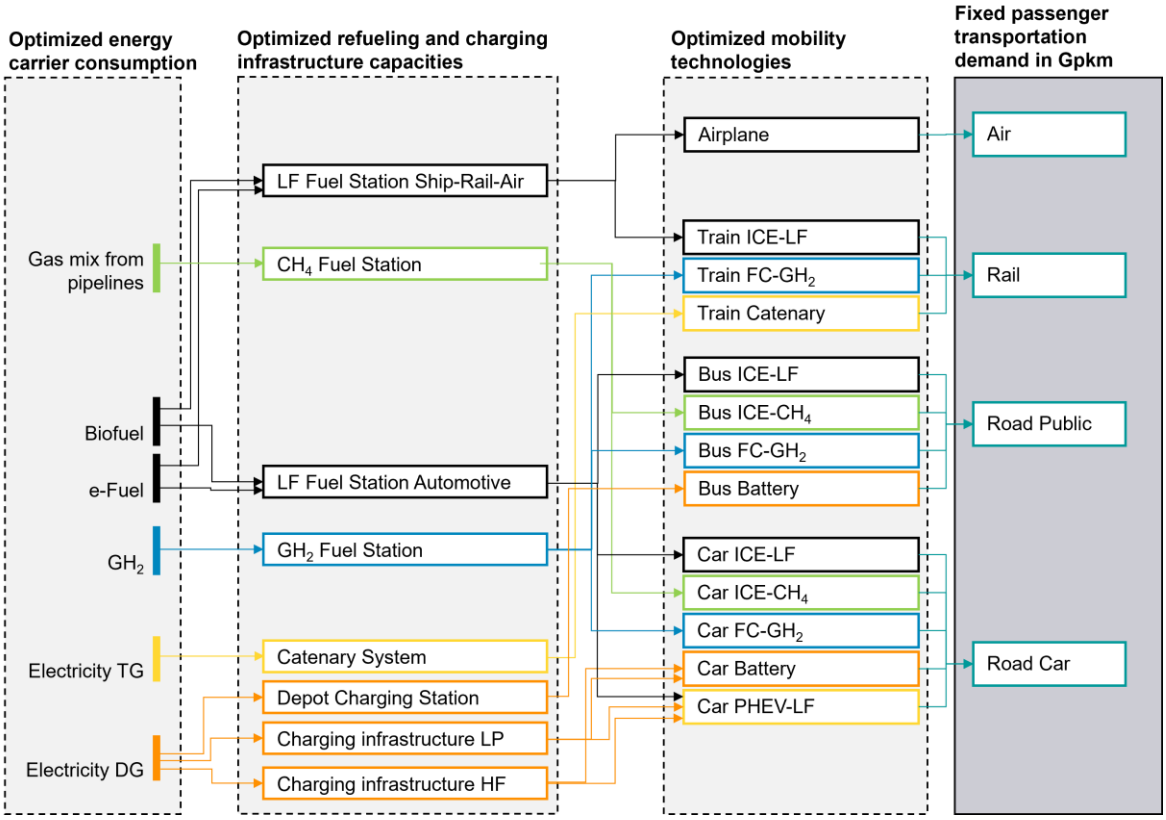

Figure 5-19 – Passenger transportation modeling. LF – Liquid Fuel; PHEV – Plug-In Hybrid Electric Vehicle; FC – Fuel Cell; TG- Transmission Grid; DG – Distribution Grid; LCH_4 – Liquified methane; LP – charging infrastructure network designed to minimize the charging peak load; HF – charging infrastructure network designed to maximize the flexibility; HDV – Heavy Duty Vehicle; LDV – Light Duty Vehicle.

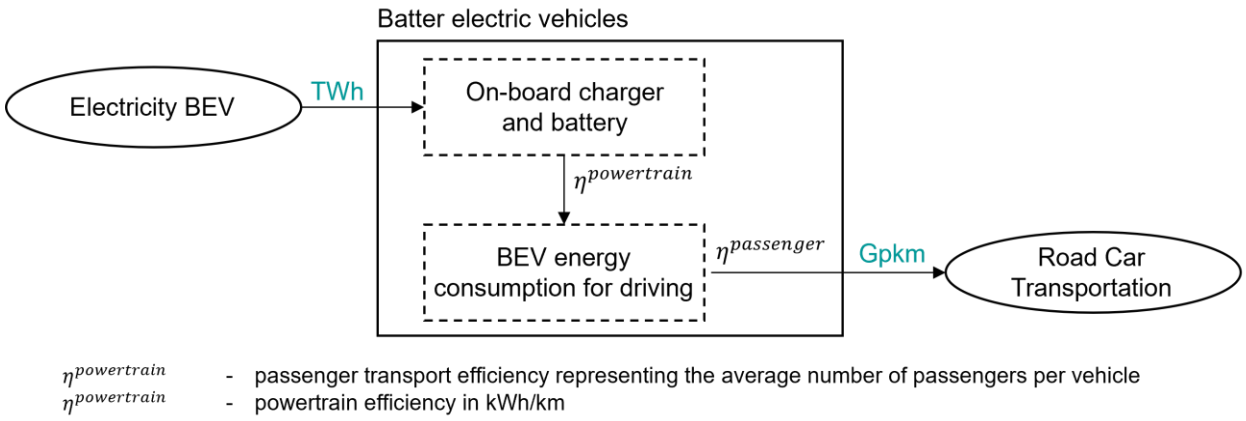

$\eta^{powertrain}$ - passenger transport efficiency representing the average number of passengers per vehicle
$\eta^{powertrain}$ - powertrain efficiency in kWh/km

Figure 5-20 – Unit conversion from TWh to Gpkm for Battery Electric Vehicles.

Furthermore, each mobility demand process is disaggregated on the NUTS2 level in analogy to [122]. The mobility demand for passenger cars and buses is distributed according to the NUTS2 population and the vehicle density in each region. The freight transportation is disaggregated based on the freight traffic performance in ton-kilometers. Aviation demand is also assumed to correlate with population density. The rail demand for freight and passenger transport is based on the number of train stations per NUTS2 region obtained from OpenStreetMap. Finally, inland shipping is based on inland port locations and their respective annual cargo handling volumes. Figure 5-21 shows the distribution of the demand. The worldwide largest inland port in Duisburg is in the NUTS2 region of Düsseldorf, which therefore dominates the regional distribution for inland shipping. In contrast, the largest demand for passenger road transport occurs in NUTS2 regions with large populations such as Düsseldorf, Upper Bavaria, Stuttgart, or Berlin.

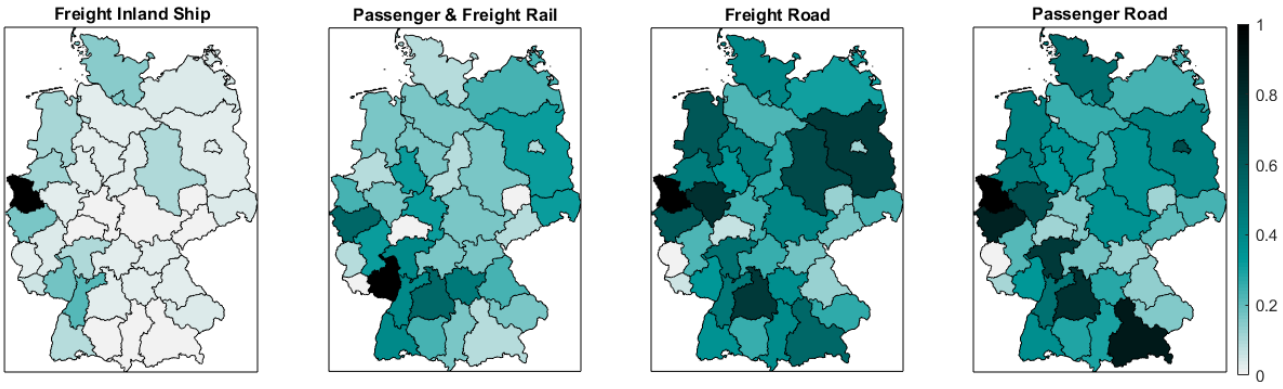

Figure 5-21 – Regional distribution of passenger and freight demand; normalized to the highest annual demand within one NUTS2 region.

All passenger transport demands are assumed to temporally align with the passenger car traffic volume in each hour of the year. The considered time series is based on traffic measurements in the year 2007 and accounts for changed traffic volumes on weekends and public holidays. For road freight transport, a time series for one representative week is derived based on [73] and extrapolated to the entire year without consideration of holidays and seasonal variations. Compared to passenger transport, one major difference is the reduced traffic

volume on Sundays in Germany, as shown in Figure 5-22. Additionally, the difference between the day and night traffic volume is lower for freight transportation by up to 60%.

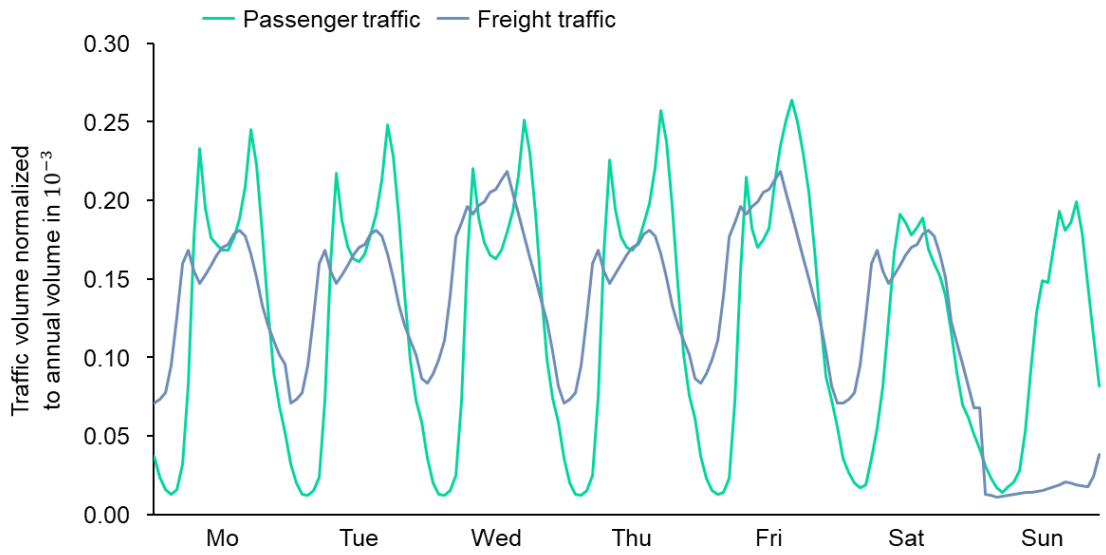

Figure 5-22 – Hourly passenger and freight traffic demand volume normalized to the annual traffic volume.

The costs of mobility technologies can vary significantly based on the vehicles' additional technical features, entertainment systems, brand, or design. In a macro-economic energy system optimization, these costs are considered non-relevant and should not depend on the vehicle's powertrain. These vehicle costs are adjusted by subtracting the cost c_v^{tech} of each transport technology *v* within one segment by costs c_{ref}^{tech} of a reference technology reflecting today's dominating technology. For passenger cars, the reference technology is an ICE car. These delta costs are divided by the average annual mileage of the vehicles segment to obtain the conversion process costs in Euro per kilometer (cf. Equation (5-27)). The applied delta costs are converted to an annuity and then considered in Equation 3.4 in ESDP. It can be interpreted as additional costs for switching from the reference technology to a new powertrain technology.

$$C_{cs}^{\text{capex}} = \frac{c_v^{\text{tech}} - c_{ref}^{\text{tech}}}{d_{y,v}^{\text{milage,avg}}} \tag{5-27}$$

All assumed techno-economic parameters for technologies in the mobility sector are listed in Appendix C.

Refueling infrastructure modeling

New technologies and energy carriers in the mobility sector require new refueling and charging infrastructure networks. It is assumed that liquid fuels from Fischer-Tropsch (FT) synthesis can use the existing distribution and refueling infrastructure at no additional costs. Costs for replacing valves or pumps are not considered since they are assumed to be significantly lower than new infrastructure investments for hydrogen and electricity refueling (cf. Section 2).

Figure 5-18 and Figure 5-19 show the considered refueling and charging technologies. Vehicles refueling at liquid fuel dispensers are assumed equally capable of running with todays' fossil liquid fuels, liquid e-fuels, or biofuels. Only one refueling technology for these fuels is modeled according to the requirements derived in Section 2. Gas fueling stations are considered, which are supplied from the pipeline gas mix within a region (cf. Section 5.3.4). Estimated costs for a methane refueling station amount to 61 thousand Euros per dispenser [5]. With an assumed refueling speed of five minutes per 500 km range, including the time for payment, with an ICE car running on methane with a consumption rate of 0.7 kWh per kilometer, the specific costs are 14.5 € per kW. Considering this technology as mature, no cost reductions until 2045 are assumed. An additional refueling station supplying LNG to trucks and ships is included assuming that the costs for both modalities are the same.

The gas can either be liquified at the refueling station or be imported in liquid form from abroad. Total refueling station costs per LNG dispenser can be estimated at 382 thousand Euros [5], presuming a liquid gas supply to the station. Assuming more powerful pumps compared to passenger cars and higher energy consumption of LNG trucks of 2.36kWh per kilometer, the refueling time for 500 kilometers is the same as for CNG cars. This results in specific costs of 54 € per kW.

Hydrogen refueling stations provide in the model hydrogen to all hydrogen consuming technologies regardless of the modality. The cost of building up an entirely new hydrogen refueling station with eight dispensers is estimated to be 3.3 million euros [5], [63]. The time to refuel the hydrogen tank at 700 bar is assumed to be five minutes. Considering a consumption rate of 0.28 kWh hydrogen per kilometer for a passenger car, the specific costs are 245 € per kW. Since no large-scale roll-out of hydrogen infrastructure occurred until 2022, the economy of scale effects can be expected if the market volume increases. Further, increasing the number of dispensers per refueling station when the fuel cell vehicle market is more mature can additionally bring down costs in the future. Therefore, a cost decline of 50% until 2045 is assumed. The same costs are considered for LNG hydrogen stations. Still, the liquefaction of gaseous hydrogen is modeled additionally as described in Section 5.3.3.

To provide electricity to vehicles, charging infrastructure and catenary systems are distinguished. Distribution grid costs are not applied to catenary systems here. The overall efficiency of delivering electricity from the transmission grid to a catenary HDVs is 89%. This includes an efficiency of 97% for the transformer, 98% for the rectifier, 95% for the catenary line, and 99% for the pantograph [172]. To build up a catenary system, high upfront investment costs are necessary. The specific costs are estimated based on [74], [173] to 889 € per kW. Furthermore, due to different power ratings, costs, and utilization of required charging stations, the charging infrastructure is distinguished for battery electric LDVs, HDVs, and busses, as well as for battery electric passenger cars (BEVs), including PHEV. A detailed approach for BEVs is relevant (cf. Section 2) and considered as described in Sections 5.1-5.2 due to its complex network structure. In contrast, charging stations for electric LDVs, HDVs and busses are assumed to be placed primarily in depots. The charging infrastructure costs can be summarized as specific costs of 492 € per kW in 2030. This considers 600 kW and 150 kW chargers supplying 20 and 0.91 vehicles on average per day for 322 € per kW and 433 € per kW, respectively [174]. A cost reduction of 20% is assumed until 2045.

If not specified otherwise, the unit kilowatt is referred to the corresponding commodity. The estimated specific costs for the refueling stations are in a similar order of magnitude as, e.g., in Helgeson and Peters [62].

Since LDVs, HDVs, and busses park at nighttime, the charging is assumed to occur mainly at night, complementary to the freight road traffic. The derived temporal distribution of the electricity demand for LDVs, HDVs, and buses is shown in Figure 5-23. To account for additional fast charging stops during the day, an adjustment factor, shown in the figure, is applied to the profile.

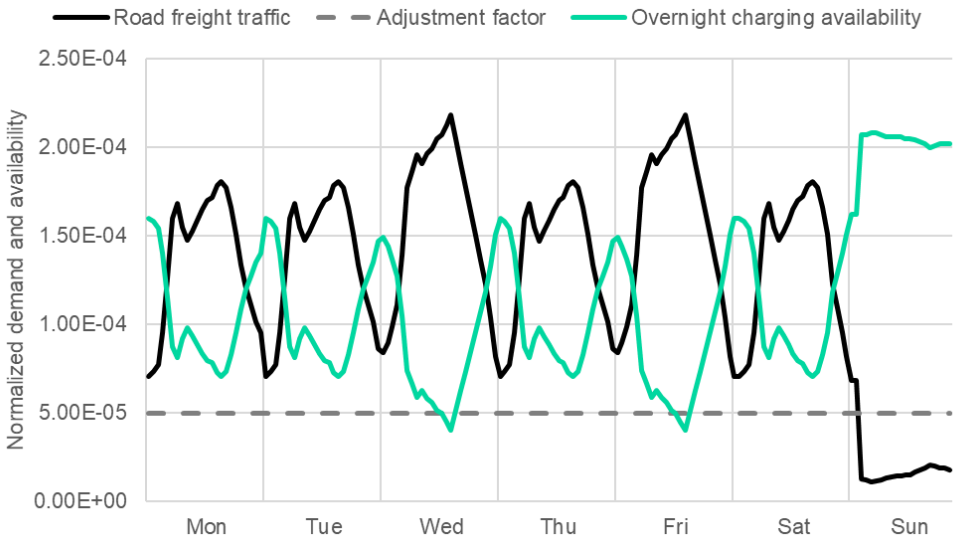

Figure 5-23 – Temporally resolved truck and bus charging demand normalized to the annual demand.

5.3.3 Hydrogen supply chain

A fundamental hydrogen supply chain representation is inevitable to model the competition between energy carriers in the mobility sector. Figure 5-24 shows the implemented conversion processes that include hydrogen generation, import, storage, transport, distribution, and demand processes. Electricity demand for the compression is also indicated in the figure. The derived parametrization of these technologies is described subsequently.

Multiple demand applications for hydrogen are implemented, such as hydrogen ready gas turbines (cf. Section 5.3.1), hydrogen boilers and furnaces (cf. Section 5.3.1), technologies in the mobility sector (cf. Section 5.3.2), and synthesis processes generating e-fuels (cf. Section 5.3.4). Methanation, FT, and methanol synthesis are assumed to be placed at central transmission pipeline hubs and require no further distribution via tailer. Contrasting, it is not assumed for gas turbines and industry since those sites are considered not to change. This follows a scenario assumption, where transmission pipelines arrive in a central hub in a NUTS2 region. This can impact the final hydrogen applications due to six cents per kilowatt-hour distribution costs, estimated based on [54], and assumed losses of five percent. A sensitivity with assumed distributed hydrogen hubs is applied to assess this assumption (cf. Section 5.4).

Since this model only considers energy applications, hydrogen as feedstock in, for instance, the steel or ammonia industry is not optimized. Since a representation of centralized hydrogen demand might impact the usage in the mobility sector and the required hydrogen supply infrastructure, an exogenously defined demand of 84 TWh is considered. This assumes a centralized hydrogen supply to 70% of the steel production in 2017, 50% of 2017's ammonia generation, and 80% of the demand in refineries. This demand is regionally distributed. Steel production locations in Germany are weighted with their steel production volume in million tons, ammonia production locations, and refinery locations weighted by their annual fuel processing capacities. The derived regional distribution is based on [175]–[177] and shown in Figure 5-25. Additional upcoming non-energetic hydrogen demand, not covered in the 84 TWh, is supposed to be supplied by on-site generation, which is not covered for non-energetic demands in the present thesis.

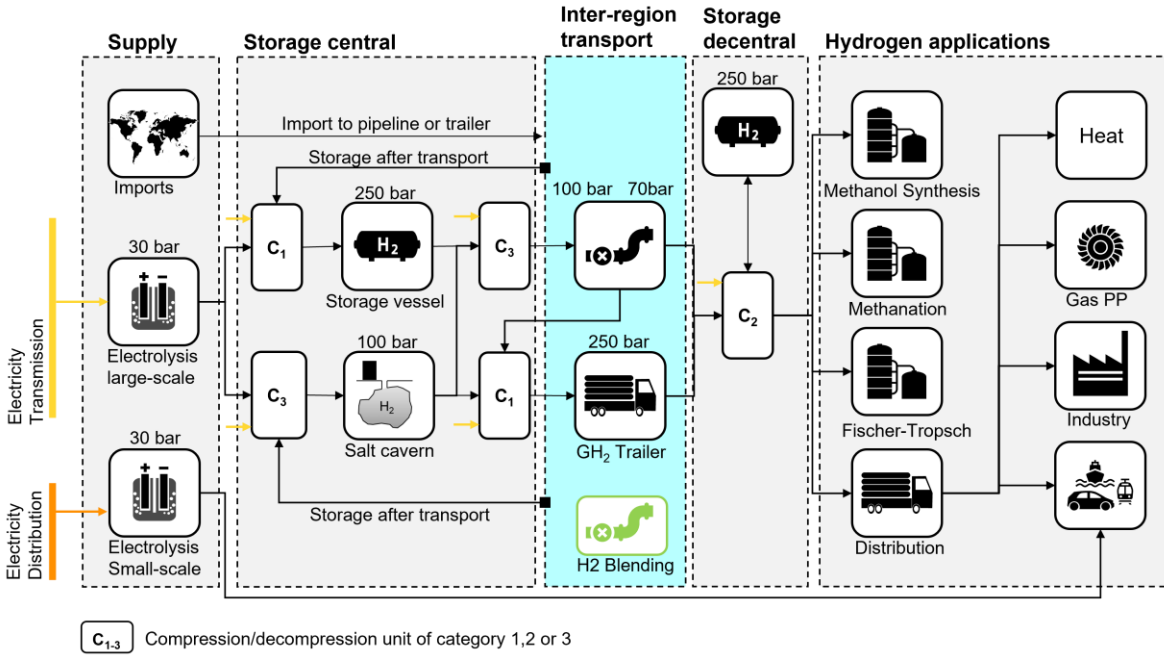

Figure 5-24 – Hydrogen supply chain modeled in ESDP.

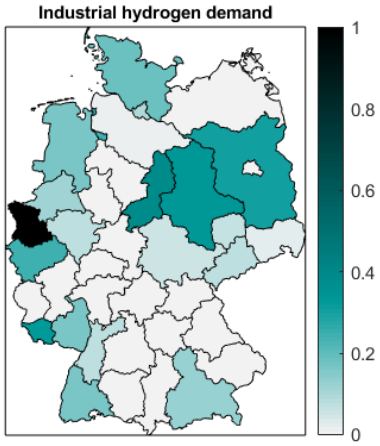

Figure 5-25 – Industrial hydrogen demand distribution (steel, ammonia, refinery) normalized to the maximum annual value within one NUTS2 region.

Import routes

Several import routes for hydrogen to Germany could be established in the future. Differences in origin, electricity source, and mode of transport are represented in the model by different import costs. The import location is highly relevant for designing a hydrogen pipeline network. Therefore, the NUTS2 import region is distinguished for each route. Following the import route options as published in [122], four different routes are implemented, as indicated in Figure 5-26. A pipeline infrastructure for importing hydrogen from Northern

Europe, Southern Europe, and Northern Africa is presumed. Those pipelines are supposed to arrive via Denmark in Schleswig-Holstein, France in Southwest Germany, and Italy and Switzerland in Freiburg. Imports from overseas arrive at the port of Rotterdam as liquid hydrogen, which is then gasified and transported via established gas pipeline routes to regions in Western Germany. All cost assumptions refer to the import costs at the German border. Varying cost assumptions in the literature are shown in Figure 5-30 and considered in the sensitivity analysis described in Section 5.3.4. Import volumes are optimized but restricted based on [178]. For the sake of security of supply and political independency, a diversification strategy for hydrogen imports is presumed. All four routes are established, delivering a minimum of about five Terawatt-hours to Germany. Natural gas imports paired with 'carbon capture and storage, and a pyrolysis system for hydrogen generation in Germany is not covered. Also, no hydrogen export is covered.

Electrolyzer

Two conversion processes generating hydrogen from electricity in Germany are optimized in the model in terms of location, capacity, and operation. One represents large-scale central electrolyzer processes, and one describes decentral small-scale on-site electrolyzers processes. The water demand of approximately nine kilogram per kilogram of generated hydrogen is not modeled here explicitly as in Germany the costs for water can be neglected compared to the costs for electricity. Table 5-5 summarizes the techno-economic parametrization of the electrolyzers.

Central electrolysis refers to large-scale systems being connected directly to an electricity generation source so that no distribution costs for electricity occur. This is represented in the model by the electrolysis being fed directly by the electricity from the transmission grid. The considered water electrolysis produces 'green hydrogen' if the electricity supply within the considered year is carbon neutral. This thesis focuses on a carbon-neutral MMES. Hence, the inland located electrolyzers generate green hydrogen. The costs are based on the long-term costs for Polymer Electrolyte Membrane Electrolysis technology as estimated in [179]. An outlet pressure of 30 bar is assumed in accordance with [54], [56]. Contrary to the modeled decentral electrolyzer, this hydrogen can be transported between NUTS2 regions.

Decentral electrolysis represents hydrogen generation from small-scale on-site electrolyzers. The hydrogen at 30 bar must be compressed for storage in a high-pressure tank at 300 bar before it is consumed at, for instance, a refueling station. This hydrogen is consumed in the model in the NUTS2 region where it is produced. Costs are based on [180] and are calculated here for a site with a maximum load of two tons of hydrogen demand per day, corresponding to a small truck refueling station with 38 served trucks per day [64]. Cost reductions and efficiency gains until 2045 are incorporated analog to the central electrolyzer. The assumed capacity of the electrolyzer is 2.78 MW_{H2}, and the corresponding compressor unit is here designed to a maximum hydrogen flow per day of 83.33 kg H2 or 2.78 MWh, respectively, with a lower heating value of 33.33 kWh/kg_{H2}. The low-pressure storage vessel is not represented in the estimated costs but modeled explicitly, as explained below. The efficiency long-term efficiency gain projected for central electrolyzers in [179] is also presumed for decentral electrolyzers here.

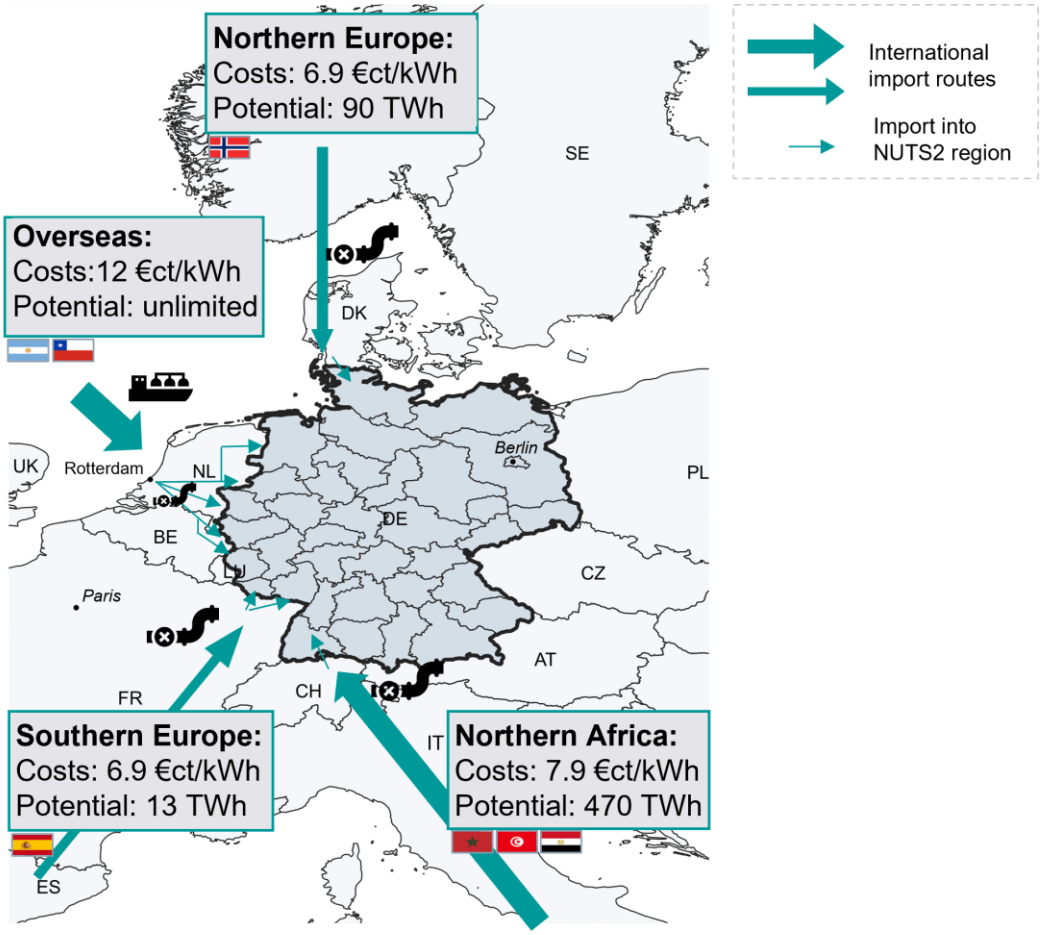

Figure 5-26 – Hydrogen import routes with maximum supply volumes and costs to Germany as assumed for the reference scenario in 2045 [122]. Assumptions are based on [40],[41],[178]. The arrow sizes do not indicate costs or volumes for an import route.

Technology	Lifetime	Investment costs in €/kW	O&M in percent of investment	Efficiency	Outlet pressure
Central Electrolyzer	20a	539	1.5%/a	74%	30bar
Decentral Electrolyzer	20a	771	4%/a	48%	30bar

Table 5-5 – Electrolyzer cost assumptions based on [179] and [180].

Hydrogen storage

Hydrogen can be stored in the model in decentral and central pressure vessels at 250 bar and in salt cavern storage. Several salt caverns suitable for gas storage exist in Germany [181], [182]. Salt caverns are already used for hydrogen storage in the United States of America and could also be utilized in Germany for large-scale hydrogen storage [182]. Since all available salt caverns in Germany differ significantly in size and costs for

realization as hydrogen storage, a model cavern is applied according to Stolzenburg et al [182]. This approach is already used in literature, for instance, in [54], [183]. The defined model cavern has a storage capacity of 133.33 GWh of H_2, holding a volume of 500,000 m^3, which represents the average size of German salt caverns. The techno-economic parameters are summarized in Table 5-6. Since compressor units are modeled individually here, the investment costs of 92 million €, according to Stolzenburg et al. [182], are reduced by the given compressor investments of 30 million €.

Large upfront investments are required to enable a salt cavern for hydrogen, especially including the overground infrastructure. Due to the characteristics of a linear program without integer variables, the application of base investment costs independent of the installed capacity is not possible. Therefore, a linear assumption of the overall costs of the model salt cavern is used here as simplification. Such a cost assumption reflects an investment into several small caverns in proximity with only one overground investment due to joint utilization of overground infrastructures. The linear cost assumptions are based on 62.6 million € for a 133.33 GWh salt cavern. A sensitivity regarding the salt caverns' availability is conducted to assess the overall impact of this simplification on the MMES (cf. Section 5.4). Further, the C-rate is fixed to 0.003 kW per kWh based on a 400 MW_{H2} output capacity. A low C-rate reflects the characteristics of salt cavern storages with a large volume in this linear approach. The assumed efficiency includes the energy demand for the drying of hydrogen. Additional electricity demand for operation of in- and outlet compressors is modeled as separate conversion processes described below. The assumed regional availability of salt caverns is based on [182], [184].

Technology	Lifetime	Investment costs in €/kWh	O&M in percent of investment	Roundtrip efficiency	Storage pressure	C-rate in kW/kWh
Model salt cavern	40a	0.47	2%/a	97.8%	>100bar	0.003
Decentral pressure vessel	30a	15	2%/a	95%	250bar	-
Central pressure vessel	30a	15	2%/a	95%	250bar	-

Table 5-6 – Techno-economic parametrization of hydrogen storage technologies based on [27], [54], [61], [182].

Compression

Compression units of hydrogen are an essential part of the hydrogen supply infrastructure. They compress gaseous hydrogen to the required pressure of the storage, pipeline, or refueling stations. Due to the volumetric density of hydrogen being lower by factor three compared to methane, more compression stages and, therefore, more energy is required to reach the same pressure level [185]. This increases the necessity to explicitly model the compression of hydrogen along its supply chain. The compression costs and required energy rely non-linearly on the inlet and outlet pressure difference and the electrical power rating [54], [186]. Figure 5-27 shows the specific costs in dependency on the power rating. Additional installation costs can be differentiated based on the application and its associated site specifications. Nexant [186] adjusts the non-linear cost function by a cost factor for a large or small installation. Reuß [54] modified the function by a long-term cost projection and differentiated the installation cost factor between the applications of a salt cavern, pipeline, and trailer. For comparison, specific cost estimation for the year 2035, without relating to the electrical power rating of the compressor, is used by Runge et al. [61] and included in Figure 5-27.

Three compression units are differentiated here based on the application and outlet pressure to represent differences in required compression work. The outlet pressure is the main driver for sizing, costs, and electricity demand [186], [187]. Table 5-7 summarizes the techno-economic parametrization. Figure 5-27 indicates that compressors 1 and 2, which compress hydrogen to 250 bar, assume a large compressor for trailer application based on the cost curve of Reuß [54]. Compressor 3 is based on the cost curve for cavern storage application

from Reuß [54], considering a 7.2 MW power rating for the model salt cavern according to Stolzenburg et al.[182]. The cost curve for pipelines from Reuß reveals a similar cost term for a 12.5 MW power rating compared to the 7.2 MW power rating for cavern application. Therefore, applying the same cost term for both applications is considered reasonable. For additional comparison of the electrical power rating, Figure 5-27 indicates the cost for a 5 MW compressor, which is the size of installed hydrogen compression units in 2020 [185], and a 16 MW compressor as the largest available commercial size according to Nexant in 2008 [186].

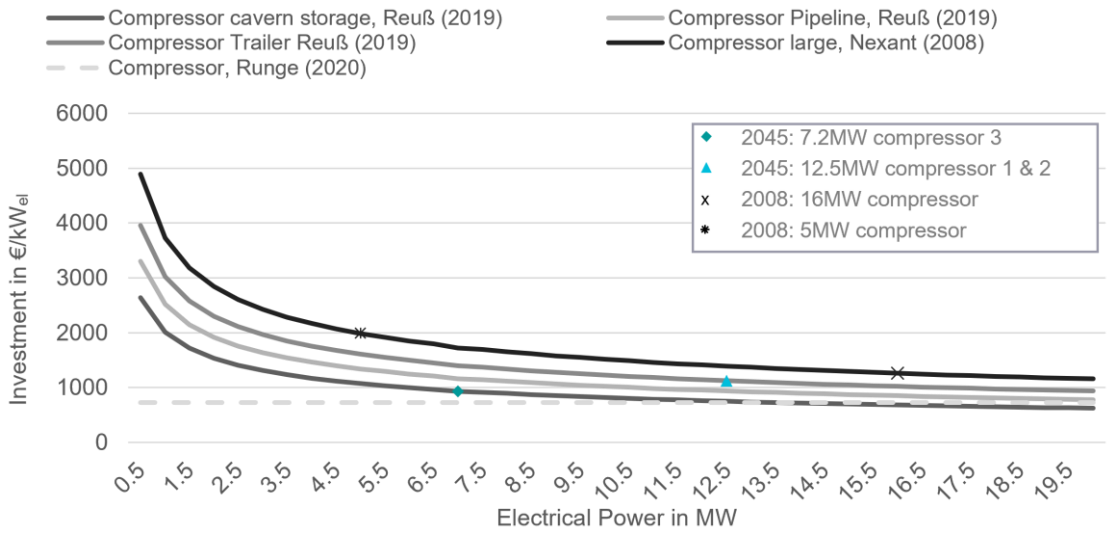

Figure 5-27 – Specific hydrogen compression costs.

Compressor category	Lifetime	Investment costs for electrical power in €/kW	O&M in €/kW/a	Efficiency (boil-offs)	In- & outlet pressure in bar	Electricity demand in percentage of LHV of H2
Compressor 1	15a	1124	30	99.5%	In: 30-100 Out: 250	4.9%
Compressor 2	15a	1124	30	99.5%	In: 100-250 Out: 250	6.5%
Compressor 3	15a	930	30	99.5%	In 30-250 Out: 100	2%

Table 5-7 – Techno-economic parametrization and categorization of hydrogen compressors based on [27], [54], [61], [182].

Pipelines and trailer

Hydrogen can be transported in the moel between NUTS2 regions via pipeline or GH_2 trailer. Both hydrogen transport capacities are optimized in the model. Hydrogen distribution within a region, for instance, to refueling stations, is assumed only via GH_2 trailer with a fixed cost term of 6.15 €/kWh, which is derived from [54]. Distribution costs vary significantly in the literature between 0.5 ct/kWh and 24 ct/kWh assuming a pipeline distribution or LH_2 trailer distribution, respectively [188]. The modeled distribution conversion process only reflects the distribution costs and losses based on the total trailer capacity within a region. In the following, the parametrization of the pipeline transport process for inter-regional hydrogen transport is elaborated.

Hydrogen pipeline costs estimations vary significantly across the literature. Reuß [54] and Reuß et al. [55] use a non-linear cost curve, shown in Figure 5-28. This curve shows the estimated costs per meter depending on the pipeline diameter. They differ in the assumed recompression costs along a pipeline section.

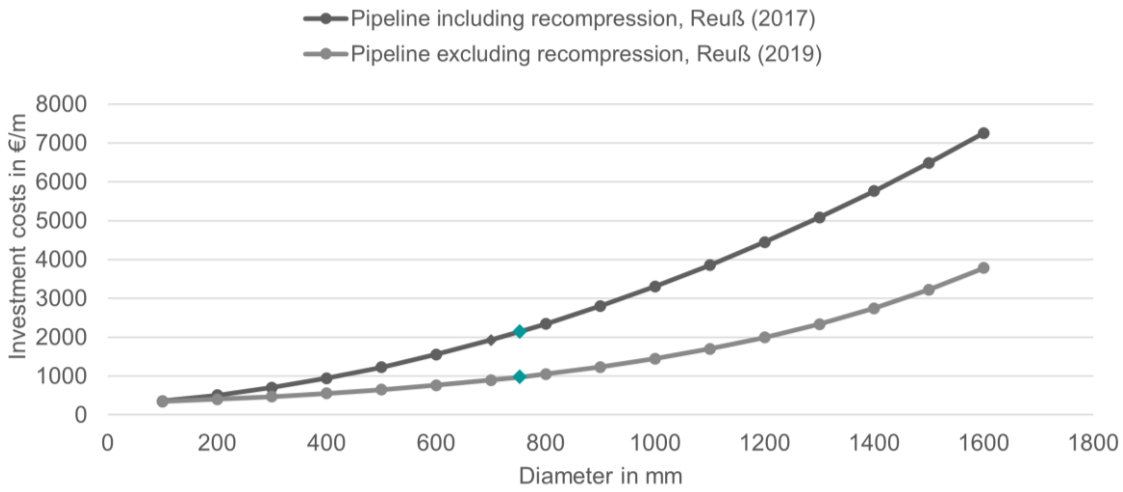

Figure 5-28 – Specific pipeline investment costs in dependency on the diameter based on Reuß [54] and Reuß et al. [55]

ESDP requires a linear parametrization of the pipeline. In the present thesis, a linear relation of the costs is assumed depending on the transport distance and the pipeline capacity. Therefore, only a diameter of 753 mm is considered as available pipeline size. This is the averaged pipeline diameter from the data set of the considered natural gas pipelines as derived from the dataset of German natural gas pipelines [163]. The pipeline capacity for hydrogen transport is considered similar to the capacity of methane transport [185]. Therefore, the capacity of a 753 mm hydrogen pipeline at 100 bar can be estimated according to Table 5-10. Then, a linear relation of the costs in dependency of the capacity is assumed (cf. Figure 5-29).

Furthermore, recompression of the hydrogen in a pipeline from 30 bar to 100 bar is required approximately every 250 km [52]. With an average center-to-center distance of 138 km between the NUTS2 regions and a compression unit explicitly modeled at the entry and exit point of an inter-region connection, a recompression unit is not considered in the estimation here. Correspondingly, the transport efficiency only includes 0.5% boil-off losses but no further energy demand for recompression. Due to the possible transport of hydrogen across several NUTS2 regions, this assumption might underestimate the hydrogen transport costs. Therefore, as described in Section 5.4, a sensitivity analysis of the pipeline costs is conducted with an alternative parametrization considering recompression costs. Thus, the cost curve from Reuß et al. [55], which is based on Krieg [52], is linearized in the same diameter, and additional energy demand of 1.8% per 250 km is modeled for the recompression according to Krieg.

Figure 5-29 compares the derived linearized costs with costs derived from a cost overview published in [188].

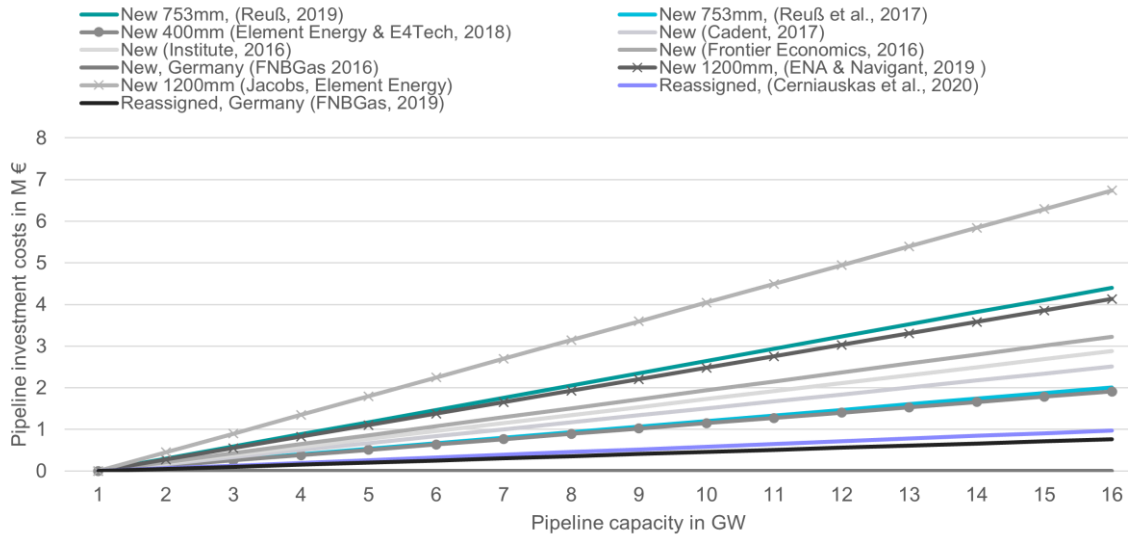

Figure 5-29 – Linearized specific hydrogen pipeline investment cost comparison for 138 km distance. The terms 'New' and 'Reassigned' indicate a newly built hydrogen and a reassigned pipeline. Costs are derived based on [54], [55], [99], [188].

Table 5-8 summarizes the techno-economic parametrization of the modeled technologies. Anyway, different pipeline assumptions, including a reassignment, are not optimized against a newly built pipeline but are considered in a sensitivity described in Section 5.4.

Finally, a linear modeling approach does not allow to model the fair competition between GH_2 trailer transport and pipeline transport since it is not possible to represent high investment base costs independent of the capacity without integer variables. Additionally, very low pipeline capacities can occur in a linear model. Still, trailers might be economically viable for low volumes and lower distances [55]. Therefore, small, unrealistic transmission pipeline sizes below 100 MW are filtered in a postprocessing.

Transport technology	Lifetime	Investment costs in €/MW/km	O&M in €/MW/km/a	Losses per 100km	Operating pressure
H2 Pipeline with recompression	40a	283	1	0.7%	70-100bar
H2 Pipeline without recompression	40a	128	1	0.005%	30-100bar
H2 Pipeline reassignment	40a	10	1	0.005%	70-100bar
GH2 trailer transport	10a	754	55	0.46%	250bar

Table 5-8 – Techno-economic parametrization of hydrogen transport technologies based on [52], [54], [55]. All pipeline cost assumptions relate to a pipeline diameter of 753mm.

5.3.4 Electricity-based fuels and methane supply chain

e-Fuels

E-fuels can be allocated from the optimizer in the mobility sector (e.g., Section 5.3.2) and in, e.g., different heat boilers and furnaces. Imported e-fuels are assumed to be generated explicitly from carbon-neutral electricity sources. This is represented in the import costs assumptions. Figure 5-30 gives an overview of different import prices estimated in the literature [61], [178], [189], [190]. If generated inland, they consume hydrogen, which is either imported or generated from the hourly electricity mix. Inland generation of e-fuels is differentiated between FT synthesis and Methanol synthesis. Additionally, e-methane can be generated by a methanation process. All three conversion steps rely on direct air capture as a CO_2 source. The e-fuel distribution costs amount to 0.1 ct/kWh, according to Helgeson and Peter [62]. E-fuels and biofuels are not differentiated in the application technologies in the model, only in their generation process. Table 5-9 summarizes the techno-economic parametrization.

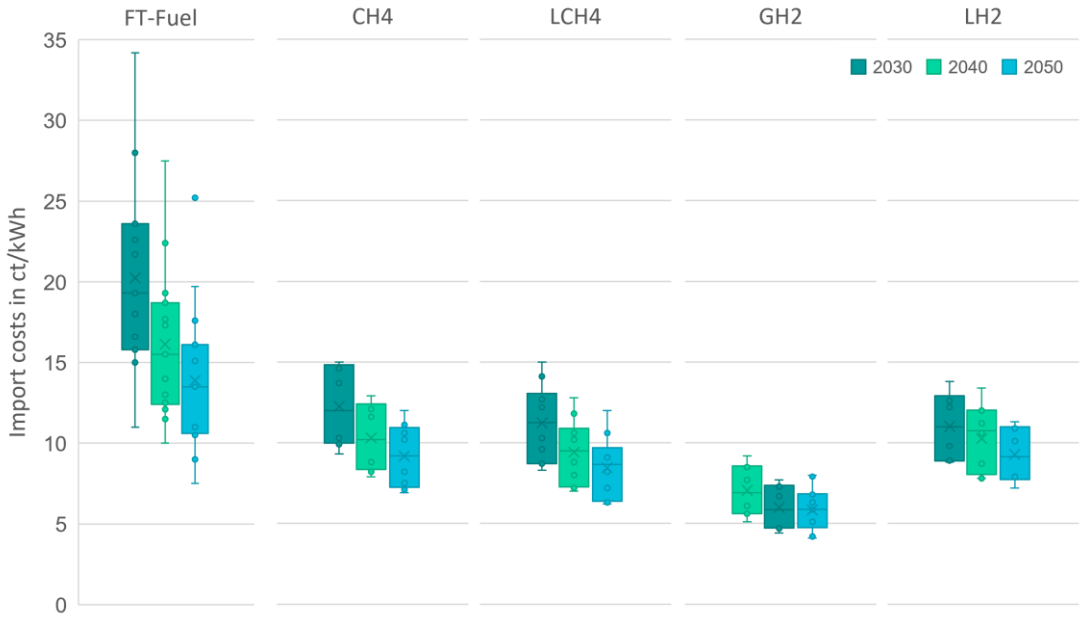

Figure 5-30 – Comparison of projected import cost for e-Fuel, e-Methane and Hydrogen based on [61], [178], [189], [190].

Technology	Lifetime	Investment costs in €/kW	O&M in % of investment	Efficiency	CO_2 costs in €/t
Methanation	30	500	4%/a	77%	50
Methanol synthesis	30	500	4%/a	79%	50
FT Synthesis	30	500	4%/a	79%	50

Table 5-9 – Techno-economic parametrization and categorization of synthesis processes based on [90], [179].

Methane

Today, natural gas is supplied to Germany from Russia, the Netherlands, Norway, and a small fraction of inland production. The latter is not considered in the model. Germany is a transit land for gas, exporting in 2015 about 1000 TWh/a of natural gas to neighboring countries [191]. In 2045 the gas export to other countries must still be guaranteed. Imports of natural gas, the transport through the modeled gas pipeline network, and the exports as in 2015 are modeled here. A decrease of 75% due to climate actions in neighboring countries is assumed, deviating from the export volume in 2015.

The modeled gas price is not distinguished between the import countries due to political influences on costs and high uncertainties. Since the model does not include carbon capture and storage, this natural gas cannot be used in a carbon-neutral energy system in Germany. Therefore, e-methane imports are established, assuming a synthetic gas production abroad from renewable electricity.

Natural gas pipelines

The third explicitly modeled energy transport infrastructure element is the natural gas transmission pipeline system in Germany, including its import and export capacities. This infrastructure can be used in the model to transport natural gas, e-methane, and biogas equivalently. In addition, up to 10% of hydrogen can be fed into the pipeline network as defined by DVGW [192]. The restriction of a maximum hydrogen share of 2% in a gas distribution grid with CNG refueling stations is neglected here. Further, inter-regional transport capacities for methane are derived as described in the following.

The gas pipeline network representation (cf. [122]) is derived based on data published in the LKD-EU project, which is also available at SciGrid Gas [163]. This data set includes geoinformation system data of nodes and pipelines, including the diameter, the operating pressure level, and the pipeline class of each pipeline. Since capacity information is covered incompletely with capacity information for only 13% of all pipelines, and for consistency, capacity information is derived based on the operating pressure and pipeline diameter. Therefore, the natural gas pipeline classification (cf. Table 5-10), published in [191], is used. A continuous operation with the maximum gas flow for 24 hours is assumed to transform the gas mass flow per day to Gigawatts. Each pipeline's entry and exit points are intersected with the NUTS2 regions. Finally, all pipelines connecting the same two NUTS2 regions are aggregated. The initial data set and the derived aggregated inter-regional capacities are shown in Figure 5-31. Compression units for operating the pipeline system are usually operated utilizing the transported gas in the pipeline itself. Therefore, the energy demand for compressing the methane for the transport along a 250 km route and additional boil-offs are represented in terms of 0.5% of transport losses [193] without additional electricity demand as assumed for hydrogen compressors.

This derived natural gas network representation is set as fixed capacity in the model. It is not further optimized in 2045 since a decrease in gas demand is expected in Germany and its neighboring countries [194], [195]. A scenario-based approach is chosen considering the reassignment of natural gas pipelines to hydrogen (cf. Section 5.4). Dismantling of pipeline capacities is not considered here.

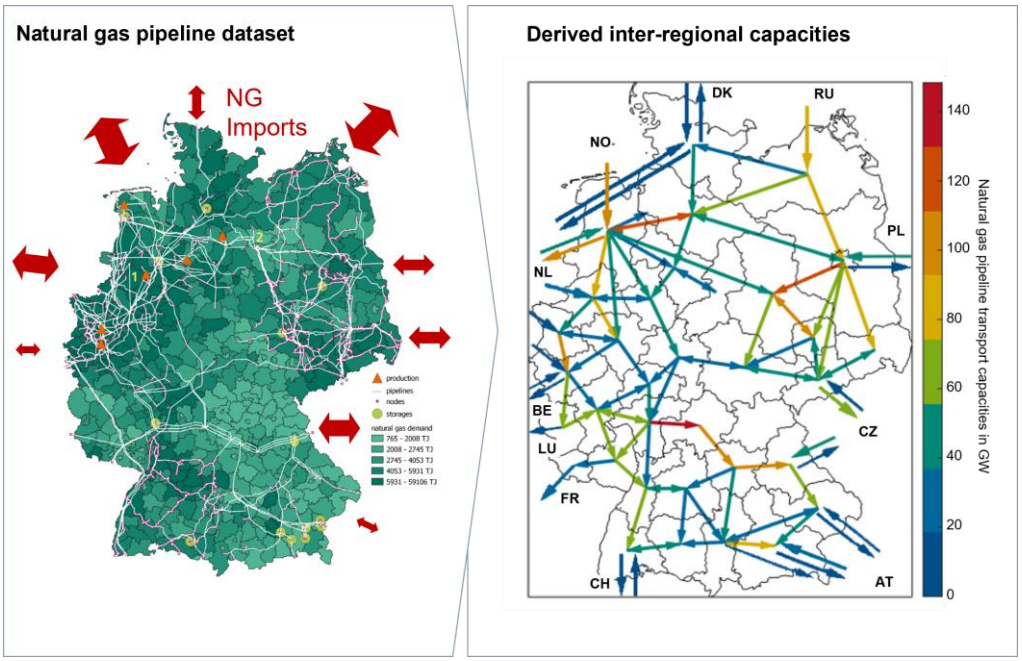

Figure 5-31 – Derived inter-regional methane transport capacities (right) from natural gas pipeline dataset (left) published by Kunz et al. [163].

	Pipeline Class	Pressure in bar	Diameter in mm	Transport capacity in GWh/day
A		100	1000 ≤ x ≤1400	651 ≤ x ≤1275
B		100	700 ≤ x ≤1000	80≤ x ≤651
C		63	500 ≤ x ≤700	41≤ x ≤201
D		25	350 ≤ x ≤500	20≤ x ≤41
E		25	250 ≤ x ≤350	4≤ x ≤20
F		63	100 ≤ x ≤200	4 ≤ x ≤16
G		63	10 ≤ x ≤100	4

Table 5-10 – Classification and capacity assignment for natural gas pipelines (adopted from [163]).

5.4 Procedure of sensitivity analysis in ESDP

A local sensitivity analysis is conducted to assess the impact of different parameters in the MMES on the decarbonization of the mobility sector. Main parameter variations are conducted and categorized into the groups ‘energy supply’, ‘energy transport’ and ‘mobility sector’. Additionally, two extreme mobility sector scenarios are defined to assess the impact of different energy carriers in the mobility sector on the MMES. The mobility sector is in these two scenarios not optimized, but a fixed technology mix is assumed. One represents

a high electrification in the mobility sector, the other represents a high usage of hydrogen in the mobility sector. All parameter variations are based on the reference scenario 'CN45-ref' targeting a carbon-neutral MMES in 2045. Table 5-11 summarizes all scenarios.

The scenarios 'Energy copper plate' and 'No Refueling Costs' are motivated from a modeler's perspective. They are used to assess the impact of these cost terms in a model, which are often neglected in energy system studies (cf. Section 1.2). A scenario assessing the impact of the availability of cavern storages is categorized in the energy transport category. Scenarios in the energy supply category vary the import or inland generation costs for different energy carriers based on the cost overview in Figure 5-30. Additionally, one scenario restricting the onshore wind turbine capacity and one scenario restricting the hydrogen inland generation are included in this category.

The 'Distributed H_2 Hubs' scenario reduces the distribution costs of hydrogen to 50% compared to the reference scenario. The costs are assumed for all technologies, including synthesis processes, to assess the impact of the assumption of no distribution costs for synthesis processes in the reference scenario (cf. Section 5.3.3). This can be interpreted in a way that optimized hydrogen pipeline networks build as center-to-center connections between two regions from the source to several distributed hubs within each region. The assumed distribution distance for the GH_2 trailer is reduced by 50% to 50-60 km for all demand processes. Synthesis processes are not directly connected to the hubs as in the reference scenario. The distribution costs decline to 2.7-3.24 ct/kWh according to [188] and are set to 3 ct/kWh in this scenario here.

Since projections for vehicle costs are highly uncertain [95], a scenario with equal vehicle costs across all technologies in the same segment is integrated to reduce the impact of vehicle costs in the model.

All scenarios in Table 5-11, but the last two, assume a charging infrastructure network design, which minimizes the charging peak load. Controlled charging using the demand side management method described in 5.2.1 is not allowed in those scenarios. BEVs charge according to their charging profiles derived based on the charge at arrival strategy.

Additionally, two scenarios are integrated to assess the impact of BEVs' flexibility and their charging infrastructure on the MMES. Therefore, controlled charging is used based on the integrated demand-side management method. One scenario uses the costs, charging profiles, and flexibility of the Low Peak charging network design and the other scenario is based on the charging network design maximizing BEV's flexibility. These scenarios are listed last in the Table.

Additional costs are parametrized in the demand side management method representing load management costs for a control box and the communication infrastructure. They are assumed for the year 2045 to 2.5% of the charging stations' capital expenditures. For public and work charging, this is assumed for a charging station with two charging points and for home charging for a charging station with only one. The specific costs are 2.1-9 €/kW plus 2% of those costs for fixed operation and maintenance costs. The cost estimation does not include compensation payments for vehicle owners or costs for occupying the charging station for longer than required.

Due to presumed grid restrictions, the maximum simultaneously occurring upshift of charging load from the original charging profile due to controlled charging is limited to 35% (Low Peak scenario) and 70% (High Flexibility scenario) of the maximum occurring charging peak load. It is assumed that the increased number of charging stations in the High Flexibility scenario allows a better distribution of flexible provision across different grid areas, which increases the overall upshift capability.

Furthermore, the 3-hour delay charging processes occur predominantly at public charging locations. It is assumed that 70% of potentially flexible public charging processes planned according to the Charge at Arrival strategy are available simultaneously for a shift. This includes a risk discount since the projected flexibility can differ from the realizable flexibility due to spontaneous decisions of drivers. The same assumption applies to home charging. Work charging is assumed to be more predictable and is therefore only limited to 90%. Those assumptions are valid for both charging infrastructure scenarios.

Identifier	Category	Motivation	Description of parameter variations	Value in the reference scenario
CN45-ref	Reference	Carbon-neutral MMES in 2045	-	-
Wind Onshore Restricted	Energy supply	Tight land restrictions for onshore wind turbines remain unchanged as in 2020	150GW maximum onshore wind capacity	250GW
Direct Air Capture expensive	Energy supply	Decelerated decrease of Direct Air Capture cost	CO_2 prices for e-fuel synthesis in Germany: 200€/t_{CO2}	50€/t_{CO2}
Low H_2 Import Costs	Energy supply	International H_2 imports are fostered by politics to guarantee the lowest H_2 import costs	GH_2: 5-10ct/kWh depending on import route; cost difference between import routes according to the reference scenario	7- 12ct/kWh
Low Fuel Costs	Energy supply	International H_2 & e-fuels (gaseous and liquid) imports fostered by politics	e-Fuel: 10.4ct/kWh e-CH_4: 7.1ct/kWh GH_2: 5-10ct/kWh	15.3ct/kWh 10.6ct/kWh 7-12ct/kWh
High Fuel Costs	Energy supply	Worldwide competition increases market prices of H_2 & e-fuels	e-fuel: 19ct/kWh e-CH_4: 16ct/kWh GH_2: 14-19ct/kWh	15.3ct/kWh 10.6ct/kWh 7-12ct/kWh
High e-Fuel Costs	Energy supply	Worldwide e-fuel demand increases market prices; H_2 import routes are not impacted	e-fuel: 19ct/kWh	15.3ct/kWh
Green LCH_4 Imports	Energy supply	Green synthetic liquid fuel imports routes are built up	LCH_4: 9.4ct/kWh	Not applicable
Low CH_4 Costs	Energy supply	E-methane import routes established cost-efficiently to substitute natural gas	e-CH_4: 7.1ct/kWh	10.6ct/kWh
100% H_2 Imports	Energy supply	Low economic viability of electrolyzers in Germany hinders investors	No inland H_2 generation	Optimized electrolysis capacity and generation

Table 5-11 – Scenario descriptions for sensitivity analysis in ESDP (part 1 of 3).

Energy Copper Plate	Energy transport	Model: impact of neglecting energy transport costs in energy system studies	All energy transports free of costs	cf. Section 5.3
Restricted Grid Expansion	Energy transport	Low acceptance of new electricity transmission lines by the population decelerates the expansion until 2045	Maximum capacity of each connection restricted to 150% of the 2017 net transfer capacities	Maximum restricted to 300%
H2 Pipe Recompression	Energy transport	Model: additional recompression along each pipeline	283€/MW/km (cf. Table 5.8)	128 €/MW/km
NG Pipe 30% Reassignment	Energy transport	Natural Gas (NG) pipeline system operators reassign a few pipelines for H_2	30% of NG pipeline capacity in Germany used for H_2 (costs: cf. Table 5.8)	0%
NG Pipe 70% Reassignment	Energy transport	NG pipeline system operators reassign most pipelines for H_2, only securing crucial European connections for NG	70% of NG pipeline capacity in Germany used for H_2 (costs: cf. Table 5.8)	0%
Only GH_2 Trailer	Energy transport	Large infrastructure pipeline projects are not realized until 2045	Only transport via GH2 trailer (costs: cf. Table 5.8)	Pipeline and trailer transport optimized
Distributed H_2 Hubs	Energy transport	Efficiently planned pipeline network from sink to a source with distributed hubs within one region minimizes the total distribution distance within each region; all applications pay the same distribution costs	3ct/kWh H_2 distribution for all applications, including synthesis processes	6.15ct/kWh for all applications, but synthesis processes (cf. Section 5.33)
No H_2 Cavern Storage	Energy transport	Cavern storages in Germany are not cost-efficiently established as large-scale H_2 storages	Maximum cavern storage capacity of 0GWh	930GWh

Table 5-11 – Scenario descriptions for sensitivity analysis in ESDP (part 2 of 3).

No Refueling Costs	Mobility sector	Model: impact of neglecting refueling and charging infrastructure costs in energy system studies	No costs for refueling and charging processes	cf. Section 5.3.2
Equal Vehicle Costs	Mobility sector	Diversification of technologies in international automotive markets	Equal costs for all mobility technologies, including road, rail, and water	Appendix C
Hydrogen Mobility	Mobility technologies fixed	Hydrogen usage in the mobility sector	Road transportation and inland shipping: 60%-95%; rail: >40% of non-electrified rail transportation	Optimized with an upper limit of 95%; rail limit of 50%
Electric Mobility	Mobility technologies fixed	Electrification of road transportation	Penetration rates: BEVs, Bus Battery, LDV Battery: 90%-95%; HDV battery 60%-95%	Optimized with an upper limit of 95% penetration rate
Controlled Charging Low Peak	Controlled Charging	Pareto optimal charging infrastructure design, which minimizes the total charging peak	Controlled charging	Charge at Arrival without controlled charging
Controlled Charging High Flexibility	Controlled Charging	Pareto optimal charging infrastructure design, which maximizes the total daily flexibility of BEVs	Controlled charging	Not considered

Table 5-11 – Scenario descriptions for sensitivity analysis in ESDP (part 3 of 3).

The model is built up in GAMS and solved with CPLEX using an interior-point approach. This solving algorithm is chosen because it is considered best practice for large linear energy system models [196].

The linear problem has a size of 7.4 Gigabytes. After pre-solving the problem in CPLEX, the model is reduced to 2.38 million rows, 4.47 million columns, and 13.55 million non-zero coefficients. Every third hour of six representative weeks is modeled to reduce the complexity and the computational effort (cf. Section 2). The total parallel computation time using 32 threads on a server is about 3 hours.

6 Results

The interactions of a decarbonized mobility sector and the energy supply, transport, refueling, and charging infrastructure requires a fundamental modeling and simulation framework. After the framework is described in the previous sections, the research questions are answered consecutively in this section.

The MMES optimization is analyzed for the target year 2045. Existing assets and planned assets, according to the NEP 2030 (2019), are set as initially installed capacities, and the capacity expansion and the technologies' operation are optimized for the target year 2045. Nuclear, lignite, and coal power plants will be phased out before 2045. The reference scenario 'CN45-ref' targets a carbon-neutral energy system in Germany in 2045. The mobility demand is assumed to increase by 14.6% compared to 2020 based on an EU reference scenario [197]. This includes, inter alia, 5.6% growth in private road transportation, 61.4% in passenger rail transportation, 11.9% in road freight transportation, and 24% growth in freight rail transportation. Weighted average costs of capital are assumed to be 7%.

The total multi-modal energy demand in the optimized reference scenario is 1898 TWh in Germany in 2045 (cf. Figure 6-1). All demands but the energy demand in the mobility sector, electricity exports, and electricity losses are exogenously fixed. Efficiency gains of, e.g., 18% for HDV IC-LF compared to 2020 and especially of 78% by BEVs compared to Car ICE-LF in 2020, reduce the mobility sector's energy consumption by a factor of 2.8 from 761 TWh to 272 TWh in 2045. Direct electrification can be cost-optimally achieved in many applications in the heat and mobility sector, which increases the share of MMES's electricity consumption from the overall end energy usage to 63%. To supply this, the electricity generation increases by 210% compared to 2019. A major share of 93% is generated by renewables with wind turbines and PV capacities of 601 GW. Since PV is the cheapest source of electricity, it is installed up to its available maximum capacity of 343 GW, including roof and ground-mounted systems. In contrast, onshore and offshore turbine capacities are not fully expanded in the model. Especially, offshore turbines are capital-intensive investments, and hence, only 15 GW are installed despite their 4170 full load hours. Additionally, offshore turbines require the largest grid investment. Presumed weighted average cost of capital of 7% further increase the costs of capital-intensive investments. Contrary, PV has the lowest capital expenditures of all three technologies and additionally the most even spatial distribution across Germany. Those advantages exceed the low availability of solar energy of on average 1140 full load hours. The volatile generation capacities are supplemented by 114 GW of the flexible assets (batteries and imports, excluding gas power plants). The latter is considered here as flexible but still relies in the model on the hourly

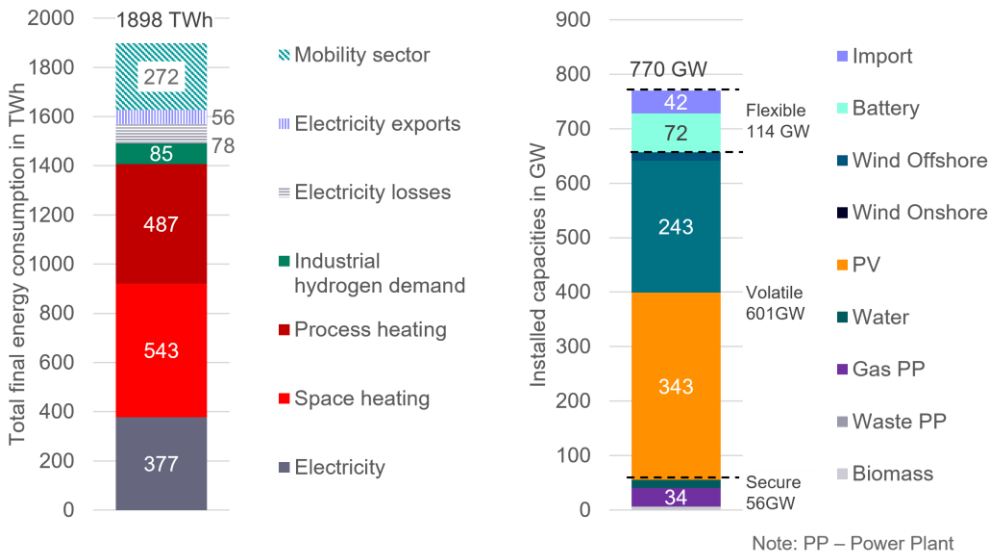

Figure 6-1 – Total final energy consumption (left) and electricity supply capacities (right) in the reference scenario.

availability of the electricity generation and the hourly demand in each country. In neighboring countries, 78 GW of gas power plants and 30 GW of battery capacity are installed.

The seasonality of electricity generation from wind turbines is contrary to PV generation (cf. Figure 6-2). While wind energy is primarily generated in January and late October, PV peaks of up to 240 GW occur predominantly from March to August. In total, 3% of the annual wind and solar energy is curtailed predominantly in January

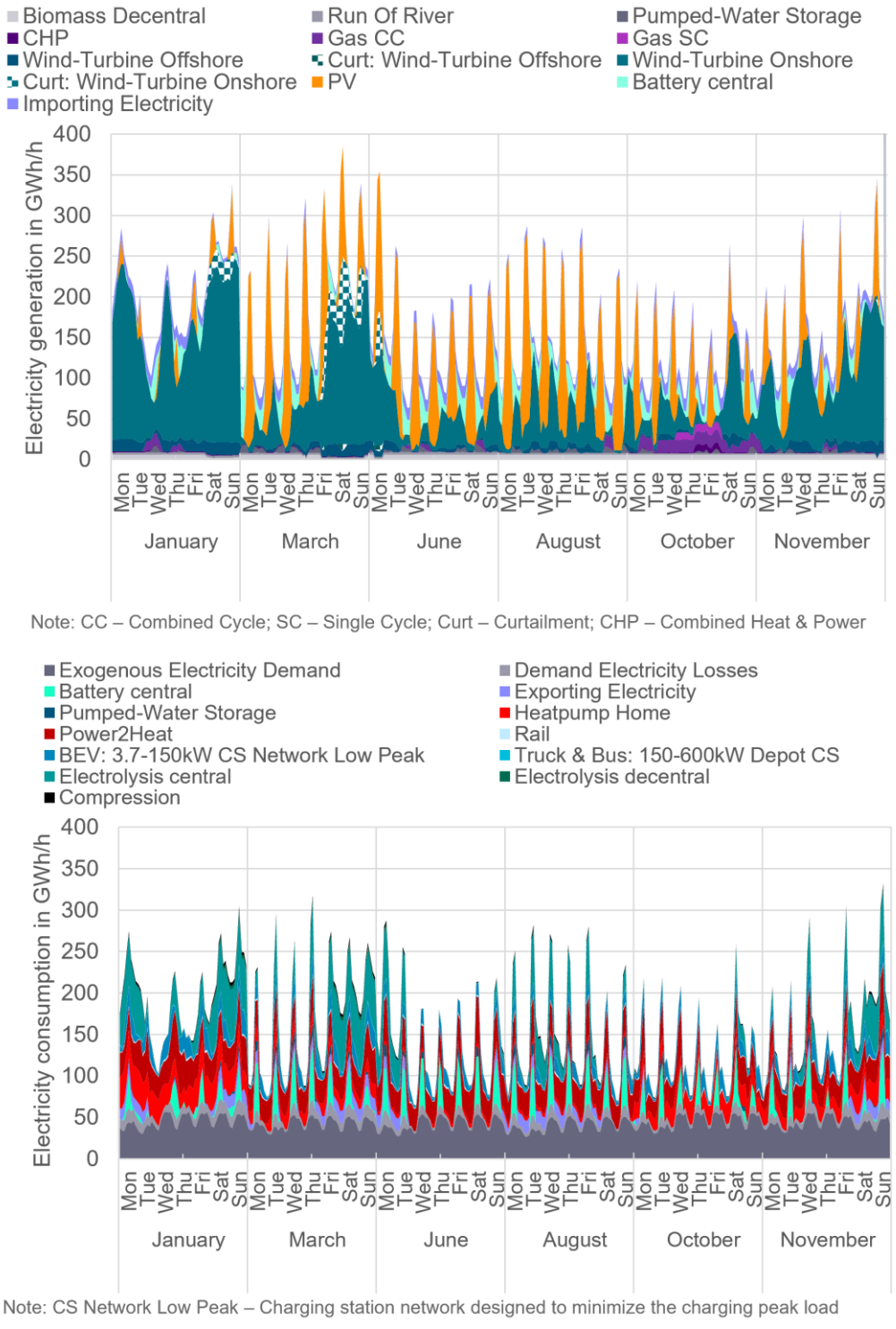

Figure 6-2 – Electricity generation (top) and demand (bottom) for six representative weeks on a three-hourly time step.

and March. The high generation of RES with a peak of more than 300 GW and a generation above 200 GW for several consecutive days drives the curtailments. In contrast, daily PV peaks in summer are not curtailed since battery storages and heat pumps provide enough short-term flexibility. Gas turbines fueled by e-methane run in times of low availability of renewable energy sources. This is mainly in October to generate electricity and heat. Hydrogen is not used in gas turbines.

The electricity peak load is supplied by volatile RES, secured capacities and flexible sources on. Including the operation of flexible demands balancing the RES, it amounts to 335 GW. This is about four times as high as in 2019, and it is mainly driven by the need to balance the increased PV and wind turbine capacities. Heat pumps, electrolyzers, and batteries are the main sources of flexibility on the demand side, whereas residential heat pumps operate primarily in winter to satisfy the space heating demand. This aligns with the higher availability of RES in winter and reduces battery utilization in winter. Batteries function as short-term storage complementing the daily PV generation. Electrolyzers operate more versatile, generating large amounts of hydrogen in January and March, which is then stored and used across the year. In summer, electrolyzers mainly operate to balance the PV peak generation.

The mobility sector's electrification is mainly driven by passenger cars and LDV. The consumed electricity of the mobility technologies transporting passengers and freights amounts with 142 TWh in 2045 to 10% of the total electricity demand. Passengers are transported to 71% by BEVs consuming 104 TWh of electricity (cf. Figure 6-3). While this is 95% of the individual passenger road transportation, fuel cell vehicles complement the segment with 5%, consuming 8 TWh. Hydrogen is not further used in the mobility sector. Inland flights, still relying on ICEs combusting e-fuels, account for 16% of the total energy demand while serving only 8% of the traveled kilometers. Public road passenger transportation by busses is split into e-fuel combustion and battery-electric powertrains. The electrification of the freight transportation is only in the LDV segment cost-optimal, and only 1% of the energy consumed by HDV is provided by Catenary powertrains. HDV-ICEs consume 90% of the road freight transportation's energy and serve 63% of the road freight transportation demand. Ships running on e-fuels demand 7.6% of the total energy of freight transportation.

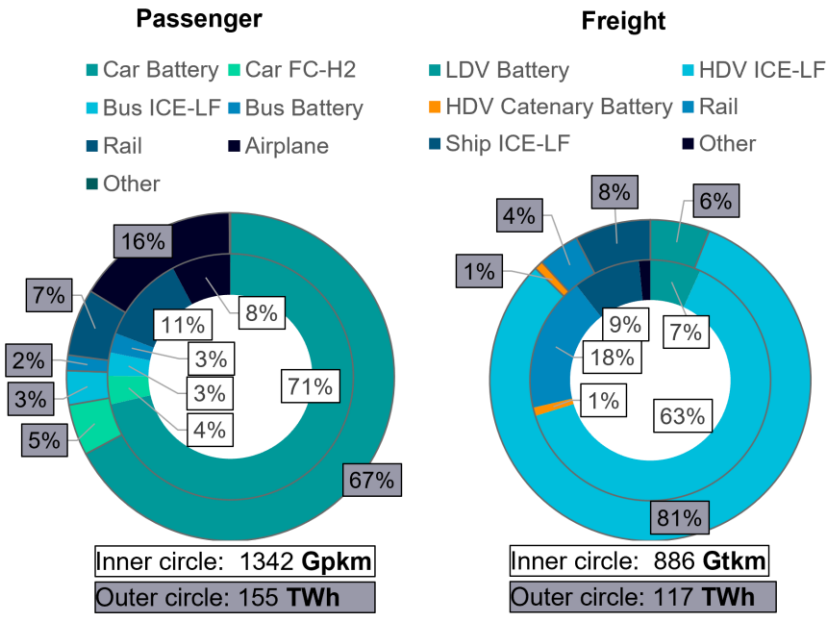

Note: FC – Fuel Cell; ICE – Internal Combustion Engine; LF – liquid fuel (e-fuel); LDV – Light Duty Vehicle; HDV – Heavy Duty Vehicle; Gpkm – Giga passenger kilometers; Gtkm – Giga tonne kilometers

Figure 6-3 – Mobility sector demand in traffic capacity (inner circle) and energy consumption (outer circle) for passenger (left) and freight (right) transportation

The optimized energy transport networks depend on the regional generation capacities of electricity and hydrogen. Figure 6-4 shows the capacities for onshore wind turbines, PV, and Electrolyzers on the NUTS2 level. PV is installed up to its maximum capacity within each region, resulting in a more balanced distribution over the entire country than wind turbines. Onshore wind turbines are primarily installed in regions with high full load hours in northern Germany (cf. Figure 5-16) and in regions with large available land areas, such as Mecklenburg-Western Pomerania, reaching a capacity of 45 GW. The optimizer allocates 37 GW of electrolyzer capacities in Germany, leading to 130 TWh of hydrogen generation in Germany. Those electrolyzers are predominantly installed in four regions: Mecklenburg-Western Pomerania (15 GW), Schleswig-Holstein (8.9 GW), Weser-Ems (7.2 GW), and Saxony-Anhalt (4.7 GW). Additionally, 59 TWh (81% of the imported hydrogen) comes from Northern Europe and lands in Schleswig-Holstein via pipeline. The marginal costs of inland generated hydrogen depend strongly on the time of operation. Electrolyzers operate to 99% in times with available electricity prices below 5 €/MWh. Operating 3000 hours of the year, the average variable hydrogen generation costs are 3.5 ct/kWh[7]. The volume-weighted average marginal costs of inland hydrogen generation are 7 ct/kWh.[8] This shows that the electrolyzer utilizes low electricity costs to generate hydrogen if the marginal costs of hydrogen stay below the import costs from Northern Europe and Southern Europe. The low electricity costs and the High Flexibility of electrolyzers explain the high amount of inland generated hydrogen in the model. It can be derived that transporting electricity is avoided by optimally allocating the electrolyzers in locations with a high renewable electricity generation potential.

The mobility sector's demand for e-fuels can be generated inland due to the low hydrogen generation costs. While a total of 206 TWh of hydrogen is consumed in 2045, only 8 TWh of hydrogen is directly used in the mobility sector. A large share of 41% is consumed in the steel and ammonia industry, but the most significant share of 55% is used in FT synthesis processes generating e-fuels for the mobility sector. It shows that this is cost-competitive against e-fuel import costs of 15.3 ct/kWh due to low hydrogen costs. Using existing vehicle technologies for e-fuels as well as transport, distribution, and refueling infrastructure favors the usage of e-fuels over hydrogen. Therefore, electricity transportation and grid extensions are reduced by converting electricity into hydrogen and e-fuels.

Figure 6-5 shows the optimized transport capacities between NUTS2 regions for hydrogen and electricity as delta capacities to the initial grid in 2017, and methane. With total electricity grid capacities up to 15 GW and hydrogen capacities up to 10 GW, both energy transport infrastructures stay 10 below the methane network. The net transfer capacities of electricity in 2017, in comparison, are 1.9 GW and reach a maximum of 5 GW. One reason for not reaching methane transport capacities is that no hydrogen exports are considered in the optimization, which could increase the hydrogen pipeline capacity between German regions. However, an enormous extension of electricity grids by factor three is required. Minimal electricity grid extensions occur in the south, south-west, and east of Germany. Larger grid extensions of 5 GW-10 GW are calculated, e.g., in Schleswig-Holstein, Hessen, between Thuringia and Upper Franconia, and between Weser-Ems and Muenster. Those extensions connect regions with low installations of wind turbines with wind-dominated regions in the North. An exception is in the North-East, from Mecklenburg-Western Pomerania and Brandenburg to other regions, where only minor electricity grid extensions are installed in wind-dominated regions. Instead, the optimizer installs hydrogen pipelines of up to 5 GW in Mecklenburg-Western Pomerania, converting wind energy to hydrogen and transporting it via pipelines to other regions. Additionally, the electricity grid is expanded between Schleswig-Holstein and Mecklenburg-Western Pomerania by up to 4 GW to increase the electricity available for the hydrogen conversion. The very high hydrogen availability by inland electrolysis and imports in Northern Germany strongly affects the structure of the hydrogen pipeline network. The hydrogen is distributed

[7] The given cost of hydrogen is here based on the hourly marginal electricity costs by multiplying the generated hydrogen in each hour with the marginal electricity costs. The marginal electricity costs are costs for an additional incremental unit of electricity demand in the model. Further, capital expenditures are not integrated in this price.

[8] This means, that 130TWh of hydrogen can be generated for marginal costs below 7 ct/kWh.

southwards to the rest of Germany with pipeline capacities of 9 GW-10 GW. Only Tubingen and Swabia in the South are supplied by trailer due to low hydrogen demands and long transport distances.

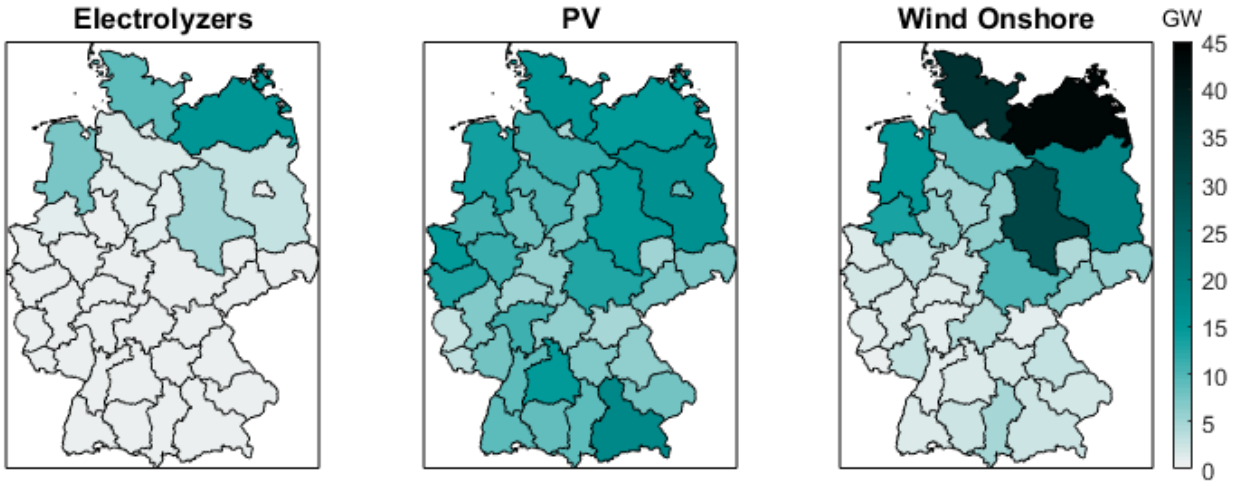

Figure 6-4 – Regional capacities for Onshore Wind Turbines, PV, and Electrolyzers (region names in Appendix B).

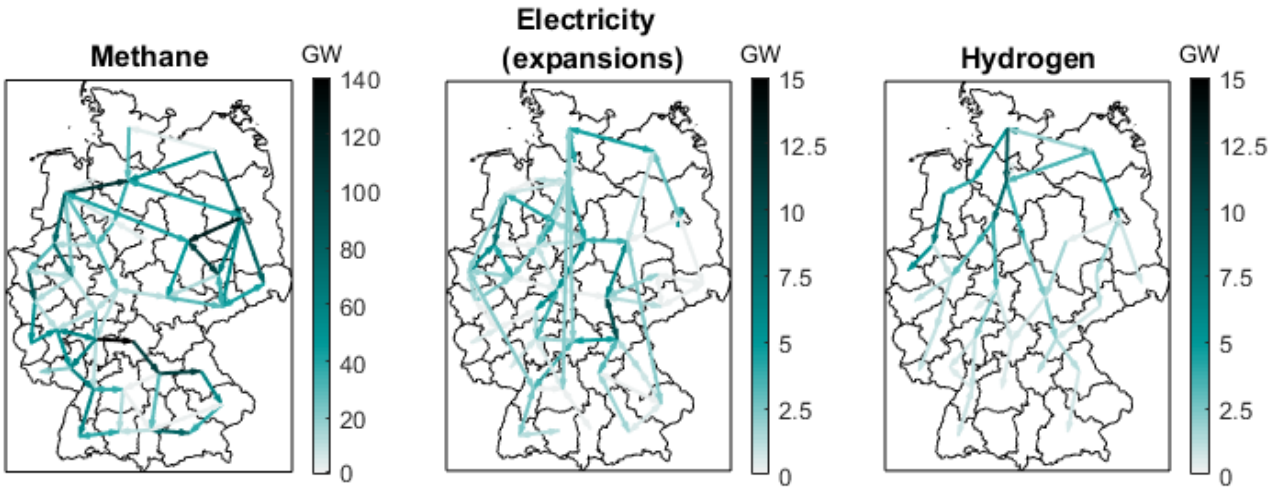

Figure 6-5 – Energy transport capacities of commodities methane, electricity (expansions to 2017), and hydrogen (region names in Appendix B).

6.1 Energy carriers in the mobility sector

The robustness of the above-presented cost-optimal energy carriers in the mobility sector is assessed in this section. Detailed insights into the technology mix of the passenger and freight transportation sectors are shown in Appendix D and mentioned throughout the following paragraphs.

The total energy demand in the mobility sector ranges from 243 TWh to 295 TWh, with its minimum and maximum energy demand occurring in the fixed mobility sector scenarios (cf. Figure 6-6). The total energy consumption in the Hydrogen Mobility scenario exceeds the consumption in the Electric Mobility scenario by

20%. This is caused by the lower efficiency of fuel cell vehicles of 40% compared to direct usage of electricity. However, the mobility sector is still electrified by 30%, reducing the total increase of energy consumption in the mobility sector.

Electricity and liquid fuels are the dominating energy carriers in most scenarios. Nevertheless, the number of scenarios showing a specific energy carrier as cost-optimal does not directly indicate their relevance. Electricity provides 46% (123 TWh) to 66% (171 TWh) of the total energy demand, excluding the Hydrogen Mobility scenario. The lowest direct electricity consumption in the mobility occurs if electricity transmission grid extensions are restricted (Restricted Grid Expansion). The restriction increases the need for flexibility, which can be provided from electrolyzers and hydrogen storage. Decreased electrification rates of 68% and 4% of busses and passenger cars, respectively, reduce the electricity demand in the mobility sector by 5% compared to the reference scenario.

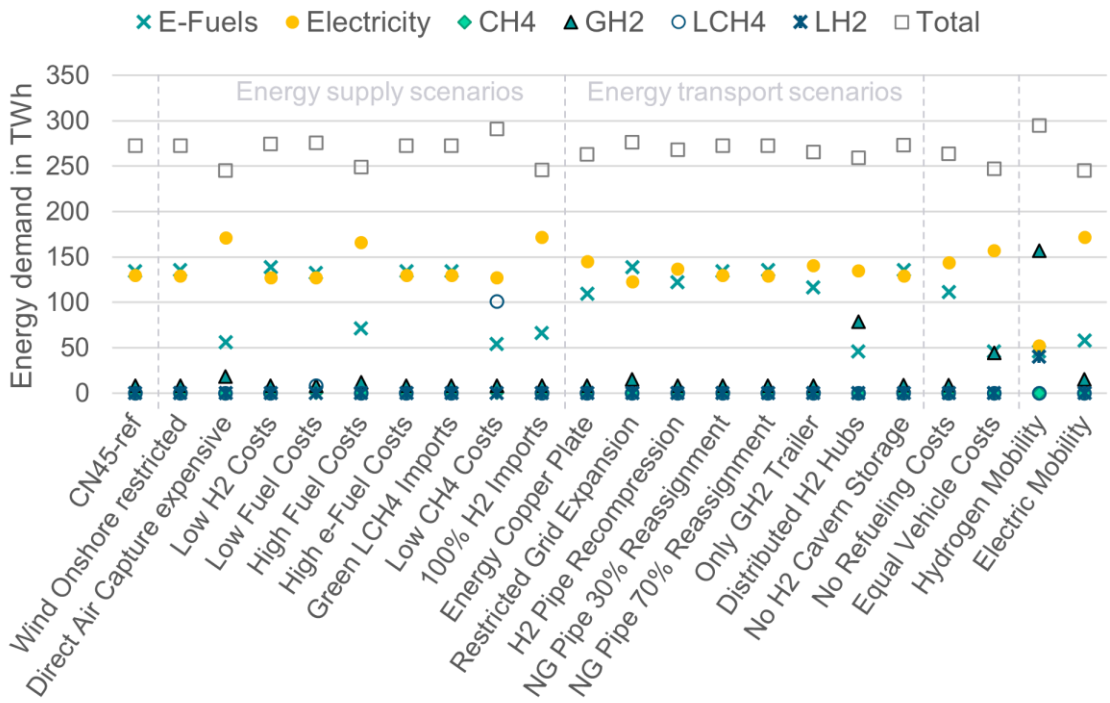

Figure 6-6 – Cost-optimal energy carriers in the mobility sector for the reference scenario CN45-ref, 19 additional scenarios, and the two fixed mobility sector scenarios Hydrogen Mobility and Electric Mobility.

Further, depending on the scenario, the e-fuel consumption is between 46 TWh and 139 TWh. Its utilization is low if both e-fuel and hydrogen costs increase simultaneously (High Fuel Costs), alternative powertrain technology costs even out with ICE costs (Equal Vehicle Costs), e-methane is available at low costs (Low CH4 Costs), energy transport or refueling costs are neglected (No Refueling Costs), hydrogen is import to 100% (100% H2 Imports), or if H2 distribution costs to refueling station decreases by simultaneously increasing the hydrogen distribution for usage in FT synthesis (Distributed H2 Hubs). The latter scenario is the only scenario with cost-optimized energy carriers in the mobility sector, in which the reduced e-fuel consumption is substituted by hydrogen.

The consumption of hydrogen in the mobility sector is below 18 TWh. It only increases to 44 TWh if the hydrogen vehicle powertrain costs are equal to other vehicle technologies (Equal Vehicle Costs) and to 79 TWh if distributed hydrogen pipeline hubs (Distributed H2 Hubs) are realized. The latter decreases the overall hydrogen distribution costs for the sake of higher hydrogen distribution costs to synthesis process locations. In contrast, a reduction of costs for hydrogen imports by 14% (lowest import route at 5.9 cents per kWh) does not increase

the hydrogen share in the mobility sector. This is due to the cost-efficient pathway of converting hydrogen into e-fuels while using existing vehicle technologies at lower costs and existing infrastructures for transport, distribution and refueling. The technology-neutral assessment here shows that the hydrogen generation or import cost itself is not the main lever for a direct hydrogen usage in the mobility sector. Increased variable synthesis costs (Direct Air Capture expensive) increase the hydrogen usage only slightly by 9 TWh in the passenger car segment. The main lever is the cost ratio between synthesis costs and hydrogen costs at the refueling station. If this is balanced (Distributed H2 Hubs), hydrogen is not converted to e-fuel but used directly in passenger cars and LDV. Simultaneously, instead of liquifying the hydrogen for usage in the HDV segment, the electrification increases by 90%.

The impact of different scenarios on the optimal energy carriers is further elaborated in Figure 6-7. The reference and the Electric Mobility scenario are dominated by electrification and e-fuels and are therefore drawn near the diagonal line. Contrary, the Hydrogen Mobility scenario is characterized by a high share of hydrogen usage and is hence offset. Compared to the Electric Mobility scenario, electrification is not substituted by e-fuels but by hydrogen. The electrification rate in the optimized scenarios ranges from 57% to 79%.

The assessed energy supply scenarios result, but in the low methane cost scenario, in substitution of e-fuels with electrification or vice versa (cf. Figure 6-7). This impact can be described in three steps.

First, three scenarios show no deviation in the mobility sector from the reference scenario. One of the scenarios is ff a restricted availability of land for onshore wind turbines is applied (Wind Onshore restricted). Even though 37% fewer wind turbines are installed in this scenario, it does not impact the electrification rate. The reduced availability of electricity is compensated primarily by reducing the share of hydrogen generation in Germany from 64% to 42% and increasing the hydrogen import volumes accordingly. Further, no deviation from the reference scenario occurs if liquid e-methane imports are enabled to 9.4 ct/kWh (Green LCH4 Imports) or if e-

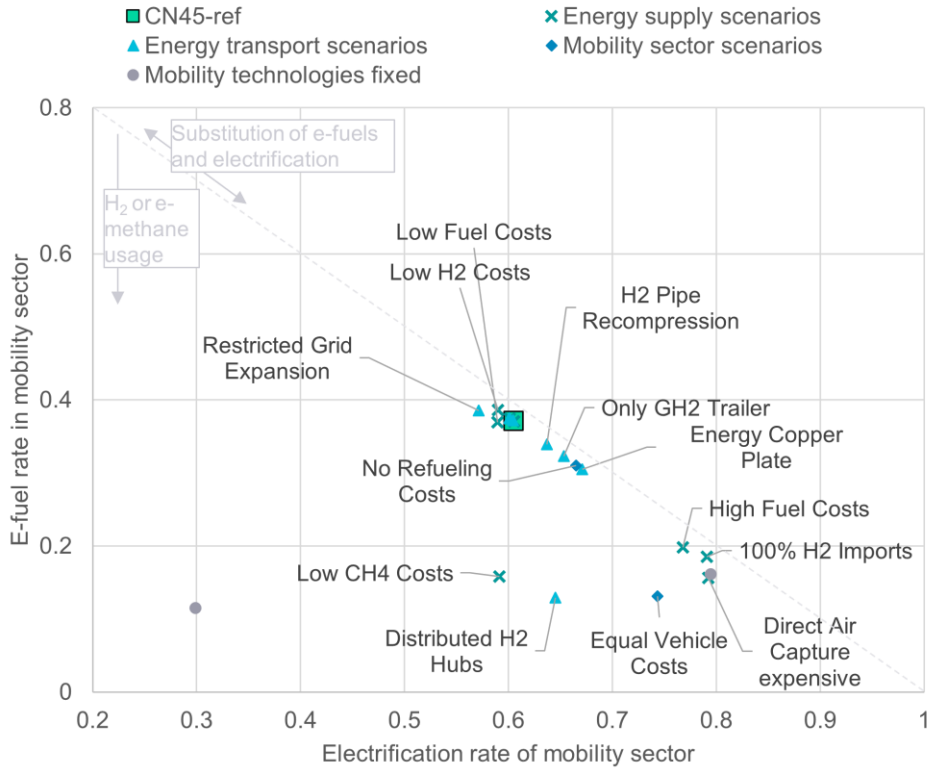

Figure 6-7 – Electrification and e-fuel rate in the mobility sector in dependency on the energy supply and transport infrastructure. Electrification and e-fuel rates are defined based on the Gpkm and Gtkm supplied by the corresponding commodity. The dashed line indicates the bisector along which e-fuels and electricity are perfectly substituted. The larger the Euclidean distance of a scenario this diagonal, the more hydrogen or methane is consumed in the mobility sector.

fuel import costs increase by 22% to 19 ct/kWh (High e-Fuel Costs). The latter scenario has no impact since the optimizer does already not import e-fuels in the reference scenario.

Second, scenarios in the energy supply category that show a reduced electrification rate by 1%. Those are scenarios with low assumed import costs either for all fuels, including e-methane and hydrogen (Low Fuel Costs), only for hydrogen (Low H2 Costs), or only for e-methane (Low CH4 Costs). In the first two of those scenarios, the electrification rate of the bus fleet decreases from 48% to 12%. If all fuels are available at low cost, an additional 7% of HDVs are switched from ICE-LF to ICE-LCH_4. If only e-methane is available to 7.1ct/kWh instead of 10.6ct/kWh (Low CH4 Costs), 87% of the HDVs are switched to ICE-LCH_4, and the ICE-LF busses increase from 53% to 82%.

Third, scenarios with high energy supply costs boost the electrification by substituting the usage of e-fuels. Those scenarios are characterized by a scarcity of low-cost e-fuels. High fuel import costs (High Fuel Costs), including e-methane and hydrogen, drive the demand for using 103 TWh of inland generated hydrogen for methanation instead of FT synthesis. Methane is required for heat and electricity generation in gas power plants. E-fuels from hydrogen imports cannot compete with the direct electrification of HDVs and busses. This argument is additionally supported by the scenario with 100% H2 imports, where the hydrogen is solely used to supply the industry and generate e-fuels for ships, aviation, and for a minor share of HDVs. Further, high e-fuel inland generation costs due to increased CO_2 prices for synthesis processes decrease the e-fuel usage (Direct Air Capture expensive). E-fuel imports at 15.3 ct/kWh are not cost-competitive compared to the electrification of the mobility sector. This shows that the impact of the scarcity of low-cost e-fuels on the cost-optimal energy carriers in the mobility sector exceeds the impact of the increased electricity costs from additional electricity demand due to an increased electrification rate. The lower efficiency of the consumption of e-fuels in the mobility sector compared to electricity is one reason for the high e-fuel sensitivity of the optimal solution. The marginal e-fuel costs at the refueling station increase by 11% to 22%, and the higher electricity demand increases the marginal electricity costs at the charging station simultaneously by 7% to 18%. The optimizer increases in all three scenarios the electrification of busses up to 87% and the electrification of HDVs up to 80%.

Furthermore, Figure 6-7 shows the impact of the modeled energy transport infrastructure parameter variations on the energy carriers in the mobility sector. The lowest electrification rate (57%) and the highest e-fuel rate (39%) are cost-optimal if the electricity grid expansion is restricted to 150% of the grid capacities in 2017 (Restricted Grid Expansion). The bus fleet's electrification rate declines in return for ICE-LF busses and increases the share of FC-H_2 Cars by 82%, consuming 14 TWh of hydrogen, compared to the reference scenario. The reduced electricity transport capacities cause increased marginal electricity costs by 6% and an increased value of the electrolyzers' flexibility. The latter is reflected in a 19% increase in the share of hydrogen inland generation.

While reduced hydrogen transport costs by reassigning gas pipelines (NG Pipe 30% Reassignment, NG Pipe 70% Reassignment) do not impact the mobility sector, increased hydrogen transport costs by a factor of two due to increased hydrogen compression demand for the pipeline transport (H2 Pipe Recompression), or by a factor greater than six due to a country-wide trailer transport (Only GH2 Trailer), increase the electrification rate by 5% and 8%, respectively. This substitution occurs in the HDV segment by introducing hybrid catenary trucks with battery systems. It is primarily reasoned by a decline of the full load hours of electrolyzers by 27%, leading to a reduction of cost-efficient FT e-fuel conversion by 54%.

If distributed hydrogen hubs are considered for hydrogen transport (Distributed H2 Hubs), 79 TWh of hydrogen is used directly in the mobility sector. While this increases the overall efficiency compared to using hydrogen in synthesis processes, it reduces the overall hydrogen demand in the MMES by 12%. It results in the following changes in the different mobility sector segments compared to the reference scenario: 46% penetration of FC-H_2 Cars compared to 5%, 88% electrification of busses compared to 46%, 59% LDV FC-H_2 compared to 5%, and 90% electrification of HDV, including full Battery and Catenary Battery HDVs. The increased electrification in the HDV and bus segment is here cost-optimal compared to direct usage of hydrogen. Increased hydrogen costs for synthesis processes trigger the substitution of e-fuels since they are assumed to be not directly located at the transport pipeline hub but require hydrogen distribution for their hydrogen supply. Finally, if energy transport

costs are neglected in the MMES (Energy Copper Plate), the electrification increases by 12% by using HDV Catenary Battery trucks.

Moreover, refueling and charging station costs, including catenary systems, and vehicle costs impact the optimal technology mix in the mobility sector as well (No Refueling Costs). If no refueling and charging station costs are considered in the MMES model, the electrification will increase by 10% (cf. Figure 6-7). The technology shift occurs in freight transportation substituting HDV ICE-LF with HDV Catenary Battery. If all transportation technology costs are equal (Equal Vehicle Costs), electrification and hydrogen will replace the ICE technologies. Busses are electrified to 96%, HDVs running on e-fuels are reduced to 5% introducing HDV Battery and Hybrid HDV Catenary ICE-LF trucks. But also, the electrification of passenger cars is reduced, and FC-H2 cars' penetration reaches 29%. Finally, only this scenario introduces fuel cell trains on today's non-electrified railways supplying 9% of the total rail transportation demand. This shows that the costs of a train are the main lever for the usage of fuel cell trains.

The analysis of the energy carriers in the mobility sector shows that e-fuels and electricity[9] are relevant in the transportation segments with capital-intensive technologies: busses, HDVs, trains, and ships[10]. Hydrogen and electricity are relevant in less capital-intensive segments: passenger cars and LDVs (cf. Appendix D). It further shows that especially busses and HDVs are affected by the sensitivities conducted in the MMES. This can be attributed to the comparatively high operational costs, with consumption rates exceeding those of ICE-LF Cars by a factor of five to six.[11]

Now, by summarizing the key findings in the current Section, Research Question 1 can be answered.

[9] Not applicable here for vessels.

[10] Airplanes can only be fueled by e-fuels in the present thesis and are therefore not further specified in the analysis here.

[11] Factor based on ICE-LF technologies for cars, busses, and HDVs.

RQ1: What are the optimal energy carriers to fuel a decarbonized mobility sector and how does the required energy supply and transport infrastructure impact the share of those energy carriers in a cost-optimally decarbonized Multi-modal Energy System?

Electrification:

(a) The introduction of electric powertrains decreases the end energy demand in the mobility sector by up to factor three compared to 2019.
(b) The electricity consumption in the mobility sector is between 123 TWh and 171 TWh, with an electrification rate in the passenger road transportation above 79%. This is only reduced to 70% if vehicle technology costs even out across all powertrains or to 55% if annually averaged marginal hydrogen costs at the refueling station are 49% lower than electricity costs.
(c) An electrification rate in the entire mobility sector between 63% and 79% is cost-optimal if liquid fuels and hydrogen are both only available at high costs, alternative powertrain costs even out with ICE powertrains, or hydrogen transport costs increase compared to the reference scenario.
(d) An increase of the electrification rate from 61% to 67% can occur if cost parameters for electricity transportation or charging and refueling infrastructure are neglected.

E-fuels and hydrogen:

(e) Between 46 TWh and 139 TWh of e-fuel is consumed with an e-fuel utilization rate in the mobility sector varying between 13% and 39%. High e-fuel usage is cost-optimal if sufficient hydrogen for synthesis processes is available below 6.9 ct/kWh or CO_2 costs from direct air capture are at 50 €/ton CO_2.
(f) Hydrogen provides between 8 TWh and 79 TWh of energy to the mobility sector. Cost-optimal usage of hydrogen is observed, if vehicle technologies even out in 2045, or if hydrogen distribution cost discrepancies between synthesis processes and hydrogen refueling stations even out at 3 ct/kWh.
(g) The e-fuels used are used in capital intensive modes of transportation (busses, HDV, trains, ships), and the hydrogen is used in segments with lower capital investments (cars, LDVs).
(h) The cost-optimal technology mix in the mobility sector and the corresponding energy carriers are more sensitive on parameter changes in transportation segments with high variable operational expenditures (busses, HDVs).

6.2 Energy infrastructure for a decarbonized mobility sector

The impact of parametrizations of the energy system on the energy carriers in the mobility sector is investigated in Section 6.1. Subsequently, the mobility sectors' impact on the MMES is assessed in the current Section. The assessment covers the electricity generation, the heat sector, and the hydrogen supply chain, including the energy transport infrastructure. While this section still includes all scenarios, the focus is on the fixed mobility sector scenarios Hydrogen Mobility and Electric Mobility, which represent extreme scenarios.

While the optimized gas power plants and PV capacities are constant in all scenarios, the optimized onshore wind turbine capacity varies significantly from 184 GW to 250 GW, excluding the scenario with limited onshore wind turbine capacities (cf. Figure 6-8). In contrast, capital intensive offshore wind turbine capacities are non-sensitive to the parameter variations and increase only from 15 GW to 37 GW or 34 GW if onshore wind turbines

are restricted to 150 GW (Wind Onshore restricted), or if both e-fuel and hydrogen import costs increase as in the 'High Fuel Costs' scenario, respectively. The total annual electricity generation increases by factor 2 to 2.6 compared to 2019. The annual electricity generation from wind turbines and PV amounts to 938 TWh to 1234 TWh, which is 90% to 93% of the annual electricity generation in Germany in 2045. Gas power plants run for 1176 to 1676 hours per year; averaged over all considered types of gas power plants, including combined heat and power plants.

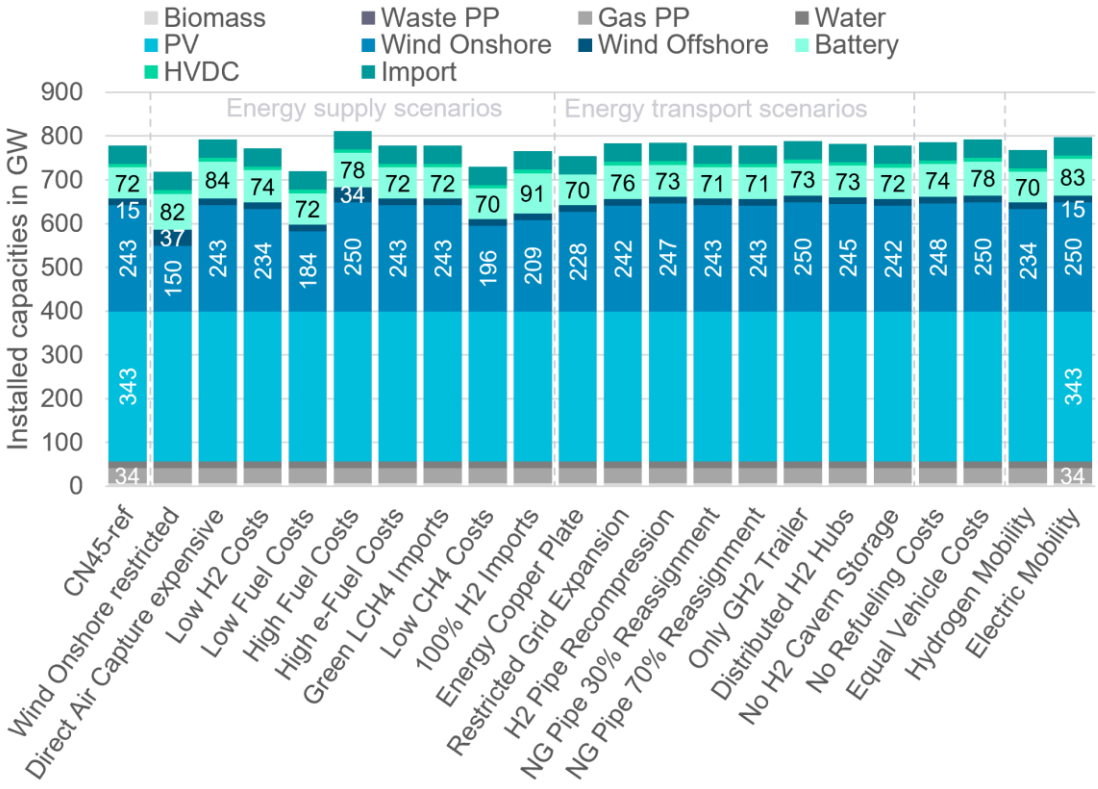

Figure 6-8 – Electricity generation capacities in 22 scenarios.

None of the above-mentioned variations in the electricity sector correlates to the energy carriers in the mobility sector but it can be attributed to the input parameter variations in the energy supply or transport infrastructure. The low impact of the energy carriers in the mobility sector on the electricity sector is additionally emphasized when comparing the two extreme scenarios, 'Electric Mobility' and 'Hydrogen Mobility'. The onshore wind turbine capacity varies in these two scenarios by less than 4% around the reference scenario (cf. Figure 6-8) even though the consumed energy carriers in the mobility sector differ significantly (cf. Figure 6-6). On the contrary, assessing the system's battery power (in GW) shows that a large share of hydrogen in the mobility sector (Hydrogen Mobility) reduces the required battery power from 72 GW in 'CN45-ref' by 2% and an increased electrification rate (Electric Mobility) increases the optimal battery power by 15%. This is without assuming controlled charging, which is investigated in Section 6.3. The indirect flexibility of the mobility sector by generation and storage of hydrogen in Germany is used to balance volatile energy sources and reduces the required battery power. If no inland generation of electrolysis is allowed in the optimization (100% H2 Imports), the electrification of the mobility sector increases significantly (cf. Figure 6-7), which in turn increases the demand for battery power by 26% up to 91 GW. This emphasizes the relevance of the indirect flexibility of the mobility sector in a cost-optimal MMES.

Further analysis of the mobility sector's impact on the energy storage capacities (GWh) in the MMES shows that the optimizer builds 250 GWh of energy storages per 10% increased electrification rate in the mobility sector (cf. Figure 6-9). This includes central heat storages (120 GWh), central battery storages (21 GWh), and GH_2 vessel storages (109 GWh). This trend is based on a linear regression with a correlation coefficient of 0.68 for battery storage, 0.74 for hydrogen storage, and 0.76 for heat storage. Those coefficients indicate a moderate positive correlation. Outliers, such as the '100% H2 import' scenario, are excluded. The regression is defined between an electrification rate of 57% to 79% for heat and hydrogen storage. For battery storage, it is defined from 30% to 79%. In comparison, almost 200 GWh of battery capacity in BEVs is installed per 10% increased electrification, considering only passenger cars and assuming an average battery capacity of 40 kWh per BEV. The potential of the BEVs' batteries in the MMES to support the energy system by controlled charging is assessed in Section 6.3.

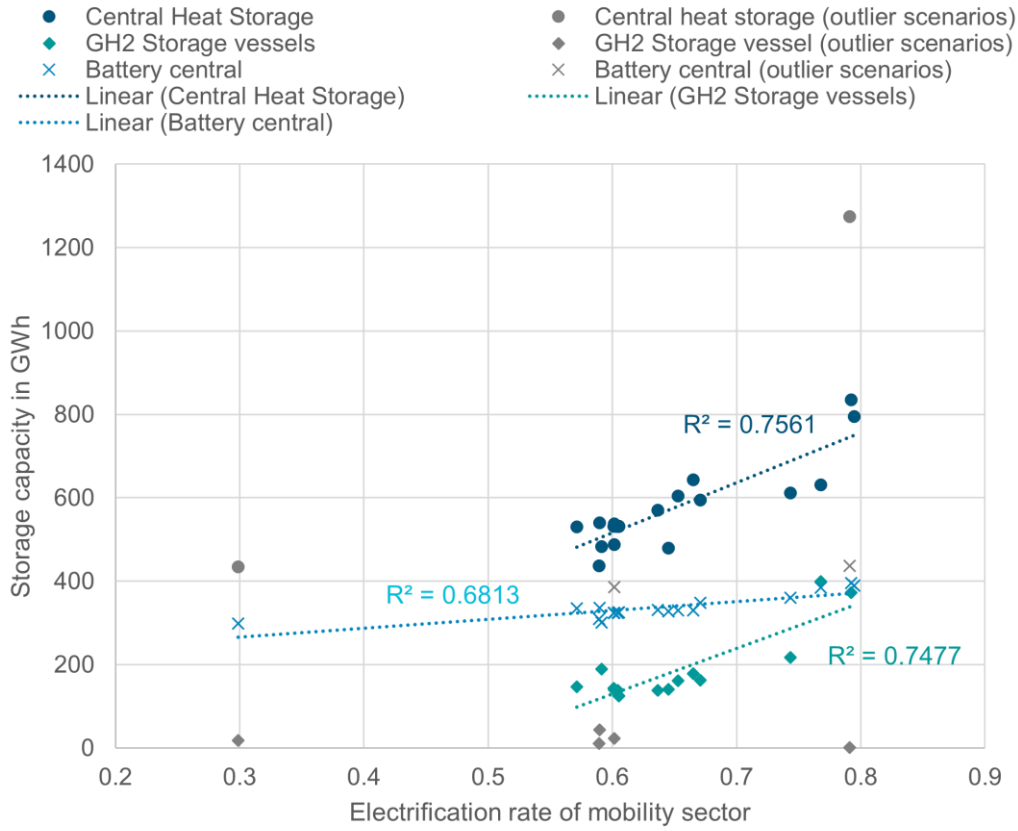

Figure 6-9 – Energy storage capacity in GWh in dependency on the mobility sector's electrification rate.

The heat sector's electrification rate is not affected by the electrification of the mobility sector (cf. Figure 6-10). The electrification of the heat sector is always cost-optimal in the assessed scenarios with an electrification rate in all scenarios above 87% and in 17 out of 22 scenarios above 91%. Solely the energy supply scenarios affect the electrification rate. This is reasoned primarily in a high efficiency of heat pumps.

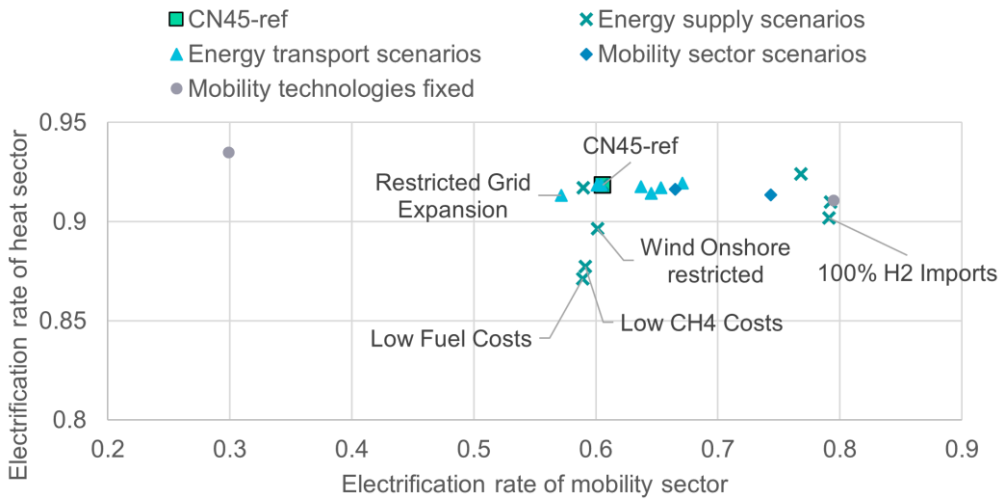

Figure 6-10 – Electrification rate in the heat and mobility sectors.

In the mobility sector, hydrogen is consumed directly in fuel cell vehicles or indirectly by combusting e-fuels. The total hydrogen demand in the MMES ranges from 104 TWh to 286 TWh (cf. Figure 6-11). Up to 119 TWh of hydrogen is used to generate e-fuels in Germany, which are used in the mobility sector. Nevertheless, a high direct hydrogen demand for passenger cars of 142 TWh increases the total hydrogen demand of the mobility sector to its maximum value of 197 TWh in the 'Hydrogen Mobility' scenario. E-fuel generation in Germany is only relevant if the mobility sector does not use hydrogen directly. Methanation of hydrogen occurs in scenarios with high import costs for all energy carriers (High Fuel Costs) or if hydrogen transported between regions is cost intense (Only GH_2 Trailer). Finally, a distributed hub concept (Distributed H2 Hubs) for hydrogen transport and distribution results in 15 TWh of hydrogen demand for combined cycle gas power plants and 6 TWh for central gas heating. However, there are no scaling effects of hydrogen usage across sectors due to an extensive usage in the mobility sector and the associated expansion of a hydrogen supply chain. This is mainly due to two reasons. First, the capital expenditures of the electrolyzers are less relevant than operational expenditures, which are minimized by only operating in low electricity cost periods. This means that an increased utilization rate of electrolyzers due to hydrogen usage across more applications is not-cost optimal. Second, the hydrogen generation and import costs are more relevant than the hydrogen transport costs. Therefore, a jointly used hydrogen pipeline network between different sectors with increasing utilization does not reduce the overall hydrogen costs sufficiently for a fuel switch to hydrogen in the electricity or heat sector.

Furthermore, 71 TWh to 215 TWh of hydrogen are supplied by electrolysis in Germany (cf. Figure 6-11). Additional low-cost hydrogen for 6.9 ct/kWh from Northern and Southern Europe is imported, reaching up to its combined assumed import limit of 103 TWh. The optimizer does not choose to import a significant amount of hydrogen from Northern Africa for 7.9 ct/kWh resulting in an inland generation share of 34% to 94%. Large-scale inland generation of 112 TWh hydrogen is cost optimal even in the 'Electric Mobility' scenario. A low share of inland generation is only triggered by low fuel import costs (Low Fuel Costs, Low CH4 Costs) and a low onshore wind turbine capacity potential (Wind Onshore restricted). The mobility sector affects the electrolyzer capacities if hydrogen is directly consumed, but other factors from the energy supply scenarios show at least a similar impact. These demand and supply structures are relevant for the required energy transport infrastructure assessed subsequently.

Figure 6-13 shows the optimized hydrogen supply regionally resolved for imports and central inland electrolysis. Electrolyzers, flexibly operated, exhaust low electricity costs. Therefore, the demand in the Hydrogen Mobility

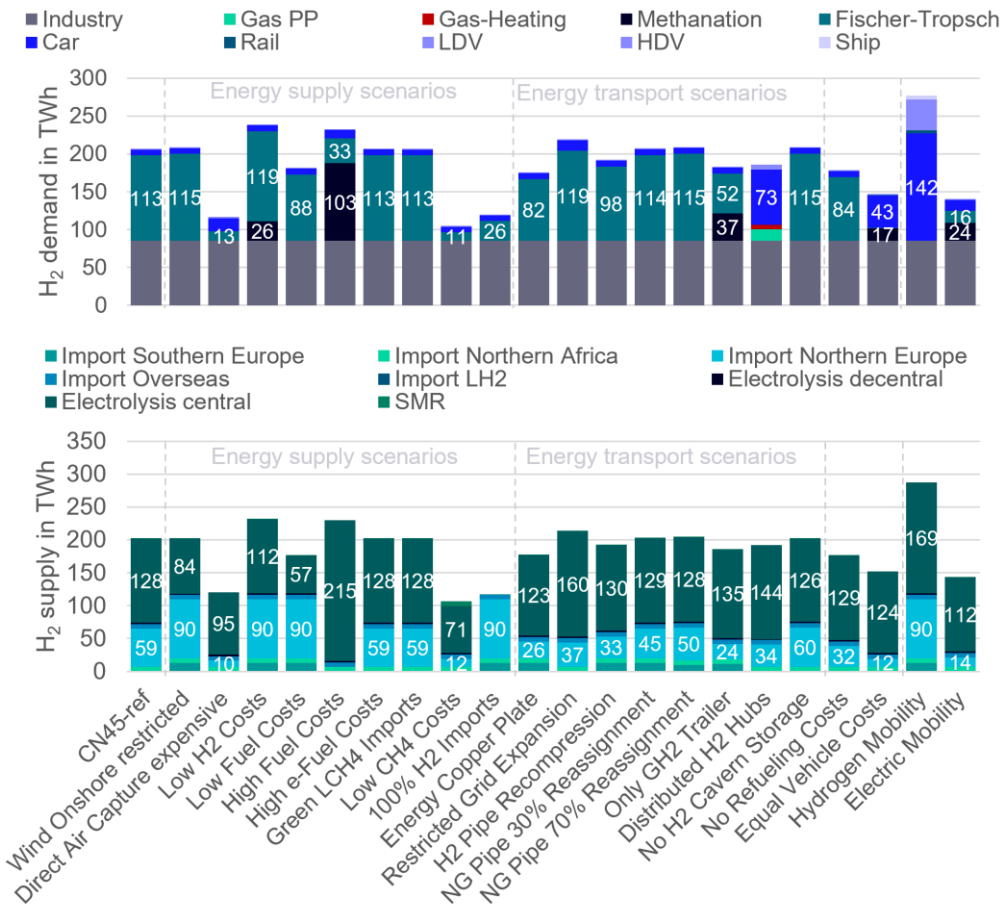

Figure 6-11 – Annual hydrogen demand (top) and supply (bottom).

scenario leads only to a minor increase in hydrogen generation from electrolysis in each region and vice versa for the Electric Mobility scenario. In contrast, the hydrogen imports vary strongly across the scenarios on a regional scale – especially in Schleswig-Holstein and Freiburg. This, in turn, leads to an increased central pipeline capacity between Schleswig-Holstein and Lueneburg from 10 GW to 18 GW (cf. Figure 6-12). Two new regions are connected to the hydrogen pipeline network in the 'Hydrogen Mobility' scenario, supplying Tubingen and Swabia. Additionally, the connections from Northern Germany through central Germany and from Brandenburg/Berlin southwards are extended compared to the reference scenario. The central pipeline segment starting in Schleswig Holstein deviates in the 'Hydrogen Mobility' scenario by 4.4 GW (+51%) and in the 'Electric Mobility' scenario by 2.8 GW (-33%) from the reference scenario. The connection from Mecklenburg Western Pomerania southwards is in the 'Electric Mobility' scenario lower by 2.5 GW (-53%) and does not significantly increase in the 'Hydrogen Mobility' scenario. Pipelines from North to West are impacted only in the 'Electric Mobility' sector by a reduction of 29% in, e.g., Muenster. The regional distribution of the hydrogen demand in the mobility sector, which is more evenly distributed than the industry demand, increases the demand for pipelines in and towards Bavaria. In contrast, pipeline capacities from Thuringia to Bavaria stay below 2 GW in the 'Electric Mobility' scenario but increase in the 'Hydrogen Mobility' scenario by up to 6 GW in Upper Franconia.

The aggregated incoming pipeline capacity in Lueneburg and further to Hannover are greater than 5.8 GW, even in the 'Electric Mobility' scenario. This shows that the hydrogen is transported via Lueneburg southwards in all scenarios, and it can be supplied from Schleswig-Holstein or Mecklenburg-Western Pomerania. Additionally, pipelines in the West from Weser-Ems to Duesseldorf are at least 5 GW. Those identified connections can be suggested here as no-regret connections.

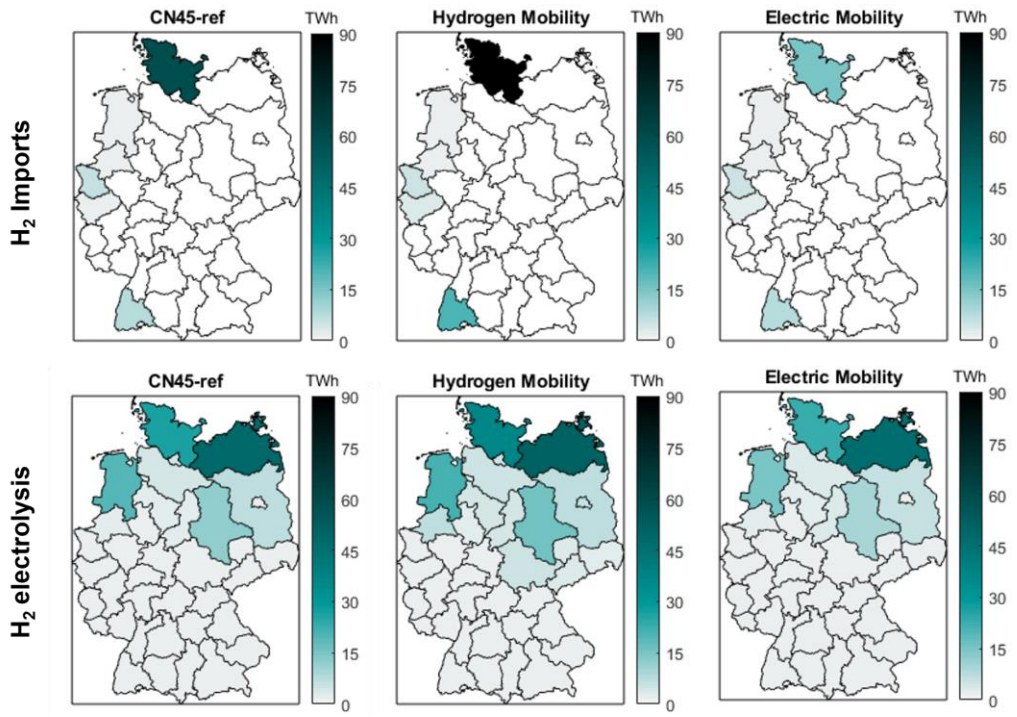

Figure 6-13 – Regional hydrogen imports and electrolysis generation per year in three scenarios.

Furthermore, no strong overall impact on the electricity transmission grid can be identified (cf. Figure 6-12). Only one grid extension varies significantly in the Hydrogen Mobility scenario requiring only half of the capacity than in the reference scenario. This East-West connection spans several inter-regional connections from Chemnitz over Thuringia, Upper Franconia, and Lower Franconia to Darmstadt. The high electricity grid expansions in Germany show that electricity grid expansions are highly relevant in a decarbonized German

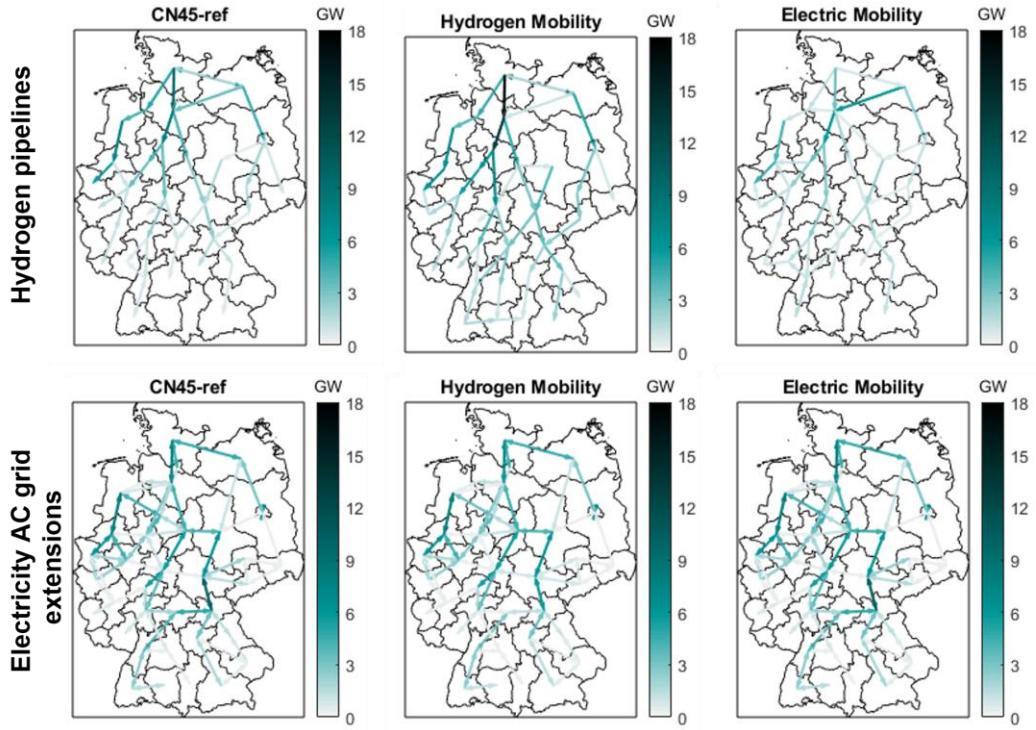

Figure 6-12 – Inter-regional hydrogen pipeline and electricity grid extension capacities in three scenarios. Grid extensions are related to the initial AC grid based on 2017.

MMES. Investments in the electricity transmission grid infrastructure are therefore cost-optimal almost independent of the here assessed scenarios. Still, the restricted grid expansion scenario shows only an increase of about 0.7% in total energy system expenditures. But even this scenario allows an increased transmission grid capacity between all neighboring regions of 50% compared to today's grid.

The impact of the mobility sector on the MMES can be summarized to answer Research Question 2 as follows:

RQ2 (part 1 of 2): How does a decarbonized mobility sector generally impact the energy supply, transport, and demand structure of the Multi-modal Energy System, and in particular, what is the impact of the charging infrastructure network design and battery electric vehicles' flexibility?

➔ The mobility sector drives in dependency of the scenario the demand for e-fuels, a hydrogen supply chain and energy storages. In case the mobility sector is intended to develop towards e-fuel or hydrogen usage, politics must enable an early buildup of the corresponding infrastructures to secure a cost-efficient supply.

<u>Energy supply and demand</u>

(i) The decarbonization of the mobility sector has no direct impact on electricity generation capacities in the cost-optimized MMES but affects the required battery power by 26%.
(j) The electrification of the mobility sector does not influence the heat sector's electrification rate, which is in all scenarios above 87%.
(k) Electrolyzers and FT synthesis capacities vary with the e-fuel utilization rate in the mobility sector, but also in dependency of non-mobility sector related measures.

➔ A strong expansion of RES is necessary and inevitable to establish cost-efficient low-cost inland hydrogen and e-fuel generation and could decrease the geopolitical dependency.

<u>Energy transport and flexibility</u>

(l) The required hydrogen pipeline network is impacted by the energy carriers in the mobility sector. A direct usage of hydrogen in the mobility sector requires especially in Southern Germany additional pipeline capacities of up to 286%. And through central Germany additional capacities of up to 4.4 GW.
(m) A no-regret hydrogen pipeline of 5.8 GW from Lueneburg to Hannover and one from Weser-Ems to Muenster of 5.5 GW is identified. Those connections emphasize the importance of the hydrogen transport from north to west and from north to central and south Germany.
(n) The indirect flexibility of the mobility sector from electrolysis and hydrogen storage reduces the required battery power by 11 GW and heat storage capacities (GW) by factor two.
(o) The cost-optimally required stationary heat, hydrogen, and battery storage capacities in the system increase with 10% electrification in the mobility sector by 250 GWh, or by about 50 kWh per vehicle.

➔ The expansion of a hydrogen pipeline network and the required central storage capacities scale with the hydrogen demand and the electrification rate in the mobility sector, respectively.

6.3 Flexibility from electric vehicles in the context of an MMES

The modelled electric vehicles follow a charge at arrival strategy without flexibility from controlled charging in all assessed scenarios above. Controlled charging has the potential to increase the provided flexibility from the mobility sector to the MMES and to reduce the large stationary energy storage capacities in the MMES for the electrification of the mobility sector (cf. Section 6.2). Following Section 5.2.3, the derived flexibility is assessed

for a charging infrastructure scenario, which minimizes the peak load of the charging processes, and for a scenario, which maximizes the available flexibility of BEVs in terms of daily shiftable energy per time step (cf. Table 5-11). The two controlled charging scenarios are based on the reference scenario with a 95% electrification rate in the passenger car segment and a 5% assumed passenger road transportation increase amounting to about 47 million BEVs in 2045.

A representative week in March is investigated, in which PV operate during the day and wind turbines operate at the end of the week, which is reflected in decreased marginal electricity costs[12] (cf. Figure 6-14). The optimizer reduces only a minor share of the charged energy of charging processes with a potential three-hour delay time between 6 am to 9 am and between 5 pm to 6 pm if controlled charging is enabled (cf. Figure 6-14). Charging processes with six-hour delay time show with a Charge at Arrival large peak loads up to 20 GW in March around 7 am to 8 am. Controlled charging reduces the peak to 7.7 GW, distributing the energy over the next six hours of the day. This load shift aligns with the PV infeed time and the corresponding lower marginal costs of electricity during midday realizing spreads of up to 44 €/MWh. Charging processes with a potential delay time of twelve-hours occur predominantly when vehicles arrive home at 5 pm. If all BEVs with access to home charging start charging immediately after arrival, the simultaneity increases the peak of those charging processes up to 13.5 GW. This peak can be reduced by factor two, shifting the charging processes into the night. Even though the electricity costs at night are up to 37 €/MWh higher, the shift is cost-optimal in the MMES. This can be explained by the benefit of a reduced electricity peak demand in the energy system. On Tuesday in March, e.g., 8.7 GWh of charging load is reduced between 5 pm and 7 pm at 116-127 €/MWh and made up for between 8 pm and 7 am at electricity costs of 147 €/MWh on average.

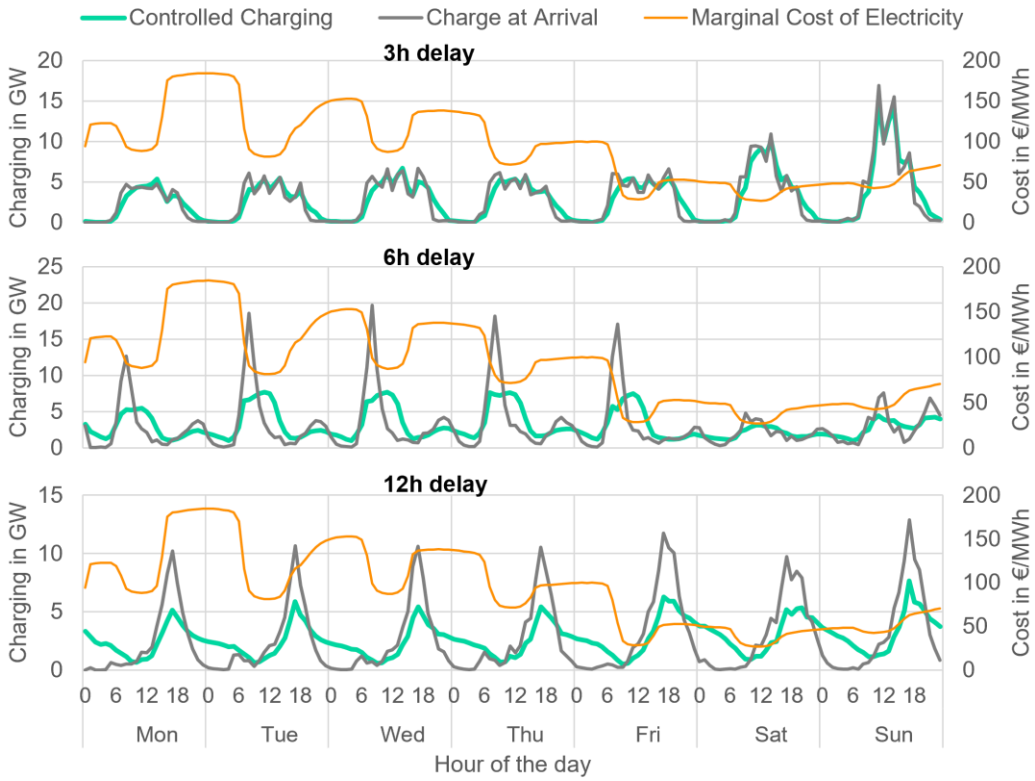

Figure 6-14 – Utilization of controlled charging potential considering a high flexibility charging infrastructure design compared to the originating 'Charge at Arrival' load profile in a representative week in March 2045 subdivided into 3-hour (top), six-hour (middle), and twelve-hour (bottom) delay time.

[12] The marginal electricity costs are not affected significantly by the load shift. Only in a few hours of the year a deviation of up to 6% occurs in the controlled charging scenario.

Aggregating all charging processes, which cannot be shifted in time, and all processes with different realizable delay times shows that 26% of the total available flexibility is utilized in both charging infrastructure scenarios in 2045 (cf. Table 6-1 and Table 6-2). Table 6-1 and Table 6-2 summarize the key statistics for the entire year for the High Flexibility and Low Peak scenario, respectively. Figure 6-15 illustrates the temporal distribution of the Controlled Charging and Charge and Arrival charging profiles for both scenarios exemplarily for a representative week in March. The optimizer shifts in the High Flexibility scenario annually 18.5 TWh and in the Low Peak scenario 14.3 TWh of charged energy in time. In the Low Peak scenario, the maximum peak load reduction amounts to 5 GW, which are realized in the evening. The load is shifted to the night, reducing the peak-to-average ratio by 14% with a maximum annual charging peak of 27 GW. The annual charging peak in the maximum flexibility scenario with controlled charging is 3 GW higher than without controlled charging in the Low Peak scenario. It shows that the difference of the two controlled charging profiles is reduced compared to the two Charge at Arrival profiles.

	Total	**12h delay**	**6h delay**	**3h delay**	**static**
Maximum peak, CaA	35.2GW	13.5GW	20.6GW	17.6GW	16.3GW
Maximum peak, CC	30.2GW	9.9GW	11.7GW	15.7GW	16.3GW
Peak reduction by CC	14.3%	26.7%	43%	10.9%	0%
Peak-to-average ratio, CaA	2.8	5.4	7.2	6.4	3.8
Peak-to-average ratio, CC	2.4	3.9	4.1	5.7	3.8
Utilized flexibility	18.5TWh/a	7.4TWh/a	8.4TWh/a	2.7TWh/a	-
Utilized flexibility in % of total available flexibility	26%	33.6%	33.4%	11.22%	-

Table 6-1 – BEV charging statistics for Charge at Arrival (CaA) and Controlled Charging (CC) with a charging infrastructure design maximizing the daily available flexibility.

	Total	**12h delay**	**6h delay**	**3h delay**	**static**
Maximum peak, CaA	27.2GW	12.33GW	9.6GW	5.5GW	16.8GW
Maximum peak, CC	23.6GW	8.7GW	9.65GW	5.29GW	16.8GW
Peak reduction by CC	13.2%	29.4%	-0.2%	3.6%	0%
Peak-to-average ratio, CaA	2.2	5	4.1	3.6	2.8
Peak-to-average ratio, CC	1.9	3.5	4.1	3.5	2.8
Utilized flexibility	14.4TWh/a	7.6TWh/a	1.1TWh/a	5.7TWh/a	-
Utilized flexibility in % of total available flexibility	25.9%	34.7%	8.2%	27.9%	-

Table 6-2 – BEV charging statistics for Charge at Arrival (CaA) and Controlled Charging (CC) with a charging infrastructure network design minimizing the overall peak load.

The utilized flexibility of both scenarios differs mainly for the six-hour delay charging processes. In the morning hours only 8.2% of this is utilized in the Low Peak scenario compared to 33.4% in the High Flexibility scenario. One reason is that the Charge at Arrival profile in the Low Peak scenario does not yield a midday valley, which is filled in the High Flexibility scenario predominantly by the six-hour delay charging processes at workplaces. Further, it cannot reduce the peak load compared to the Charge at Arrival profile.

The low utilization of the flexibility from the charging processes with up to six-hour delay times reveals that the timing of all charging processes and their corresponding flexibility significantly impact the value of flexibility. Furthermore, the analysis of the results shows that the flexibility is in a system cost-optimization not primarily used to charge BEVs when the electricity price is low but to reduce the charging peak load. This indicates, even though not further analyzed in the present thesis, that the peak load provision is more cost-intense than the benefit from aligning charging profiles with the volatile renewable electricity generation. A peak load reduction is beyond that also beneficial for the electricity grid integration of BEVs.

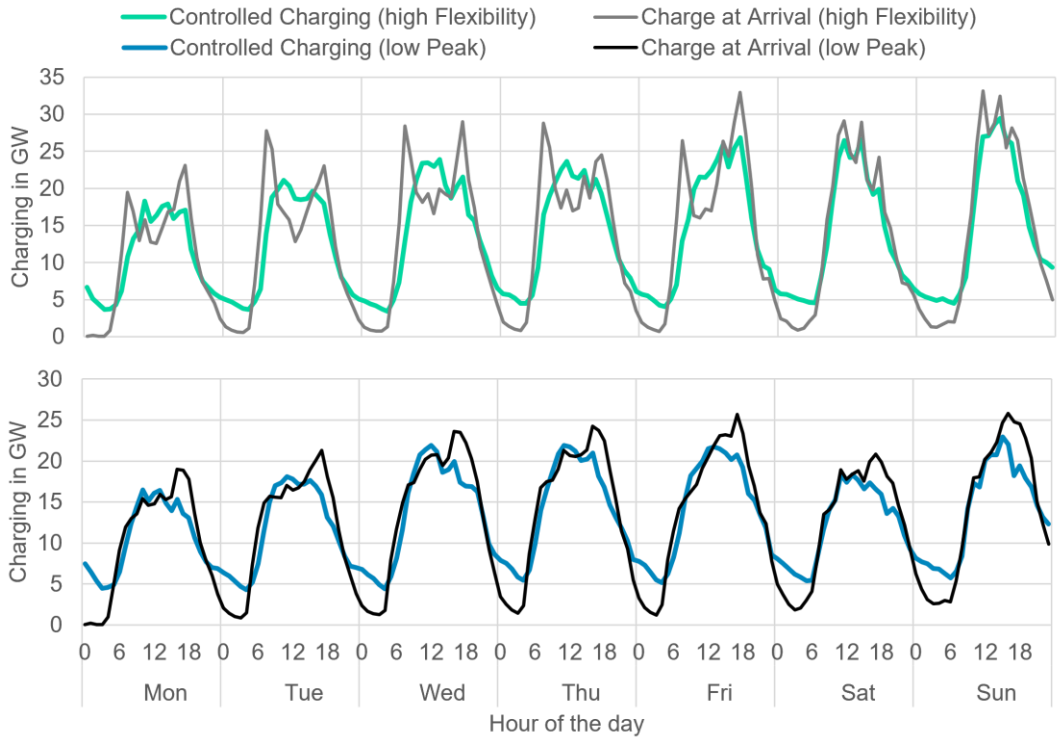

Figure 6-15 – Total utilization of controlled charging potential considering a high flexibility (top) and low flexibility (bottom) charging infrastructure design in an exemplary week in March.

The usage of additional flexibility from BEVs impacts the required energy storage capacities in the MMES (cf. Figure 6-16). Figure 6-16 shows that the installed central heat, hydrogen vessel, and battery storage capacities in the reference scenario (CN45-ref) amount to 972 GWh. Flexibility from BEVs can reduce this storage capacity to 928 GWh or 911 GWh, depending on the charging infrastructure design. This is a reduction of at least 4.5% and up to 6.3% if the charging infrastructure is designed to maximize the flexibility provision. Heat storage capacities are reduced by 23 GWh by controlled BEV charging. However, the charging infrastructure design has only a minor impact of 0.7% on this reduction.

Furthermore, the most significant impact of controlled charging is observed on central battery storage capacities. Compared to the reference scenario, the optimizer reduces in the MMES 45 GWh battery capacity and 10.5 GW of battery power, or 13.8% and 14.6%. The charging infrastructure design is responsible for 24.4% and 34.4% of this battery capacity and power reduction, respectively. No other flexible electricity generation capacities are impacted by controlled charging.

However, the significance of the impact on the stationary battery storage in the system must also be assessed in terms of system costs. Controlled charging reduces the annual capital expenditures of the MMES by 0.5% due to lower storage capacity investments if a Low Peak charging infrastructure design is rolled out. This includes the additional costs for load management described in Section 5.4 but no compensation payments for the vehicle owners. The investigated charging infrastructure design with High Flexibility is more cost intense than a Low Peak infrastructure design. This exceeds the savings from reduced storage capacities and increases the total annual capital expenditures by 0.6%. The operational expenses change accordingly but affect the MMES operational expenditures less than 0.05%. However, the reference scenario (CN45-ref) assumes the Low Peak charging infrastructure design. A reduction of system costs by controlled charging in the High Flexibility scenario could be expected if compared to a reference scenario without controlled charging but the same charging infrastructure design.

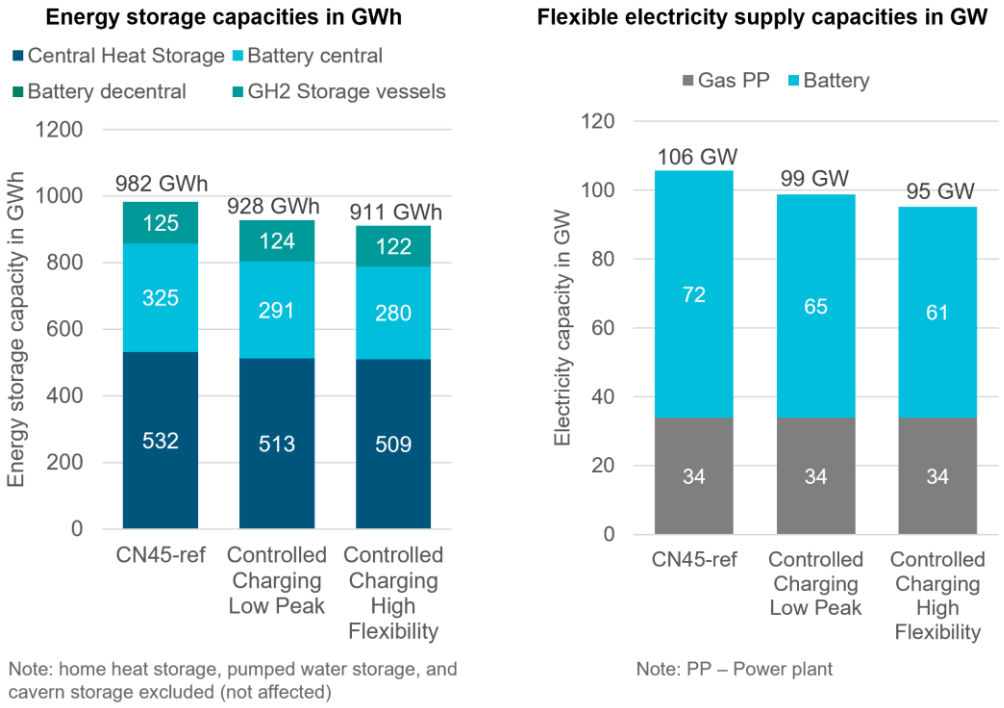

Figure 6-16 – Impact of flexibility from BEVs on Energy storage systems in the MMES. Pumped hydro storage, decentral home storage, and cavern storage are not impacted and excluded here.

In addition to the answers to research question 2 in the previous section, the impact of charging infrastructure and the BEVs flexibility can be added to the summary as follows:

RQ2 (part 2 of 2): How does a decarbonized mobility sector generally impact the energy supply, transport, and demand structure of the Multi-modal Energy System, and in particular, **what is the impact of the charging infrastructure network design and battery electric vehicles' flexibility?**

(a) A charging peak load reduction of factor two can be cost optimally realized in the MMES by shifting charging processes towards the night, even though the electricity costs at night are up to 37 €/MWh higher. The benefit of a peak load reduction in the MMES exceeds the drawback of the higher electricity costs for charging.
(b) Charging infrastructure impacts the value and the total dispatched volume of the BEV's flexibility by up to 28%. This is due to different temporal availabilities of the flexibility, and the temporal distribution and peak load of the original charging profile in dependency on the charging infrastructure design.
(c) Up to 18.5 TWh of flexibility per year are dispatched in the MMES cost-optimally. This is 26% of the available flexibility of BEVs or 19% of the energy dispatch from batteries in the reference scenario.
(d) Controlled charging reduces the combined heat, hydrogen, and storage capacity by up to 6.3%. The charging infrastructure design accounts for 27% of this reduction.
(e) Controlled charging reduces 45 GWh and 10 GW of battery capacity and power. The charging infrastructure design affects the reduction by 24.4% and 34.4%, respectively.
(f) Utilizing the flexibility of BEVs reduces the MMES total expenditures by 0.5% if the charging infrastructure design minimizes the peak load. Otherwise, the MMES total expenditures can increase by 0.6%.

6.4 Charging infrastructure design for electric vehicles

BEVs are cost-optimally used for the decarbonization of road passenger transportation in the assessed scenarios (cf. Sector 6.1). The analysis in Section 6.3 emphasizes that the charging infrastructure for BEVs is an essential factor for the decarbonization of the MMES. The charging infrastructure network design significantly affects the MMES's storage capacities and capital expenditures. A well-planed charging infrastructure design is therefore important. Subsequently, an analysis for designing charging infrastructure is conducted, based on the ABM eMob and the sensitivity analysis described in Section 5.1.

In this section, six scenarios are investigated differentiating between a rural and an urban region (cf. Table 5-1) for low (1%), mid (20%), and high (80%) BEV penetration rates in the passenger road transportation sector. The assessed design targets the number, and the combination of different required charging stations with different power ratings at different locations within a region. All results in the following paragraphs are normalized to 1000 BEVs for comparability between different BEV penetration rates. This means, that the numbers – if not other indicated – must be multiplied by the expected number of BEVs in a region divided by 1000 at a certain penetration level for an interpretation on the NUTS2 or country-level.

Figure 6-17 shows all investigated charging infrastructure combinations for both regions and all three penetration levels. Simulations are filtered by their SQCI using the mean value over all simulation runs (sample size 40) (cf. Section 5.1). All scenarios covered by a colored area are according to Equation (5-1) in the solution space and can be considered suitable charging infrastructure designs in the context here.

A fast-charging network with a high availability of fast charging points and a coverage of 25 km on highways and up to 5 km in cities reduces the need for public chargers in rural areas at low penetration by factor two to three (cf. Figure 6-17). The assessed rural area requires at a low penetration rate at least 50 public charging points and

if the fast-charging network coverage in the city and highway is low at least 200. If the number of work chargers is halved from 200 to 100 chargers, the minimum number of public chargers must increase by 32%. While the total number of work and public chargers cannot drop below 140 without violating the SQCI constraint, building up a charging infrastructure network without relying on work chargers is possible by increasing the number of public chargers to 200. However, this additionally requires a fast-charging coverage of 25 km on highways and 5 km in the city. Supposing the fast-charging infrastructure network on highways does not exceed the coverage of 100 km in an early market phase, the required total number of chargers doubles. An additionally low coverage of fast chargers of 25 km within cities requires at least 200 public charging points per 1000 BEVs. This is independent of the availability of charging infrastructure at workplaces.

The demand for public chargers in urban areas at low penetration of at least 200 is up to 200% higher than in rural areas. The total work and public charger demand in urban areas exceed the demand in rural areas by factor 1.4. Two reasons are identified: the assumed 29% lower home charger availability in urban areas and the 31% increased number of BEVs in urban areas compared to rural areas due to inter-regional commuters. This finding is further supported by an analysis of the size of the solution space. Of all simulations, 6% at low penetration, 55% at mid penetration, and 68% at high penetration are within the solution space for urban areas and 16%, 85%, and 91% for rural areas. That means that even at high penetration levels, 34% more work and public charger combinations are reasonable in rural areas than in urban areas. It shows that following a demand-oriented buildup of charging infrastructure networks in urban areas requires more charging stations than in urban areas.

At mid penetration level in a rural area, the demand for charging points per 1000 BEVs can be minimized to a total of 24 work and public chargers. Supposing a dense DCFC network with 5 km in the city and 25 km coverage on highways, no more than 24 public and four work chargers or 32 public and ten work chargers are sufficient. Even with a low coverage of fast-charging stations, only a total of 22 work and public chargers are needed additionally. This increases the opportunities of designing and tailoring the charging infrastructure to an area's requirements compared to an initial charging infrastructure network. Figure 6-17 shows that increasing the fast-charging coverage in the city reduces the need for public chargers by factor three. Contrary, increasing the number of fast chargers on highways reduces the number of work chargers that need to be installed. The latter is caused by inter-regional travelers traveling relatively long distances into the area for work. If no charging station is available at work, it raises the need for charging on the highway. A high penetration charging network design differs only slightly from the mid penetration design in rural areas decreasing the minimal total charger demand per 1000 BEVs in rural areas by four chargers at work.

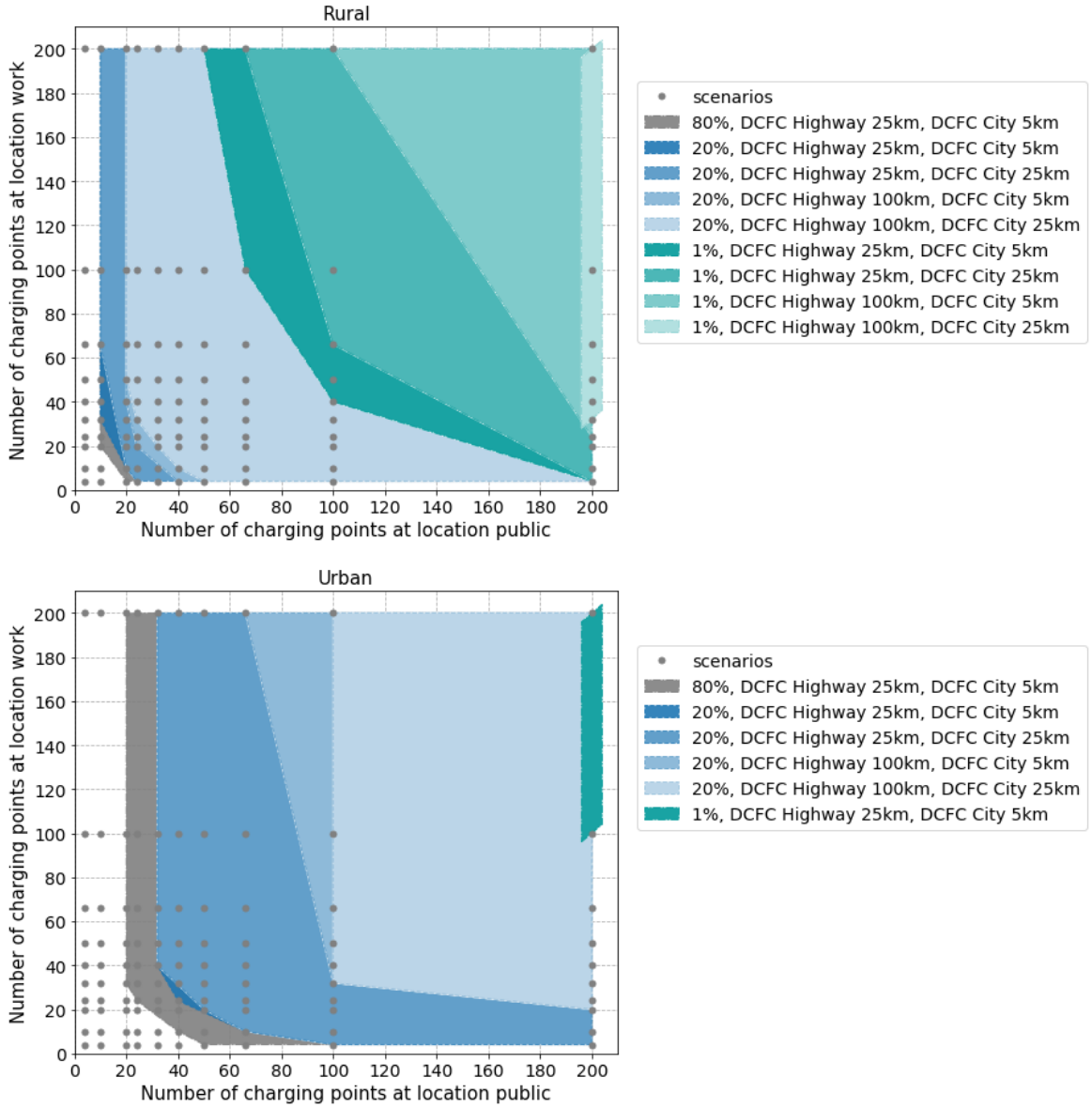

Figure 6-17 – Charging infrastructure network designs with sufficient charging stations to cover the BEVs' charging demand at a BEV penetration rate of 1%, 20%, and 80% in (top) a rural and (bottom) an urban area. Points indicate simulated combinations of the number of public and work chargers. The colored areas indicate simulations with sufficient charging infrastructure. Each color represents another BEV penetration level scenario, and its brightness differentiates between different the assessed fast charging scenarios. Areas overlay each other so that only the additional design combinations are shown for, e.g., higher penetration rates.

Urban areas at mid penetration require 217% more AC chargers than rural areas at a minimum. Especially the highway fast-charging network can reduce the need for public chargers by factor three. Minimal design combinations are 40 work and 32 public, or ten work and 66 public chargers. Reaching a high penetration, the number of chargers per 1000 BEVs decreases in urban areas to 54. This shows that the difference between urban and rural areas is most significant in low and mid penetration scenarios. Additionally, highway charging impacts the public charger needs at mid penetration in urban areas significantly. Large infrastructure investments are required especially in urban areas. Enabling the buildup of home charging in shared garages and on-street-charging, if no private parking is available, is crucial to reach a home charger availability in urban areas of 60%.

Further, companies can contribute significantly to supplying the charging demand. Work charging must therefore be enabled and might even be subsidized. It could additionally support the initial market ramp-up of BEVs.

To conclude, the answers to research question 3 are summarized following:

RQ3 (part 1 of 2): How to design charging infrastructure networks and how does the infrastructure affect the battery electric vehicles' charging peak load and available flexibility?

(a) The minimum required number of chargers per 1000 BEVs in urban areas is 125% higher than in rural areas due to the higher charging demand in urban areas, caused by inter-regional commuters, and the lower home charging availability.
(b) In rural areas: a dense DCFC infrastructure reduces the demand for an intensive slow charger network at an early BEV market penetration in rural areas by up to factor three.
(c) In urban areas: a dense DCFC network at highway locations is required to satisfy the demand at low penetration and it decreases the need for slow chargers at mid penetration by factor three.
(d) From statement (b) and (c) it can be derived that building up a fast-charging network should be fostered already in an early stage of the market ramp up of BEVs.
(e) Urban areas require 50% more AC chargers at mid penetration with 20 public and 12 work chargers per 1000 BEVs compared to 5 public and 16 work in rural areas.
(f) While a dense highway fast-charging network reduces especially the need for work chargers, and a dense city fast-charging network reduces the need for public chargers.

Integrating BEVs into a region's mobility concept can pose different challenges in each region. Those challenges are, for instance, required distribution grid extensions or the integration of RES with BEVs' charging demand. A reasonable charging infrastructure design helps mitigate upcoming challenges. In Section 5.1, a Pareto-optimal design is introduced for a high penetration scenario based on maximizing the flexibility of BEVs and minimizing the total electricity charging peak load. Figure 6-18 compares the lever of charging infrastructure regarding the availability flexibility of BEVs and the charging peak load. The assessed flexibility is the total daily shiftable charging energy without differentiation of different delay times.

The peak load per 1000 BEVs ranges from 930 kW to 1490 kW and 840 kW to 1160 kW in urban and rural areas. The daily flexibility of those charging processes ranges from 4 MWh to 6.7 MWh and from 5.4 MWh to 7 MWh in urban and rural areas, respectively. Thus, charging infrastructure in urban areas can be designed to decrease the peak load by up to 38% and increase the flexibility by 68%. In rural areas, the lever on the absolute peak load reduction is 57% lower than in urban areas, the lever on the flexibility increase is 59% lower. This is because the peak load is primarily dominated by home charging in rural areas but not in urban areas. This difference is due to a higher home charger availability and by longer travel distances towards home in rural areas resulting in larger recharging demands and hence, increased simultaneity. The drawn area's shape and orientation indicate that the peak load in urban areas increases with increasing available flexibility. Rural areas show no direction of correlation. Only for low penetration flexibility increase and peak load decrease correlate.

The charging infrastructure design is most relevant at mid to high penetration rates since its impact at low penetration on the peak load is four times (urban) and two times (rural) lower than in the high penetration scenario. Rural areas can especially benefit from the flexibility lever to integrate the charging demand with, e.g., rooftop PV. However, especially urban areas can leverage charging infrastructure by a holistic charging infrastructure network planning, which is even more relevant due to the expected higher charging peak in urban areas. A targeted charging infrastructure design can lead in the urban area of Kiel at mid penetration with 22 thousand BEVs to a potential peak load mitigation of 15 MW and a flexibility increase of 28 MWh/day. This increase of flexible electricity charging demand is approximately as much as 3400 two-person households

consume per day[13]. The total minimum available flexibility in urban areas amounts at mid penetration to 100 MWh per day, an equivalent of twelve thousand households.

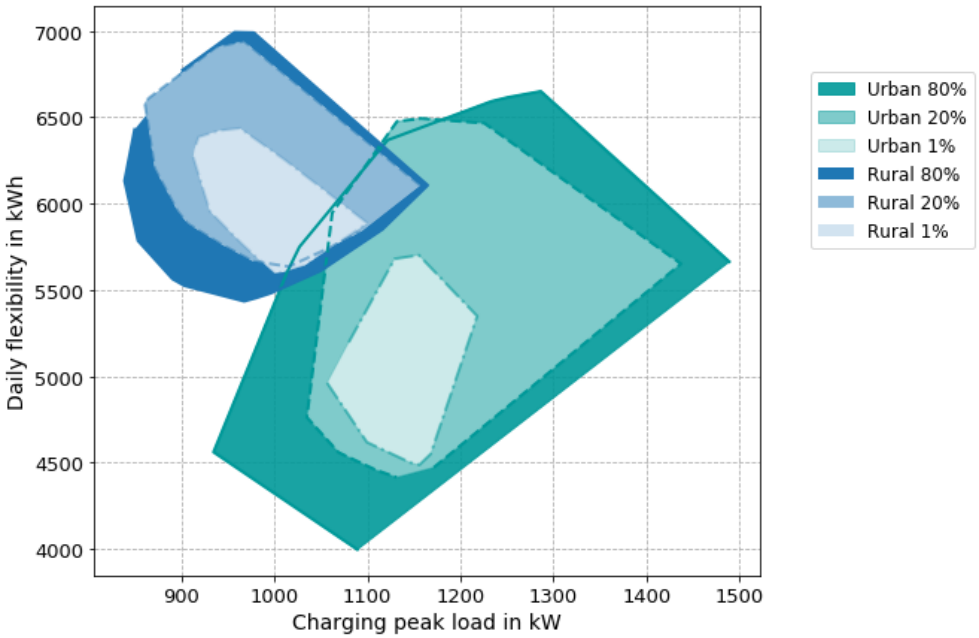

Figure 6-18 – Comparison of resulting flexibility and charging peak load for all charging infrastructure scenarios normalized to 1000 BEVs for an urban and rural area at 1%, 20%, and 80% BEV penetration rate. The figure shows the minimal convex hull, including the averaged values of all simulations for each charging infrastructure scenario.

Subsequently, the design options of a charging infrastructure network to increase the flexibility and reduce the peak load are further investigated. Figure 6-19 shows the impact of work and public chargers on the flexibility and peak load normalized to 1000 BEVs for all six scenarios. The first column of plots shows the effect of varying the number of public chargers. The second plot shows the impact of varying the number of work chargers on the flexibility on the ordinate and the charging peak on the abscissa. The first three rows show the results for an urban area for 1%, 20%, and 80% penetration, and the last three rows for the rural region.

Considering all penetration rates, an increasing number of work chargers increases the available flexibility. In urban areas, a tipping point is reached between 100 and 200 charging points at work where the peak load increases with an increasing number of work chargers up to 200 kW above the maximum peak value with less than 100 charging points. This is when the work charging peak in the morning exceeds the evening peak load. If large numbers of charging points are installed in a region, the balance between work and public charging must therefore be assessed carefully.

In contrast, work chargers in rural areas decrease the peak load while increasing the flexibility. The additional work chargers reduce the charging demand at home, which is most relevant for the rural area's peak. It can therefore be recommended to incentivize work charging in rural areas. The number of public chargers correlates positively with the daily flexibility and the peak load in the region. The benefit of the additional flexibility must therefore be assessed carefully. Furthermore, the flexibility and the peak load correlate in urban areas but not in rural areas.

[13] 3MWh electricity consumption per year assumed for a two-person household.

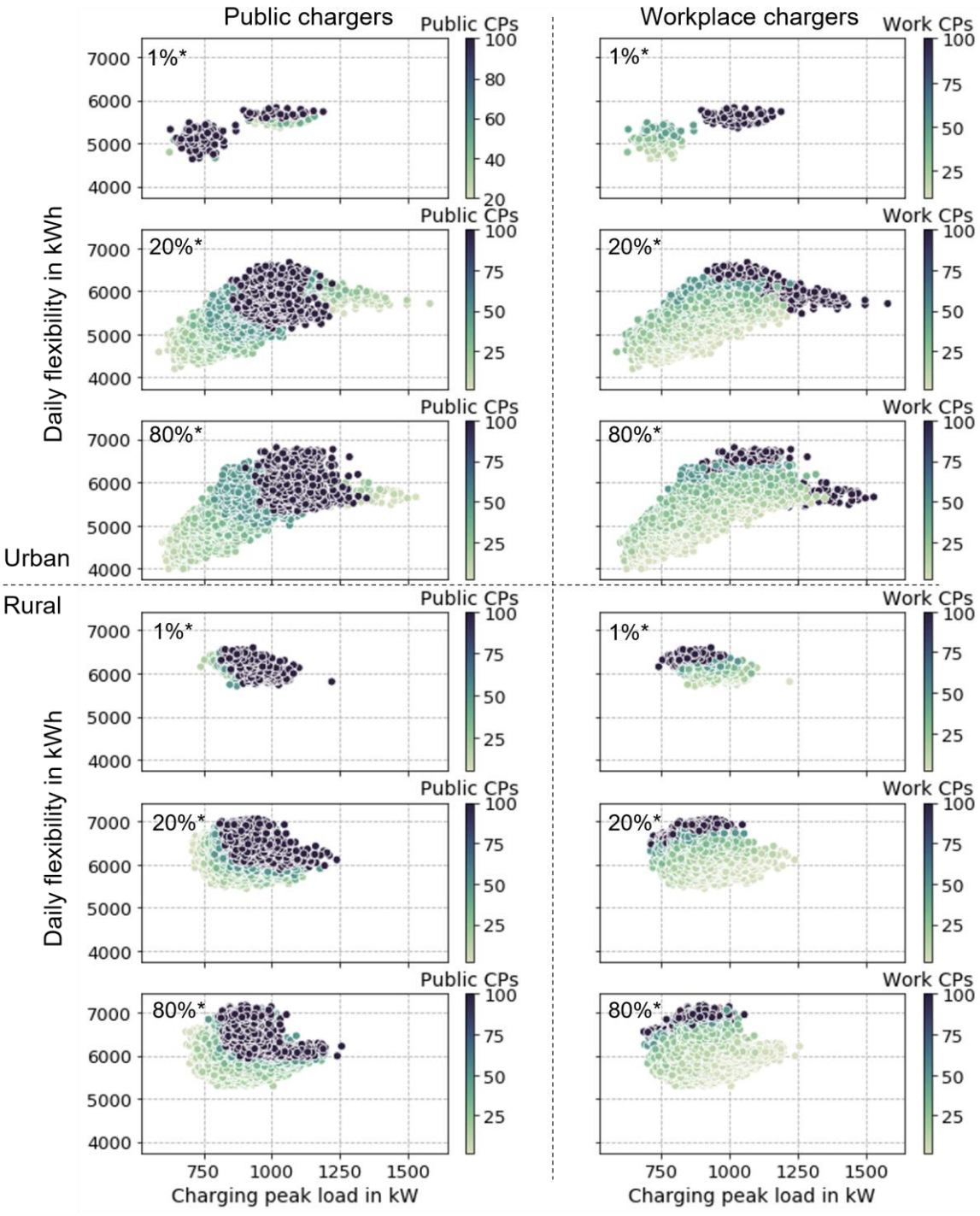

* Battery electric vehicle penetration rate (scenario)
CPs – Charging Points

Figure 6-19 – Impact of charging infrastructure design on flexibility and charging peak load. Each point represents one simulation, and its color indicates the simulated number of work and public charging points.

The following summarizes the key findings to answer Research Question 3:

RQ3 (part 2 of 2): How to design charging infrastructure networks and **how does the infrastructure affect the battery electric vehicles' charging peak load and available flexibility?**

(g) The total charging peak load per 1000 BEVs varies in dependency on the charging infrastructure design between 930 kW to 1490 kW, and 840 kW to 1160 kW in urban and rural areas, respectively.
(h) The total daily flexibility of 1000 BEVs varies in dependency on the charging infrastructure design between 4 MWh to 6.7 MWh and from 5.4 MWh to 7 MWh in urban and rural areas, respectively.
(i) The design of a charging infrastructure network can decrease the BEVs' peak load by up to 38% and increase the flexibility by up to 67%.
(j) Work chargers in rural areas should be incentivized since they increase the flexibility while decreasing the charging peak load. In contrast, work chargers in urban areas can increase the charging peak load, if more than 100 charging points per registered 1000 BEVs are installed.
(k) An increasing number of public chargers increases the peak load and the flexibility in rural and urban areas.

➔ These results suggest fostering fast charging networks already at a low BEV market penetration, while in a later stage the flexibility and peak load provision from charging processes at AC chargers should be integrated into the planning to lever the potential of BEVs for the energy system.

7 Discussion

The applied framework of the ABM eMob and an MMES optimization allows not only to focus on BEVs' flexibility and charging infrastructure network designs but to also assess the interactions of the mobility sector simultaneously with the MMES.

The role of the mobility sector in the MMES

The assessed carbon-neutral mobility sector and its cost-optimal energy carriers should be interpreted from an energy system perspective. Analyzing a carbon-neutral MMES in 2045 using a total system cost-optimization is a reasonable approach, which can be used for designing regulations to steer towards a cost-optimal system. However, the MMES model does not project energy technology or automotive market developments. Especially in a highly heterogenous mobility sector, where the vehicle owners do not necessarily buy vehicles based on a cost-optimal decision. Still, the interactions between the mobility sector and the MMES are indicative for relevant macro-economic or political decisions such as building up a hydrogen pipeline network and expanding the electricity grid.

The MMES optimization results must further be considered in the context of a linear model without integer variables. Therefore, large infrastructure investments in pipelines, cavern storage, or the electricity grid can be inaccurate. This is especially the case if, e.g., hydrogen pipelines with very low capacities or very high capacities are built by the optimizer. A linear model formulation allows a continuous buildup of, e.g., cavern storage having large upfront investments. This behavior can favor one technology over the other. Anyway, sensitivities are used here for assessing the robustness of the results.

The analysis showed, that the decarbonization of the mobility sector can be achieved in different ways with total annual system expenditures varying by 6%.[14] The energy transport infrastructure and the charging and refueling infrastructure have a share of 3% and 1% of the total MMES costs, respectively. If energy transport or charging and refueling infrastructure costs are not considered in a MMES, the electrification of the mobility sector might be overestimated. While energy transport costs and restrictions showed an impact on the mobility sectors electrification especially a required hydrogen pipeline network would be affected significantly from hydrogen usage in Germany. A hydrogen pipeline network for the transportation sector, as assessed in [52]–[54], might therefore be considered as maximum required pipeline network. The interactions between the energy transport infrastructure and the mobility sector shown in the present thesis emphasize the need for integrated, sector-coupling energy system studies.

The energy transport infrastructure is impacted by the size of a NUTS2 region. Regions with a large land area, such as the NUTS2 regions in Northern Germany, offer more area for onshore wind turbines. In the approach here, the number of grid extensions is still reduced to a single connection independent of the regions size. A higher resolution of the model might deviate from the results shown in this thesis. Further, the optimized hydrogen pipeline network shows the required hydrogen energy transport capacities in Germany, but it neglects exports, which could increase the demand for pipelines with Germany as hydrogen transit country. This effect is counterweighted by a neglectable amount of distributed electrolyzers in the model. Especially if building up a sufficient hydrogen pipeline network is delayed, more distributed electrolyzers are expected to be installed [198]. However, the simplifications made here allow optimizing a full MMES, including electricity, hydrogen, and methane transport infrastructures. The effect on the mobility sector's decarbonization of the different assessed energy transport elements is still valid, even though the quantification might deviate with a higher degree of detail in the model. Interpreting the marginal hydrogen cost difference between NUTS2 regions as hydrogen transport costs, the costs amount to 0.4 ct/kWh hydrogen in the reference scenario, 0.8 ct/kWh if

[14] Variation assessed between Controlled Charging Low Peak scenario and Hydrogen Mobility scenario. Assessed scenarios with cost variations for vehicle technologies or energy imports are not considered in the estimation here.

recompression costs are included, and 1.3ct/kWh if only GH_2 trailers are allowed.[15] This is in line with the lower cost assumptions for hydrogen transport via pipeline from Robinius et al. ranging from 0.6 ct/kWh to 1.7 ct/kWh [27]. Estimates summarized in a meta study from the European Commission vary between 0.5 to 4.5 ct/kWh hydrogen [188]. The lower cost estimation here for pipeline transport might be due to the lower spatial resolution of the considered hydrogen pipeline network, which is here modeled as center-to-center connection between NUTS2 regions.

The inland hydrogen generation is based on regionally occurring marginal electricity prices in the model. It does not reflect spot market prices, which do not incorporate grid congestions. Hence, the hydrogen inland generation costs below 7 ct/kWh reflect marginal costs but cannot be interpreted as costs for generating hydrogen in Germany for investors. It does not mean necessarily that it is economically viable for investors. This could sufficiently reduce the installed electrolyzer capacity in Germany in the future and impact the cost-optimal energy carrier mix in the mobility sector. However, the resulting full load hours of 2200 h to 2900 h of electrolyzers in the MMES and the allocation of electrolyzers in regions with a high availability of wind energy aligns with results from Robinius et al. and assumptions in the Grid Development Plan 2037/2045 (2023) [27], [198]. While their study calculates 62 GW of electrolyzers in Germany in 2050 the present thesis shows a range between 29 GW and 69 GW of electrolyzers in 2045. The inland generation in Robinius at et al. is with 180 TWh larger than in the here assessed scenarios. This value is exceeded by 19% in the MMES only if high fuel import costs, including e-methane and hydrogen, are assumed. The German Grid Development Plan 2037/2045 (2023) assumes an inland generation of 35% which is in the range with the resulting inland generation in the MMES of 59 TWh to 171 TWh [198].

The usage of hydrogen differs across studies. The assessed scenarios from Robinius et al. target an 80% and 95% CO_2 emission reduction and show in the latter 400 TWh of hydrogen demand in the system primarily in the industry and mobility sector. This is 1.4 times as much as the scenario in this thesis with the highest hydrogen demand. A high share of hydrogen usage in the mobility sector in this study might be due to the equal vehicle cost assumptions for all powertrains in the passenger car sector. Still, the freight transport costs for a fuel cell powertrain technology are assumed higher than other technology costs. The new scenario draft of the German Grid Development Plan 2037/2045 (2023) projects for 2045 a hydrogen demand of 240 TWh to 450 TWh [198] with a major share in the industry. The study ‚Klimaneutrales Deutschland 2045' from Agora Energiewende projects 265 TWh of hydrogen demand [41]. This is primarily for power and heat generation but also partly in the mobility sector for freight transportation. The meta studies [198], [199] show that the here assumed hydrogen demand is at the lower range of other studies. One reason is a relatively low hydrogen demand in the mobility sector in most scenarios and the fixed industry demand here of 84 TWh, which might be exceeded in future.

In contrast to the results here, e-fuels are only imported in the above-mentioned studies as well as in the Langfristszenarien from the BMWi [7]. Helgeson and Peter and the dena study with a European context show a generation potential in the EU [62], [88]. The latter study of up to 600 TWh per year [88]. However, the inland e-fuel generation of 119 TWh here is caused by three main factors. First, the availability of up to 130 TWh of hydrogen for costs below 7 ct/kWh. Second, the assumed optimal location of synthesis plants at central hydrogen hubs, which reduces the hydrogen distribution costs compared to a direct hydrogen usage by up to 6 ct/kWh. Third, the assumed CO_2 costs from direct air capture of 50 €/t. These assumptions are highly uncertain and can be challenged. Therefore, they are tested in this thesis in a sensitivity analysis. It shows, that when changing those assumptions, the inland generation of e-fuels drops to values between zero and 13 TWh. This is not in favor of imported e-fuels for 15 ct/kWh in the MMES but changes the decarbonization in the mobility sector towards increased electrification or a direct hydrogen usage. Large-scale imports of e-fuels are not relevant in any scenario. This result can only be achieved through the advantage of a full sector-coupling energy system optimized applied here. Even low e-fuel costs of 10.4 ct/kWh do not change this result[16]. Nevertheless,

[15] This is exemplarily calculated for the annually averaged marginal hydrogen cost difference between Mecklenburg-Western Pomerania (high generation) and Duesseldorf (high demand). The distance between both regions is about 600 km.

[16] The reduced e-fuel import costs are assumed here simultaneously with reduced hydrogen and e-methane import costs.

an assessment of reduced e-fuel import costs with a fixed e-fuel demand in the system is out of scope in this thesis.

Even though a carbon-neutral system in the year 2045 is assessed, the e-fuel usage in the mobility sector must be considered in the context of the transformation pathway towards the carbon-neutral system. If the CO_2 reduction targets foster a technology switch in the mobility sector before low-cost e-fuels are largely available, lock-in effects could occur favoring the electrification or the usage of hydrogen in the mobility sector. The e-fuel usage in the mobility sector must here be interpreted in a way, that the transformation towards this system enables an early availability of e-fuels before ICE powertrains are faded out.

The here cost-optimally derived high share of electrification for passenger cars and LDVs is within the consensus in the literature [7], [41], [62], [198]. The studies [7], [74] show depending on the scenario additional usage of e-fuel for passenger cars. Contrary, the MMES analysis shows fuel cell electric vehicles as the second relevant passenger transportation technology. This aligns with the study from Robinius et al., who show a fuel cell electric vehicle penetration of up to 40% [27]. Here, a penetration rate between 30% and 45% of fuel cell vehicles is reached in the optimization only if vehicle costs across powertrain technologies are balanced or if hydrogen is available at the refueling station below 8 ct/kWh compared to about 10 ct/kWh in the other scenarios.[17] This is approximately a third of the costs at hydrogen refueling stations in Germany in 2022 [100].

There is less agreement on the energy carriers used in the HDV segment. The uncertainty is supported by the findings in this thesis showing that the cost-efficient energy carrier is more sensitive to parameter variations. A partial electrification is assumed in Helgeson and Peter and in the Langfristszenarien. While in Helgeson and Peter methane is one major energy carrier for HDVs, the Langfristszenarien and Robinius et al. show scenario-dependent a usage of e-fuels or hydrogen [7], [27], [62]. However, the analysis here shows that e-methane is only relevant if available at low costs while hydrogen and e-fuels are more expensive. Since e-methane might be generated from hydrogen, this assumption depends on the development of international markets and the buildup of alternative supply chains towards Germany compared to methane.

The analysis here shows the range of possible decarbonization pathways and the sensitivity to the input parameters. It is not intended to state here if one energy carrier is more relevant than the other. Economic viability and geopolitics are major factors, which are not assessed here but could be highly relevant for the availability of low-cost energy carriers. If the increase of gas and oil prices continues due to geopolitical conflicts, the transition towards other technologies might be enforced earlier, which decreases alternative vehicle technology costs in 2045 and could cause lock-in effects. Nevertheless, the analysis shows that the electrification of the mobility sector is a reasonable way to reduce the dependency on foreign oil and gas imports and could at least in the passenger car segment be considered as no-regret solution. Additionally, the electrification of the heat sector should gain momentum as soon as possible reducing the international dependency and simultaneously targeting climate-neutrality. Current actions foster non-climate neutral alternatives to natural gas imports from Russia, such as LNG [200]. Methane is also supported in the Directive 2014/94/EU for the mobility sector. However, the analysis shows, that other energy carriers are suitable and if targeting a carbon-neutral system, methane might only be relevant in the mobility sector if available at much lower costs than other energy carriers. The results presented here suggest that an early ramp-up of alternative energy carriers should be fostered within the next years, while increasing the speed of electrifying the heat and mobility sector.

At the core of the transformation is inevitably a fast ramp-up of RES [7], [27], [41], [198]. The here required RES capacities are in the assumed range of the literature and require an increase of onshore wind turbine capacities of up to factor five, offshore capacities of factor two, and PV of factor ten compared to 2020. Especially the PV ramp-up with a required annual installation rate of 12 GW[18] needs incentives for house owners to install roof-top PV. This exceeds the currently annual installed PV capacities by more than factor two. However, this is below the required annual ramp-up until 2030 calculated from the 'Energiewirtschaftliches Institut an der Uni zu Köln (EWI)' in an analysis considering the coalition negotiations in 2021 [201]. The ramp-up of onshore wind

[17] Marginal electricity costs at the refueling station are across the assessed scenarios between 14 ct/kWh and 16 ct/kWh.

[18] Assuming a linear ramp-up from 2020 to 2045.

capacities of 5 GW, as stated in the analysis from the EWI, must be exceeded for the here assessed scenarios by up to 3 GW. This is especially challenging considering an average annual installation rate of 3 GW between 2010 and 2020 and a rate of 1 GW to 2 GW between 2018 and 2020. The challenge is not only regarding the social acceptance and political decisions but additionally in terms of required materials and production capacities for wind turbines and PV assets. A reduced ramp-up of 4 GW is considered here in one scenario. This scenario does not show a significant deviation from the electrification strategy in the mobility sector but only reduced inland electrolysis capacities.

Charging Infrastructure design and BEVs' flexibility

The charging infrastructure design is based on the aggregated charging peak load within a region and its aggregated daily flexibility. The results of integration of BEVs' flexibility show that those objectives are reasonable for an energy system assessment. The optimizer uses the flexibility to decrease the charging peak load of the fleet of 47 million BEVs in Germany. One advantage of focusing on those aggregated parameters is that different regional and urban systems can be compared. Other parameters might be suitable as well. When focusing on integrating BEVs and RES, e.g., a residual load minimization could be targeted for the charging infrastructure design. However, this depends on the historical weather data and increases the uncertainty of the approach.

One challenge is to integrate BEVs into the electricity distribution grid. This is not in the scope of the present thesis, but it can significantly impact the charging infrastructure design. For this, the aggregated peak is not a sufficient measure but locally arising charging peaks and voltage quality need to be considered. Further, the measure of daily shiftable electricity demand does not incorporate potential delay times or the time of the available flexibility.

The analysis in the present thesis shows that the timing is an important measure for the value of flexibility in an MMES context. Measuring the share of the flexible charging process during peak load times could overcome the drawback of considering a daily shiftable energy demand. Further, a combined approach of those measures could be suitable. The implemented framework is able to incorporate additional parameters in the multi-objective Pareto optimization. It is suggested to precisely analyze the upcoming challenges of a specific region in terms of BEV integration into the energy system and derive the suitable measures individually to design a regional charging infrastructure network. Finally, with the present thesis focusing on a system cost optimization, the economic viability of charging stations is not considered. An analysis of the utilization rate of individual public charging stations showed that the number of public charging stations in a region is an important measure for a projected utilization rate of a charging station.

The here developed charging infrastructure design method relies on the SQCI, which is one measure for the sufficiency of the charging infrastructure in a region. Different methods can incorporate detours or optimize the required charging infrastructure under the constraint of supply being equal to the demand [202]. The latter guarantees a sufficient supply but does not incorporate the dynamics of the charging demand.

A range of different vehicle parameters regarding the consumption and battery size is assumed here to represent the heterogeneity of the future automotive market. Nevertheless, the projected consumption rates and battery sizes are highly uncertain and impact the ABM eMob output significantly (cf. Figure 4-11). This can especially result in different charging peak loads and different requirements for the number of charging stations. Lower consumption rates would reduce the charging peak and the number of required chargers, and a higher demand would increase both outputs.

The analysis of the required charging infrastructure at different penetration levels shows, that an initial DCFC network is reasonable already at an early market penetration of BEVs reducing the demand of AC chargers by up to factor three. This can be compared with the strategy of Tesla rolling-out more than 1000 Supercharger's at 112 locations until beginning of 2022 and planning to equip another 68 locations in the same year. The DCFC coverage represents here the availability of DCFC chargers. The simplified approach can result in an underestimation of the required DCFC chargers. This is because no competition around DCFC chargers is modeled in the ABM eMob. Furthermore, the resulting number of AC charges in the results is restricted to the

discrete values simulated in the scenarios. Especially scenarios with many charging points, such as at low penetration, are prone to overestimate the required number of chargers. This is especially the case when the step size between the number of chargers from one to the other scenario increases up to 100. The number of chargers further relies on the assumption that no comfort reduction is accepted by drivers. Otherwise, lower numbers might be possible.

The results of this thesis show that at 20% BEV penetration, the number of public chargers in urban areas can drop to 20 per 1000 BEVs. This means that 50 BEVs share one charging point. The Pareto optimal scenarios reveal a demand for public chargers between 20 and 66 chargers per 1000 BEVs, which corresponds to 15-50 BEVs per charging point at 80% penetration. In comparison, the 'Masterplan Ladeinfrastruktur' from the German government targets 10 BEVs per charging point [11]. The present analysis shows that this number is reasonable for an initial charging infrastructure network. Still, the number of BEVs' sharing one public charging point can be reduced at mid and high penetration. Further, for a large-scale roll-out, the different needs of a roll-out must be considered.

Attention must be paid interpreting the resulting peak load values. They cannot be interpreted in a way that one BEV increases the peak load at a local grid feeder by approximately 1 kW but in a way, that on average, for each vehicle in the city, an additional 1 kW of electricity peak generation must be guaranteed. The local feeder impact might be significantly higher. This interpretation is in line with the system view in this thesis.

A decreasing number of flexible electricity generators until 2045 in the energy system increases the need for batteries to secure the load when low wind and PV energy generation occurs. The electricity grid connection of a region to the transmission grid could also help ensure the supply of the regional peak load. Nevertheless, the BEVs' flexibility can be leveraged to reduce the impact on the electricity distribution system. The transmission grid expansion in the assessed MMES is not impacted by the flexibility of BEVs, which is in line with the findings in Robinius et al. [14]. The authors additionally state that BEVs flexibility reduces the renewable energy that has to be curtailed. This cannot be confirmed in the present thesis since it mainly substitutes stationary energy storage capacities. The different findings are due to the here technology-neutral and full multi-modal consideration of the energy system. The cost-optimal dispatch of the BEVs fleet in the MMES shows that the peak load reduction is a cost-optimal dispatch of BEVs' flexibility on the country energy system level. Still, this flexibility here is a theoretical upper value, which must be incentivized for BEV owners to participate. A combined incentive for different challenges could be suitable since the MMES optimization showed that only 26% of the flexibility was utilized. This leaves additional flexibility for, e.g., regional grid congestions. Nevertheless, a prioritization cannot be made here. Further, different applications for flexibility could require flexibility at peak time, which would therefore be more valuable than the midday flexibility.

A common way of assessing the potential flexibility of BEVs is to refer to the total battery storage capacity in all registered vehicles [23]. This might significantly overestimate the available flexibility since the batteries are primarily used to satisfy the mobility demand. The utilized flexibility in the optimized MMES from BEV charging reaches up to 18 TWh/a, substituting 45 GWh of central battery storage or 61 GWh of total central storage capacities in the model. This is 26% of the total annual flexibility of a 95% electrified passenger car sector, which sums up to 69 TWh/a. Supposing an average BEV's battery capacity of 45 kWh, 47 million BEVs would have a battery storage capacity of more than 2 TWh in a 95% electrified passenger car segment. If it is compared to stationary batteries and assuming two full battery cycles every week it would result in a flexible energy dispatch of 208 TWh/a. If that is compared to the theoretically available flexibility of 69 TWh, it reveals that approximately one-third of the battery's capacity would be available for dispatch throughout the year. The assessed BEVs' flexibility in the ABM eMob is already an upper limit, and batteries could operate more than two cycles a week, which further reduces the share. However, the flexibility of BEVs is still significant and must be levelized efficiently to integrate BEVs into energy systems to reduce overall system costs and drive the energy transition.

In future BEVs could also operate on, e.g., the frequency reserve market [203]. Therefore, the total energy is not only the measure of relevance but also the power within each time step. While BEVs could theoretically shift up to 78% of all charging processes during evening peak load, the flexible power provision could reach an order of magnitude of 36 GW, assuming 1 kW per BEV charging peak load. Anyway, also this is highly uncertain due to

the strong dependency on the time of the day. Pooling of BEVs and primarily incentivizing the flexibility of BEVs efficiently is one key element for the energy transition. Lastly, bidirectional charging might increase the available flexibility of BEVs if incentivized efficiently.

To realize the transformation towards an electrified passenger car sector, the buildup of charging infrastructure is inevitable. For a 95% electrified passenger car sector in 2045, 4.5 million AC charger (11 kW-22 kW) are required at public and workplaces in Germany and additionally 329 thousand fast charging points (50 kW-150 kW).[19] The total charging infrastructure investment costs amount to 68 billion € to 87 billion €.[20] A linear ramp-up would require 200 thousand 11 kW and 22 kW charging points per year or 4000 per week.[21] As shown in the analysis, lower penetration rates require even more charging stations per BEV, which would increase the required number of annually installed chargers in the next years significantly. This ramp-up must be subsidized and start immediately gaining momentum in the electrification of the automotive market. It is a no-regret measure towards a carbon-neutral energy system.

[19] This refers to the Pareto-optimal low peak charging infrastructure design identified here. The numbers are valid if home charging is widely available, and 31 million home charging points are installed for 47 million BEVs.

[20] Lower value estimated based on 2020 charging station costs, upper value based on 2045 cost estimations.

[21] About 300 charging points are build up per week at the end of 2021 [204].

8 Conclusion and outlook

RES must be utilized in the electricity, heat, and mobility sector in a decarbonized MMES. The interactions between a carbon-neutral mobility sector and an MMES must be understood to cost-optimally steer the transformation towards climate-neutrality. Especially new, disruptive infrastructure elements such as the hydrogen supply and charging infrastructure require increased attention in the assessment of a decarbonized MMES. The present thesis identified interactions that are relevant to consider while planning the decarbonization of the mobility sector.

The multi-modal approach here extends former research by incorporating electricity, methane, and hydrogen transport infrastructure in a linear energy system optimization while optimizing the mobility sector as part of the MMES. This allows assessing the impact of different measures in the energy system on the energy carriers in a cost-optimally decarbonized mobility sector. Since the level of detail and heterogeneity of individual stakeholders, such as electric vehicle drivers, is limited in a country energy system model, an agent-based model is coupled with the energy system model for an in-depth analysis of BEVs and their required charging infrastructure. This allows reducing the gap in research of understanding the impact of the design of charging infrastructure networks on the energy system.

The analysis here shows that a high electrification of the mobility sector is cost-efficient and primarily in the passenger car and light duty vehicle segment a non-regret decision. The uncertainty of energy import and transport costs as well as realizable expansion pathways for the inland electricity and hydrogen generation are especially relevant for recommending cost-efficient transportation technologies in capital-intensive transportation segments such as heavy-duty vehicles and busses. However, only a range of selected scenarios is assessed here. Quantifying tipping points between different technologies in large energy system models would require new methods capable of assessing significantly more scenarios. Future work could pick up on that to extend the analysis. An additional micro-economic perspective for different stakeholders in the mobility sector, such as car manufacturers and charging station operators, would further enrich the analysis and improve the quality of recommendations.

An integrated approach must be chosen for planning a hydrogen supply chain since the required buildup of a hydrogen transport network is significantly affected by the hydrogen usage in the mobility sector. If the buildup does not keep pace with the developments in the mobility sector, the risk of increased hydrogen prices at refueling stations could finally lead to a non-optimal system. Therefore, it is highly recommended to extend the analysis of interactions between different sectors in a MMES by incorporating transition pathways of the energy system until 2045.

In any case, it is inevitable to ramp-up wind and PV electricity generation capacities independently of the energy carriers in mobility sector. The number of hours with low electricity prices can be sufficient in a carbon-neutral system to generate hydrogen on a large-scale in Germany. Whether the hydrogen is then used directly in the mobility sector or processed in Fischer-Tropsch synthesis systems highly depends on the hydrogen distribution costs charged for both applications. Contrary to the narrative in former studies and literature, the analysis here showed that e-fuel generation might be cost-efficient in Germany in a carbon-neutral energy system if synthesis processes are allocated at central hydrogen hubs minimizing the hydrogen distribution costs. A low-cost e-fuel transport, distribution, and refueling system based on existing infrastructure can then be used, increasing the competitiveness of e-fuels compared to hydrogen. Nevertheless, the buildup of international supply chains should be compared in future work macro-economically to the inland generation considering the findings from this thesis. It is further recommended to include geopolitical uncertainties in future analysis of international energy supply chains.

Flexible charging of BEVs has a large potential to contribute to a cost-efficient energy system mainly by reducing the aggregated charging peak load and by alignment with PV electricity generation times. It should not be assumed that controlled charging of BEVs reduces the curtailment of renewable electricity generation directly, but it rather reduces the need for stationary storage systems. However, the flexibility must be incentivized efficiently to leverage its potential. Studying the most effective incentive schemes is of upmost relevance for further research. Additionally, future research could focus on suitable applications for the flexibility from BEVs

such as peak load reduction, avoidance of grid congestions, avoidance of expansions in the distribution grid, flexibility provision for the transmission grid, economic benefits for charging station operators or BEV drivers.

A previously unassessed effect regarding the relevance of charging infrastructure planning for the integration of BEVs with the energy system is analyzed. It shows that charging infrastructure can be used as a lever to reduce the charging peak and to increase the flexibility. This can finally reduce overall energy system costs. At an early stage, the charging infrastructure design must focus on realizing a large ramp-up to accelerate the transformation towards BEVs. In this early stage, fast-charging points reduce the total number of required slow chargers significantly. If the BEV penetration increases, an integrated planning of charging infrastructure and the energy system becomes increasingly important to first, reduce the overall charging peak load, and second to enable more flexible charging. It is highly recommended to consider the lever of efficiently designing charging infrastructure networks in urban and rural areas. While the relevance of an efficient charging infrastructure design is identified here focusing on the country energy system, further research should integrate local renewable electricity potential and distribution grid congestions into the charging infrastructure planning process. This should allow targeting the design to specific challenges in different regions. Incorporating geoinformation system data is highly recommended for this.

Acronyms

AC	Alternating Current
BEV	Battery Electric Vehicle
DC	Direct Current
DCFC	Direct Current Fast Charging
FT	Fischer-Tropsch
HDV	Heavy Duty Vehicle
ICE	Internal Combustion Engine
LDV	Light Duty Vehicle
MiD17	Mobility in Germany 2017 [136]
MMES	Multi-modal Energy System
RES	Renewable Energy Sources
SOC	State of Charge
SQCI	Service Quality of deployed Charging Infrastructure

Nomenclature

Indices, Sets, Variables and Parameters in the mathematical optimization model (ESDP):

Index	Set	Description
co	CO	Commodity
cp	CP	Conversion process describing a conversion technology in the model, which consists of one or multiple conversion subprocesses cs
cs	CS	Conversion subprocess describing an energy conversion steps
t, tt	T	Time step
x	X	Region
y	Y	Year

Variable	Description
e	energy
g	Capacity of a transport process between two regions
k	Capacity of a conversion process defined by a single conversion subprocess
k^{dsm}	Demand side management capacity of a conversion subprocess
o	CO_2 emissions
p	power within each time step
e^{st}	Stored energy
γ^{down}	Load in one time step that is shifted down from an originating load profile
γ^{up}	Load in one time step that is shifted up from an originating load profile

Parameters	Description
C	Costs as capital expenditures (capex) or operational expenditures (opex)
F	Discount factor
I	Indicator defining if a commodity requires transport infrastructure two be transported between regions
K	Maximum demand side management shift capacity of a conversion subprocess
L	Distance between two regions
N	Annuity of conversion process
O	CO_2 emission limit
V	Technical availability of conversion subprocess / technology
η	Efficiency of a conversion subprocess
w	Weighting factor for time steps

δ	Maximum time to shift load from one time step to another

Indices, Sets, Variables and Parameters in the agent-based simulation model (ABM eMob):

Index	**Set**	**Description**
i	I	Index of battery electric vehicle
j	J	Charging point
places		Type of location
t	T	Time step within simulation period T
z	Z	Location of fast charging station

Variable	**Description**
$\mathrm{p}^{\mathrm{charge}}$	Power supply from charging point to electric vehicle
f^{charge}	Available shiftable energy of a BEV's charging process
SOC	State of Charge of vehicle's battery

Parameters	**Description**
C	Consumption rate of electric vehicle
D	Driven distance in one time step
K	Battery capacity of electric vehicle
M	Number of modeled locations of the same type
M^{BEV}	Number of modeled battery electric vehicles
$\mathrm{N}^{\mathrm{cars}}$	Total number of cars in a region
$\mathrm{N}^{\mathrm{tot}}$	Total number of potential charging sites in a region
S^{BEV}	Share of battery electric vehicles in relation to $\mathrm{N}^{\mathrm{cars}}$
$T^{ambient}$	Ambient temperature for entire simulation period

Bibliography

[1] Bundesministerium für Wirtschaft und Energie (BMWi), "Datenübersicht zum achten Monitoring-Bericht.xlsx." Energiewende, Mar. 25, 2021. Accessed: Oct. 14, 2021. [Online]. Available: https://www.bmwi.de/Redaktion/DE/Binaer/datenuebersicht-fortschrittsbericht-2018-2019.xls?__blob=publicationFile&v=6

[2] Kraftfahrt-Bundesamt, "Verkehr in Kilometern (VK), Zeitreihe 2014-2020." Jun. 2021. Accessed: Oct. 17, 2021. [Online]. Available: https://www.kba.de/DE/Statistik/Kraftverkehr/VerkehrKilometer/vk_inlaenderfahrleistung/vk_inlaenderfahrleistung_node.html;jsessionid=66820693C12D6DA80B5F9C50AE159FA4.live21301

[3] Umweltbundesamt (UBA), "Energieverbrauch nach Energieträgern und Sektoren," May 10, 2021. https://www.umweltbundesamt.de/daten/energie/energieverbrauch-nach-energietraegern-sektoren#allgemeine-entwicklung-und-einflussfaktoren (accessed Oct. 23, 2021).

[4] Bundesministerium für Verkehr und digitale Infrastruktur, "Verkehr in Zahlen 2020/2021," Flensburg, 49. Jahrgang, Sep. 2020.

[5] U. Kramer, F. Ortloff, S. Stollenwerk, and R. Thee, "Defossilisierung des Transportsektors - Optionen und Voraussetzungen in Deutschland," Research Association for Combustion Engines (FVV), Frankfurt, Germany, R586, 2018.

[6] Umweltbundesamt (UBA), "Nationale Trendtabellen für die deutsche Berichterstattung atmosphärischer Emissionen 1990 - 2019." Jan. 15, 2021. Accessed: Oct. 14, 2021. [Online]. Available: Internet: http://www.umweltbundesamt.de/emissionen

[7] BMWi, "Langfristszenarien für die Transformation des Energiesystems in Deutschland 3," 2021. https://www.langfristszenarien.de/enertile-explorer-de/

[8] Bundesverband der Deutschen Industrie (BDI), "Klimapfade für Deutschland 2.0 - Ein Wirtschaftsprogramm für Klima und Zukunft," Germany, Oct. 2021. Accessed: Nov. 12, 2021. [Online]. Available: https://bdi.eu/publikation/news/klimapfade-2-0-ein-wirtschaftsprogramm-fuer-klima-und-zukunft/

[9] Bundesregierung Deutschland, "Climate Change Act 2021," Jun. 25, 2021. https://www.bundesregierung.de/breg-de/themen/klimaschutz/climate-change-act-2021-1936846 (accessed Oct. 20, 2021).

[10] The European Parliament and the Council, *Directive 2014/94/EU on the deployment of alternative fuels infrastructure (AFID)*. 2014.

[11] Bundesregierung Deutschland, "Masterplan Ladeinfrastruktur der Bundesregierung - Ziele und Maßnahmen für den Ladeinfrastrukturaufbau bis 2030." 2019. Accessed: Dec. 11, 2020. [Online]. Available: https://www.bmvi.de/SharedDocs/DE/Anlage/G/masterplan-ladeinfrastruktur.pdf?__blob=publicationFile#:~:text=Mit%20dem%20Ma%C3%9Fnahmenpaket%20Elektromobilit%C3%A4t%20vom,15.000%20Ladestationen%20bis%20Ende%202020.

[12] Bundesregierung Deutschland, "Verkehr," *Verkehr*, 2021. https://www.bundesregierung.de/breg-de/themen/klimaschutz/verkehr-1672896 (accessed Mar. 28, 2022).

[13] T. Gnann, S. Funke, N. Jakobsson, P. Plötz, F. Sprei, and A. Bennehag, "Fast charging infrastructure for electric vehicles: Today's situation and future needs," *Transportation Research Part D: Transport and Environment*, vol. 62, pp. 314–329, Jul. 2018, doi: 10.1016/j.trd.2018.03.004.

[14] M. Robinius *et al.*, "Comparative Analysis of Infrastructures - Hydrogen Fueling and Electric Charging of Vehicles.pdf," IEK-3, Forschungszentrum Jülich GmbH, H2MOBILITY, Jülich, Germany, Volume 408, 2018. [Online]. Available: http://hdl.handle.net/2128/16709

[15] Agora Verkehrswende, Agora Energiewende, and Regulatory Assistance Project (RAP), “Verteilnetzausbau für die Energiewende - Elektromobilität im Fokus,” p. 114, Aug. 2019.

[16] M. F. Felgenhauer, “Battery and fuel cell electric vehicles in the context of the energy transition. Cross-sectoral assessment of electric vehicles in Germany and California,” Technical University of Munich, Munich, Germany, 2016.

[17] D. Castelvecchi, “Electric cars and batteries: how will the world produce enough?,” *Nature*, vol. 596, no. 7872, pp. 336–339, Aug. 2021, doi: 10.1038/d41586-021-02222-1.

[18] W. He, M. King, X. Luo, M. Dooner, D. Li, and J. Wang, “Technologies and economics of electric energy storages in power systems: Review and perspective,” *Advances in Applied Energy*, vol. 4, p. 100060, Nov. 2021, doi: 10.1016/j.adapen.2021.100060.

[19] R. Peters *et al.*, “Future Power Train Solutions for Long-Haul Trucks,” *Sustainability*, vol. 13, no. 4, p. 2225, Feb. 2021, doi: 10.3390/su13042225.

[20] M. Yugo and A. Soler, “A look into the role of e-fuels in the transport system in Europe (2030–2050) (literature review),” No. 1, Oct. 2019.

[21] P. Sterchele, *Analysis of technology options to balance power generation from variable renewable energy: case study for the German Energy System with the Sector Coupling Model REMod*. Düren: Shaker Verlag, 2019.

[22] H. C. Gils, H. Gardian, and J. Schmugge, “Interaction of hydrogen infrastructures with other sector coupling options towards a zero-emission energy system in Germany,” *Renewable Energy*, vol. 180, pp. 140–156, Dec. 2021, doi: 10.1016/j.renene.2021.08.016.

[23] J. Figgener *et al.*, “The development of battery storage systems in Germany – A market review (status 2022),” p. 15, 2022.

[24] H.-K. Ringkjøb, P. M. Haugan, and I. M. Solbrekke, “A review of modelling tools for energy and electricity systems with large shares of variable renewables,” *Renewable and Sustainable Energy Reviews*, vol. 96, pp. 440–459, Nov. 2018, doi: 10.1016/j.rser.2018.08.002.

[25] L. Kotzur *et al.*, “A modeler’s guide to handle complexity in energy systems optimization,” *Advances in Applied Energy*, vol. 4, p. 100063, Nov. 2021, doi: 10.1016/j.adapen.2021.100063.

[26] Deutsche Energie-Agentur GmbH (dena), “dena-Leitstudie Integrierte Energiewende - Impulse für die Gestaltung des Energiesystems bis 2050,” Berlin, Germany, Jul. 2018. [Online]. Available: https://www.dena.de/fileadmin/dena/Dokumente/Pdf/9262_dena-Leitstudie_Integrierte_Energiewende_Ergebnisbericht.pdf

[27] M. Robinius *et al.*, *Wege für die Energiewende - Kosteneffiziente und klimagerechte Transformationsstrategien für das deutsche Energiesystem bis zum Jahr 2050*, vol. Schriften des Forschungszentrum Jülich. 2020. [Online]. Available: www.fz-juelich.de/zb/openaccess

[28] P. Sterchele *et al.*, “Studie: Wege zu einem klimaneutralen Energiesystem - Die deutsche Energiewende im Kontext gesellschaftlicher Verhaltensweisen,” Frauenhofer Institut für Solare Energiesysteme ISE, Freiburg, Feb. 2020. [Online]. Available: https://www.ise.fraunhofer.de/content/dam/ise/de/documents/publications/studies/Fraunhofer-ISE-Studie-Wege-zu-einem-klimaneutralen-Energiesystem.pdf

[29] M. Robinius *et al.*, “Linking the Power and Transport Sectors—Part 2: Modelling a Sector Coupling Scenario for Germany,” *Energies*, vol. 10, no. 7, p. 957, Jul. 2017, doi: 10.3390/en10070957.

[30] Bartholdsen *et al.*, “Pathways for Germany’s Low-Carbon Energy Transformation Towards 2050,” *Energies*, vol. 12, no. 15, p. 2988, Aug. 2019, doi: 10.3390/en12152988.

[31] R. Bramstoft, A. Pizarro-Alonso, I. G. Jensen, H. Ravn, and M. Münster, “Modelling of renewable gas and renewable liquid fuels in future integrated energy systems,” *Applied Energy*, vol. 268, p. 114869, Jun. 2020, doi: 10.1016/j.apenergy.2020.114869.

[32] T. Brown, D. Schlachtberger, A. Kies, S. Schramm, and M. Greiner, “Synergies of sector coupling and transmission reinforcement in a cost-optimised, highly renewable European energy system,” *Energy*, vol. 160, pp. 720–739, Oct. 2018, doi: 10.1016/j.energy.2018.06.222.

[33] M. S. Lester, R. Bramstoft, and M. Münster, “Analysis on Electrofuels in Future Energy Systems: A 2050 Case Study,” *Energy*, vol. 199, p. 117408, May 2020, doi: 10.1016/j.energy.2020.117408.

[34] M. Metzger *et al.*, “Pathways toward a Decarbonized Future—Impact on Security of Supply and System Stability in a Sustainable German Energy System,” *Energies*, vol. 14, no. 3, p. 560, Jan. 2021, doi: 10.3390/en14030560.

[35] C. Müller *et al.*, “Modeling framework for planning and operation of multi-modal energy systems in the case of Germany,” *Applied Energy*, vol. 250, pp. 1132–1146, Sep. 2019, doi: 10.1016/j.apenergy.2019.05.094.

[36] A. Palzer, *Sektorübergreifende Modellierung und Optimierung eines zukünftigen deutschen Energiesystems unter Berücksichtigung von Energieeffizienzmaßnahmen im Gebäudesektor*. Stuttgart: Fraunhofer Verlag, 2016.

[37] Öko-Institut e.V and Frauenhofer Institut für Solare Energiesysteme (ISI), “Klimaschutzszenario 2050 – 2. Endbericht,” Berlin, Germany, Dec. 2015. [Online]. Available: https://www.isi.fraunhofer.de/de/competence-center/energiepolitik-energiemaerkte/projekte/klimaszenario-2050_3305311.html

[38] H. Hecking, M. Hintermayer, D. Lencz, and J. Wagner, “Energiemarkt 2030 und 2050 – Der Beitrag von Gas- und Wärmeinfrastruktur zu einer effizienten CO2-Minderung,” Cologne, Germany, Endbericht, Nov. 2017.

[39] F. Ausfelder *et al.*, *“Sektorkopplung” - Untersuchungen und Überlegungen zur Entwicklung eines integrierten Energiesystems*. München: acetech - Deutsche Akademie der Technikwissenschaften e.V, 2017.

[40] N. Gerhardt *et al.*, “Interaktion EE-Strom, Wärme und Verkehr,” Fraunhofer-Institut für Windenergie und Energiesystemtechnik, Sep. 2015.

[41] M. Weiß, M. Wünsch, and I. Ziegenhagen, “Klimaneutrales Deutschland 2045. Wie Deutschland seine Klimaziele schon vor 2050 erreichen kann,” Jun. 2021.

[42] Fernleitungsnetzbetreiber (FNB Gas), “Netzentwicklungsplan Gas 2020-2030,” Fernleitungsnetzbetreiber Gas e.V, Berlin, Germany, May 2021.

[43] Übertragungsnetzbetreiber, “Netzentwicklungsplan Strom 2035 (2021), zweiter Entwurf.” Apr. 26, 2021.

[44] Deutsche Energie-Agentur GmbH (dena), “dena-Zwischenbericht - Energieinfrastrukturen im klimaneutralen Energiesystem,” Oct. 2021.

[45] J. Egerer, C. Gerbaulet, and C. Lorenz, “European Electricity Grid Infrastructure Expansion in a 2050 Context,” *EJ*, vol. 37, no. 01, Sep. 2016, doi: 10.5547/01956574.37.SI3.jege.

[46] European Commission, “e-Highway 2050: Europe’s future secure and sustainable electricity infrastructure,” Nov. 2015. [Online]. Available: https://docs.entsoe.eu/baltic-conf/bites/www.e-highway2050.eu/e-highway2050/e-highway2050-modular-development-plan-of-the-pan-european-transmission-system-2050/

[47] M. Fürsch, S. Hagspiel, C. Jägemann, S. Nagl, D. Lindenberger, and E. Tröster, “The role of grid extensions in a cost-efficient transformation of the European electricity system until 2050,” *Applied Energy*, vol. 104, pp. 642–652, Apr. 2013, doi: 10.1016/j.apenergy.2012.11.050.

[48] A. Schroeder, P.-Y. Oei, A. Sander, L. Hankel, and L. C. Laurisch, “The integration of renewable energies into the German transmission grid—A scenario comparison,” *Energy Policy*, vol. 61, pp. 140–150, Oct. 2013, doi: 10.1016/j.enpol.2013.06.006.

[49] J. Haumaier, P. Hauser, H. Hobbie, and D. Möst, “Grünes Gas für die Gaswirtschaft – Regionale Power-to-Gas-Potentiale aus Onshore-Windenergie in Deutschland,” *Z Energiewirtsch*, Apr. 2020, doi: 10.1007/s12398-020-00274-w.

[50] B. Gillessen, H. Heinrichs, J.-F. Hake, and H.-J. Allelein, “Natural gas as a bridge to sustainability: Infrastructure expansion regarding energy security and system transition,” *Applied Energy*, vol. 251, p. 113377, Oct. 2019, doi: 10.1016/j.apenergy.2019.113377.

[51] P. Hauser, S. Heidari, C. Weber, and D. Möst, “Does Increasing Natural Gas Demand in the Power Sector Pose a Threat of Congestion to the German Gas Grid? A Model-Coupling Approach,” p. 22, 2019.

[52] D. Krieg, “Konzept und Kosten eines Pipelinesystems zur Versorgung des deutschen Straßenverkehrs mit Wasserstoff,” Forschungszentrum Jülich, Jülich, 2012.

[53] M. Robinius, Forschungszentrum Jülich GmbH, and Z. Verlag, “Strom- und Gasmarktdesign zur Versorgung des deutschen Straßenverkehrs mit Wasserstoff,” 2016.

[54] M. Reuß, “Techno-ökonomische Analyse alternativer Wasserstoffinfrastruktur,” RWTH Aachen University, 2019. [Online]. Available: https://publications.rwth-aachen.de/record/765438/files/765438.pdf

[55] M. Reuß, T. Grube, M. Robinius, P. Preuster, P. Wasserscheid, and D. Stolten, “Seasonal storage and alternative carriers: A flexible hydrogen supply chain model,” *Applied Energy*, vol. 200, pp. 290–302, Aug. 2017, doi: 10.1016/j.apenergy.2017.05.050.

[56] F. Stöckl, W.-P. Schill, and A. Zerrahn, “Optimal supply chains and power sector benefits of green hydrogen,” *Sci Rep*, vol. 11, no. 1, p. 14191, Dec. 2021, doi: 10.1038/s41598-021-92511-6.

[57] S. Samsatli, I. Staffell, and N. J. Samsatli, “Optimal design and operation of integrated wind-hydrogen-electricity networks for decarbonising the domestic transport sector in Great Britain,” *International Journal of Hydrogen Energy*, vol. 41, no. 1, pp. 447–475, Jan. 2016, doi: 10.1016/j.ijhydene.2015.10.032.

[58] S. Samsatli and N. J. Samsatli, “The role of renewable hydrogen and inter-seasonal storage in decarbonising heat – Comprehensive optimisation of future renewable energy value chains,” *Applied Energy*, vol. 233–234, pp. 854–893, Jan. 2019, doi: 10.1016/j.apenergy.2018.09.159.

[59] TenneT and Gasunie, “Phase 2 - Pathways to 2050,” Feb. 2020.

[60] B. Koirala, S. Hers, G. Morales-España, Ö. Özdemir, J. Sijm, and M. Weeda, “Integrated electricity, hydrogen and methane system modelling framework: Application to the Dutch Infrastructure Outlook 2050,” *Applied Energy*, vol. 289, p. 116713, May 2021, doi: 10.1016/j.apenergy.2021.116713.

[61] P. Runge, C. Sölch, J. Albert, P. Wasserscheid, G. Zöttl, and V. Grimm, “Economic Comparison of Electric Fuels Produced at Excellent Locations for Renewable Energies: A Scenario for 2035,” *SSRN Journal*, 2020, doi: 10.2139/ssrn.3623514.

[62] B. Helgeson and J. Peter, “The role of electricity in decarbonizing European road transport – Development and assessment of an integrated multi-sectoral model,” *Applied Energy*, vol. 262, p. 114365, Mar. 2020, doi: 10.1016/j.apenergy.2019.114365.

[63] F. Grüger, “Initialinfrastruktur für Wasserstoffmobilität auf Basis von Flotten,” RWTH Aachen University, 2019.

[64] P. Rose, “Modeling a potential hydrogen refueling station network for fuel cell heavy-duty vehicles in Germany in 2050,” 2020, doi: 10.5445/IR/1000119521.

[65] M. Melaina and J. Bremson, “Refueling availability for alternative fuel vehicle markets: Sufficient urban station coverage,” *Energy Policy*, vol. 36, no. 8, pp. 3233–3241, Aug. 2008, doi: 10.1016/j.enpol.2008.04.025.

[66] T. Grube, A. Linke, D. Xu, M. Robinius, and D. Stolten, “Kosten von Ladeinfrastrukturen für Batteriefahrzeuge in Deutschland,” p. 12, 2017.

[67] S. Á. Funke, F. Sprei, T. Gnann, and P. Plötz, “How much charging infrastructure do electric vehicles need? A review of the evidence and international comparison,” *Transportation Research Part D: Transport and Environment*, vol. 77, pp. 224–242, Dec. 2019, doi: 10.1016/j.trd.2019.10.024.

[68] P. Jochem, E. Szimba, and M. Reuter-Oppermann, “How many fast-charging stations do we need along European highways?,” *Transportation Research Part D: Transport and Environment*, vol. 73, pp. 120–129, Aug. 2019, doi: 10.1016/j.trd.2019.06.005.

[69] M. Nicholas and S. Wappelhorst, “Regional charging infrastructure requirements in Germany through 2030.” Oct. 2020. Accessed: Oct. 17, 2021. [Online]. Available: https://theicct.org/sites/default/files/publications/germany-charging-infrastructure-20201021.pdf

[70] W. Brost, T. Funke, R. Philipsen, T. Brell, and M. Ziefle, “Integrated Model Approach STELLA Method of Site Identification for Charging Infrastructure,” *IFAC-PapersOnLine*, vol. 51, no. 9, pp. 206–211, 2018, doi: 10.1016/j.ifacol.2018.07.034.

[71] R. Pagany, A. Marquardt, and R. Zink, “Electric Charging Demand Location Model—A User- and Destination-Based Locating Approach for Electric Vehicle Charging Stations,” *Sustainability*, vol. 11, no. 8, p. 2301, Apr. 2019, doi: 10.3390/su11082301.

[72] VDE|FNN and BDEW, “Metastudie Forschungsüberblick Netzintegration Elektromobilität,” FGH e.V., Aachen, Germany, Study, Dec. 2018. [Online]. Available: https://shop.vde.com/de/metastudie-netzintegration-elektromobilitaet

[73] F. Hacker *et al.*, “eMobil 2050 - Szenarien zum m?glichen Beitrag des elektrischen Verkehrs zum langfristigen Klimaschutz,” Öko-Institut e.V., 2014.

[74] P. Kasten, M. Mottschall, W. Köppel, and C. Degünther, “Erarbeitung einer fachlichen Strategie zur Energieversorgung des Verkehrs bis zum Jahr 2050,” Umweltbundesamt, Dessau-Roßlau, Nov. 2016.

[75] L. B. Weger, J. Leitão, and M. G. Lawrence, “Expected impacts on greenhouse gas and air pollutant emissions due to a possible transition towards a hydrogen economy in German road transport,” *International Journal of Hydrogen Energy*, vol. 46, no. 7, pp. 5875–5890, Jan. 2021, doi: 10.1016/j.ijhydene.2020.11.014.

[76] V. Matthias *et al.*, “Modelling road transport emissions in Germany – Current day situation and scenarios for 2040,” *Transportation Research Part D: Transport and Environment*, vol. 87, p. 102536, Oct. 2020, doi: 10.1016/j.trd.2020.102536.

[77] M. Millinger, P. Tafarte, M. Jordan, A. Hahn, K. Meisel, and D. Thrän, “Electrofuels from excess renewable electricity at high variable renewable shares: cost, greenhouse gas abatement, carbon use and competition,” *Sustainable Energy Fuels*, p. 10.1039.D0SE01067G, 2021, doi: 10.1039/D0SE01067G.

[78] R. Bramstoft and K. Skytte, “Decarbonizing Sweden’s energy and transportation system by 2050,” *International Journal of Sustainable Energy Planning and Management*, vol. 14, pp. 3–20, 2017, doi: 10.5278/ijsepm.2017.14.2.

[79] O. Ruhnau, S. Bannik, S. Otten, A. Praktiknjo, and M. Robinius, “Direct or indirect electrification? A review of heat generation and road transport decarbonisation scenarios for Germany 2050,” *Energy*, vol. 166, pp. 989–999, Jan. 2019, doi: 10.1016/j.energy.2018.10.114.

[80] D. Chakraborty, J. H. Efthi, East Delta University, M. Khanom, and I. M. Mahbubul, “Prospective and Challenging Issues of Biofuels,” *EJCEE*, vol. 1, no. 1, pp. 4–10, Aug. 2020, doi: 10.46603/ejcee.v1i1.5.

[81] Umweltbundesamt (UBA), “Bioenergie,” Jun. 26, 2020. https://www.umweltbundesamt.de/themen/klima-energie/erneuerbare-energien/bioenergie#Reststoffe (accessed Nov. 12, 2021).

[82] C. Stan, *Alternative Propulsion for Automobiles*. Cham: Springer International Publishing, 2017. doi: 10.1007/978-3-319-31930-8.

[83] European Commission. Joint Research Centre., *JEC well-to-tank report V5: JEC well to wheels analysis : well to wheels analysis of future automotive fuels and powertrains in the European context : passenger car.* LU: Publications Office, 2020. Accessed: Nov. 13, 2021. [Online]. Available: https://data.europa.eu/doi/10.2760/557004

[84] F. Hacker *et al.*, "StartOn - Bewertung und Einführungstrategien für oberleitungsgebundene schwere Nutzfahrzeuge - Endbericht," Berlin, Germany, Feb. 2020. Accessed: Mar. 13, 2022. [Online]. Available: https://www.oeko.de/publikationen/p-details/straton-bewertung-und-einfuehrungsstrategien-fuer-oberleitungsgebundene-schwere-nutzfahrzeuge

[85] International Energy Agency (IEA), "Global Hydrogen Review 2021," Paris, France, Oct. 2021. [Online]. Available: https://iea.blob.core.windows.net/assets/e57fd1ee-aac7-494d-a351-f2a4024909b4/GlobalHydrogenReview2021.pdf

[86] C. Bae and J. Kim, "Alternative fuels for internal combustion engines," *Proceedings of the Combustion Institute*, vol. 36, no. 3, pp. 3389–3413, 2017, doi: 10.1016/j.proci.2016.09.009.

[87] International Energy Agency, Ed., *Transport, energy and CO_2: moving toward sustainability*. Paris: International Energy Agency, 2009.

[88] dena, "The potential of electricity-based fuels for low-emission transport in the EU." Nov. 2017. [Online]. Available: https://www.dena.de/fileadmin/dena/Dokumente/Pdf/9219_E-FUELS-STUDY_The_potential_of_electricity_based_fuels_for_low_emission_transport_in_the_EU.pdf

[89] A. Soler, "Role of e-fuels in the European transport system. Literature review," 14/19, 2020.

[90] A. Tremel, P. Wasserscheid, M. Baldauf, and T. Hammer, "Techno-economic analysis for the synthesis of liquid and gaseous fuels based on hydrogen production via electrolysis," *International Journal of Hydrogen Energy*, vol. 40, no. 35, pp. 11457–11464, Sep. 2015, doi: 10.1016/j.ijhydene.2015.01.097.

[91] M. Aslam, H. Masjuki, M. Kalam, H. Abdesselam, T. Mahlia, and M. Amalina, "An experimental investigation of CNG as an alternative fuel for a retrofitted gasoline vehicle," *Fuel*, vol. 85, no. 5–6, pp. 717–724, Mar. 2006, doi: 10.1016/j.fuel.2005.09.004.

[92] S. Schemme, R. C. Samsun, R. Peters, and D. Stolten, "Power-to-fuel as a key to sustainable transport systems – An analysis of diesel fuels produced from CO 2 and renewable electricity," *Fuel*, vol. 205, pp. 198–221, Oct. 2017, doi: 10.1016/j.fuel.2017.05.061.

[93] D. U. Bünger, H. Landinger, W. Weindorf, R. Wurster, J. Zerhusen, and D. W. Zittel, "Vergleich von CNG und LNG zum Einsatz in LKW im Fernverkehr - Eine Expertise für die Open Grid Europe GmbH, Abschlussbericht," Ludwig Bölkow Systemtechnik, May 2016.

[94] M. Zerta *et al.*, "Strombasiert Kraftstoffe für Brennstoffzellen in der Binnenschifffahrt," NOW GmbH, Munich,Hamburg,Berlin, Germany, Sep. 2019. Accessed: Dec. 11, 2021. [Online]. Available: https://www.now-gmbh.de/wp-content/uploads/2020/09/now_studie-ship-fuel-1.pdf

[95] P. E. Dodds and W. McDowall, "Methodologies for representing the road transport sector in energy system models," *International Journal of Hydrogen Energy*, vol. 39, no. 5, pp. 2345–2358, Feb. 2014, doi: 10.1016/j.ijhydene.2013.11.021.

[96] E. Shafiei, B. Davidsdottir, J. Leaver, H. Stefansson, and E. I. Asgeirsson, "Energy, economic, and mitigation cost implications of transition toward a carbon-neutral transport sector: A simulation-based comparison between hydrogen and electricity," *Journal of Cleaner Production*, vol. 141, pp. 237–247, Jan. 2017, doi: 10.1016/j.jclepro.2016.09.064.

[97] Nationale Plattform Zukunft der Mobilität (NPM), "Wekstattbericht Antriebswechsel Nutzfahrzeuge - Wege zur Dekarbonisierung schwerer LKW mit Fokus der Elektrifizierung," Bundesministerium für Verkehr und digitale Infrastruktur, Berlin, Germany, Dec. 2020.

[98] M. Taljegard, S. Brynolf, M. Grahn, K. Andersson, and H. Johnson, “Cost-Effective Choices of Marine Fuels in a Carbon-Constrained World: Results from a Global Energy Model,” *Environ. Sci. Technol.*, vol. 48, no. 21, pp. 12986–12993, Nov. 2014, doi: 10.1021/es5018575.

[99] S. Cerniauskas, A. Jose Chavez Junco, T. Grube, M. Robinius, and D. Stolten, “Options of natural gas pipeline reassignment for hydrogen: Cost assessment for a Germany case study,” *International Journal of Hydrogen Energy*, vol. 45, no. 21, pp. 12095–12107, Apr. 2020, doi: 10.1016/j.ijhydene.2020.02.121.

[100] H2 MOBILITY Deutschland GmbH & Co. KG, “H2.live,” 2021. https://h2.live/en/ (accessed Nov. 15, 2021).

[101] VNG and enervis, “Metastudie Sektorenkopplung: ‘Analyse einer komplexen Diskussion.’” Apr. 2018. [Online]. Available: https://vng.de/sites/default/files/vng_meta_studie_sektorenkopplung_enervis.pdf

[102] W. Biener and K. R. Garcia Rosas, “Grid reduction for energy system analysis,” *Electric Power Systems Research*, vol. 185, p. 106349, Aug. 2020, doi: 10.1016/j.epsr.2020.106349.

[103] K.-K. Cao, J. Metzdorf, and S. Birbalta, “Incorporating Power Transmission Bottlenecks into Aggregated Energy System Models,” *Sustainability*, vol. 10, no. 6, p. 1916, Jun. 2018, doi: 10.3390/su10061916.

[104] M. Groissböck, “Are open source energy system optimization tools mature enough for serious use?,” *Renewable and Sustainable Energy Reviews*, vol. 102, pp. 234–248, Mar. 2019, doi: 10.1016/j.rser.2018.11.020.

[105] L. Welder, D. S. Ryberg, L. Kotzur, T. Grube, M. Robinius, and D. Stolten, “Spatio-temporal optimization of a future energy system for power-to-hydrogen applications in Germany,” *Energy*, vol. 158, pp. 1130–1149, Sep. 2018, doi: 10.1016/j.energy.2018.05.059.

[106] M. Reuß *et al.*, “Modeling hydrogen networks for future energy systems: A comparison of linear and nonlinear approaches,” *International Journal of Hydrogen Energy*, vol. 44, no. 60, pp. 32136–32150, Dec. 2019, doi: 10.1016/j.ijhydene.2019.10.080.

[107] P. Hauser, “A modelling approach for the German gas grid using highly re- solved spatial, temporal and sectoral data (GAMAMOD-DE),” ZBW- Leibniz Information Center of Economics, Kiel, Hamburg, Germany, Working Paper, 2019. [Online]. Available: http://hdl.handle.net/10419/197000

[108] K. Trepper, M. Bucksteeg, and C. Weber, “Impacts of renewables generation and demand patterns on net transfer capacity: implications for effectiveness of market splitting in Germany,” *IET Generation, Transmission & Distribution*, vol. 9, no. 12, pp. 1510–1518, Sep. 2015, doi: 10.1049/iet-gtd.2014.1063.

[109] M. Moreno-Benito, P. Agnolucci, and L. G. Papageorgiou, “Towards a sustainable hydrogen economy: Optimisation-based framework for hydrogen infrastructure development,” *Computers & Chemical Engineering*, vol. 102, pp. 110–127, Jul. 2017, doi: 10.1016/j.compchemeng.2016.08.005.

[110] M. M. Frysztacki, J. Hörsch, V. Hagenmeyer, and T. Brown, “The strong effect of network resolution on electricity system models with high shares of wind and solar,” *Applied Energy*, vol. 291, p. 116726, Jun. 2021, doi: 10.1016/j.apenergy.2021.116726.

[111] S. Pfenninger, A. Hawkes, and J. Keirstead, “Energy systems modeling for twenty-first century energy challenges,” *Renewable and Sustainable Energy Reviews*, vol. 33, pp. 74–86, May 2014, doi: 10.1016/j.rser.2014.02.003.

[112] N. Wulff, F. Steck, H. C. Gils, C. Hoyer-Klick, B. van den Adel, and J. E. Anderson, “Comparing Power-System and User-Oriented Battery Electric Vehicle Charging Representation and Its Implications on Energy System Modeling,” *Energies*, vol. 13, no. 5, p. 1093, Mar. 2020, doi: 10.3390/en13051093.

[113] H. C. Gils *et al.*, “Methods to improve computing times in linear energy system optimization models,” presented at the IFORS Conference, Quebec City, Jul. 17, 2017. Accessed: Dec. 11, 2021. [Online]. Available: https://elib.dlr.de/113913/1/IFORS2017_Gils_Speed-up_Energy_System_Models_final.pdf

[114] Kueppers, Martin, “Data-Driven Modeling of Decarbonization Pathways for Worldwide Energy Systems Based on Archetypes and Spatial Clustering Methods,” Technical University of Darmstadt, Darmstadt,

Germany, 2021. Accessed: Feb. 26, 2022. [Online]. Available: https://tuprints.ulb.tu-darmstadt.de/id/eprint/19824

[115] K. Siala and M. Y. Mahfouz, “Impact of the choice of regions on energy system models,” *Energy Strategy Reviews*, vol. 25, pp. 75–85, Aug. 2019, doi: 10.1016/j.esr.2019.100362.

[116] H. Teichgraeber and A. R. Brandt, “Time-series aggregation for the optimization of energy systems: Goals, challenges, approaches, and opportunities,” *Renewable and Sustainable Energy Reviews*, vol. 157, p. 111984, Apr. 2022, doi: 10.1016/j.rser.2021.111984.

[117] D. Husarek, S. Paulus, M. Huber, M. Metzger, and S. Niessen, “The Contribution of Carbon-optimized Battery Electric Vehicle Charging to the Decarbonization of a Multi-modal Energy System,” presented at the 3rd E-Mobility Power System Integration Symposium, Dublin, Ireland, Oct. 2019.

[118] D. Husarek, V. Salapic, S. Paulus, M. Metzger, and S. Niessen, “Modeling the Impact of Electric Vehicle Charging Infrastructure on Regional Energy Systems: Fields of Action for an Improved e-Mobility Integration,” *Energies*, vol. 14, no. 23, p. 7992, Nov. 2021, doi: 10.3390/en14237992.

[119] DKE, VDE|FNN, BDEW, ZVEH, VDA, and ZVEI, “Technischer Leitfaden Ladeinfrastruktur Elektromobilität - Version 4.” Oct. 2021. [Online]. Available: https://www.vde.com/resource/blob/988408/87ed1f99814536d66c99797a4545ad5d/technischer-leitfaden-ladeinfrastruktur-elektromobilitaet---version-4-data.pdf

[120] K. Schaber, F. Steinke, and T. Hamacher, “Transmission grid extensions for the integration of variable renewable energies in Europe: Who benefits where?,” *Energy Policy*, vol. 43, pp. 123–135, Apr. 2012, doi: 10.1016/j.enpol.2011.12.040.

[121] S. Raths *et al.*, “The Energy System Development Plan (ESDP),” presented at the ETG Congress, Bonn, Germany, 2015. [Online]. Available: https://publications.rwth-aachen.de/record/561436

[122] D. Husarek, J. Schmugge, and S. Niessen, “Hydrogen supply chain scenarios for the decarbonisation of a German multi-modal energy system,” *International Journal of Hydrogen Energy*, vol. 46, no. 76, pp. 38008–38025, Nov. 2021, doi: 10.1016/j.ijhydene.2021.09.041.

[123] T. Kolster, R. Krebs, S. Niessen, and M. Duckheim, “The contribution of distributed flexibility potentials to corrective transmission system operation for strongly renewable energy systems,” *Applied Energy*, vol. 279, p. 115870, Dec. 2020, doi: 10.1016/j.apenergy.2020.115870.

[124] M. Kueppers *et al.*, “Decarbonization pathways of worldwide energy systems – Definition and modeling of archetypes,” *Applied Energy*, vol. 285, p. 116438, Mar. 2021, doi: 10.1016/j.apenergy.2021.116438.

[125] M. Kueppers *et al.*, “Data-Driven Regionalization of Decarbonized Energy Systems for Reflecting Their Changing Topologies in Planning and Optimization,” *Energies*, vol. 13, no. 16, p. 4076, Aug. 2020, doi: 10.3390/en13164076.

[126] P. Mancarella, G. Andersson, J. A. Pecas-Lopes, and K. R. W. Bell, “Modelling of integrated multi-energy systems: Drivers, requirements, and opportunities,” in *2016 Power Systems Computation Conference (PSCC)*, Genoa, Italy, Jun. 2016, pp. 1–22. doi: 10.1109/PSCC.2016.7541031.

[127] H. Van Dyke Parunak, R. Savit, and R. L. Riolo, “Agent-Based Modeling vs. Equation-Based Modeling: A Case Study and Users’ Guide,” in *Multi-Agent Systems and Agent-Based Simulation*, vol. 1534, J. S. Sichman, R. Conte, and N. Gilbert, Eds. Berlin, Heidelberg: Springer Berlin Heidelberg, 1998, pp. 10–25. doi: 10.1007/10692956_2.

[128] A. Harbrecht, R. McKenna, D. Fischer, and W. Fichtner, “Behavior-oriented Modeling of Electric Vehicle Load Profiles: A Stochastic Simulation Model Considering Different Household Characteristics, Charging Decisions and Locations,” Karlsruhe, Apr. 2018. doi: 10.5445/IR/1000082537.

[129] F. J. Soares, J. A. Pecas-Lopes, P. M. Rocha Almeida, C. L. Moreira, and L. Seca, “A stochastic model to simulate electric vehicles motion and quantify the energy required from the grid,” Stockholm, Sweden, Aug. 2011, p. 7.

[130] P. Sokorai, A. Fleischhacker, G. Lettner, and H. Auer, “Stochastic Modeling of the Charging Behavior of Electromobility,” *WEVJ*, vol. 9, no. 3, p. 44, Oct. 2018, doi: 10.3390/wevj9030044.

[131] N. Daina, A. Sivakumar, and J. W. Polak, “Modelling electric vehicles use: a survey on the methods,” *Renewable and Sustainable Energy Reviews*, vol. 68, pp. 447–460, Feb. 2017, doi: 10.1016/j.rser.2016.10.005.

[132] K. H. van Dam, I. Nikolic, and Z. Lukszo, *Agent-based modelling of socio-technical systems*. Springer, 2018.

[133] Q. Han, B. de Vries, and G. Kanters, “An agent-based multi-objective optimization model for allocating public charging stations for electric vehicles,” Cambridge, MA, Jul. 2015, p. 17.

[134] M. van der Kam, A. Peters, W. van Sark, and F. Alkemade, “Agent-Based Modelling of Charging Behaviour of Electric Vehicle Drivers,” *JASSS*, vol. 22, no. 4, p. 7, 2019, doi: 10.18564/jasss.4133.

[135] U. Wilensky, “NetLogo, http://ccl.northwestern.edu/netlogo/.” Center for Connected Learning and Computer-Based Modeling, Northwestern University, Evanston, IL, 1999. [Online]. Available: http://ccl.northwestern.edu/netlogo/

[136] MiD, “Mobilität in Deutschland (MiD) 2017,” Bundesministerium für Verkehr und digitale Infrastruktur, Study, 2017.

[137] C. Nobis and T. Kuhnimhof, “Mobilität in Deutschland - Ergebnisbericht,” infas,DLR,IVT and infas 360, Bonn, Berlin, Germany, 2018. Accessed: Mar. 02, 2022. [Online]. Available: http://www.mobilitaet-in-deutschland.de/pdf/MiD2017_Ergebnisbericht.pdf

[138] A. Schmidt, “Flottenbetrieb von elektrischen und autonomen Serviceagenten im städtischen Personennahverkehr,” Karlsruher Institut für Technologie, Karsruhe, 2016.

[139] M. Nicholas, D. Hall, and N. Lutsey, “Quantifying the electric vehicle charging infrastructure gap across U.S. markets,” Jan. 2019.

[140] I. Frenzel, J. Jarass, S. Trommer, and B. Lenz, “Erstnutzer von Elektrofahrzeugen in Deutschland. Nutzerprofile, Anschaffung, Fahrzeugnutzung.,” Deutsches Zentrum für Luft- und Raumfahrt e. V. (DLR), Berlin, 2. überarbeitete Auflage, 2015.

[141] H. H. Alhelou, P. Siano, M. Tipaldi, R. Iervolino, and F. Mahfoud, “Primary Frequency Response Improvement in Interconnected Power Systems Using Electric Vehicle Virtual Power Plants,” *WEVJ*, vol. 11, no. 2, p. 40, May 2020, doi: 10.3390/wevj11020040.

[142] S. Gottwalt, A. Schuller, C. Flath, H. Schmeck, and C. Weinhardt, “Assessing load flexibility in smart grids: Electric vehicles for renewable energy integration,” in *2013 IEEE Power & Energy Society General Meeting*, Vancouver, BC, 2013, pp. 1–5. doi: 10.1109/PESMG.2013.6672854.

[143] E. C. Kara, J. S. Macdonald, D. Black, M. Bérges, G. Hug, and S. Kiliccote, “Estimating the benefits of electric vehicle smart charging at non-residential locations: A data-driven approach,” *Applied Energy*, vol. 155, pp. 515–525, Oct. 2015, doi: 10.1016/j.apenergy.2015.05.072.

[144] A. Nayak, R. Rana, and S. Mishra, “Frequency Regulation by Electric Vehicle during Grid Restoration using Adaptive Optimal Control,” *IFAC-PapersOnLine*, vol. 52, no. 4, pp. 270–275, 2019, doi: 10.1016/j.ifacol.2019.08.210.

[145] C. Hecht, S. Das, C. Bussar, and D. U. Sauer, “Representative, empirical, real-world charging station usage characteristics and data in Germany,” *eTransportation*, vol. 6, p. 100079, Nov. 2020, doi: 10.1016/j.etran.2020.100079.

[146] Kraftfahrt-Bundesamt (KBA), “Der Fahrzeugbestand im Überblick,” *Kraftfahrt-Bundesamt (KBA) - Zahlen, Daten Fakten*, 2019. https://www.kba.de/DE/Statistik/Fahrzeuge/Bestand/Jahrebilanz_Bestand/fz_b_jahresbilanz_node.html;jsessionid=51D389C13873FDD51E0409454234A8C3.live11292 (accessed Feb. 27, 2022).

[147] Bundesnetzagentur, “Ladesäulenregister Bundesnetzagentur.” Dec. 03, 2020. Accessed: Dec. 14, 2020. [Online]. Available: https://www.bundesnetzagentur.de/DE/Sachgebiete/ElektrizitaetundGas/Unternehmen_Institutionen/HandelundVertrieb/Ladesaeulenkarte/Ladesaeulenkarte_node.html

[148] G. E. B. Archer, A. Saltelli, and I. M. Sobol, “Sensitivity measures,anova-like Techniques and the use of bootstrap,” *Journal of Statistical Computation and Simulation*, vol. 58, no. 2, pp. 99–120, May 1997, doi: 10.1080/00949659708811825.

[149] A. Saltelli, P. Annoni, I. Azzini, F. Campolongo, M. Ratto, and S. Tarantola, “Variance based sensitivity analysis of model output. Design and estimator for the total sensitivity index,” *Computer Physics Communications*, vol. 181, no. 2, pp. 259–270, Feb. 2010, doi: 10.1016/j.cpc.2009.09.018.

[150] A. Saltelli, “Making best use of model evaluations to compute sensitivity indices,” *Computer Physics Communications*, vol. 145, no. 2, pp. 280–297, May 2002, doi: 10.1016/S0010-4655(02)00280-1.

[151] Y. Gan *et al.*, “A comprehensive evaluation of various sensitivity analysis methods: A case study with a hydrological model,” *Environmental Modelling & Software*, vol. 51, pp. 269–285, Jan. 2014, doi: 10.1016/j.envsoft.2013.09.031.

[152] G. ten Broeke, G. van Voorn, and A. Ligtenberg, “Which Sensitivity Analysis Method Should I Use for My Agent-Based Model?,” *JASSS*, vol. 19, no. 1, p. 5, 2016, doi: 10.18564/jasss.2857.

[153] M. Jaxa-Rozen and J. H. Kwakkel, “PyNetLogo: Linking NetLogo with Python,” *JASSS*, vol. 21, no. 2, p. 4, 2018, doi: 10.18564/jasss.3668.

[154] R. Oudkerk and Contributors, “Multiprocessing - Python package.” 2008.

[155] D. Husarek, S. Paulus, and S. Niessen, “Pareto optimal design of charging infrastructure within a region,” in *ETG Congress 2021*, Berlin, Offenbach, May 2021, vol. ETG Fachbericht 163: ETG Kongress, pp. 832–837.

[156] Prognos, “Lade-Report,” EnBW Energie Baden-Würtemberg AG, Feb. 2020. Accessed: Mar. 09, 2021. [Online]. Available: https://www.prognos.com/sites/default/files/2021-01/20200207_prognos_lade-report_2020.pdf

[157] German National Platform for Electromobility (NPE), “Progress Report 2018 – Market ramp-up phase,” Federal Government’s Joint Agency for Electromobility (GGEMO), Berlin, Germany, May 2018. [Online]. Available: https://www.plattform-zukunft-mobilitaet.de/en/2download/progress-report-2018-market-ramp-up-phase/

[158] A. Zerrahn and W.-P. Schill, “On the representation of demand-side management in power system models,” *Energy*, vol. 84, pp. 840–845, May 2015, doi: 10.1016/j.energy.2015.03.037.

[159] J. Dorfner, “urbs: A linear optimisation model for distributed energy systems,” *urbs: A linear optimisation model for distributed energy systems*, Feb. 07, 2022. https://urbs.readthedocs.io/en/latest/Users_guide.html

[160] A. Zerrahn and W.-P. Schill, “Long-run power storage requirements for high shares of renewables: review and a new model,” *Renewable and Sustainable Energy Reviews*, vol. 79, pp. 1518–1534, Nov. 2017, doi: 10.1016/j.rser.2016.11.098.

[161] Arbeitsgemeinschaft Energiebilanzen e.V. (AGEB), “Anwendungsbilanzen zur Energiebilanz Deutschland - Endenergieverbrauch nach Energieträgern und Anwendungszwecken - Detaillierte Anwendungsbilanzen der Endenergiesektoren für 2019 und 2020 sowie zusammenfassende Zeitreihen zum Endenergieverbrauch nach Energieträgern und Anwendungszwecken für Jahre von 2010 bis 2020.” May 2021. Accessed: Mar. 11, 2022. [Online]. Available: https://ag-energiebilanzen.de/wp-content/uploads/2020/10/ageb_20v_v1.pdf

[162] Bundesministerium für Wirtschaft und Energie (BMWi), “Energieeffizienz in Zahlen 2020 - Entwicklungen und Trends in Deutschland 2020,” Berlin, Germany, Sep. 2020.

[163] F. Kunz *et al.*, “Reference Data Set: Electricity, Heat, And Gas Sector Data For Modeling The German System.” Zenodo, Dec. 27, 2017. doi: 10.5281/ZENODO.1044463.

[164] Heat Roadmap Europe, “Profiles and Baselines for heating and cooling energy demands in 2015 for EU28 countries,” *Heat Roadmap Europe*, Sep. 21, 2021. https://heatroadmap.eu/heating-and-cooling-energy-demand-profiles/

[165] D. G. Erbs, S. A. Klein, and J. A. Duffie, “Estimation of the diffuse radiation fraction for hourly, daily and monthly-average global radiation,” *Solar Energy*, vol. 28, no. 4, pp. 293–302, 1982, doi: 10.1016/0038-092X(82)90302-4.

[166] European Commission, Joint Research Centre (JRC), “ENSPRESO - INTEGRATED DATA. European Commission, Joint Research Centre (JRC) [Dataset] PID: http://data.europa.eu/89h/88d1c405-0448-4c9e-b565-3c30c9b167f7,” 2021. https://data.jrc.ec.europa.eu/dataset

[167] 50Hertz Transmission GmbH, Amprion GmbH, TenneT TSO GmbH, and TransnetBW GmbH, “Szenariorahmen für die Netzentwicklungspläne Strom 2030 - Entwurf der Übertragungsnetzbetreiber.” 2019. [Online]. Available: www.netzentwicklungsplan.de

[168] ENTSO, “TYNDP 2020 - Scenario Data.” Jun. 2020. Accessed: Mar. 11, 2022. [Online]. Available: https://www.entsos-tyndp2020-scenarios.eu/download-data/#download

[169] Transmission Grid Operators, “Netzentwicklungsplan Strom 2030, Version 2019 - 2.Entwurf der Übertragungsnetzbetreiber.” Apr. 15, 2019. Accessed: Mar. 17, 2022. [Online]. Available: https://www.netzentwicklungsplan.de/sites/default/files/paragraphs-files/NEP_2030_V2019_2_Entwurf_Teil1.pdf

[170] D. Hess, M. Wetzel, and K.-K. Cao, “Representing node-internal transmission and distribution grids in energy system models,” *Renewable Energy*, vol. 119, pp. 874–890, Apr. 2018, doi: 10.1016/j.renene.2017.10.041.

[171] D. Most *et al.*, “A Novel Modular Optimization Framework for Modelling Investment and Operation of Energy Systems at European Level,” ZIB-Report (20-08), Mar. 2020. Accessed: Mar. 19, 2022. [Online]. Available: https://opus4.kobv.de/opus4-zib/frontdoor/index/index/docId/7807

[172] I. Mareev and D. Sauer, “Energy Consumption and Life Cycle Costs of Overhead Catenary Heavy-Duty Trucks for Long-Haul Transportation,” *Energies*, vol. 11, no. 12, p. 3446, Dec. 2018, doi: 10.3390/en11123446.

[173] M. Wietschel *et al.*, “Machbarkeitsstudie zur Ermittlung der Potentiale des Hybrid-Oberleitungs-Lkw,” Karlsruhe, Feb. 2017. Accessed: Mar. 12, 2022. [Online]. Available: https://www.bmvi.de/SharedDocs/DE/Anlage/G/MKS/studie-potentiale-hybridoberleitungs-lkw.pdf?__blob=publicationFile

[174] F. Unterlohner, “Comparison of hydrogen and battery electric trucks - Methodology and underlying assumptions.” Jun. 2020. Accessed: Mar. 12, 2022. [Online]. Available: https://www.transportenvironment.org/discover/comparing-hydrogen-and-battery-electric-trucks/

[175] Industrieverband Agrar e.V., “Wichtige Zahlen 2019-2020 - Düngemittel, Produktion, Markt, Landwirtschaft,” Frankfurt, Germany, Dec. 2020. Accessed: Mar. 13, 2022. [Online]. Available: https://www.iva.de/publikationen/wichtige-zahlen-2019-2020

[176] “Raffinerien und Produktion,” *en2x - Raffinerien und Produktion*, Dec. 09, 2021. https://en2x.de/positionen/raffinerien-und-produktion/ (accessed Mar. 13, 2022).

[177] Wirtschaftsvereinigung Stahl, “Fakten zur Stahlindustrie in Deutschland 2020,” Aug. 2020. Accessed: Mar. 13, 2022. [Online]. Available: https://www.stahl-online.de/publikationen/fakten-zur-stahlindustrie/

[178] G. Brändle, M. Schönfisch, and S. Schulte, “Estimating Long-Term Global Supply Costs for Low-Carbon Hydrogen,” *EWI Working Paper*, p. 72, Nov. 2020.

[179] International Energy Agency (IEA), “IEA G20 Hydrogen report Assumptions.” Dec. 2020. Accessed: Mar. 19, 2022. [Online]. Available: https://iea.blob.core.windows.net/assets/29b027e5-fefc-47df-aed0-456b1bb38844/IEA-The-Future-of-Hydrogen-Assumptions-Annex_CORR.pdf

[180] Ø. Ulleberg and R. Hancke, “Techno-economic calculations of small-scale hydrogen supply systems for zero emission transport in Norway,” *International Journal of Hydrogen Energy*, vol. 45, no. 2, pp. 1201–1211, Jan. 2020, doi: 10.1016/j.ijhydene.2019.05.170.

[181] D. G. Caglayan *et al.*, “Technical potential of salt caverns for hydrogen storage in Europe,” *International Journal of Hydrogen Energy*, vol. 45, no. 11, pp. 6793–6805, Feb. 2020, doi: 10/gh6j9c.

[182] K. Stolzenburg *et al.*, “Integration von Wind-Wasserstoff-Systemen in das Energiesystem - Abschlussbericht,” Oldenburg, Germany, Mar. 2014. Accessed: Mar. 13, 2022. [Online]. Available: https://www.planet-energie.de/de/media/Abschlussbericht_Integration_von_Wind_Wasserstoff_Systemen_in_das_Energiesystem.pdf

[183] L. Welder *et al.*, “Design and evaluation of hydrogen electricity reconversion pathways in national energy systems using spatially and temporally resolved energy system optimization,” *International Journal of Hydrogen Energy*, vol. 44, no. 19, pp. 9594–9607, Apr. 2019, doi: 10.1016/j.ijhydene.2018.11.194.

[184] Energie Informationsdienst (EID), “Underground Gas Storage in Germany,” *Erdöl Erdgas Kohle 131 Jg. 2015*, vol. 131, no. 11, 2021. Accessed: Mar. 13, 2022. [Online]. Available: https://www.lbeg.niedersachsen.de/energie_rohstoffe/erdoel_und_erdgas/untertagegasspeicher/publikation_untertageerdgaspeicherung/publikation-zur-untertage-gasspeicherung-in-der-zeitschrift-erdoel-erdgas-kohle-898.html

[185] P. Adam and F. Heunemann, “Hydrogen infrastructure – the pillar of energy transition,” p. 32, 2020.

[186] Nexant, Inc. *et al.*, “H2A Hydrogen Delivery Infrastructure Analysis Models and Conventional Pathway Options Analysis Results, Interim Report: DE-FG36-05GO15032: Hydrogen Delivery Infrastructure Options Analysis,” DE-FG36-05GO15032, May 2008.

[187] G. T. Simbolotti, “Hydrogen Production & Distribution, IEA-ETSAP Technology Brief P12.” Feb. 2014. [Online]. Available: https://iea-etsap.org/E-TechDS/PDF/P12_H2_Feb2014_FINAL%203_CRES-2a-GS%20Mz%20GSOK.pdf

[188] European Commission. Directorate General for Energy., Guidehouse., and Tractebel Impact., *Hydrogen generation in Europe: overview of costs and key benefits.* LU: Publications Office, 2020. Accessed: Mar. 20, 2022. [Online]. Available: https://data.europa.eu/doi/10.2833/122757

[189] J. Hampp, M. Düren, and T. Brown, “Import options for chemical energy carriers from renewable sources to Germany,” *arXiv:2107.01092 [physics]*, Jul. 2021, Accessed: Feb. 09, 2022. [Online]. Available: http://arxiv.org/abs/2107.01092

[190] Agora Verkehrswende, Agora Energiewende, and Frontier Economics, “The Future Cost of Electricity-Based Synthetic Fuels,” Cologne, Germany, Sep. 2018. Accessed: Mar. 20, 2022. [Online]. Available: https://www.agora-verkehrswende.de/en/publications/the-future-cost-of-electricity-based-synthetic-fuels/#:~:text=Costs%20can%20fall%20to%2010,in%20electrolysers%20and%20CO2%20absorbers.

[191] F. Kunz, “Electricity, Heat and Gas Sector Data for Modelling the German System.” 2017. [Online]. Available: https://www.diw.de/documents/publikationen/73/diw_01.c.574130.de/diw_datadoc_2017-092.pdf

[192] DVGW, “DVGW G 260: Gas Quality.” Sep. 2021. [Online]. Available: https://www.beuth.de/de/technische-regel/dvgw-g-260/345469197

[193] J. Mischner and P. Schley, “System- und netzplanerische Aspekte der Wasserstoffeinspeisung in Erdgasnetze - Teil 1,” *gwf - Gas | Erdgas*, no. 01-02 2015, p. 10, Jan. 02, 2015.

[194] Navigant, “Gas for Climate. The optimal role for gas in a net zero emissions energy system,” Utrecht, Netherlands, Mar. 2019. Accessed: Mar. 20, 2022. [Online]. Available: https://gasforclimate2050.eu/wp-content/uploads/2020/03/Navigant-Gas-for-Climate-The-optimal-role-for-gas-in-a-net-zero-emissions-energy-system-March-2019.pdf

[195] H. Scharf, F. Arnold, and D. Lencz, “Future natural gas consumption in the context of decarbonization - A meta-analysis of scenarios modeling the German energy system,” *Energy Strategy Reviews*, vol. 33, p. 100591, Jan. 2021, doi: 10.1016/j.esr.2020.100591.

[196] Y. Scholz, B. Fuchs, F. Borggrefe, K.-K. Cao, and M. Wetzel, “Speeding up Energy System Models - a Best Practice Guide,” Jun. 2020. Accessed: Mar. 11, 2022. [Online]. Available: https://elib.dlr.de/135507/1/EnergySystemModel_SpeedUp_BestPracticGuide.pdf

[197] European Commission, Directorate-General for Energy, European Commission, Climate Action DG, European Commission, and Directorate General for Mobility and Transport, *Energy, transport and GHG emissions, trends to 2050: EU reference scenario 2016*. Luxembourg: EUR-OP, 2016.

[198] Übertragungsnetzbetreiber, “Szenariorahmen zum Netzentwicklungsplan Strom 2037 mit Ausblick 2045, Version 2023 - Entwurf.” Jan. 2022. Accessed: Apr. 07, 2022. [Online]. Available: https://www.netzentwicklungsplan.de/sites/default/files/paragraphs-files/Szenariorahmenentwurf_NEP2037_2023.pdf

[199] Kopernikus-Projekt Ariadne, “Ariadne Kurzdossier - Durchstarten trotz Unsicherheiten: Eckpunkte einer anpassungsfähigen Wasserstoffstrategie.” Nov. 2021. Accessed: Apr. 07, 2022. [Online]. Available: https://ariadneprojekt.de/media/2021/11/Ariadne_Kurzdossier_Wasserstoff_November2021.pdf

[200] N. J. Kurmayer and EURACTIV.com, “Germany signs initial contract to build first LNG terminal,” *EURACTIV.com*, Mar. 07, 2022. https://www.euractiv.com/section/energy/news/germany-signs-first-stage-contract-to-build-first-lng-terminal/

[201] M. Gierkink, J. Wagner, F. Arnold, B. Czock, N. Namockel, and P. Theile, “EWI-Analyse - Auswirkungen des Koalitionsvertrags auf den Stromsektor 2030.” Dec. 06, 2021. Accessed: Apr. 07, 2022. [Online]. Available: https://www.ewi.uni-koeln.de/cms/wp-content/uploads/2021/12/211206_EWI-Analyse_Auswirkungen-des-Koalitionsvertrags-auf-den-Stromsektor-2030_final.pdf

[202] R. Pagany, L. Ramirez Camargo, and W. Dorner, “A review of spatial localization methodologies for the electric vehicle charging infrastructure,” *International Journal of Sustainable Transportation*, vol. 13, no. 6, pp. 433–449, Jul. 2019, doi: 10.1080/15568318.2018.1481243.

[203] International Renewable Energy Agency, “Innovation outlook: Smart charging for electric vehicles,” Abu Dhabi, 2019.

[204] ecomento, “VDA: E-Auto-Hochlauf gefährdet, Deutschland hängt bei Ladeinfrastruktur „extrem hinterher“,” *ecomento.de*, Dec. 27, 2021. https://ecomento.de/2021/12/27/vda-e-auto-hochlauf-gefaehrdet-deutschland-haengt-bei-ladeinfrastruktur-extrem-hinterher/ (accessed Apr. 08, 2022).

[205] J.-S. Lee *et al.*, “The Complexities of Agent-Based Modeling Output Analysis,” *JASSS*, vol. 18, no. 4, p. 4, 2015, doi: 10.18564/jasss.2897.

[206] B. Helgeson and J. Peter, “The Role of Electricity in Decarbonizing European Road Transport – Development and Assessment of an Integrated Multi-Sectoral Model,” p. 67, Jan. 2019.

[207] Umweltbundesamt (UBA), “Endenergieverbrauch und Energieeffizienz des Verkehrs,” *umweltbundesamt.de*, 2021. https://www.umweltbundesamt.de/daten/verkehr/endenergieverbrauch-energieeffizienz-des-verkehrs#endenergieverbrauch-steigt-seit-2010-wieder-an (accessed Jun. 26, 2021).

Appendix A ABM eMob sample size

The required sample size for a sensitivity analysis using the ABM eMob can be determined based on the stabilization of the coefficient of variance for all model outputs of interest as suggested in [152], [205]. The coefficient of variation is defined as

$$c_{V,k} = \frac{\sigma_k}{\mu_k}, \forall k \in \{p, f\}$$

with the standard deviation σ, the mean μ over a simulations and k the output parameter of interest. The minimum number n_{min} of repetitions for a scenario is then defined by the number of repetitions, for which $c_{V,k}$ stabilizes for all considered model outputs k = {p, f} (cf. Eq. 5.39). It is in the following assessed for sample sizes of $N = \{1, \dots, 200\}$.

$$n_{min} = \ argmax_k |c_{v,k}(n-1) - c_{v,k}(n)| < \epsilon, \forall k \in \{p, f\}$$

When applying this measure, the confidence interval of the output variable needs to be sufficiently greater than zero [205], which is the case for all investigated outputs of the model. Figure A-1 shows for a parametrized rural region with 1000 simulated BEVs the stabilization of the coefficient at a sample size of $n_{min} = 38$. The threshold ϵ is a subjective measure and is here set to 0.1%.

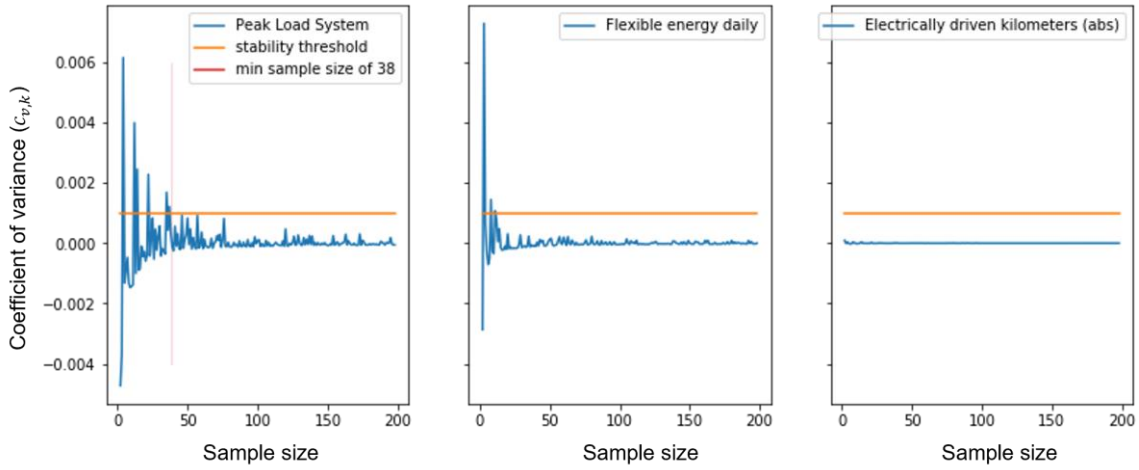

Figure A-1 – Minimum required sample size based on stabilization of coefficient of variation.

Appendix B NUTS2 naming convention

The regional resolution on the NUTS2 level is referred to in this thesis. Figure B-2 shows the naming convention of all 38 NUTS2 regions in Germany.

Figure B-2 – NUTS2 resolution and naming convention.

Appendix C Mobility sector technology costs

Techno-economic parameter assumptions for the year 2045. Airplanes are not listed since no competing technologies are optimized.

Transportation technology	Consumption in kWh/km	Investment costs in thousand € per vehicle	Maintenance costs in % of investment per year	Average annual mileage in km	Average number of passengers per vehicle	Lifetime in years
Car ICE-LF	0.4	23	3%	14700	1.4	15
Car ICE-CH4	0.45	24.3	3%			
Car Battery (BEV)	0.15	24.7	2%			
Car FC-GH2	0.21	24.8	3%			
Car PHEV-LF	0.4|0.15*	26	3%			

Table C-3 – Technical and economical passenger car vehicle parameters in 2045. Own assumptions based on [27], [74], [206]. * First number applies for ICE and second for electric powertrain.

Transportation technology	Consumption in kWh/km	Investment costs in thousand € per vehicle	Maintenance costs in % of investment per year	Average annual mileage in km	Average number of passengers per vehicle	Lifetime in years
Bus ICE-LF	2.42	187	3%	57000	16.1	17
Bus ICE-CH4	2.96	205.8	3%			
Bus Battery	1.35	213.8	2%			
Bus FC-GH2	2.24	212.9	3%			

Table C-4 - Technical and economical parameters in 2045 for busses and coaches. Own assumptions based on [27], [74], [206].

Transportation technology	Consumption in kWh/km	Investment costs in thousand € per vehicle	Maintenance costs in % of investment per year	Average annual mileage in km	Average load in t per vehicle	Lifetime in years
LDV ICE-LF	0.48	45	3%	35000	2	11
LDV ICE-CH4	0.54	45.7	3%			
LDV Battery	0.23	46	2%			
LDV FC-GH2	0.3	46	3%			

Table C-5 - Technical and economical parameters in 2045 for Light Duty Vehicles (LDV). Own assumptions based on [27], [74], [206].

Transportation technology	Consumption in kWh/km	Investment costs in thousand € per vehicle	Maintenance costs in % of investment per year	Average annual mileage in km	Average number of passengers per vehicle	Lifetime in years
HDV ICE-LF	2.09	83	3%	60000	12.5	11
HDV ICE-LCH4	2.48	90.4	3%			
HDV Battery	1.28	97.1	2%			
HDV FC-LH2	1.7	99.5	3%			
HDV Catenary-LF	1.77 | 1.28*	102	3%			
HDV Catenary-LCH4	1.77 | 1.28*	102	3%	130000		
HDV Catenary-Battery	1.28	112.1	2%			

Table C-6 - Technical and economical parameters in 2045 for Heavy Duty Vehicles (HDV). Own assumptions based on [27], [74], [206]. * First number applies for ICE and second for electric powertrain.

Transportation technology	Consumption in kWh/tkm	Investment costs in million € per train	Maintenance costs in % of investment per year	Average annual mileage in km	Average load in t per train	Lifetime in years
Train Catenary	0.03	4.185	2%	200000	1*	40
Train ICE-LF	0.12	4.185	2%			
Train FC-GH2	0.06	5.6	2%			

Table C-7 - Technical and economical parameters in 2045 for trains. Own assumptions based on [27], [207]. * Assumptions already based on tkm.

Transportation technology	Consumption in kWh/tkm	Investment costs in million € per vessel	Maintenance costs in % of investment per year	Average annual mileage in km	Average load in t per vessel	Lifetime in years
Ship ICE-LF	0.11	17.5	2%	84000	1*	60
Ship ICE-LCH4	0.11	18.6	2%			
Ship FC-LH2	0.11	19.4	2%			

Table C-8 - Technical and economical parameters in 2045 for ships. Own assumptions based on [98].

Appendix D Resulting technology mix in mobility sector

Resulting technology mix in the mobility sector for passenger transportation (cf. Figure D-9) and freight transportation (cf. Figure D-10) in all assessed scenarios in the MMES optimization for the year 2045. Additionally, the electrification rate in the passenger and freight transportation sector is shown in Figure D-11.

Naming conventions are: LF – Liquid Fuel; PHEV – Plug-In Hybrid Electric Vehicle; FC – Fuel Cell; HDV – Heavy Duty Vehicle; LDV – Light Duty Vehicle.

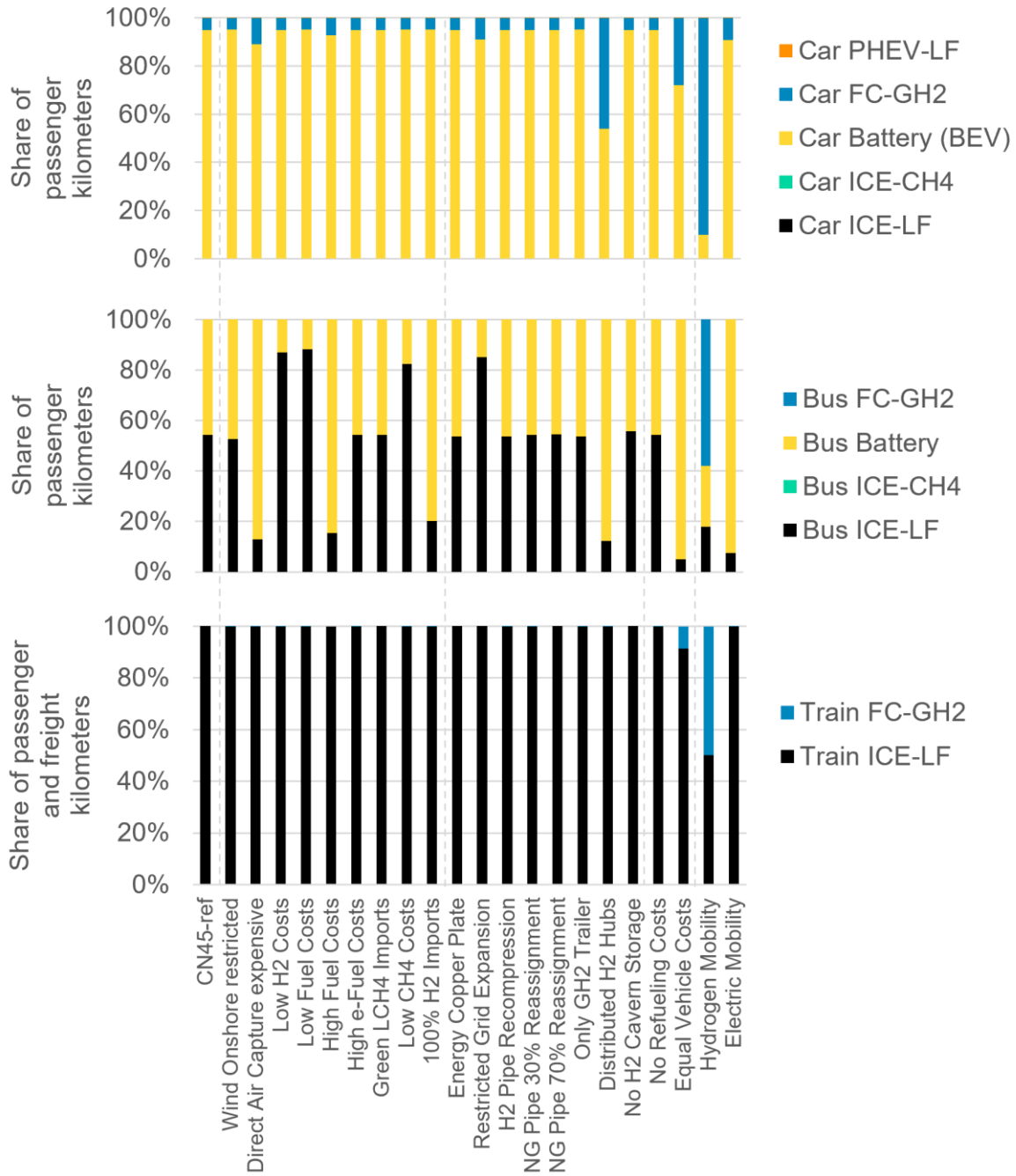

Figure D-9 – Technology mix in the passenger transportation sector as share of passenger kilometers in the corresponding segment. From top to bottom it shows cars, busses, and trains. Trains only show the non-electrified railway systems and contain additionally the freight transportation.

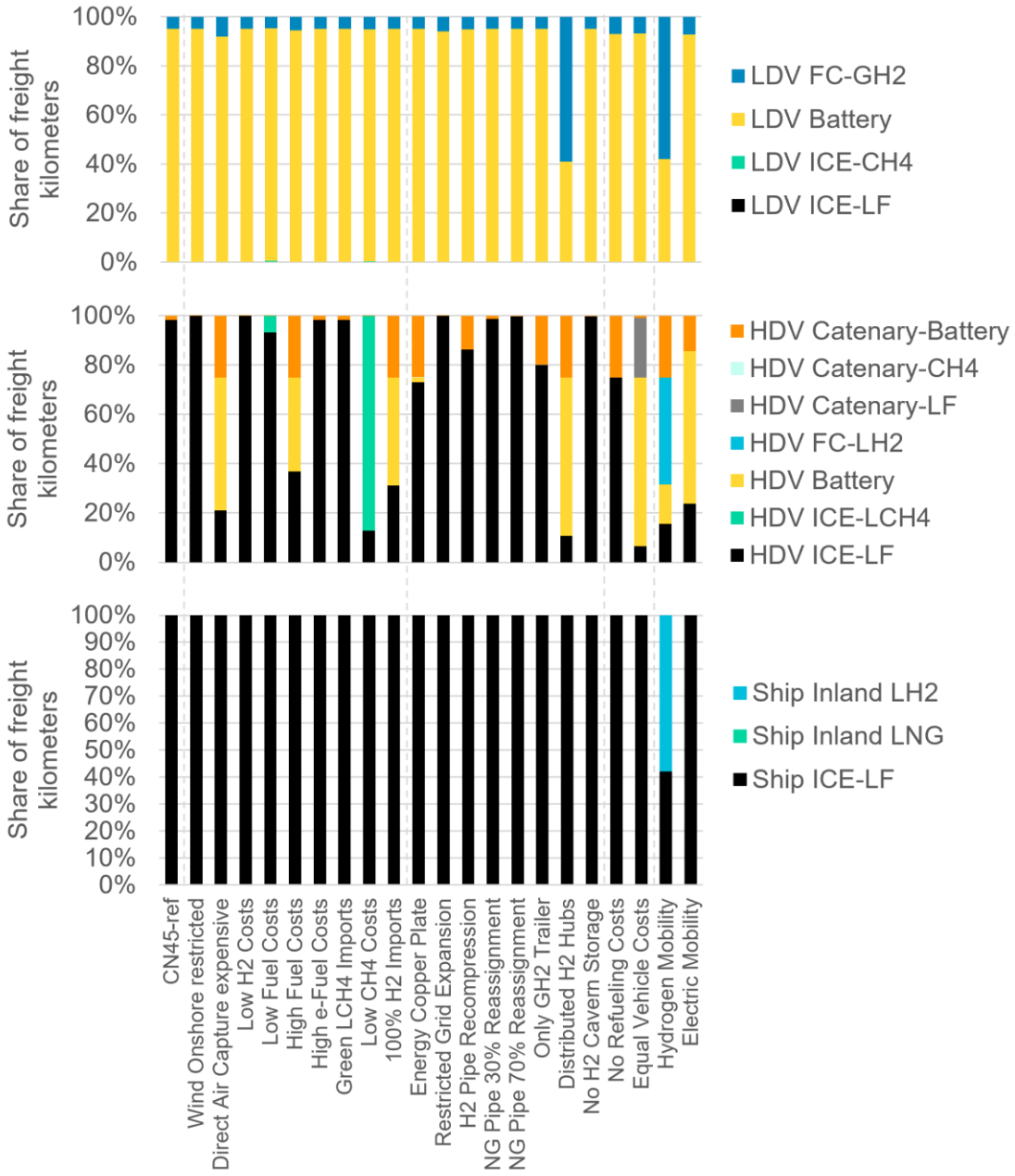

Figure D-10 – Technology mix in the freight transportation sector as share of ton kilometers in the corresponding segment.

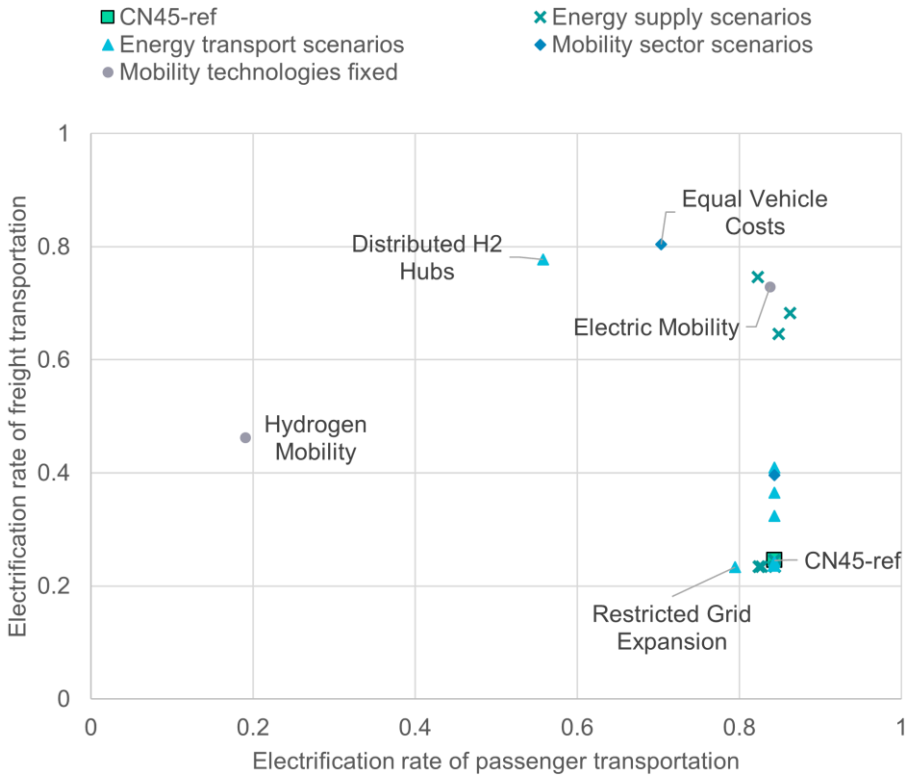

Figure D-11 – Electrification rate in the passenger and freight transportation sector in different scenarios compared to the reference scenario CN45-ref. The electrification rate is based on the electrified Gpkm and Gtkm.